T.C.
INONU UNIVERSITY
GRADUATE SCHOOL OF NATURAL AND APPLIED SCIENCES

DEVELOPMENT OF FUNCTIONAL CARRIER SYSTEMS FOR BIOTECHNOLOGICAL ENZYME DRUGS BY USING UPCONVERTING NANOPARTICLES

DOCTORAL THESIS

Samir Abbas Ali NOMA

DEPARTMENT OF CHEMISTRY

Supervisor
Prof. Dr. Burhan ATEŞ

MALATYA

APRIL, 2021

T.C.
INONU UNIVERSITY
GRADUATE SCHOOL OF NATURAL AND APPLIED SCIENCES

DEVELOPMENT OF FUNCTIONAL CARRIER SYSTEMS FOR BIOTECHNOLOGICAL ENZYME DRUGS BY USING UPCONVERTING NANOPARTICLES

DOCTORAL THESIS

Samir Abbas Ali NOMA
(D3616130002)

DEPARTMENT OF CHEMISTRY

Supervisor
Prof. Dr. Burhan ATEŞ

MALATYA

APRIL, 2021

ACKNOWLEDGEMENTS

First, I thank God for keeping me in the faith power, and heath to finish this Ph.D. thesis. Subsequently, I would like to express my huge gratitude to my supervisor Prof. Dr. Burhan ATEŞ, who has been helping me. Thank you for your motivation, guidance, endless discussions, and for the example of a professional that I will take throughout my career.

I would like to thank Prof. Dr. Meltem ASİLTÜRK and Assist Prof. Dr. Seda Demirel TOPEL for their help in the synthesis and characterization of UCNP nanoparticles.

Thanks for my thesis supervision committee members Prof. Dr. İsmet YILMAZ and Prof. Dr. Süleyman KÖYTEPE.

Special thanks for Prof. Dr. Mehmet ODABAŞI for his support and encouragement.

Thanks for my friends Dr. Ahmet ULU, Canbolat GURSES, İmren ÖZCAN, Ali KURUÇAY, and Fakhriy MUHAMMAD.

Special thanks for my dear friend Assist Prof. Dr. Ömür ACET and Dr. Selda SEZER, and special thanks to Gülşah KARADOL and Zehra TUTUK for their supports.

Special and much thanks to my parents, brothers, and sister for their support, and encouragement, they have great merit upon me for their unconditional support throughout my degree. Without them, I would not have the ability to study and finish this Ph.D.

This study was supported by Technological Research Council of Turkey (TUBITAK, Project number: 119Z962). I would like to thank TUBITAK, which provided financial support.

DECLARATION

I hereby declare that I wrote this Doctoral Thesis titled “Development of Functional Carrier Systems for Biotechnological Enzyme Drugs by Using Upconverting Nanoparticles”, in consistent with the thesis writing guide of the Graduate School of Natural and Applied Sciences, Inonu University. I also declare that all information in it is correct, that I acted according to scientific ethics in producing and presenting the findings, cited all the references I used, express all institutions or organizations or persons who supported the thesis financially. I have never used the data and information I provide here in order to get a degree in any way.

Samir Abbas Ali NOMA

LIST OF CONTENTS

LIST OF TABLES

LIST OF FIGURES

ABBREVIATIONS

ALL	Acute Lymphoblastic Leukemia
DCM	Dichloromethane
DMEM	Dulbecco′s Modified Eagle′s Medium
DMSO	Dimethyl Sulfoxide
DMF	N, N-Dimethyl Formamide
DSC	Differential Scanning Calorimeter
E. coli	*Escherichia Coli*
Ea	Activation Energy
EU	Enzyme unit
FDA	Food and Drug Administration
FTIR / ATR	Fourier Transform Infra Red-Attenuated Total Reflection
GO	Graphene Oxide
GPTMS	3-Glycidyloxypropyl Trimethoxysilane
ICPTES	3-Isocyanatopropyl Triethoxysilane
L-Asn	L-Asparagine
L-ASNase	L-Asparaginase
L-Asp	L-Aspartic acid
L-Glu	L-Glutamic acid
MNP	Magnetic Nanoparticle
MTT	3-(4,5-dimethylthiazol-2-yl) -2,5-diphenyltetrazolium bromide
NIR	Near-infrared
PEI	Polyethylenimine
PEG	Polyethylene glycol
TCA	Trichloroacetic acid
TGA	Thermogravimetric Analysis
TEM	Transmission electron microscopy
UCNPs	Upconversion nanoparticles
XRD	X-ray diffraction
HL-60	Human leukemia cell

ÖZET

Doktora Tezi

UPCONVERTING NANOPARTİKÜLLER KULLANILARAK BİYOTEKNOLOJİK ENZİM-İLAÇLAR İÇİN FONKSİYONEL TAŞIYICI SİSTEMLERİN GELİŞTİRİLMESİ

Samir Abaas Ali NOMA

İnönü Üniversitesi
Fen Bilimleri Enstitüsü
Kimya Bölümü

178 + XVII sayfa

2021

Danışman: Prof. Dr. Burhan ATEŞ

L-Asparaginaz (LASNaz) Akut Lenfeblast Lösemi (ALL) tedavisi için anahtar kemoterapötik ilaçdır. Polietilen glikol (PEG) ile modifiye edilmiş L-ASNaz formu, hastalarda bağışıklık tepkisini en aza indirmek için kullanılmaktadır. Bununla birlikte, bu enzimin kullanımı ve erişilebilirliği, kısa plazma yarı ömrü ve pahalı olması nedeniyle sınırlıdır. Ayrıca enzim immobilizasyonu sonrası meydana gelen enzim aktivitie kayıplarını ortadan kaldıran yeni taşıyıcı sistemlere ihtiyaç mevcuttur. Tez kapsamında klinikte kullanılan en önemli enzim ilaçlardan biri olan L-ASNaz için biyouyumlu ve fonksiyonel uç gruba sahip UCNP'lerin hazırlanması, PEG-L-ASNaz enziminin immobilizasyonu, NIR etkisi ile aktivitesinin tetiklenerek arttırılması ve mekanizmasına yönelik çalışmalar gerçekleştirilmiştir. Ayrıca hazırlanan immobilize sistemin *in vitro* biyouyumluluk özellikleri de belirlenmiştir.

Çalışmada öncelikle 980 nm'de indüklenenen $NaYF_4$:Yb^{3+}, Er^{3+} ve 808 nm'de indüklenenen $NaYF_4$:Nd^{3+}, Yb^{3+}, Er^{3+} UCNP'leri hidrotermal yöntemle sentezlenmiş ve yapısal ve termal karakterizasyonları sırasıyla XRD, DLS, Zeta-metre, TEM, FTIR, TGA, XPS ve floresans spektrometresi ile belirlenmiştir. PEG-L-ASNaz enziminin immobilizasyonu, PEI, GPTMS ve ICPTES ile modifiye nanopartiküller üzerinde fiziksel (elektrostatik) ve kimyasal (kovalent) yöntemler kullanılarak gerçekleştirilmiştir. Daha sonra, enzim içeren taşıyıcı platformlar için NIR tetikleme parametreleri olarak lazer yoğunluğu, maruz kalma süresi ve mesafe çalışmaları gerçekleştirilmiştir. İmmobilizasyon parametreleri (immobilizasyon verimliliği, optimum pH, sıcaklık, termal stabilite, yeniden kullanılabilirlik, *in vitro* yarılanma ömrü, depolama stabilitesi, tripsin sindirimi vb.) detaylı olarak incelenmiş ve serbest enzimle karşılaştırılmıştır. UCNP'ler ve UCNP-PEG-L-ASNazlar için *in vitro* toksisite çalışmaları, L-929 hücre hattı üzerinde gerçekleştirilmiştir.

Sonuç olarak PEG-L-ASNaz, bu tez kapsamında ilk kez 980 ve 808 nm'de indüklenebilen UCNP'lere immobilize edilmiş ve enzimin NIR ile indüklenebileceği gösterilmiştir. NIR ile L-ASNaz enzim aktivitesinin indüksiyon oranlarında yaklaşık % 547'ye ulaşılarak mevcut sistemlerden daha iyi bir taşıyıcı sistem ($NaYF_4$: Nd^{3+}, Yb^{3+}, Er^{3+}/ICPTES) geliştirilmiştir. Ek olarak, bu taşıyıcı sistemin insanlar için toksik olmaması nedeniyle biyoteknolojik enzim ilaçları için umut verici bir sistem gibi görünmektedir.

Anahtar Kelimeler: L-asparaginaz, UCNP, NIR, Enzim immobilizasyonu, Enzim-ilaç.

ABSTRACT

Ph.D. Thesis

Development of Functional Carrier Systems for Biotechnological Enzyme Drugs by Using Upconverting Nanoparticles

Samir Abaas Ali NOMA

Inonu University
Graduate School of Natural and Applied Sciences
Chemistry Department

178 + XVII pages

2021

Supervisor: Prof. Dr. Burhan ATEŞ

L-Asparaginase (LASNase) is the key chemotherapeutic drug for the treatment of Acute Lymphatic Leukemia (ALL). The L-ASNase form modified with polyethylene glycol (PEG) is used to minimize the immune response in patients. However, the use and accessibility of this enzyme are limited due to its short plasma half-life and expensive. In addition, there is a need for new carrier systems that eliminate the loss of enzyme activity after enzyme immobilization. Within the scope of the thesis, for L-ASNase, one of the most important enzyme drugs used in the clinic, the preparation of biocompatible and functional end group UCNPs immobilization of the PEG-L-ASNase enzyme, triggering its activity by NIR effect and its mechanism was carried out. In addition, the *in vitro* biocompatibility properties of the prepared immobilized system were determined.

In this study, $NaYF_4$: Yb^{3+}, Er^{3+} induced at 980 nm and $NaYF_4$: Nd^{3+} Yb^{3+}, Er^{3+}, induced at 808 nm UCNPs were firstly synthesized by hydrothermal method, and their structural and thermal characterizations were performed with XRD, DLS, Zeta-meter, TEM, FTIR, TGA, XPS and fluorescence spectrometry. Immobilization of PEG-L-ASNase on UCNP modified with PEI, GPTMS, and ICPTES was carried out using physical (electrostatic) and chemical (covalent) methods. Later intensity, exposure time, and laser distance studies were performed as NIR triggering parameters for carrier platforms containing enzymes. Immobilization parameters (immobilization efficiency, optimum pH, temperature, thermal stability, reusability, *in vitro* half-life, storage stability, trypsin digestion, etc.) were examined in detail and compared with the free enzyme. *In vitro* toxicity studies for UCNPs and UCNP-PEG-L-ASNases were performed on the L-929 cell line.

In the conclusion, PEG-L-ASNaz was immobilized to UCNPs that can be induced at 980 and 808 nm for the first time within the scope of this thesis, and it has been shown that the enzyme can be induced by NIR. A better carrier system ($NaYF_4$:Nd^{3+}, Yb^{3+}, Er^{3+}/ICPTES) than existing systems has been developed by reaching approximately 547 % in the induction rates of L-ASNase enzyme activity with NIR. In addition, the fact that this carrier system appears to be a promising system for biotechnological enzyme drugs due to no toxic to humans.

Key Words: L-asparaginase, UCNP, NIR, Enzyme immobilization, Enzyme-drug.

1. INTRODUCTION

The development of drug delivery systems requires a number of scientific instruments and a specific disciplinary approach. One clear example for the creation of drug delivery mechanisms is based on many specific pharmaceutical approaches, notably; bioconjugate chemistry and molecular biology in accordance to the regulation of pharmacokinetics, pharmacodynamics, immunogenicity, toxicity, bio-information, and drug effectivity. Moreover, a broad range of drug delivery and targeting mechanisms in mitigating drug degradation and declines are currently under development to prevent adverse side effects as well as improving the bioavailability of medications and fractions of drugs that are stored at the desired site.

A number of enzymes have been utilized as a medicament in the treatment of metabolic diseases. The common feature of medicinal enzyme treatment is the scavenging of substrates which present in the human blood circulatory system. The catalytic activity and *in vivo* half-life of the enzyme drugs significantly affect the accomplishment of the treatment. In contrast, since most of these drugs are biotechnological products, a sophisticated and expensive manufacturing process takes place. As well as high dose administration leads to serious side effects among patients. It is widely noted that both diminishing the side effects of these clinical enzymes and increasing the half-life *in vivo* immobilization are crucial. However, the obstacle of the immobilization process is the reduction of the catalytic activity of the enzyme. Hence, innovative approaches are required to increase the catalytic activity of immobilized enzyme drugs. In several references, it has been implied that the increase of enzymatic activity relies on platform inducement by UV light or magnetic fields which is also toxic and limited access into internal tissue. Moreover, NIR excitation potentially becomes an important alternative in this area with low toxicity and higher accessibility to internal tissues.

NIR has extensive applications in the medical field such as imaging, controlled drug release, and photodynamic therapy. However, the NIR has not previously been tested to increase the catalytic activity of the enzyme drugs. The aim of this research is to construct the bond between enzyme and upconverting nanoparticles (UCNP), which relies on the conformation molding between substrate and enzyme active center due to NIR radiation in a certain wavelength. Subsequently, recovery of products from the active center with simultaneous increase of catalytic activity will take place by the

mechanism of Förster Resonance Energy Transfer (FRET). Apart from this, NIR light emits heat so that it does not damage the healthy cells in the region, thus, it can be easily applied to the patient.

Recently, scientists and private companies have been conducting wide and detailed research in the field of drug delivery systems. By including these drugs, L-ASNase has been chosen as a suitable enzyme-drug due to L-ASNase is can not found in all human tissue and have an anti-cancer effect in the circulatory system. L-ASNase is used as the primary chemotherapeutic agent in the therapy of remission induction, which is the initial stage of Acute Lymphoblastic Leukemia (ALL), as well as the therapy of subsequent pathogenesis of the disease. L-ASNase is usually administered to patients by intravenous injection 2-3 times a week. On the other hand, L-ASNase modified with polyethylene glycol (PEG) is applied to reduce the immune response that occurs during administration. Nevertheless, its use and accessibility are limited due to organ damage caused by the side effects of the enzyme and the short half-life of the plasma enzyme-drug. Also, a continuous injection during the chemotherapy process and dependence on the hospital triggers psychological depression in patients. Consequently, it is crucial to solving the encountered issue of disease treatment by emphasizing in children and adults as well as creating new approaches.

UCNPs transform NIR light to UV or visible light in UCNP-assisted photochemistry. Simultaneously, $NaYF_4$: Yb/Tm UCNPs ($NaYF_4$-host doped by Yb^{3+} and Tm^{3+}) and $NaYF_4$: Yb/Er ($NaYF_4$-host doped with Yb^{3+} and Er^{3+}) UCNPs are two common types UCNPs. One clear example, Yb^{3+} is the sensitizer for these UCNPs to harvest NIR light and transfers energy to Tm^{3+} or Er^{3+}. The transmission of energy from Yb^{3+} to Tm^{3+} or Er^{3+} will take place many times so that Tm^{3+} or Er^{3+} can be excited. Meanwhile, Tm^{3+} is an emitter of UV/blue; while Er^{3+} an emitter of green/red.

In this thesis, the well-dispersed biocompatible UCNPs in an aqueous solution having functional end groups have been prepared to immobilize the L-ASNase for the first time. Studies on the mechanism of triggering and increase the activity of the immobilized PEG-L-ASNase by NIR light effect have been performed. In the scope of this thesis, firstly, $NaYF_4$, Yb^{3+}, Er^{3+} (induced at 980 nm) and $NaYF_4$, Yb^{3+}, Er^{3+}, Nd^{3+} (excited at 800 nm) UCNP's have been synthesized via hydrothermal method. For physical (electrostatic) immobilization of the PEG-L-ASNase, UCNPs were functionalized with PEI, while for chemical (covalent) immobilization of the PEG-L-ASNase, UCNP were modified with ICPTES and GPTMS having the optimum

properties (particle size, surface area, radiation properties, etc.). The surface morphology, crystal phase, functional groups, thermal properties, and photophysical properties of the synthesized UCNPs were characterized by TEM, XRD, FTIR, XPS, TGA, and fluorescence spectrometry, respectively. In addition, the parameters affecting enzyme immobilization such as particle size distribution, zeta potential, and DLS.

In the following stage, UCNP-PEG-L-ASNases were prepared with the physically and chemically immobilization of PEG-L-ASNase on functionalized UCNPs. Firstly, NIR triggers parameters such as laser intensity and expose time studies were performed for carrier platforms containing enzymes. Meanwhile, the comparison and detail measurement between free and immobilized enzymes were carried out for a number of immobilization parameters such as immobilization efficiency, optimum pH, temperature, thermal stability, reusability, *in vitro* half-life, storage stability, and trypsin digestion. Adsorption and diffusion models for UCNP-PEG-L-ASNases were carried out to reveal the mechanism of NIR excitation. *In vitro* toxicity studies for UCNPs and UCNP-PEG-L-ASNases were performed on the L-929 mouse fibroblast cell line. UCNP and UCNP-PEG-L-ASNase subjected to stability and plasma coagulation.

The outcome of this thesis, a novel carrier platform was designed for PEG-L-ASNase enzyme-based drugs, which improve their stability and usability against. In addition, this enzyme drug is currently utilized for the treatment of metabolic diseases. The catalytic activity of this enzyme increased by the appropriate NIR excitation and maximum bioavailability is provided from the enzymes. This way can be providing added value by reducing the treatment cost. Therefore, this methodology could lead to the development of similar approaches to other enzymes.

2. THEORETICAL INVESTIGATION

2.1. L-Asparaginase

L-ASNase (EC 3.5.1.1) is a type of enzyme that plays a significant role in chemotherapeutic agents for the treatment of ALL since the 1970s [1], and other types of hematopoietic cancer. L-ASNase is an essential chemotherapeutic agent due to the ability to hydrolyze of L-Asparagine (L-Asn) amino acid to L-aspartic acid (L-Asp) and ammonia. It is widely recognized that L-Asn roles as the substrate of protein synthesis in both normal cells as well as leukemic cells as its dependents on the bloodstream supply of L-Asn. However, L-ASNase diminishes L-Asns in the bloodstream which prevents utilization by leukemic cells. This leads to famine and subsequent death of the malignant lymphoid cells [2].

L-ASNase for clinical purposes is purified from *E. coli* or E. *chrysanthemi*, with a quaternary molecular weight distribution of 136 320 Da 140 320 Da respectively [3,4]. In clinical practice, there are currently three types of L-ASNase. Two of these enzymes are derived from *Escherichia coli* (native), whereas a third L-ASNase is derived from *E. chrysanthemi* [5]. *E.coli* L-ASNase is used as the first-line for the treatment of ALL, although *E. chrysanthemi* L-ASNase is used as second due to the highest treatment of hypersensitivity to the first type [6].

In the early fifties, L-ASNase was discovered by Kidd, and he was reported that the anti-tumor activity of serum guinea pig (Ginepig) against murine lymphoma. The serum of guinea pig is capable of halting the development of murine lymphoma. During this procedure, the mouse was grown with lymphoma cells and they received repeated intraperitoneal doses with normal guinea pig serum. This procedure culminated in the lymphoma retreat and existence of treated the mouse, while the control mouse eventually developed lymphoma and died within 20-30 days [7]. However, Clementi, in his study serum guinea pig-rich exporter of L-ASNase and have anti-lymphoma efficiency. At the beginning of the sixties, lymphoma cells from serum guinea pigs were grown in a cell culture medium free from L-Asn amino acid. This austerity of L-Asn amino acid reduced the population of cells, but some cells endure and survived and started to redouble. Hence, it declared that L-ASNase in serum guinea pigs shows anticancer activity [8]. The cytotoxicity of serum guinea pigs was later reported by Broome, as being due to a high L-ASNase level in the serum blood.

The theory behind cytotoxicity effect it's based on, leukemia cells cannot synthesize L-Asns, that leukemia cells have a disability to synthesize proteins and depended on external donations including blood plasma and tissues. The rule of the L-ASNase enzyme breaks down the accumulated free exporter of L-Asn, which leads to starving and killing cancer cells [9]. The first L-ASNase clinical research was made by Dolowy, L-ASNase have efficacy chemotherapeutic agent [10]. Tallal et al., 1970, mentioned that L-ASNase was capable of handling solid tumors together with lymphatic cancers in children [11]. After a period of time, the toxicity, pharmacology, and resistance mechanism of L-ASNase which implicated immunological clearance were investigated by McCredie [12]. From the start of L-ASNase discovery, L-ASNase still has a serious material for researchers who examine microbial sources that are cheap or easily accessible for the purification of the enzyme with relative ease. In the ALL treatment, formulations of L-ASNase have been utilized for a long time, but these formulations cause undesirable reactions. Therefore, researching alternative sources of this enzyme that will not cause side effects or developing formulations is an important area for researchers.

2.1.1. Structure of L-ASNase

In 1976, Murthy and Knox performed small-angle X-ray scattering studies on *E. coli* L-ASNase solutions. Which the structure was recognized as a tetramer. In contrast purification from various sources founded certain alterations for example monomeric, dimeric and hexameric. Meanwhile, most bacterial L-ASNase exhibits quaternary and tertiary structures [13]. In the various researches, it has been focused on two types of bacterial L-ASNase structure, notably *E. coli* and *Erwinia sp.* due to it has identical three-dimensional structures as well as both demonstrated details of the structure [14]. In accordance to X-ray crystallographic data, the L-ASNase enzyme that was purified from *E. coli* is a tetrameric protein and widely used for clinical purposes. The molecular formula for L-ASNase is $C_{1377}H_{2208}N_{382}O_{442}S_{17}$ and an average molecular weight of 35.6 kDa for each identical subunit. [15]. In a study of Maita et al., elected the Edman degradation to determine the amino acid sequence of L-ASNase [16]. In the 1980 Illarionova et al., characterize the L-ASNase secondary structure of *E. coli* in a broad range of pH [17]. The structure of L-ASNase from *E. coli* was also described by Swain et al. that reported two areas as well as the identification of active site

between N and C terminals [15]. Nevertheless, Lubkowski et al they found the insignificant L–ASNase difference of amino acid structure between bacterial and *Wolinella succinogenes* during the characterization of tertiary structure and amino acid classification [18]. In 2001, Aghaiypour et al., described Thr15 and Try29 residues play a substantial role in the catalytic activity of L-ASNase in bacteria [19]. In the collection of 327 amino acids in two monomers it was found that 14 α-strands, and β-helix and two domains, a large N-terminal domain and a small C-terminal domain [20]. The active site is existing between two adjacent monomers (A and C: B and D). Each active site is generated by the transport of amino acids in two adjacent monomers. The amino acids in the active center are Thr15, Tyr29, Ser62, Glu63, Thr95, Asp96, Ala120, and Lys168, and the adjacent monomer contains only one residual Ser254 [21,22]. In which, Thr15 and Thr95 are residues accountable for the enzyme catalytic activity. Enzyme originating from *E. carotovora* formed with two tetramers (ABCD and EFGH), each consisting of four identical monomers (A to H) (Figure 2.1).

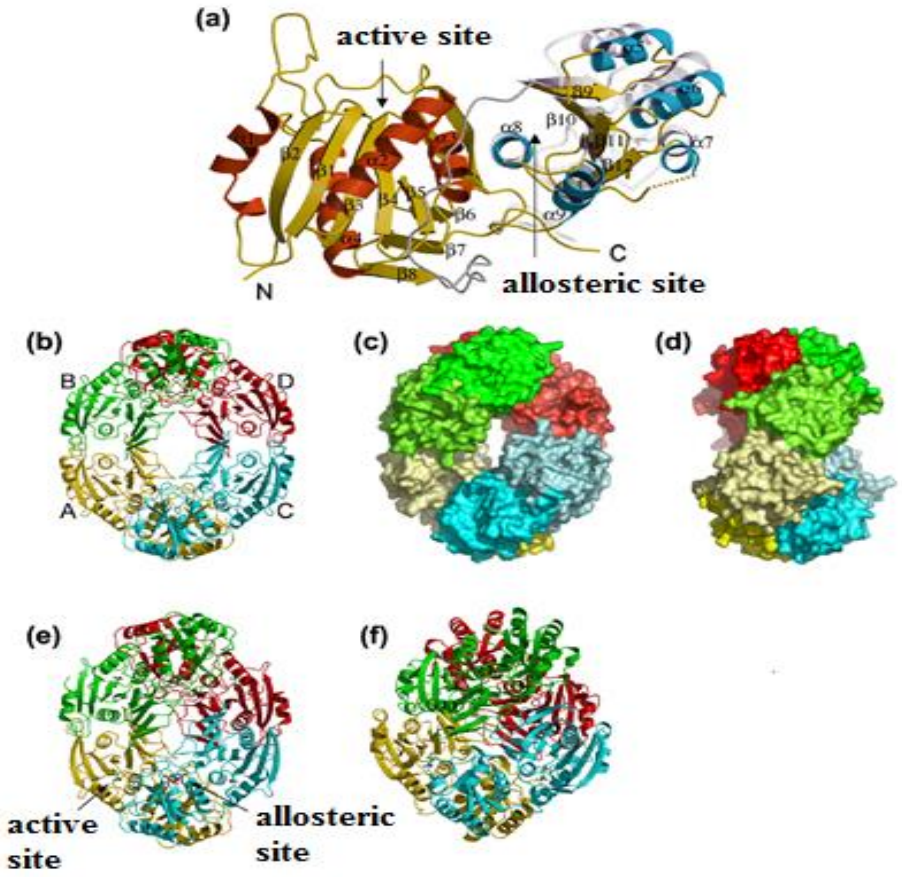

Figure 2.1: A strip display of the monomer of E. coli L-ASNase, showing secondary structural elements [23].

2.1.2. The action mechanism of L-ASNase

Owing to the hydrolysis reaction of L-ASNase, it is a major drug used for the treatment of hemopoietic illness such as ALL in children. ALL is the most common acute leukemia in child nearly 80 % of childhood leukemia and 20 % of adult leukemia. The antineoplastic activity of L-ASNase is according to the efflux of L-Asn, which leads to ceasing protein synthesis in leukemia cells. L-Asn amino acid is required for both normal (healthy) and leukemic cells for protein synthesis and metabolic needs [24]. L-Asn can be synthesized in healthy cells due to the availability of L-Asparagine synthetase and transaminase enzymes in healthy cells. L-aspartate can be synthesis from oxaloacetate by transaminase enzyme as an intermediate, the synthesized L-Asn from the glutamate to the oxaloacetate lead to generated aspartate and α-ketoglutarate. Ultimately, the healthy cells transform L-Asp to L-Asn by using the asparagine syntheses enzyme. L-ASNase synthetase is not found in neoplastic cells, in which the L-Asn synthesis incapability drives the amino acid intake from external sources notably blood circulation for the life and reproduction of neoplastic cells. Injection of the L-ASNase into blood circulation led to breaks of L-Asn amino acid, which result in the famine of cancer cells and subsequent cell death.

The process of hydrolysis mechanism of L-Asn by L-ASNase takes place in two steps with the formation of the intermediate product of *β*-acyl-enzyme (Figure 2.2). In the first step of the mechanism, (NH_2) strong base activated the nucleophilic residue of the enzyme and hence attacking the amide C atom of L-Asn, thus cause of *β*-acyl-enzyme product as an intermediate product. In the second step, attacking the R-C=O ester carbon by nucleophile activated by an H_2O molecule. And finally, products are Asp and NH_3. This mechanism is similar to serine-proteases because the activities rely on amino acid groups classified as catalytic threesomes. These catalytic triumvirates are formed by a nucleophilic amino acid such as His, Ser, Asp, base, and an acid characteristic amino acid, all bound by hydrogen bonds. There are other reactions catalyzed by L-ASNase, L-ASNase produced by *Serratia marcescens* can hydrolysis L-glutamine (L-Glu) compared to L-Asn. L-Glu is a competitive inhibitor of L-Asn, because of similarity in their structure. Moreover, L-ASNase can hydrolyze the *β*-aspartyl peptide amide bond, with the insufficient quantity of reaction [25].

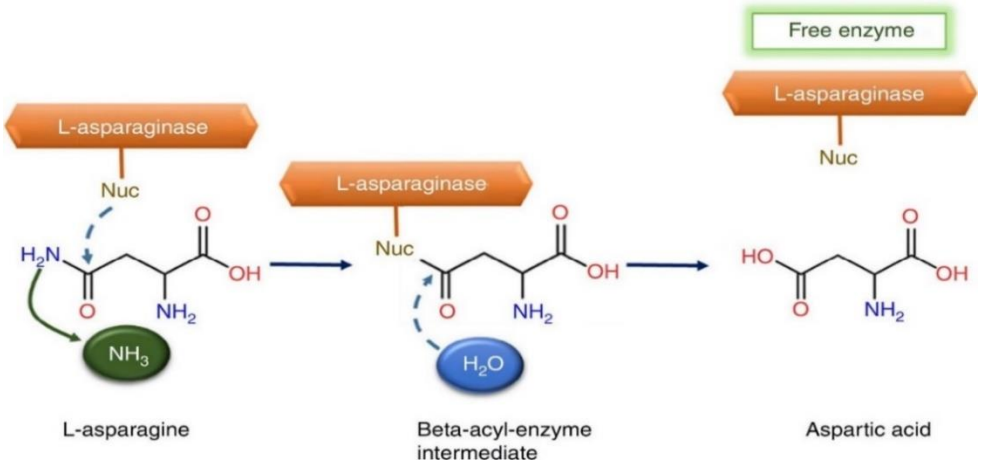

Figure 2.2: The general reaction mechanism of hydrolysis L-ASNase enzyme [26].

2.1.3. Sources of L-ASNase

L-ASNase is widely purified from diverse sources of organisms, animals, plants, and microorganisms except for humans. L-ASNase has high yields and easy isolate in microorganisms such as bacteria, fungi, yeasts, and actinomycetes that make attention for many researchers.

2.1.3.1. Bacteria sources

One clear example, a number of enzymes that have been isolated from bacterial have commercial purpose is widely distinguishable and investigated for the multilateral effects such as enhanced temperature and pH probability apply to the largest environments in which these bacteria live. L-ASNase can be isolated from (Gram + and Gram -) bacteria species in a terrestrial and nautical environment. L-ASNase obtained from Gram-negative and Gram-positive bacteria from the past to currently shown in (Table 2.1).

Table 2.1: The sources of L-ASNase from Gram-positive and Gram-negative bacteria.

Gram-positive	Reference	Gram-negative	Reference
Mycobacterium phlei	[27]	*Proteus vulgaris*	[42]
Bacillus mesentericus	[28]	*Citrobacter species*	[43]
Staphylococcus species	[29]	*Acinetobacter calcoaceticus*	[44]
Bacillus polymyxa	[30]	*Vibrio succinogenes*	[45]
Bacillus licheniformis	[31]	*Escherichia coli*	[46]
Staphylococcus aureus	[32]	*Thermus aquaticus*	[47]
Bacillus species	[33]	*Erwinia cartovora*	[48]
Bacillus subtilis	[34]	*Erwinia chrysanthemi*	[49]
Mycobacterium bovis	[35]	*Pseudomonas stutzeri*	[50]
Bacillus circulans MTCC8574	[36]	*Helicobacter pylori*	[51]
Bacillus circulans	[37]	*Enterobacter cloacae*	[52]
Corynebacterium glutamicum	[38]	*Thermus thermophiles*	[53]
Streptomyces gulbargensis	[39]	*Serratia marcescens*	[54]
Staphylococcus epidermidis	[40]	*Pseudomonas aeruginosa*	[55]
Paenibacillus barengoltzii,	[41]	*Acinetobacter baumannii*	[56]

2.1.3.2. Fungal sources

Fungi is an alternative source of L-ASNase as the bacterial have broad side effects. In addition, fungal L-ASNase indicates closer phylogeny to human L-ASNase rather than bacterial counterparts. As a result of easier purification of fungal L-ASNase, it has gained a major important source. The fungal sources of L-ASNase from the past to current were listed in (Table 2.2).

Table 2.2: The sources of L-ASNase from Fungi.

Fungi	Reference	Fungi	Reference
Fusarium roseum	[57]	*Penicillium notatum,*	[64]
Cylidrocapron obtusisporum	[58]	*Fusarium oxysporum*	[65]
Mucor Species	[59]	*Beauveria bassiana*	[66]
Aspergillus tamarii	[60]	*Taxomyces andreanae*	[67]
Aspergillus niger	[61]	*Fusarium culmorum ASP-87*	[68]
Aspergillus oryzae	[62]	*Fusarium equiseti*	[69]
Helminthosporium (RF3)	[63]	*Aspergillus fumigatus*	[70]

2.1.3.3. Yeast sources

Apart from bacterial and fungal, yeast is a source of L-ASNase in which its isolation is less detrimental than other sources. The list of yeast L-ASNase from past to current is shown in Table (Table 2.3).

Table 2.3: The sources of L-ASNase from Yeast.

Yeast	Reference	Yeast	Reference
Fusarium roseum	[71]	*Mucor Species*	[78]
Saccharomyces cerevisiae	[72]	*Aspergillus tamarii*	[79]
Pichia polymorpha	[73]	*Aspergillus niger*	[80]
Aspergillus nidulans	[74]	*Aspergillus oryzae*	[81]
Cylidrocapron obtusisporum	[75]	*Candida bombicola*	[82]
candida utilis	[76]	*Alternaria species*	[83]
Rhodosporidium toruloides	[77]	*Candida guilliermondii*	[84]

2.1.3.4. Actinomycete sources

Actinomycetes are an alternative source for L-ASNase isolation. Owing to its considerable distribution in nature, water, and soil. L-ASNase that can be isolated from fish-dwelling with high activity. Furthermore, actinomycetes are a preferable exporter of L-ASNase rather than bacteria and fungi, L-ASNase isolates from actinomycetes from earlier to nowadays show in (Table 2.4).

Table 2.4: The sources of L-ASNase from Actinomycete.

Actinomycete	Reference	Actinomycete	Reference
Streptomyces griseus	[85]	*Streptomyces albidoflavus*	[90]
Streptomyces collinus	[86]	*Actinomyces species*	[91]
Thermoactinomyces vulgaris	[87]	*Streptomyces albidoflavus*	[92]
Streptomyces plicatus	[88]	*Streptomyces tendae*	[93]
S. longsporus flavus	[89]	*Nocardia species*	[94]

2.1.4. L-ASNase application as cancer therapy

L-ASNase has widely been implemented as a chemotherapeutic agent for ALL disease treatments such as Hodgkin's disease, acute myelocytic leukemia, chronic lymphocytic leukemia, and lymphosarcoma [95]. L-Asn is an important amino acid for several tumor cells used to synthesize proteins and cell growth. However, the main principle of L-ASNase is to converting the L-Asn to L-Asp, in which the existence of L-ASNase prevents the nutrition intake of the cancer cell which inhibits its development by leading to asparagine deficiency and subsequent death of tumor cells. The representation of the chemotherapeutic effect of L-ASNase in cancer cells is shown in (Figure 2.3). On the other hand, in the foodstuffs industry, L-ASNose also has a significant function to resolve the issue of undesired acrylamide production, which is a carcinogenic agent in certain food products such as potato chips, etc.

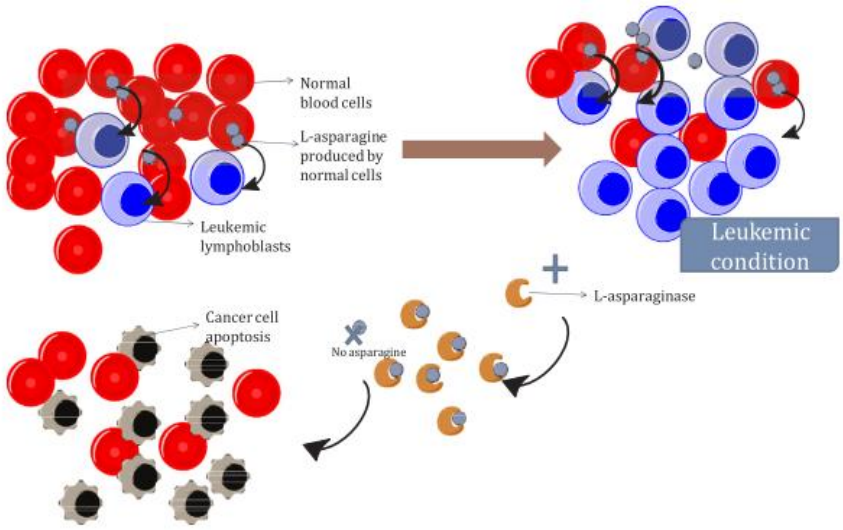

Figure 2.3: Schematic representation L-ASNase cytotoxicity in cancer cells [96].

2.1.5. L-ASNase side effects

2.1.5.1. Some aspect of the impact of L-ASNase as an enzyme drug

In spite of, its antileukemic properties, L-ASNase treatment of ALL induces certain side effects such as allergic (edema), vomiting, fever, rash in the skin, dysfunction of the liver, diabetes, pancreatitis, leukopenia, and hemorrhage may occur after L-ASNase utilize [97]. In addition, Radulovic et al. reported that neutropenic enterocolitis (NE) has been detected as an uncommon acute complication of

neutropenia, relate to leukemia and lymphoma [98]. Moreover, Chen and his group observed that patients with ALL treatment suffer from urethral obstruction due to L-ASNase utilization [99]. Furthermore, Moola et al. mention that hypersensitive, mild allergic, and anaphylactic shock were observed after treatment from ALL by L-ASNase drug application [100]. On the other hand, Pochedly mentioned in his study that teenagers have a higher possibility of neurotoxicity caused by L-ASNase, which results in fatigue, depression, drowsiness, agitation, and dizziness [101].

2.1.5.2. Coagulation disorder

A diversity of abnormality-associated coagulation is also probably driven by L-ASNase due to deficiency of serine protease enzyme which encompasses antithrombin and aα1 antitrypsin. The occurrence of such impediments has been reported as 2.1–15% for free L-ASNase and 1.1–4% for PEG-L-ASNase [102]. Meanwhile, several previous types of research have determined the harmonic alteration in the anti-thrombin molecule that comes from L-ASNase may diminish enzyme activity and protein aggregate formation in endoplasmic reticulum cisterns [103]. In addition, L-ASNase therapy maybe leads to a decrease in protein C and S levels, while rising the level of thrombin, which symptoms as bleeding and thrombosis risk [104]. Inclusively, 15-65% of patients will be at risk to suffer from hypofibrinogenemia in the later time of L-ASNase therapy.

2.1.5.3. Hypersensitivity

A number of immunological reactions take place after injection of bacterial proteins for example erythema transitory, urticaria rash localized, respiratory distress, and acute life-threatening anaphylaxis. These hypersensitive side effects are probably due to serum illness, extremities itching and swelling, hypersensitive reactions, anaphylaxis, urticaria, edema, and other clinically relevant reactions. In addition, L-ASNase therapy inflicts liver dysfunction, organ poisoning, pancreatitis ketoacidosis, and associated hyperglycemia, glucosuria, and cerebral dysfunction, reduce the protein synthesis, hypofibrinogenemia, hypercoagulable state-coagulopathy [105]. Hypersensitivity reactions have been detected in almost 60 % of patients during *E. coli* L-ASNase therapy. Even polyethylene glycol-L-ASNase derived from *E. coli* has been

reported to cause hypersensitive reactions [106]. Therefore, the research of alternative forms of L-ASNase is crucial because of these disadvantages.

2.1.5.4. Pancreatitis, hyperglycemia, hepatotoxicity

Despite the cause behind the negative side effects of the L-ASNase enzyme drug is not well defined yet, it is assumed or hypothesized that L-ASNase probably leads to disorder in protein synthesis. After L-ASNase therapy several side effects appear such as liver toxicity, reduce hepatic protein synthesis, glutamine deficiency, oxidative stress, and beta-oxidation impairment in the mitochondria have been reported [107,108]. In addition, L-ASNase therapy potentially rise the levels of amylase and lipase in pancreatic in which L-Asn regulates the reduction of these enzymes. The deficiency of L-Asn, enzymes leads to serious complications in the pancreas [109]. Notably, the increase of diabetes risk which consequently the deficiency in insulin synthesis by affecting both endocrine (insulin-secreting) and pancreatic exocrine (digestive enzyme secreting) cells. A broad range of drawbacks is overcoming by immobilization which is defined as the addition of natural enzyme of the solid carrier as well as diminishing its mobility. Because of immobilization, the lifetime of the enzyme is increased compared to the free enzyme and shows higher stability against allergic reactions. Up to now, L-ASNase has been immobilized on many natural, synthetic, and hybrid carrier matrices using various chemical/physical methods.

2.1.6. The L-ASNase formulations use in the treatment

Apart from mammals, L-ASNase is found in a broad range of living creatures such as birds, plants, bacteria, and fungi. Moreover, not all L-ASNase possess the capability for ALL treatment, there are only two forms of L-ASNase which has been widely implemented in medical fields; the first one is from *E. coli*, while the second one from *E. chrysanthemi*, and their subalterns. In the USA, three L-ASNase formulations are commonly used to treat ALL (Table 2.5). These; natural E. coli ASNase (Elspar®; Merck & Co., Inc., West Point, PA, USA), Pegylated form of L-ASNase Oncaspar® (Enzon, Inc. Bridgewater, NJ, USA) and *Erwinia chrysanthemi* (Ipsen-Speywood Pharmaceuticals Ltd, UK), the name of the product is Erwinase®.

The second formulation L-ASNase is advisable in the UK as second-line therapy in patients with hypersensitivity to the previous two models. These natural L-ASNase

combinations are available under various trademark names; In Europe and Asia, Medac® (Kyowa Hakko, Kogyo, Japan), Crasnitin® (Bayer AG, Leverkusen, Germany), Leunase® (Sanofi-Aventis, Paris, France) Paronal® and Kidrolase®, etc. However, some of these are no longer available and are only available in the literature (Table 2.8) [106].

Table 2.5: Three common forms of L-ASNase with frequently administered doses.

Formulation	Elimination Half life	Dosage
Natural E. coli ASNase	26 – 30 hours	6000 IU/m2 three times / week
PEG- ASNase	5.5 – 7 days	2000 – 2500 IU/m2 every 2 or 4 weeks
Erwinia ASNase	16 hours	6000 IU/m2 daily × ten doses, then three doses weekly, or 30000 IU/m2 daily × ten doses in induction

Table 2.6: L-ASNase formulations used as therapy in different countries.

Region	First Line	Second Line
North America, UK, Australia, New Zealand	E. coli- ASNase or PEG- ASNase	Erwinia ASNase or PEG- ASNase
Europe	E. coli- ASNase or PEG- ASNase	Erwinia ASNase
Other Countries	E. coli- ASNase	Erwinia ASNase or PEG- ASNase

Currently, PEGylation (Figure 2.4) is the most efficient strategy is the covalent binding of L-ASNase with polyethylene-glycol (PEG), which increases the life cycle of many therapeutic agents and reduces their immunogenicity and antigenicity. Owing to the principle the L-ASNase isolated from *E. coli* is modified covalently with monomethoxypolyethylene glycol (mPEG), represented pharmacokinetic alterations rather than free L-ASNase counterpart [110]. The simultaneous rise of molecular dimension and inhibition of steric hindrance is lead by the protein enzyme coating of PEG. Meanwhile of PEG-ASNase resemble the native L-ASNase from *E. coli* (optimum temperature: 50 °C, pH maximum: 7.0, isoelectric: 5.0) [111]. One clear example Oncaspar® is widely utilized as a PEG-L-ASNase formulation from *E.coli* in most countries meanwhile slight difference is also found in the similar formulation in other countries. The PEG-ASNase from *E. coli* produced by Merck, Sharp, and Dohme is produced in the USA by Sigma-Tau and marketed as Oncaspar®, while it is obtained from the Kyowa Hakko natural ASNase protein in Europe [112]. PEG-ASNase has 5

times half-life longer than *E. coli* and 9 times longer than that formulation of *Erwinia*. This longer half-life the number of injections needed to maintain treatment effectiveness in patients and increases the level of treatment significantly [113].

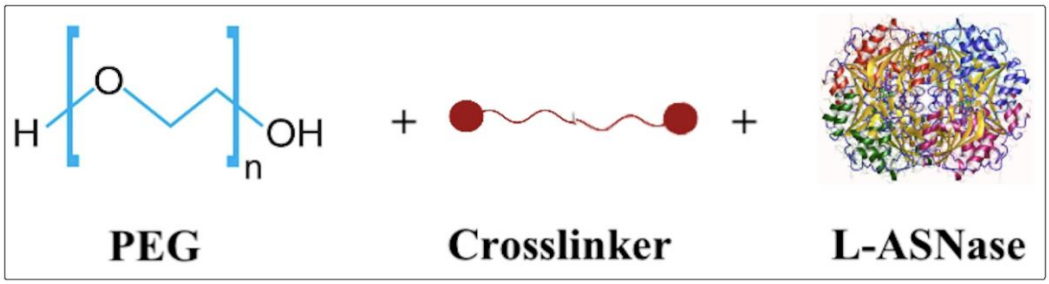

Figure 2.4: Image of the L-ASNase PEGylating process.

2.2. Enzyme Immobilization

Owing to the main feature of catalyst which accelerates the reaction and diminishes activation energy, it is noted that enzyme is biocatalyst in certain biochemical processes with a specific substrate. In addition, enzymes can work only under very mild conditions such as pH and temperature it must be in aqueous solutions. The transformation of a substrate (S) into the target product (P) takes place at the enzyme active site (E), which is composed of a number of specific amino acid residues that regulate binding to the substrate molecule [114]. Enzymes reduce the activation energy ($\Delta G^{\ddagger}$) and simultaneously increase the reaction rate. The activation energy is a variation between the ground state energy levels and the transition state of the substrate. Working with enzymes at optimum pH and temperature, lead the enzyme to reach the highest catalytic activity. The pH will affect on the ionization states of amino acids, whereas an ideal collision between enzymes and substrates is influenced by the temperature. Enzymes normally have the ideal temperature at 37 °C which is body temperature [115]. High catalytic activity, selectivity, specificity, and biodegradability are the benefits of the enzyme. Nevertheless, enzymes are unable for repeated use which leads to working with enzymes become more expensive.

The immobilization procedures are capable to solve this weakness by principally facilitates an easy recapture of the enzyme, fast termination, and repeated enzyme assay, which leads to a decrease in the expense of enzyme. However, it is exhausted and laborious to extract and recover enzymes after the enzyme reaction processes. Therefore, the separation of enzymes is one of the important goals for immobilization.

Without centrifugation, the separation of the enzyme from support materials can occur with matrices such as magnetic nanoparticles, membranes, and capillary columns. Moreover, good storage stability, pH, and thermal tolerance are normally increased after immobilization. These advantages have led to the wide use of immobilized enzymes in a wide variety of fields including pharmaceutical, food, waste water treatment, textile, and others. In addition, the supportive materials for immobilization procedures are also important for the immobilization enzymes. The carrier such as nanoparticles, neutral polymers, and inorganic materials widely used for immobilization enzymes [116].

2.2.1. Immobilization methods

In accordance to the mode of interaction between enzymes and support carriers, a broad range of approaches is applicable for enzyme immobilization (Figure 2.6) Physical methods can be broadly classified as weak associations that occur between the enzyme and supporting material. In contrast, chemical methods; rely on covalent bonds which are formed between the enzyme and the supporting materials. In particular, several associations in the support of enzymes are utilized for the immobilization of enzymes.

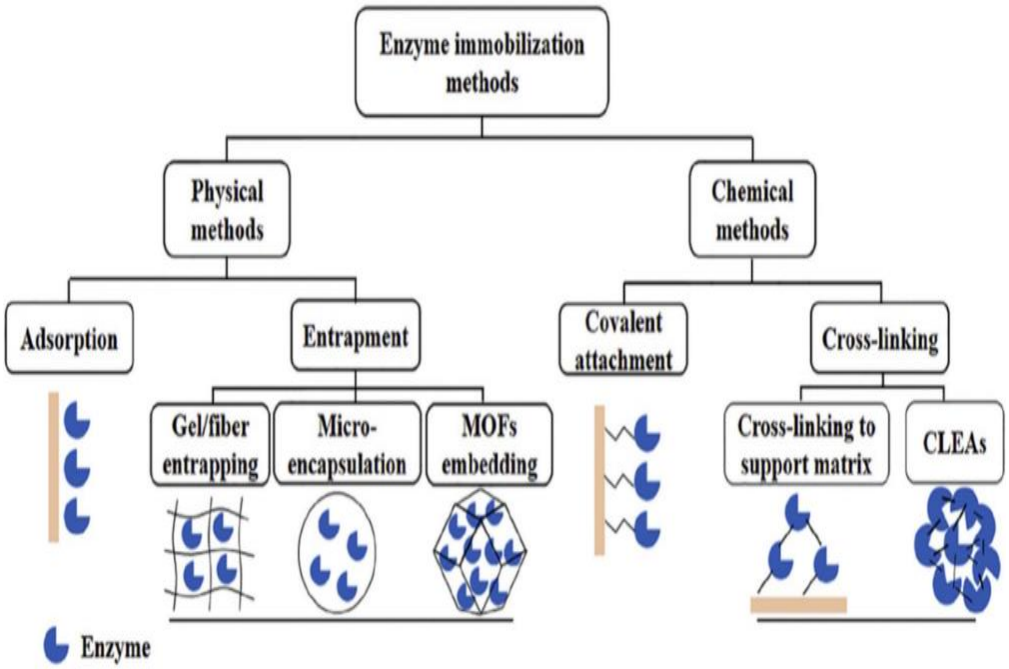

Figure 2.5: The methods for enzyme immobilization [117].

2.2.1.1. Physical methods

In physical methods, there is two main part for enzyme immobilization adsorption and entrapment parts. Adsorption is a simple and functional method of immobilizing enzymes, which involves reversible interactions of the surface between the enzyme and the supportive substance. In addition, a multitude of weak forces are adsorbed between enzymes and the surfaces of support carriers in the adsorption process, for example, hydrogen bond, van der Waals, electrostatic attraction, and /or hydrophobic [118]. Moreover, cation and anion exchange resins, activated carbon, silica gel, alumina, regulated pore, and ceramics are the most common supporters used in this immobilization mode. This process is generally one of the most durable and mostly used in large-scale production. Owing to the absence of chemical activation, the possibility of the enzyme conformational modifications is reduced and quickly carried out with low costs and simply combining them over a certain incubation duration. Additional binding agents and modification steps for the immobilization of enzymes are not needed in this process. Consequently, the activity of the enzyme is usually sustained or enhanced after the immobilization. Besides, the conditions for immobilization are slightly destructive for enzymes and thus their original catalytic processes are retained. Nevertheless, the major weakness is that the interactions between enzyme and supportive carriers are generally weak and reversible, which drives the enzyme to leak out from the support [119, 120].

To diminish the leakage of the enzyme, it is crucial to carry out the selective election of material. Also, the pH control regulates the net surface charges on the enzyme and the matrix. Election of solution pH requires selectivity by involving matrix and isoelectric point (pI) of a specific enzyme which improves the electrostatic forces between enzyme and matrix [121]. The surface areas of the enzyme molecules are able to carry either a positive or negative charge to use electrostatic forces during enzyme immobilization which depends on the comparative distinction between the isoelectric point of enzyme and solution pH. The ionic and highly polar interaction of the enzyme can be immobilized against the oppositely charged carrier matrix. Layer-by-layer deposition (LBL) and electrochemical doping are two important techniques in electrostatic bonding immobilization [122]. Moreover, hydrophobic interactions between support and enzyme molecules are another adsorption immobilization strategy. These hydrophobic associations are regulated by entropy development during

immobilization by the removal of water molecules from the enzyme molecules and carrier matrix [123]. The intensity of interaction relied on the simultaneous hydrophobicity of enzyme and adsorbent. Hence, a number of specific parameters in enzyme immobilization are widely implemented to alter the interaction between enzyme and matrix notably pH, temperature, and ion concentration [124].

A method of physical adsorption is widely implemented to improve the enzymatic biosensors. Owing to the principle, the carrier matrix requires immersion in an enzyme solution and subsequent incubation within a specific period. Overall, this approach has advantages that include simplicity, reusability, and cost-reducing, but it takes a long time. Furthermore, the substrate can block from reaching enzyme active sites because of enzyme cannot be homogeneously immobilized into the carrier matrix [122].

In the entrapment immobilization method, the enzyme is not directly bound to the surface of the carrier matrix. Otherwise, the enzyme is restrictive to a polymer matrix which only is allowing the substrate and products to move out from the model, as well as simultaneously maintains the enzyme activity and prevents the diffusion of enzymes. Although the enzyme is limited physical to the polymers, by the absence of chemically interacting with the polymer. This method of immobilization is achieved in two steps: enzyme blending into a monomer solution and subsequent chemical reaction of polymerizing monomers. It is a potentially realistic solution to prevent enzyme aggregation, by improving enzyme stability as well as reduce leaching, denaturation, and low the cost of the enzyme. Also, the additional benefit of the process is achieved by the optimization of the enzyme's microenvironment which adjusting the encapsulating material to obtain optimum pH, polarity, and amplitude.

However, mass transfer resistance is the major drawback due to the length of the polymerization chain which prevents the substrate from complete accession into the substrate into the enzyme site. One of the major weaknesses of this method is poor immobilization efficiency and the carrier matrix will be broken down due to the effects of polymerization. There are a number of procedures used in entrapment immobilization such as electro-polymerization, photopolymerization, sol-gel processing for mesh or fiber type, and microcapsule type microencapsulation [122]. Various materials such as chitosan, collagen, calcium alginate, cellulose triacetate, polyacrylamide, gelatin, agar, synthetic rubber, polyvinyl alcohol, and polyurethane are applicable for the preparation of the entrapment matrix.

2.2.1.2. Chemical methods

In the chemical strategy, there are two major parts for enzyme immobilization first one is covalent attached and the second one is cross-linker. Covalent immobilization involves the interaction between the enzyme and support substance by a covalent bond. Which usually forms between functional groups that present on the support material and amino acids of enzymes such as lysine, cysteine, aspartic, and glutamic acid residues [125,126]. In addition, amino, carboxyl, imidazole, and phenolic hydroxyl groups are preferable for the formation of covalent bonds [127]. This type of immobilization process is normally carried out in two stages. Activation of support matrix by reagent and binding of the matrix into the enzyme. One of the key advantages of the technique is the stability to preventing enzyme leakage from supporting matrices [128]. However, chemical reactions between enzyme molecules and support matrices will inactivate the enzyme active sites, which leads to a decrease in catalytic activity. The major drawback of this method is a conformational change of the enzyme which is always observed and subsequent partial loss of the activity. However, the covalent binding process can lead to a loss in the flexibility enzyme conformation, which drives the alteration in the activity, particularly if the covalent binding occurs to an essential part or near the active site [129].

Cross-linking immobilization is an irreversible method, which relies on the intersection between enzymes with various cross-linkers via their amino or carboxylic groups. Immobilization of enzymes has been developed by cross-linking the enzyme with covalent bonds, to other molecules of protein or functional groups of insoluble matrixes [130]. Enzymes are tightly immobilized to maximize reusability and stabilization. However, during the cross-linking process, enzymes potentially lose their catalytic activities in which are driven by binding agent reagent. One clear example, glutaraldehyde is the most widely used bifunctional reagents to synthesize cross-linked enzyme aggregates, they are probably related to each other. The active sites of the enzyme are covered and catalytic processes are maintained after aggregation. The micro-environmental modification for the enzyme using suitable stabilizing agents through surface complementarity is another benefit of the procedure, which helps to increase the stability. However, the use of glutaraldehyde drives significant modifications to the enzyme and it could contribute to the conformational alteration of the enzyme which leads to a loss in activity. Hence, the addition of inert

protein particularly gelatin and bovine serum albumin is applicable to reduce the complex alteration of the enzyme during immobilization which reduces the difficulty [131].

2.2.2. Carrier matrices used for enzyme immobilization

It is crucial to employ the supporting matrix as enzyme carriers for the determination of performance and output of immobilization. The following properties should belong in the carrier matrix;

- Economical and eco-friendly.
- Completely inert and not inhibit the catalytic activity after immobilization.
- Resistant to heat and mechanical impact, which facilitates the utilization of immobilized enzyme in various operating conditions.
- Stable.
- Maintain a high degree of reusability for the immobilized enzyme.
- Raise the specificity of the enzyme.
- Allow immobilization of large amounts of enzymes, by relying on porosity plays an important role. In accordance to reducing the surface area of the big pore and preventing protein entry by a small pore, a suitable pore diameter is required. [132].
- Able to shift the optimum pH and target value.
- Antimicrobial properties and non-specific adsorption.

The researcher continues to work to develop and increase the matrix that can be used for immobilized enzymes. Consequently, the importance to find and implement novel materials with the desired properties has recently increased. Organic as well as inorganic materials demonstrate excellent thermal and chemical stability and mechanical characteristics. In addition, these support materials are widely generated in several morphological types, mostly nanoscale, with manageable particle size, making them ideal for use with enzymes. These materials have different functional groups to facilitate enzyme binding and surface modification. Notably, in the last decade, hybrid and composite materials with a variety of advantageous qualities have received more interest. As a result of those needs and properties, new utilized materials in enzyme immobilization are described below.

2.2.2.1. Common materials used for enzyme immobilization

One of the most influential issues is the removal of enzymes from the reaction mixture following catalytic therapy. Which is overcome by coupling the enzyme molecules to external magnetic field magnetic iron oxide nanoparticles (MNP). MNP is a promising material for researchers due to a number of advantages for example ideal magnetic characteristics non-toxicity, small size, large surface, relatively cheap synthesis, biocompatibility, and strong mechanical features. Moreover, MNP has been widely implemented in various fields for examples such as controlled drug delivery [133], biosensors [134], hyperthermia [135], gene therapy [136], and catalysis [137]. One clear example Fe_3O_4 is one of the most common nanoparticles due to its strongest magnetic properties, easy stability, easy functionality, synthesis and separation, low cost, and low toxicity [138]. At the same time, Fe_3O_4 nanoparticles have the potential to encapsulate bioactive molecules such as protein, enzyme, and anti-core or immobilize these molecules. Meanwhile, MNPs are well recognized for their wide surface area and excess of OH groups which make the surface area easy modification and enable strong (covalent) attachment of the enzyme [139]. Enzyme immobilization on magnetic nanoparticles is able to increase enzyme activity due to the high surface area that leads to the higher interaction between the enzyme and the substrate.

Mesoporous is potentially advantageous as enzyme immobilization supports material due to insolubility in water, large surface area, small pore size distribution, well-defined pore geometry, thermal and mechanical stability as well as biocompatibility [140]. In fact, the silica surface is also easily chemically modified easily by different functional groups [141]. Both the stability and enzyme immobilization performance is increased by modifying nanoparticles. One clear example, covalent binding of the encapsulation is the way to immobilized enzymes, which relies on strong dipole-dipole attractions between magnetic nanoparticles that subsequently lead nanoparticles aggregate in an aqueous medium. Furthermore, there are few reactive functional groups of hydroxyl groups on its surface, which may be reacted with other molecules such as enzymes and proteins. These disadvantages probably delay enzyme applications in industrial areas [142]. To overcome these disadvantages nanoparticles modification with various molecules is important techniques such as precious metals [143], carbon [144], SiO_2 [145], MCM-41 [146], and polymers [147]. Carbon nanotube **(**CNTs), improved prospects of immobilization

indicate due to their distinguishing characteristic for example electrical, regular, large surface area, mechanical features, thermal behavior, and strong biocompatibility. Carbon nanotubes are also ideal to enhance their affinity and allow strong enzyme-matrix interactions to grow, due to the improvement of electron transfer between the substrate and immobilized enzyme in comparison with other materials [148]. Graphen (G), which possess two-dimensional (2D) single-atom-thick carbon atom network, has attracted increasing interest in various rapidly emerging fields due to special characteristic such as its high surface area, solid mechanical strength, and extraordinary electrical, thermal and optical characteristics. [149]. Due to the above extraordinary properties, G tends to be an optimal carrier for enzymes immobilizing, because its enormous surface area assists to raise the loading capacity of enzyme and improve the reusability with a desirable mechanical strength. Graphene oxide (GO), is considered an excellent carrier of enzyme immobilization due to its super-high area surface, excellent thermal and mechanical properties. Also, the significant oxygen-containing functional groups of GO are favorable for enzyme immobilization such as carboxyl, epoxy, and hydroxyl. A number of catalytic activities have been observable during GO nano-support enzyme immobilization with various methods while the reduced one (rGO) indicated a deficiency in surface functional groups.

Metallic Nanomaterials notably gold nanomaterials are widely used materials for enzyme immobilization, due to their big surface area, thermal and mechanical properties, simplified functionality, and desirable biocompatibility. Furthermore, gold nanomaterials are often bound to other nano-carriers to immobilized enzymes [150]. In biosensors, enzyme immobilized gold nanoparticles have been widely used due to the enzyme capability to attach the gold nanomaterial by covalent interaction between gold and the amino or thiol side of the enzyme. Also, TiO_2 nanomaterials have high biocompatibility and large surface area properties, they are commonly used for enzyme immobilization and other applications such as biosensors, catalytic action, wastewater treatment, and more. Bare or functional Au and TiO_2 nanomaterials have been applied for enzyme immobilization by different forces including covalent attachment [152], physical adsorption [151], cross-linking method [153], chemical adsorption [154], cross-linking [155]. ZnO nanomaterials are attractive carriers for the immobilization of enzymes due to their different properties including strong biocompatibility, non-toxicity, chemical stability, wide surface area, and low cost. Nano-ZnO is positively in immobilization solution, which is almost 9.5 due to its high isoelectric point, which

is preferable for electrostatic adsorption of the low isoelectric point enzyme which is negatively charged in the solution.

Polymeric materials have taken attention toward application in recent decades with various morphologies and features as carrier platforms for many enzymes. Enzymes may be either bound to the surface of the polymers or encapsulated in hollow structures, or incorporated into the porous network of polymers. This technique takes attention to various biotechnological applications such as biocatalysts, bio-separation, imaging, bio-sensing, *in vitro* biotransformation, and drug delivery or therapy [156,157]. Polymeric micelles have a dimeter between (100–200 nm), with nanoscopic core-shell structures created by amphiphilic block co-polymers–which consists of a hydrophobic part inside the core as well as hydrophilic part outside the core. Subsequently, the conjugation of enzyme takes place in the outer hydrophilic part of micelles as modification of corona which optimization of physicochemical and biological properties is modified in the micelle. Dendrimer a multi-branched high-density polymer molecule with sizes is ranged between 100 and 200 nm drives its micellar behavior from emanating a central hydrophobic core that subsequently regulates covalent bonding for efficient enzyme immobilization [158].

Similarly, electrospun materials are potential an efficient supporting matrix for enzyme immobilization according to special characteristics notably higher porosity in nanometer sizes and larger surface areas. Moreover, sizes of fiber regulate the inhibition of low mass transfer and diminish the diffusion constrains electrospun's assisted materials also provide advantages in terms of bio-compatibility, biodegradability, high mechanical efficiency, and hydrophilicity. In addition, the presence of functional group diversity on the surface, nanomaterials are able to facilitate the enzyme binding as well as subsequent actions rapidly. The development of electrospun carriers has been implemented by a number of biopolymers such as chitin, CHI, alginate, and celluloses as well as synthetics counterparts such as PVA, polystyrene, polyacrylamide, and polyurethane. Consequently, enzyme immobilization of these materials is regulated by a broad mechanism for example adsorption, encapsulation, and covalent attachment. [159].

2.2.3. L-ASNase immobilization

Bio-compatibility and biodegradable features of polymeric and nanomaterials have been emphasized as crucial properties of carrier formulations used for the immobilization of the L-ASNase. Various literatures enlist a number of matrices such as chitosan [160], colominic acid [161], Nylon tubing [162], Polyacrylamide entrapment [163], Polyimide [164], PANI nanofiber covalent binding [165], calcium alginate-gelatin cross-linking [166], Fe_3O_4 coated with MCM-41[167], MOF [168], hybrid nanoflowers [169], and others. Several improvements of crucial parameters have been accounted for in these materials for example kinetic parameters, half-life, and storage stability.

A study made by Monajati et al., uses graphene oxide (GO) an appropriate carrier matrix for immobilization of L-ASNase, due to its high specific surface area which principally relies on GO was functionalized with L-aspartic acid (GO-Asp), then L-ASNase immobilization on GO-Asp with physical or chemical conjugation. It was also reported that the covalent immobilization efficiency was 100%. While the stability of free and immobilized L-ASNase has been studied for enzyme activity at various temperatures (20–60 °C) and pH (5-9). Covalently immobilized L-ASNase showed higher activity at pH 8 than free enzyme. It was also noted that the enzyme showed 42% activities after 8 consecutive used at 60 °C, and as well as the absence of kinetic parameter significant alteration after immobilization. As a result, it was predicted that the L-ASNase of GO-Asp nanomaterials immobilization is potentially applicable in the industrial field [170].

Apart from this, the *E. coli* L-ASNase was immobilized in calcium alginate nanoparticles by microencapsulation technique, by employing sodium alginate, calcium chloride, and the load concentration of enzymes to investigate the optimum parameters. As a result, the proportional relationship was indicated between the increase of sodium alginate amount and L-ASNase enzyme activity upgrade at any $CaCl_2$ concentration as well as enzyme residual activity upgrade by moderate amount loading [171].

On the other hand, the study of *E. coli* L-ASNase was covalently immobilized in aluminum oxide pellets by the assist of glutaraldehyde as a crosslinking agent by the optimum efficiency as 85.0 %. In addition, both free and immobilized L-ASNase optimal activity was reported at 37 °C was founded the optimal activity and pH 7.5. It

was observed that the immobilized enzyme has a higher affinity (low Km) and relatively more stable in the presence of some solvents (ethyl acetate, acetone, and acetonitrile), metal ions (Ag^{+}, Zn^{2+}), and β-mercaptoethanol. The immobilized enzyme was reused in a glass column reactor for up to nine successive cycles of substrate hydrolysis with no loss of activity. In addition, it has been reported that the immobilized enzyme has a shelf life of 30 days and is effective in lowering the level of L-Asn in blanched potato chips [172].

2.2.4. L-ASNase inducing

Several references emphasized that a broad range the carrier materials either natural or synthetic polymer, as well as nanoparticles, are capable to immobilize L-ASNase in which half-life, as well as reusability and thermal stability are enhanced. Nevertheless, a number of drawbacks which are emerged from enzyme immobilization for example diminishing immobilized enzyme activity compared to the initial activity, and lower reaction rate compared with native enzymes. On the other hand, additional costs for carriers as well as the absence of the spent immobilized enzyme, reduce the enzyme activity by binding to the enzyme active site. Therefore, the research and finding of novel methods of enzyme immobilization that simultaneously improving enzyme activity are crucial.

Despite the widespread debate of L-ASNase inducement enzyme activity methods in the last few years, it was only found in two studies in the literature. The first study was reported by Uygun et al. (2017) which immobilized L-ASNase enzyme to Au/ Ni/Au/PEDOT-PPy-COOH nanowires by ultrasonic induction, which concluded that free L-ASNase inhibited the growth of EL4 lymphoma cells by 17.3 %, while ultrasonically stimulated (5V, 2.83 MHz) counterpart inhibited 22.9 %. In addition, the immobilized enzyme inhibited the growth of lymphoma cells by 28 %, while the ultrasonically stimulated counterpart inhibited at a rate of 92 %. Therefore, it was noted that higher activity by ultrasonic stimulation reached 1.32-fold for free enzyme while the immobilized counterpart reached 3.28-fold [173].

The second study of L-ASNase by Ates et al., (2018), which relied on Fe_3O_4-chitosan magnetic nanoparticles immobilization of L-ASNase with the main purpose of magnetic and frequency inducement of L-ASNase activity. At the end of the study,

it was distinguished that the relative activity of the L-ASNase enzyme increased approximately 300 % at 3Hz and 30 mT magnetic field conditions [174].

The following explanation can be rendered as a general consequence of these two studies: Under suitable circumstances, external stimulus agents can have effects on the reactions of enzymes and substrates and their microenvironment, inducing L-ASNase enzyme activity at the molecular level. The triggering effect plays an important role, make a favorable position and accelerate the interaction between enzyme and substrate, and thus increase the product. These two studies have indicated that ultrasonic and magnetic platforms can increase *in vitro* the activity of the L-ASNase enzyme. However, these two trigger platforms have limitations in the application of human L-ASNase induction. High-frequency range as the ultrasonic waves used are between 2-12 MHz, make it difficult to subjected solid tumor tissues by using ultrasonic probes for treatment. However, the magnetic field frequency in comparison to ultrasonic waves is incredibly weak. However, the magnetic field also has a radiosity drawback. Therefore, the activation process that will induce the L-ASNase enzyme should not be likely to disrupt biological structures.

2.2.5. Near-infrared (NIR) Light

Several external stimulating factors have been applied to monitor enzymatic activity for example pH, temperature and light. One clear example, in recent times, light inducing systems in various wavelength application to induce enzyme activity owing to the incapability of UV and visible light to reach deeper tissue as well as damage of biological system from UV light, NIR is implemented in accordance to its capability to infiltrate deeper as well as low damage into tissue compared to the UV light as shown in (Figure 2.7a) [175]. NIR stimulation is extensively researched in scientific studies for the treatment of numerous cancer diseases involving solid tumor tissue. The simultaneous two-photon absorption induces NIR photographic reactions [176]. A UV-sensitive compound must simultaneously absorb two NIR photons. NIR photographic reactions at double-photon absorbing interfaces have been widely researched for future lithographic and controlled drug release applications [177]. In comparison, only laser focus can absorb two photons. The two-photon absorption technique is unworkable to induce deep tissue photoreactions since a femtosecond laser is defocused when traveling through the tissue.

In this thesis, the NIR trigger method is potentially capable as a significant alternative in L-ASNase application. Due to the NIR has a harmlessness effect on the human body, it is extendable to the whole body when it's needed. Owing to the current example, NIR sauna therapy baths are used for detoxification which does not put the health at risk. It is assumed that the compatibility between NIR and body tissues would bring a tremendous benefit. In accordance to the two studies in the literature, it is regarded that NIR is capable of the activation of enzymes. The first study by Gao et al., prepared photoactivable bio-catheters to remotely trigger or obstruct the biochemical pathways in living organisms at a targeted time and place, which relied on a photoactivatable enzyme platform with NIR using protein kinase A (PKA) as a fundamental enzyme in cell biology due to trigger properties to other enzymes [178].

The second study, although not directly related to enzyme immobilization and triggering, involves determining the effect of NIR triggering on sensor measurements in an environment with glucose oxidase enzyme in sensor development for glucose measurement [179]. NIR stimulation consists of two primary targets, the first one enhancing the drug release directed from the carrier system suitable for NIR inducing (UCNPs) in the objective tumor. The second goal is to assist photodynamic therapy with multiple initiators. Until recent times, positive effects have been achieved with photodynamic combination therapies. The main subject of this study is to create a triggering mechanism by using immobilized enzyme and NIR induction against the decreases in enzyme activity that occurs during the PEGylating process of L-ASNase and elevating enzymatic activity (Figure 2.7 b).

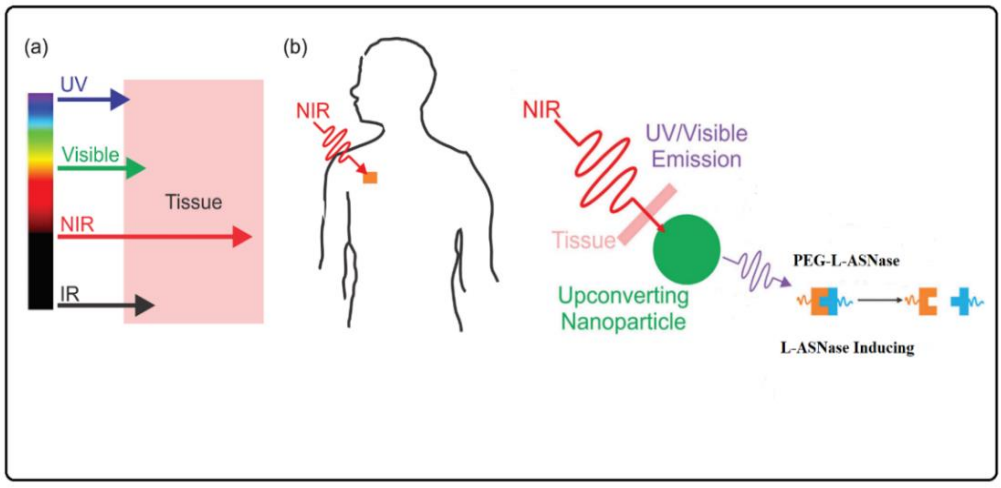

Figure 2.6: NIR penetration into the tissue (A), and triggering UCNP-linked L-ASNase with NIR (B).

2.2.6. Up-conversion nanoparticles (UCNPs)

Recently, lanthanide-doped up-conversion nanoparticles (UCNPs) have produced NIR photoreactions [180] which rely on the capability of the UCNPs to turn NIR light into UV or visible light [181]. The UC has a possess short-wavelength light that can induce to start the photosensitive reactions, by the approach namely as UCNP-supported photochemistry. The exciting power for UCNP-aided photochemistry is in several orders less than for two-photon absorptions. Which is powered by low-cost laser NIR diodes and does not need high-intensity costly femtosecond lasers. Besides, NIR light is shown to induce UCNP-assisted photoreactions after crossing a tissue of a few millimeters of thickness [182]. Therefore, UCNPs are a new promising revolution of bio-imagery which relies upon sequential absorption of many photons notable ladder energy of trivalent Lanthanide ions with sufficient inorganic host lattice to achieve higher anti-Stokes's luminescence [183]. Outstandingly, the NIR light carries out the transformation of two or more photons with low energy excitement into shorter wavelength emission for example visible and UV.

Moreover, UCNPs are potentially applicable in drug delivery, imagery, and therapy theragnostic due to UCNP's several beneficial properties which are led by the excitement of NIR optic window such as the absence of blinkness diffusion and capability of deeper penetration of the tissue. Also, the UCNP theranostic route uses hierarchically designed nanostructures to combine UC photoluminescence (PL) imaging with other imaging modalities for both *in vitro* and *in vivo* application such as magnetic resonance imaging (MRI) [184], computed tomography (CT) [185], single-photon emission tomography (SPECT) [186], positron emission tomography (PET) [187], as well as with therapeutics of photothermal therapy (PTT) [188], gene and drug delivery [189]. A recent crucial development on the application of nano-chemistry for the use of theranostic UCNP's was conducted by enabling nano-control of its optical features to increase the up-conversion at a selected wavelength [190], modification of the surface area for the transmission phases, and biomarker surface binding chemistry [191].

The host structures of UCNPs are radiant, whereas the trivalent lanthanide ions in a proper dielectric host with a network less than (100 nm) are distributed as a guest. Dopant lanthanides are optically active centers producing emissions when are excited. UCNPs can selectively upgrade the NIR into shorter NIR (blue, green, red) with

wavelength (colored) and UV using careful choice of lanthanide dopes. Normally, The UC PL is typically provided from *4f−4f* orbital electronic transformations with concurrent wave functions located within one single lanthanide ion. Protecting effect of *4f* electrons from external shells *5s* and *5p* contributes to linear sharp emissions, which have a high photo blinding and photochemical degradations resistance. Lanthanide ion transitions *intra-4f* are electric dipoles forbidden by quantum mechanical selection laws, which are induced by local crystal areas with relaxed inter-mixing of the *f* states with superior electro-configuration [192]. The fundamental interdiction of transformation *4f−4f* leads to extremely long lives for lanthanide ion energy levels. Thus, it facilitates consecutive excitations of a lanthanide ion's energies in excited states and enables favorable ion-ion interactions with two or more lanthanide ions in excited states, facilitating energy transfers between these two or more lanthanide ions.

The UCNPs are similar to the bulk forms' optical characteristics. In general, they generate the same UC PL peaks, because of the electronic transitions well-shielded of *4f−4f* by the *5s* and *5p* external shells. However, due to nano-size induced surface lead the efficiency and the relative intensity of UCNP pinnacles are quite distinct from their bulk counterpart. Given the big surface area compare to the volume of UCNP ratio, the majority of lanthanide doping products are surface exposed to disablement because of surface defects and the high-phonon energy ligands and solvents. Two approaches include deactivation on the surface.

- The dopants on or around the surface of the nanoparticles may be specifically disabled by surrounding centers of the quenching surface.
- Dopant energy at the core of the UCNPs may move randomly and travel a long distance or directly to the surface scrub site to/from the dopant surface.
- All UCNPs are required for higher efficiency to improve the limit of detection (LOD) in sensing high SBR bio-imaging and enhanced the therapy impact. A multicolor emission of single wavelengths is crucial for the multiplexing of the imagery and/or the enhanced by-course of bioassays (the simultaneous identification of multiple analytes and targets in samples).
- The single size and the uniform shape are needed to have similar optical properties for intracellular theranostics as well as cellular and biological effects, meanwhile specific stoichiometric composition to regulating the concentration of the

lanthanide dops which subsequently manage the optical qualities of these substances is required.

- ❖ The UCNPs are as-synthesized because of their capping by hydrophobic ligands of the long chain. For biological applications, it is important to construct the region of UCNPs to permit its dispersion in an aqueous phase.
- ❖ UCNP should be non-toxic to cells and the body and biocompatible properties.

Furthermore, UCNPs have no target groups to classify areas of body concern such as angiogenic tumor areas. Adequate chemical couplings must be integrated onto nanoparticle surfaces by a combination of antibodies, peptides, biotin, avidin, and proteins.

2.2.7. Upconversion mechanisms

There are five fundamental UC pathways. The cooperative mechanism for upconversion luminescence is not well studied, since in UCNPs it is a method inefficient until now.

2.2.7.1. Excited state absorption (ESA)

The ESA takes on the form of a three-level system for two sequential photon absorption of one ion in a consecutive absorption, because of the ladder-like form of a basic multilevel system. The existence of this process is due to the similar distinction between ground state (G) and excited states (E1 and E2), as well as the intermediate-level E1 reservoir capacity. As an ion is excited from a G to E1, a separate pump photon will promote the ion from E1 to the higher phase. State E2 owing to E1's long existence, until its decline to the ground. Therefore, upgraded emissions from the E2 stage will arise. A ladder-like configuration of lanthanide energy levels is desired to obtain the extremely efficient ESA. Only a few lanthanides ions including Er^{3+}, Ho^{3+}, Tm^{3+}, and Nd^{3+} they have some energy level structures [193], which are also well correlated with the performance of the commercially available diode laser with the good excitation wavelength at (~975 nm and/or 808 nm).

2.2.7.2. Energy transfer upconversion (ETU)

As ESA is operated within one lanthanide ion, ETU consists of two nearby ions. In the ETU phase, an ion 1 called the sensitizer; first the ion gets excited by absorbing

a pump photon phase from the ground level until to the stable stage E1; it subsequently transfers its extracted energy to ground-state (G) and excited-state E1 ion 2, that considered as the activator, exciting ion 2, into its highest emission stage E2, while sensitizer 1 relieves itself two times back to ground-state G. The upconversion performance of the ETU method is subject to the mean stretch between the surrounding sensitizer activator, calculated by dopant concentrations. Unlike ETU, the performance of ESA is independent of the dopant amount because of its single ion property. The ETU mechanism has an extremely significant role in UCNPs, Yb^{3+}/Tm^{3+}, Yb^{3+}/Er^{3+}, and Yb^{3+}/Ho^{3+} ion pairs have crucial theranostic UCNPs (sensitizer/activator) and used to improve the excitation at ~975 nm [194,195]. It should be mentioned that the biological tissues have very little dispersion and absorption at 975 nm, which is inside the tissue's "optical transparency window". In this case, Yb^{3+} acts excellently as a sensitizer, since its absorption cross-section is sufficiently high for the NIR area at 975 nm.

In addition, its optimized concentration (20−100 % for fluoride nanoparticles) can be sustained at a high level without evoking deleterious cross-relaxation since Yb^{3+} has the structure of just two energy levels. Most attempts to grow Yb^{3+} sensitized UCNPs with a pumping capability of around 975 nm date have been made. Also, effective ETU can be seen with single lanthanide-doped systems, structures using the lanthanide ion itself as the sensitizer. For example, in Er^{3+}-doped $LiYF_4$ when excited at 1490 nm [196], or in Ho^{3+}-doped $NaGdF_4$ when excited at 1200 nm [197]. Utilization of other sensitizers can be used to quench and enhance certain emission bands. Different ion has been utilized as sensitizers (Nd^{3+}, Ce^{3+}, and Ho^{3+}) to improve the blue emission band of Tm^{3+}, red emission band of Ho^{3+}, and NIR emission band of Tm^{3+} [198].

2.2.7.3. Cooperative sensitization upconversion (CSU)

CSU is the interacting mechanism of three ion centers, with ion 1 and ion 3 normally of the same form, which is both excited after receiving photons excitation level. Subsequently, both interact mutually with ion 2 and transfer energy to stimulate higher levels of ion 2. By emitting an upconverted photon, the exciting form of ion 2 will return to the planet. CSU efficiency is generally less than the ESA or ETU phase because during transformations it requires quasi-virtual pair levels, which is a higher

order of perturbation must be defined mechanically as quantum. Despite this, the required for limited excitation to compensate for the low performance may provide a possibility to obtain high-resolution imaging that is not possible from the other UC mechanisms. The CSU mechanism has been reported for Yb^{3+}/Tb^{3+}, Yb^{3+}/Eu^{3+}, and Yb^{3+}/Pr^{3+} ion pairs [199].

2.2.7.4. Cross relaxation (CR)

CR is formed as a result of ion-ion interaction, in which ion 1 transfers a portion of its exciting energy into ion 2 through a mechanism of E2 (ion 1) + G (ion 2) → E1 (ion 1) + E1 (ion 2). Ion 1 and ion 2 can be similar or various, ion 2 maybe also in the excited state in some cases. The CR mechanism is an essential product of ion-ion interaction; its efficiency is directly linked to the concentration of dopants. CR is the major reason for the notable "concentration quenching mechanism" of emission, alternatively it is capable for purpose using to change the color production in UCNPs or creating successful photon avalanche mechanisms.

2.2.7.5. Photon avalanche (PA)

PA is a mechanism that generates UC above a certain threshold of excitation power. Sparse amount of transformed fluorescence is produced under the threshold, while PL intensity rises by magnitude orders above the pump threshold. In fact, PA is an ESA looping method for excitation light and effective CR generating. In the beginning, non-resonant poor ground state absorption populates ion 2 level E1. Owing to ESA protocol the initiation of looping begins by raising ion 2 at E1 level to E2. Subsequently a successful is driven as CR process of E2 (ion 2) + G (ion 1) → E1 (ion 2) + E1 (ion 1) between ion 1 and ion 2. Finally, ion 1 passes its energy to ion 2 by populating its level E1to create a complete loop. The net result of the loop technique is that an ion 2 creates two ion 2's in this state with the metastable E1 state. When the method of looping follows, two ion 2’s at the E1 state will release four; four will release eight, evocative of a population landslide effect ion 2 in its E1 state, and thus the PA UC from the emitting level of E2. PA Identifying it is simple, although the pump threshold typically takes a long (second) period to build up. Furthermore, UC PL relies incredibly highly on pump power around the threshold pump power.

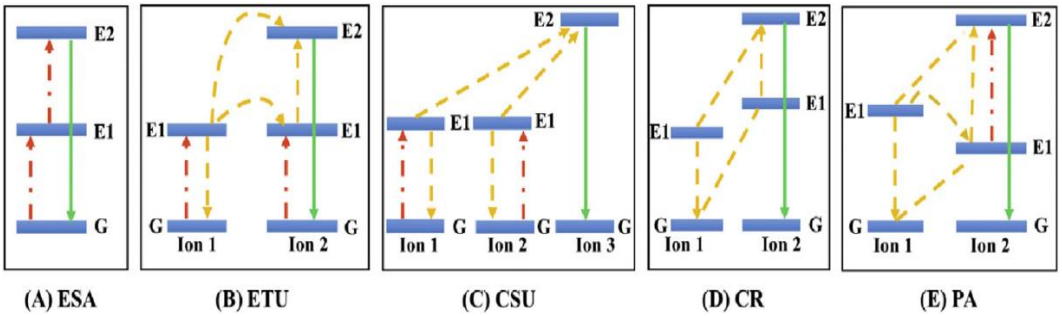

Figure 2.7: Principal UC processes for lanthanide-doped UCNPs: ESA (A), ETU (B), CSU (C), CR (D), and PA (E). The red, violet, and green lines represent photon excitation, energy transfer, and emission processes, respectively [200].

2.3. The Aim of Thesis

L-ASNase is usually administered to patients by intravenous (intravenous) injection 2-3 times a week. Meanwhile, the PEG immobilized L-ASNase is used to reduce the immune response that occurs during administration. However, its use and accessibility are limited because of organ damage caused by the side effects of the enzyme, and its short plasma half-life, and high cost. In addition, a continuous injection during the chemotherapy process and dependence on the hospital cause psychological depression in patients. At this point, it is crucial to overcome encountered problems in the treatment, which is crucial for children and some adults as well as providing new approaches. Immobilization is capable to solve all the problems above, however the enzyme catalytic and sensitivity to substrate decrease after immobilization.

Therefore, it is crucial to construct novel enzyme carriers which capable to increase the enzymatic activity as well as diminish side effects with a better result than free enzyme. In the scope of the thesis, the synthesis of 6 different UCNP's with biocompatible properties were initially carried out. Then PEG-L-ASNase enzyme was immobilized onto these 6 UCNPs. Afterward, the immobilization parameters were measured such as enzyme unit, incubation time, optimum pH, optimum temperature, reusability, storage stability, and subsequently activation measurement of the enzyme by NIR.

3. MATERIAL AND METHOD

3.1. Materials

All chemicals were used without any purification process. The manufacturer company and some properties of these chemicals were given in (Table 3.1).

Table 3.1. Chemicals used in the scope of the thesis.

Material	Properties	Manufacturer
Yttrium (III) chloride hexahydrate	%99.9	ChemPur
Ytterbium (III) chloride hexahydrate	%99.9	Fluorochem
Erbium (III) chloride hexahydrate	%99.9	Fluorochem
Neodymium (III) chloride hexahydrate	%99.9	Fluorochem
Ammonium fluoride	≥%97.0	Merck, USA
Sodium hydroxide pellet	≥%97.0	Merck, USA
Sodium chloride	≥%97.0	Merck, USA
Poly (ethylene imine)	≥%97.0	Merck, USA
3- (Triethoxilyl) propyl isocyanate	≥%98.0	Merck, USA
(3-Glycidyloxypropyl)trimethoxy silane	≥%98.0	Merck, USA
Ammonium hydroxide	≥%98.0	Merck, USA
Tetraethyl ortho silicate	≥%99.0	Sigma, USA
Hexane	%≥99.9	Merck, USA
Dimethyl sulfoxide	%≥99.9	Merck, USA
Mercury (II) iodide	≥%99.0	Merck, USA
L-Asn	≥%98	Sigma, USA
PEG-L-ASNase	≥ 96%, isolated from E. coli ASI.357	Leunase, Japan
Potassium iodide	≥%99.5	Merck, USA
Sodium chloride	≥%99.0	Merck, USA
Sodium citrate	≥99.5%	Sigma-Aldrich, USA
Trichloroacetic acid (TCA)	≥%99.0	Sigma-Aldrich, USA
Tris-HCl	≥%99.0	Sigma-Aldrich, USA
BSA	≥%99.0	Sigma-Aldrich, USA
DMEM	≥%99.0	Capricorn Scientific, Germany
MTT	%98	Sigma-Aldrich, USA
Trypsin	% 98	Biological industries, USA

Acetic acid	≥%99.85	Sigma-Aldrich, USA

3.2. Devices Used For Characterization

The list of devices used in the thesis were given in (Table 3.2).

Device	Institution / Organization
FTIR / ATR Spectrophotometer (Perkin Elmer)	Akdeniz University
Zetameter (Malvern Nano-ZS)	Akdeniz University
Dynamic light scattering (DLS)	Akdeniz University
Thermogravimetric analysis (TGA, Perkin-Elmer)	Akdeniz University
X-Ray Photoelectron Spectroscopy (XPS) techniques	Akdeniz University
Transmission electron microscopy analysis TEM	Middle East Technical University
X-ray diffraction (XRD, Rigaku, Rad B-Dmax II)	Middle East Technical University
Diode laser (808 nm)	Inonu University
Diode laser (980 nm)	Inonu University
ELISA plate reader (BioTek)	Inonu University
Water bath (WiseBath)	Inonu University
Cold centrifuge (Core, NF 800 R)	Inonu University
Orbital mixer (Daihan, SHO-1 d)	Inonu University
Electronic balance (Shimadzu ATX224)	Inonu University

3.3. Synthesis and Modification of Upconverting Nanoparticles

Synthesis of upconverting nanoparticles: UCNPs were synthesized by the hydrothermal method which resulted in UCNPs with high emission efficiency, well dispersibility in aqueous solution, and high reaction yield [201]. Within the scope of the thesis, UCNPs have irradiated under 980 and 800 nm NIR lasers.

3.3.1. Synthesise of UCNPs containing $NaYF_4$: Yb^{3+}, Er^{3+} glowing green at 980 nm

For preparation UCNPs containing $NaYF_4$, Yb^{3+}, Er^{3+} with several stages, firstly, the reaction mixtures were prepared with yttrium (III) chloride hexahydrate ($YCl_3.6H_2O$) (1.6 mmol), ytterbium (III) chloride hexahydrate ($YbCl_3.6H_2O$) (0.36 mmol), erbium (III) chloride hexahydrate ($ErCl_3.6H_2O$) lanthanide salts (0.04 mmol), NaCl (2 mmol) salts, and this solution mixture was added to the Teflon vessel, which

is part of the hydrothermal synthesis system. Thereafter, ammonium fluoride (NH_4F) (10 mmol) was dissolved in 60 mL of anhydrous ethanol and added to the reaction mixture. Teflon vessel was placed in the hydrothermal unit in a steel container and heated to 200 °C for 4 hours. After the reaction was completed, the white solid was centrifuged at 10.000 rpm for 15 minutes and removed from the solvent medium. The white precipitates were washed 3 times with a mixture of ethanol: water (1:1), filtered and dried overnight at 40 ° C in a vacuum oven.

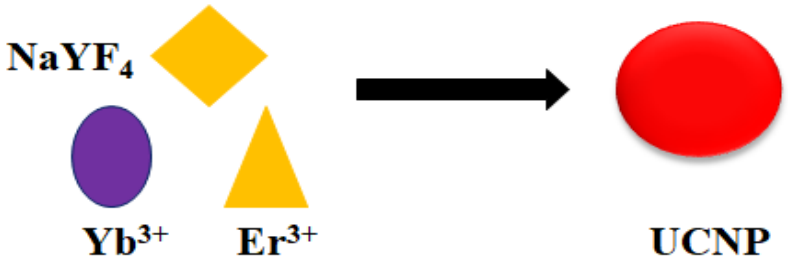

Figure 3.1: Synthesis of upconverting nanoparticles for 980 nm laser trigger.

3.3.1.1. Modification of $NaYF_4$: Yb^{3+}, Er^{3+} with PEI

The charge of the PEG-L-ASNase enzyme is negative at pH 7.4. Therefore, UCNPs were modified with polyethyleneimine (PEI, branched MW: 25.000), which has a positive surface charge, in order for PEG-L-ASNase to interact electrostatically with UCNPs. For surface modification studies of UCNPs that emit blue and green light, which are planned for excitation at 980 nm, two approaches such as during and after synthesis were applied. Since the modification during the synthesis contributes to the reduction of the additional process step, saving the solvent and controlling the particle size, the modification process to be applied for the physical interactions was done *in situ*. In the experimental procedure followed in the modification process, the amount of PEI to be used over the yield of naked UCNP synthesis was determined. For this purpose, PEI solution (1 g/ 30 mL water) was added to the synthesis medium of UCNPs. Then, PEI-coated-UCNPs were taken from the mixture by centrifugation at 10.000 rpm for 15 minutes. The product was washed 3 times with a mixture of ethanol: water (1: 1), filtered and dried overnight at 40 ° C in a vacuum oven to remove excess PEI.

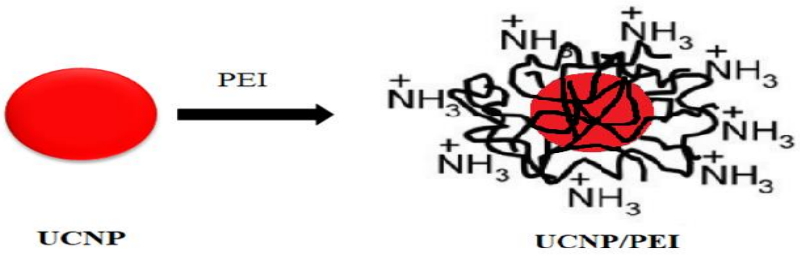

Figure 3.2: $NaYF_4$: Yb^{3+}, Er^{3+} UCNP modification with PEI.

3.3.1.2. Modification of $NaYF_4$: Yb^{3+}, Er^{3+} with GPTMS

To functionalize UCNPs with the covalent group on their surface, UCNPs nanoparticles were dispersed in dry iso-propanol (IPA) (60 mL), and epoxy (3-glycidyloxypropyl) trimethoxysilane (GPTMS) was added to the medium at a ratio of 0.542 of UCNPs (w/w). The mixture was refluxed at 110 °C overnight, after cooling to room temperature, it was centrifuged at 10.000 rpm for 15 minutes, and GPTMS modified-UCNPs were removed from the mixture. To remove the excess silane derivatives from the environment, it was washed with iso-propanol twice, washed 2 times with ethanol, filtered and dried overnight at 40 ° C in a vacuum oven.

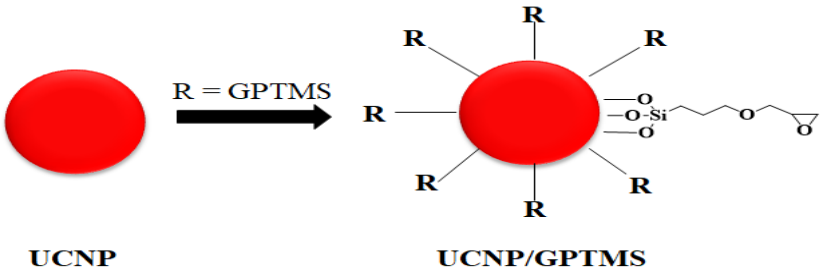

Figure 3.3: $NaYF_4$: Yb^{3+}, Er^{3+} UCNP modification with GPTMS.

3.3.1.3. Modification of $NaYF_4$: Yb^{3+}, Er^{3+} with ICPTES

For covalent modification of UCNPs with 3-isocyanatetopropyl triethoxysilane (ICPTES) structure, UCNPs nanoparticles were dispersed in dry iso-propanol (IPA) (60 mL), and then ICPTES was added to the medium at a ratio of 0.542 of UCNPs (w/w). The mixture was refluxed at 110 °C overnight, after cooling to room temperature, it was centrifuged at 10.000 rpm for 15 minutes, and ICPTES modified-UCNPs were removed from the mixture. To remove the excess silane derivatives from

the environment, it was washed with iso-propanol twice and washed 2 times with ethanol then filtered and dried overnight at 40 ° C in a vacuum oven.

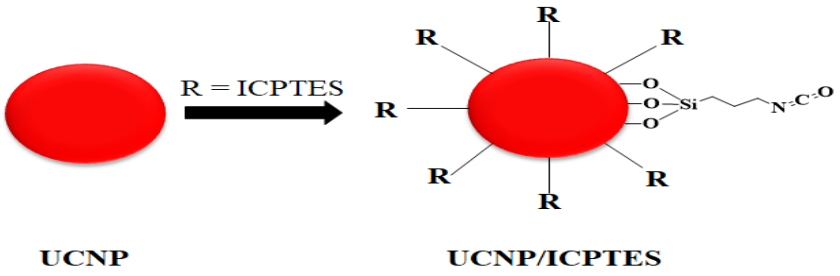

Figure 3.4: $NaYF_4$: Yb^{3+}, Er^{3+} UCNP modification with ICPTES.

3.3.2. Synthesis of UCNPs containing $NaYF_4$: Nd^{3+}, Yb^{3+}, Er^{3+} glowing green at 808 nm

For the synthesized of UCNPs containing $NaYF_4$: Nd^{3+}, Yb^{3+}, Er^3, the reaction mixture was included yttrium (III) chloride hexahydrate ($YCl_3.6H_2O$) (1.6 mmol), ytterbium (III) chloride hexahydrate ($YbCl_3.6H_2O$) (0.36 mmol), erbium (III) chloride hexahydrate ($ErCl_3.6H_2O$) (0.04 mmol), and neodymium (III) chloride hexahydrate ($NdCl_3.6H_2O$) (0.02 mmol) lanthanide salts and sodium chloride (NaCl) (2 mmol), and these solutions were mixed in Teflon vessel. After loading the mixture into a Teflon container, ammonium fluoride (NH_4F) (10 mmol) dissolved in 60 mL of anhydrous ethanol was added to the Teflon vessel, then it was placed in the hydrothermal unit in a steel container and heated to 200 °C for 4 hours. After the reaction was completed, the solid product in the system cooled to room temperature was separated from the solvent medium by centrifuged at 10.000 rpm for 15 minutes. The white precipitates were washed 3 times with a mixture of ethanol: water (1:1), filtered and dried overnight at 40 ° C in a vacuum oven.

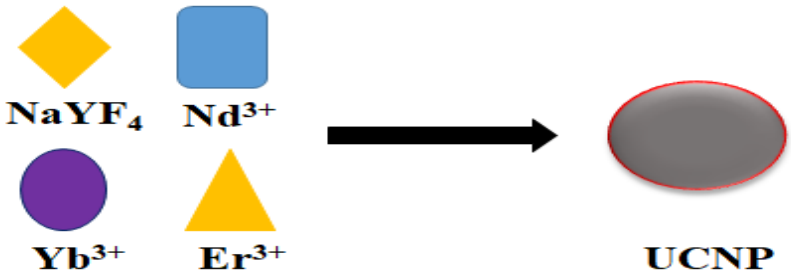

Figure 3.5: Synthesis of upconverting nanoparticles for 808 nm laser trigger.

3.3.2.1. Modification of $NaYF_4$: Nd^{3+}, Yb^{3+}, Er^{3+} with PEI

UCNPs were modified with polyethyleneimine (PEI, branched MW: 25.000), which has a positive surface charge, in order for PEG-L-ASNase to interact electrostatically with Nd-UCNPs. For surface modification studies of Nd-UCNPs that emit blue and green light, which are planned for excitation at 808 nm, two approaches such as during and after synthesis were applied. In the experimental procedure followed in the modification process, the amount of PEI to be used over the yield of naked UCNP synthesis was determined. For this purpose, PEI solution (1 g / 30 mL water) was added to the synthesis medium of Nd-UCNPs. Then, PEI-coated- Nd-UCNPs were taken from the mixture by centrifugation at 10.000 rpm for 15 minutes. The product was washed 3 times with a mixture of ethanol: water (1: 1), filtered and dried overnight at 40 ° C in a vacuum oven to remove excess PEI.

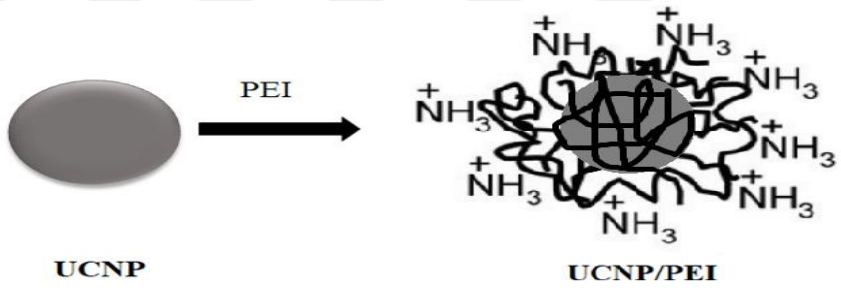

Figure 3.6: $NaYF_4$: Nd^{3+}, Yb^{3+}, Er^{3+} UCNP modification with PEI.

3.3.2.2. Modification of $NaYF_4$: Nd^{3+}, Yb^{3+}, Er^{3+} with GPTMS

The surface modification of Nd-UCNPs has been performed as follows; UCNPs were dispersed in dry iso-propanol (IPA) (60 mL). (3-glycidyloxypropyl) trimethoxysilane (GPTMS) was added to the medium at a ratio of 0.542 of UCNPs (w/w). The mixture was refluxed at 110 °C overnight, after cooling to room temperature, it was centrifuged at 10.000 rpm for 15 minutes, and GPTMS modified-UCNPs were removed from the mixture. To remove the excess silane derivatives from the environment, it was washed with iso-propanol twice, washed 2 times with ethanol, filtered and dried overnight at 40 ° C in a vacuum oven.

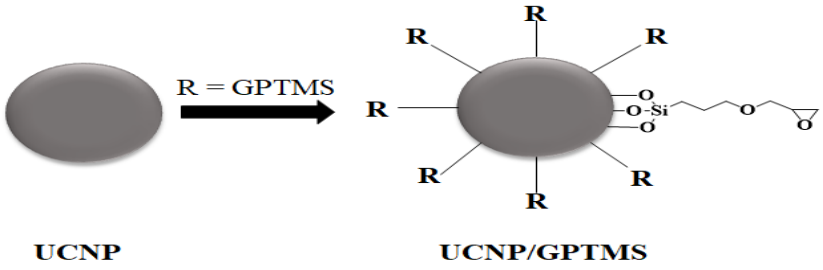

Figure 3.7: $NaYF_4$: Nd^{3+}, Yb^{3+}, Er^{3+} UCNP modification with GPTMS.

3.3.2.3. Modification of $NaYF_4$: Nd^{3+}, Yb^{3+}, Er^{3+} with ICPTES

UCNPs were dispersed in dry iso-propanol (IPA) (60 mL) then ICPTES was added to the medium at a ratio of 0.542 of UCNPs (w/w). The mixture was refluxed at 110 °C overnight, after cooling to room temperature, it was centrifuged at 10.000 rpm for 15 minutes, and ICPTES modified- Nd-UCNPs were removed from the mixture. To remove the excess silane derivatives from the environment, it was washed with iso-propanol twice and washed 2 times with ethanol then filtered and dried overnight at 40 ° C in a vacuum oven.

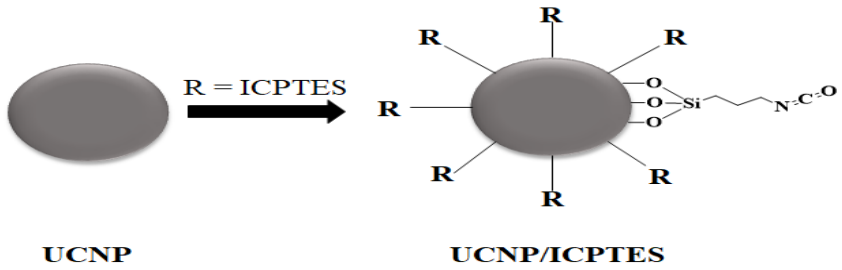

Figure 3.8: $NaYF_4$: Nd^{3+}, Yb^{3+}, Er^{3+} UCNP modification with ICPTES.

3.4. Characterization

Synthesized pure and surface modified UCNPs; crystal phases were characterized by X-Ray Diffraction Spectroscopy (XRD), Fourier Transform Infrared Spectroscopy (FTIR), Zetameter, Transmissive Electron Microscopy (TEM), Thermal Analysis (TGA), and X-ray Photoelectron Spectroscopy (XPS) techniques. The photo-physical properties of all particles, whose surfaces are bare or coated, under laser excitation at the relevant wavelength (980 and 808 nm) were determined by a fluorescence spectrophotometer.

3.5. L-ASNase Immobilization and Parameters

3.5.1. Immobilization of PEG-L-ASNase on $NaYF_4$: Yb^{3+}, Er^{3+}/PEI

To find out the optimum enzyme unit for physical immobilization of enzyme on UCNP, 25 mg of $NaYF_4$: Yb^{3+}, Er^{3+}/ PEI UCNP nanoparticle was incubated with a different unit (5, 10, 25, 50, 75, 100 U) of PEG-L-ASNase enzyme, the immobilization was made at +4 °C overnight. Then, the nanoparticles were taken and separated by a cold centrifuge, the supernatants were removed and keep, while the nanoparticles were washed with Tris-HCl buffer to remove the unbound enzyme.

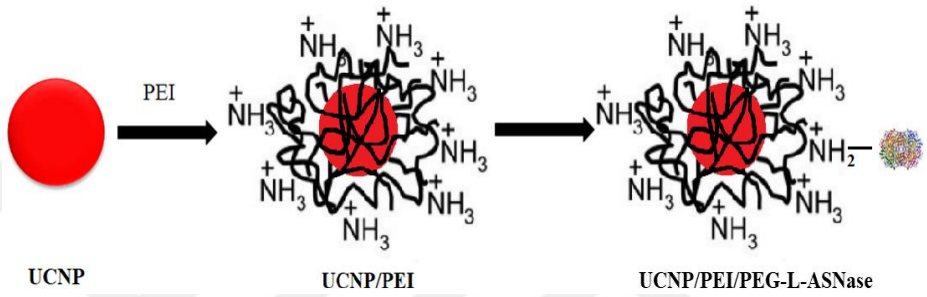

Figure 3.9: Immobilization of PEG-L-ASNase on modified $NaYF_4$: Yb^{3+}, Er^{3+} by PEI.

3.5.2. Immobilization of PEG-L-ASNase on $NaYF_4$: Yb^{3+}, Er^{3+}/GPTMS

To determine the optimum enzyme unit for covalent enzyme immobilization with UCNP, 25 mg of $NaYF_4$:Yb^{3+}, Er^{3+}/GPTMS nanoparticle were incubated with a different unit (5, 10, 15, 20, 25, and 50 U) of PEG-L-ASNase, the immobilization has occurred at +25 °C, pH 9.0 for 24 hours. Then, the nanoparticles were taken and separate from supernatants by cold centrifuge, the supernatants were removed and stored for further calculations, while the nanoparticles were washed with Tris-HCl buffer to remove the unbound enzyme.

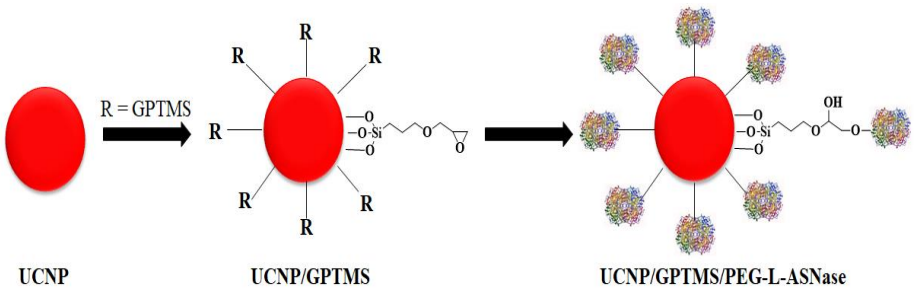

Figure 3.10: Immobilization of PEG-L-ASNase on modified $NaYF_4$: Yb^{3+}, Er^{3+} by GPTMS.

3.5.3. Immobilization of PEG-L-ASNase on $NaYF_4$: Yb^{3+}, Er^{3+}/ICPTES

25 mg of $NaYF_4$:Yb^{3+}, Er^{3+}/ ICPTES nanoparticle were incubated with a different unit (5, 10, 15, 20, 25, 30, 35, 50, and 75 U) of PEG-L-ASNase, and the immobilization has occurred at +40 °C, pH 9.0 for 24 hours. Then, the nanoparticles were taken and separated from supernatants by cold centrifuge, the supernatants were removed and stored for further calculations, while the nanoparticles were washed with Tris-HCl buffer to remove the unbound enzyme.

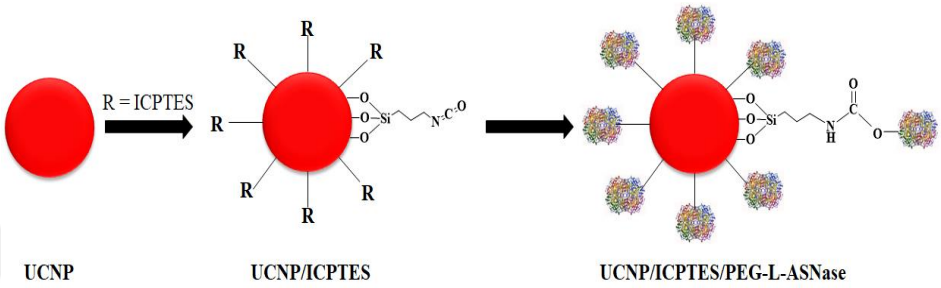

Figure 3.11: Immobilization of PEG-L-ASNase on modified $NaYF_4$: Yb^{3+}, Er^{3+} by ICPTES.

3.5.4. Immobilization of PEG-L-ASNase on $NaYF_4$: Nd^{3+}, Yb^{3+}, Er^{3+}/PEI

To determine the optimum enzyme unit for physical immobilization, 25 mg of $NaYF_4$: Nd^{3+}, Yb^{3+}, Er^{3+}/ PEI UCNP nanoparticles were incubated with a different unit (5, 10, 25, 50, 75, and100 U) of PEG-L-ASNase enzyme, and the immobilization was made at +4 °C overnight. Then, the nanoparticles were taken and separated by a cold centrifuge, the supernatants were removed and the nanoparticles were washed with Tris-HCl buffer to remove the unbound enzyme.

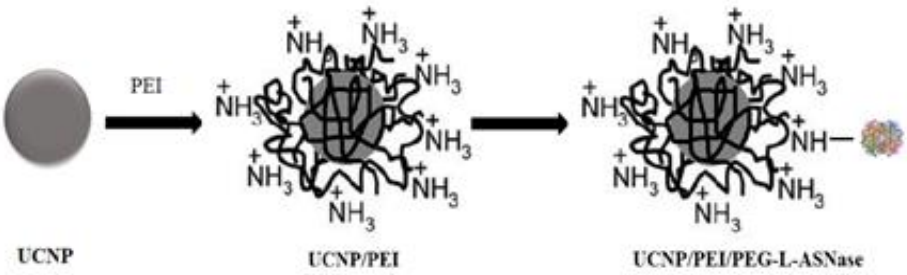

Figure 3.12: Immobilization of PEG-L-ASNase on modified $NaYF_4$: Nd^{3+}, Yb^{3+}, Er^{3+} by PEI.

3.5.5. Immobilization of PEG-L-ASNase on $NaYF_4$: Nd^{3+}, Yb^{3+}, Er^{3+}/GPTMS

To determine the optimum enzyme unit for covalent enzyme immobilization, 25 mg of $NaYF_4$: Nd^{3+}, Yb^{3+}, Er^{3+}/GPTMS nanoparticle were incubated with different enzyme unit (5, 10, 15, 20, 25, and 50 U), the immobilization has occurred at +25 °C, pH 9.0 for 24 hours. Then, the nanoparticles were taken and separate from supernatants by cold centrifuge, the supernatants were removed and stored for further calculations, while the nanoparticles were washed with Tris-HCl buffer to remove the unbound enzyme.

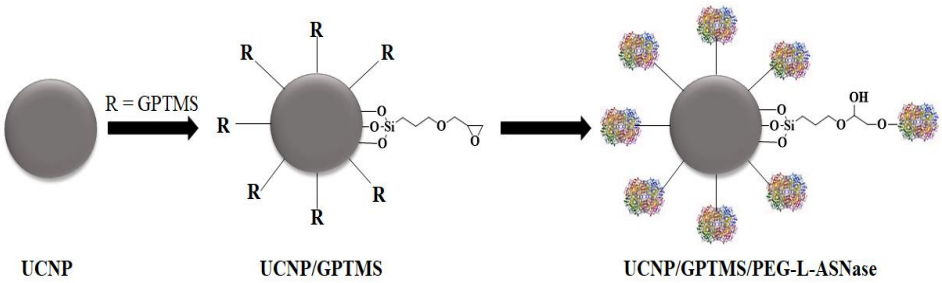

Figure 3.13: Immobilization of PEG-L-ASNase on modified $NaYF_4$: Nd^{3+}, Yb^{3+}, Er^{3+} by GPTMS.

3.5.6. Immobilization of PEG-L-ASNase on $NaYF_4$: Nd^{3+}, Yb^{3+}, Er^{3+}/ICPTES

To determine the optimum enzyme unit for covalent enzyme immobilization with UCNP, 25 mg of $NaYF_4$: Nd^{3+}, Yb^{3+}, Er^{3+}/ICPTES nanoparticle were incubated with a different unit (5, 10, 15, 20, 25, 30, 35, and 50 U) of PEG-L-ASNase, the immobilization has occurred at +40 °C, pH 9.0 for 24 hours. Then, the nanoparticles were taken and separated from supernatants by cold centrifuge, the supernatants were removed and stored for further calculations, while the nanoparticles were washed with Tris-HCl buffer to remove the unbound enzyme.

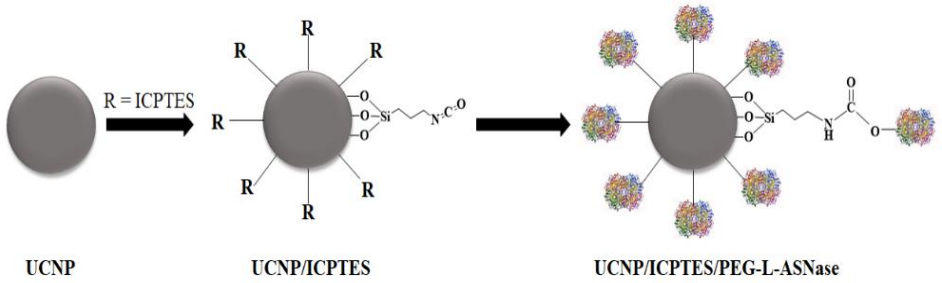

Figure 3.14: Immobilization of PEG-L-ASNase on modified $NaYF_4$: Nd^{3+}, Yb^{3+}, Er^{3+} by ICPTES.

3.5.7. L-ASNase activity

The L-ASNase enzyme activity was measured by the nesslerization technique [202]. This technique is based on the approach of colorimetric measurement of the ammonia formed by hydrolysis of L-Asn by L-ASNase. The method is briefly as follows: Free and immobilized enzymes are placed in a tube and a solution of a freshly prepared substrate (10 mM, 1 mL) with Tris-HCl (50 mM, pH 8.6) buffer is added. The reaction solution was incubated for 15 minutes at the optimum temperature. Then, the enzymatic reaction was terminated by adding TCA solution (1.5 M, 100 µL). Then, 100 µL of the solution was added to the 96 well plates and reacted with Nessler reagent (K_2HgI_4, 100 mL) and a yellow-orange color was observed. The absorbance of the obtained color was measured spectrophotometrically at 480 nm with a microplate reader device after 10 minutes of incubation at room temperature. One unit of enzyme activity (IU) is defined as the amount of enzyme that releases 1 µmol of ammonia per minute under optimum conditions. All experiments were performed using three parallel samples and the data obtained were graphically presented as mean ± SD (standard deviation). Results were calculated as 100% the highest activity and given as relative activity.

3.5.8. Enzyme unit and incubation time

To find the optimum enzyme unit for immobilization, different unite of PEG-L-ASNase enzyme and 25 mg of UCNPs were incubated overnight. Then the immobilized enzyme was removed from the reaction solution by a cooled centrifuge and the supernatants were collected. The carrier nanoparticles were washed with Tris-HCl buffer to remove the unbound enzyme. Immobilization yield (*IY*), activity yield (*AY*), and immobilization efficiency (*IE*) were calculated by using the equations below.

$$IY(\%) = \frac{C_i - C_s}{C_i} x100 \quad \text{..... (3.1)}$$

Where, C_i presents the total protein concentration of the enzyme, while C_s the total protein concentration of the unbound enzyme in the supernatant and washing solutions.

$$AY(\%) = \frac{A_i}{A_f} x100 \quad \text{..... (3.2)}$$

As for activity yield, here, A_i and A_f express the activity of the UCNP-L-ASNase and the free L-ASNase, respectively.

$$IE(\%) = \frac{AY}{IY} x100 \quad \ldots\ldots (3.3)$$

Immobilization efficiency, *AY* is activity yield, and *IY* immobilization yield.

For incubation time, the optimum enzyme unit was incubated with a constant amount of UCNP nanoparticles for a different time.

3.5.9. Optimum pH and temperature

To calculate the optimum pH value of the free and immobilized enzymes, the enzyme activities were measured by using substrate solutions prepared with different pH buffers. Buffers used in this parameter; citrate buffer 50 mM (pH 4.0, 5.0 and 6.0), phosphate buffer 50 mM (7.0, 7.5 and 8.0) and Tris-HCl 50 mM (pH 8.5, 9.0 and 10.0). The pH value is reported as the optimal pH value with the highest enzyme activity. Determined the optimum temperature, free and immobilized L-ASNase were incubated at different temperature degrees for 30 min then added 1 mL of substrate prepare in optimum pH buffer. The highest enzyme activity at temperature degree will be recorded as optimum temperature.

3.5.10. Thermal and pH stability

The thermal stability was measured when the free and immobilized L-ASNase were incubated in a water bath at 50 °C. The activity of the enzyme was calculated at 6 h intervals. The remainder of the free and immobilized activities were then contrasted with the initial activities which were considered to 100% activity. While for the pH stability both free and immobilized L-ASNase were incubated at (pH 4 and 9) for 6h the initial activities, which was considered to 100% activity.

3.5.11. Effect metal ion and solvent

The effect of metal ions on free and immobilized enzyme activity was invested with different ions such as Na^{1+}, Ag^{1+}, Ba^{2+}, Ca^{2+}, Co^{2+}, Cu^{2+}, Mg^{2+}, Ni^{2+}, Sr^{2+}, Zn^{2+}, Al^{3+}, and Cr^{3+}, both enzyme samples were incubated for 24 hours with prepared metal ion and inhibitor (10 mM) solutions. Enzyme activities were measured under optimum

conditions after incubation. However, the solvent effect on free and immobilized enzyme was invested by used (5 %) of organic solvents such as 1-pentanol, 2-propanol, acetonitrile, chloroform, ethanol, ethyl acetate, *n*-hexane, isoamyl alcohol, DCM, DMF, DMSO, and THF were incubated for 24 h at room temperature, the activities were determined. The results were calculated by considering the enzyme activity not exposed to any chemicals as 100 %.

3.5.12. Reusability

To investigate the reusability of UCNP-PEG-L-ASNase, the activity was measured repeatedly for twenty times under optimum conditions. After each activity cycle, the sample removed from the reaction system then washed with ultra-deionized water. After that, a fresh substrate solution is added to the same sample and residual activity was measured according to the standard enzyme procedure. The first enzyme activity was assumed to be 100 % and subsequent activities were calculated relatively.

3.5.13. Storage stability

To determine the storage stability of the free and immobilized enzyme, both enzyme samples were stored at +4 °C and room temperature (~25 °C) for 4 weeks. Then the activity of both enzyme samples was measured every week according to the enzyme activity method specified. The first enzyme activity was considered as 100 %, and subsequent activities were calculated relatively.

3.5.14. Trypsin resistance

The biggest problem of bacterial enzymes used as pharmaceuticals is their low stability against proteases. Therefore, to measure the resistance of both free and immobilized enzymes to trypsin, 2 U of PEG-L-ASNase and UCNP-PEG-L-ASNase was tacked and 10 µL (1.0 mg /mL) of trypsin solution was added and the mixture was incubated with taking the interval 0-2 hours. Then the enzyme was hydrolyzed at certain intervals and their residual activities were measured.

3.5.15. Kinetic parameter

K*m* and V*max* values of free and immobilized enzymes were determined by using Lineweaver-Burk plot by measuring reaction rates at different substrate concentrations.

$$\frac{1}{v} = \left(\frac{K_m}{V_{max}}\right)\left(\frac{1}{S}\right) + \frac{1}{V_{max}} \quad \ldots\ldots (3.4)$$

3.5.16. Activation energy

The activation energy of the free and immobilized enzyme was calculated. The activation energy (*Ea*) represents the energy difference between reactants and the transition state (or activated complex) in a reaction. Ea will be determined using Arrhenius law.

$$ln\,(\mathrm{V}) = \mathrm{lnA} - \mathrm{Ea} \,/\, (\mathrm{RT}) \quad \ldots\ldots (3.5)$$

A is a constant for a given reaction, V is the relative enzyme activity, temperature (T) in Kelvin (*K*), the gas constant (R = 8.314 J mol^{-1} K^{-1}). The activation energy of the free and immobilized enzyme will be calculated from the slope of the graph obtained for the region where the activity increases with temperature.

3.5.17. Laser power, laser distance, and laser exposure time

To determine the optimum laser power for the inducing mechanism the distance and the amount of UCNP-PEG-L-ASNase kept constant, while the laser powers were change to find the optimum power. The laser power was scanned between the range (0-5000 mW) for both 980 nm and 808 nm of the diode laser.

After the optimizing of laser power to find the right distance between laser light and UCNP-PEG-L-ASNase. Keep fixed the laser power and the amount of nanoparticles, while the change in the distance between the diode laser and the tube that contains UCNP-PEG-L-ASNase from (0-5 cm).

Laser exposure time is another parameter to optimizing the work of the laser. To find out if the laser has side effects when exposed for time. After fined the optimum of laser power and distance, keeping constant these two parameters and change the exposure time and starting from zero minutes until 120-minute afterword the reaction was stoped by added TCA, then the activity was measured.

3.5.18. Stability of UCNP-PEG-L-ASNase by laser

The stability of UCNP-PEG-L-ASNase in PBS was investigated by incubated the immobilized nanoparticle with PBS (50 mM, pH 7.4) at 37°C for one week and the activities were measured every single day by induced UCNP-PEG-L-ASNase to its optimum parameter of laser power and distance.

3.5.19. *In vitro* half-life

In order to show the advantage of immobilization, free and immobilized L-ASNase samples (PEG-L-ASNase and UCNP-PEG-L-ASNase) incubated for 1 week at +37 ° C with rat blood serum samples. Then, the activity of the free and immobilized enzyme was measured and their *in vitro* half-lives were calculated [203].

3.5.20. Plasma coagulation

To investigate the effects UCNP-PEG-L-ASNase on plasma coagulation, blood samples were collected from rats with a tube containing 3.2 % sodium citrate then plasma was isolated by centrifugation at 2500 g for 15 minutes at 20 °C. In the next, 200 µL of plasma was mixed with 50 µL UCNP-PEG-L-ASNase and 50 and 200 µg mL^{-1} as final concentrations were prepared. Samples were incubated at 37 ° C for 3 minutes. Then, the Prothrombin time (PT) and active partial thromboplastin time (APTT) of blood samples were determined by an automatic coagulometer [203]. (These parameters were realized through service procurement from Inonu University Turgut Özal Medical Center).

3.5.21. *In vitro* cytotoxicity

In cytotoxicity studies, L-929 mouse fibroblast cells were grown in Dulbecco's Modified Eagle's medium (DMEM) contain 10 % FBS, 1 % penicillin /streptomycin, and incubate at 37 ° C in an atmosphere of 5 % CO_2. The cells were seeded into 96-well plates with 10^4 cells per well to grow for 24 hours. Then different concentrations (12.5, 25, 50, 100, 200 µg mL^{-1}) of UCNP and UCNP-PEG-L-ASNase solutions prepared with DMEM, were applied to the cells and were incubated at (37°C under 5 % CO_2) for 24, 48, and 72 hours in cytotoxicity studies. Thereafter, the medium was removed and replaced with an MTT test. After the application for 24, 48, and 72 hours

the medium removed and 90 µL of fresh DMEM, then 10 µL of 5 mg/mL of MTT((3-(4,5-dimethylthiazol-2-yl)-2,5-diphenyltetrazolium bromide) in PBS solution was applied to the cells incubated under the same conditions for 4 hours. After 4 hours, the DMEM and MTT were removed and replaced with 100 µL of DMSO. The resulting color was measured with a microreader reader at 540 nm. Cell viability results were given in % relative.

3.5.22. *In vitro* catalytic activity

Human acute leukemia (HL-60) cells were used to examine the *in vitro* catalytic activity of the $NaYF_4$:Nd^{3+}, Yb^{3+}, Er^{3+}/ICPTES-PEG-L-ASNase selected according to greater NIR inducement ratio. HL-60 ALL cells were grown by using RPMI solution containing 10 % FBS and 1 % penicillin /streptomycin in an atmosphere of 5 % CO_2 at 37 °C [204]. Groups were determined as $NaYF_4$:Nd^{3+}, Yb^{3+}, Er^{3+}/ICPTES, PEG-L-ASNase, NIR, $NaYF_4$:Nd^{3+}, Yb^{3+}, Er^{3+}/ICPTES+NIR, $NaYF_4$:Nd^{3+},Yb^{3+}, Er^{3+}/ ICPTES-PEG-L-ASNase, and $NaYF_4$:Nd^{3+}, Yb^{3+}, Er^{3+}/ICPTES-PEG-L-ASNase+ NIR. NIR exposure time and NIR power values were applied 30 minutes and 150 milliwatts, respectively, as optimum values determined as a result of UCNP-PEG-L-ASNase triggering studies. The *in vitro* catalytic activity of the samples was correlated with the inhibition of the growth of HL-60 cells. Cell viability was determined by the MTT test described before.

4. RESULTS

4.1. Characterization

4.1.1. Characterization of UCNPs radiating green at 980 nm ($NaYF_4$: Yb^{3+}, Er^{3+})

4.1.1.1. X-Ray Diffraction (XRD)

XRD spectra of UCNP radiating under at 980 nm laser excitation are presented in Figure 4.1. The XRD pattern of the polyethyleneimine and functional silica-coated nanoparticles is similar. The planes where the peaks are mixed indicate that the hexagonal crystal structure was formed and its sharpness indicated the degree of purity. As expected, PEI added during synthesis did not change the crystal structure. After coating with different silane compounds GPTMS and ICPTES, the surfaces of particles have hexagonal crystal structure with silane compounds, no change in the crystal structure was observed.

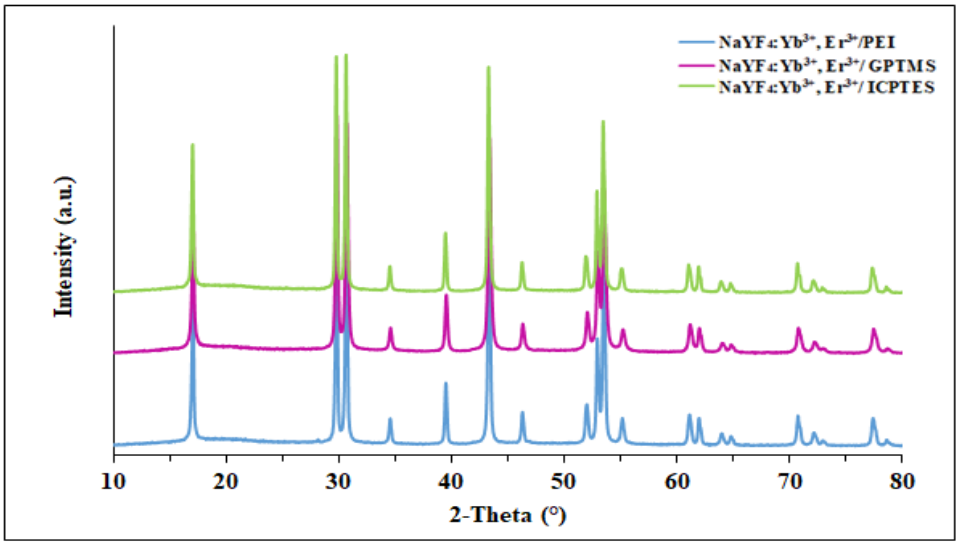

Figure 4.1: XRD spectra of $NaYF_4$:Yb^{3+}, Er^{3+}/PEI, $NaYF_4$: Yb^{3+}, Er^{3+}/GPTMS and $NaYF_4$: Yb^{3+}, Er^{3+}/ICPTES.

4.1.1.2. Fourier-Transform Infrared Spectroscopy (FTIR)

In the spectrum, the peaks at 3400-3300 cm^{-1} and 3000-2850 cm^{-1} correspond to N-H stretching, and C-H stretching, respectively, due to PEI. The peaks of N-H in-plane bending vibrations are observed between 1600 cm^{-1} and 900-700 cm^{-1}. The characteristic C-N bond stretching is seen in the range of 1120-1050 cm^{-1}. The signal observed at 470 cm^{-1} is the tensile vibrations of the PEI bond. While the signals of the presence of isocyanate (ICPTES) and epoxy (GPTMS) functionalized UCNPs, C = N

stretching vibrations were observed at 1558 cm^{-1} due to the isocyanate functional group. Stretching of the epoxy functional ring was observed at 1739 cm^{-1} (C-C), 1605 cm^{-1} (C-O), and 1397 cm^{-1} (C-H). The sharp peaks seen in the samples at 930 cm^{-1} and at 1055 cm^{-1} belong to Si-OH and Si-O-Si vibrations are the most important signs of the presence of silane coating on the surface as shown in Figure 4.2.

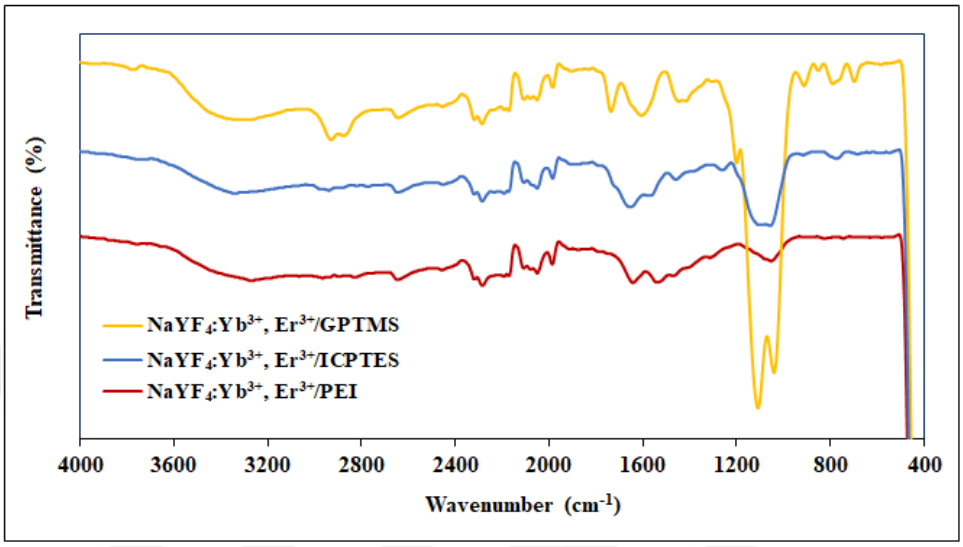

Figure 4.2: FTIR spectra of $NaYF_4$: Yb^{3+}, Er^{3+}/PEI, $NaYF_4$: Yb^{3+}, Er^{3+}/GPTMS and $NaYF_4$:Yb^{3+}, Er^{3+}/ICPTES.

4.1.1.3. Thermogravimetric (TGA) and zeta potential

The decrease in surface charge is due to the silica coating. As can be seen from the thermograms given in Figure 4.3, the weight losses caused by the organic polymer and organic polymer-silica coatings on the surface are quite low. This anticipated situation indicates that the coatings are extremely thin. As can be seen from the TG curves, the surface coated with GPTMS particle is higher stability than the others.

The zeta potential of the particle determined in the fixed electrolyte environment indicates the presence of groups on the surface. Hydrodynamic diameters and surface charge measurements of synthesized $NaYF_4$: Yb^{3+}, Er^{3+}/PEI, $NaYF_4$: Yb^{3+}, Er^{3+} /GPTMS and $NaYF_4$: Yb^{3+}, Er^{3+}/ICPTES up-converting particles were measured. The tendency to agglomerate increases due to the tendency to reduce the rising surface energy as the particle size gets smaller. The zeta potential values of the bare silane coated UCNPs whose surfaces contain different functional groups are presented in Table 4.1. As can be seen from the table, zeta potentials decreased after the particle surfaces were coated with silane compounds.

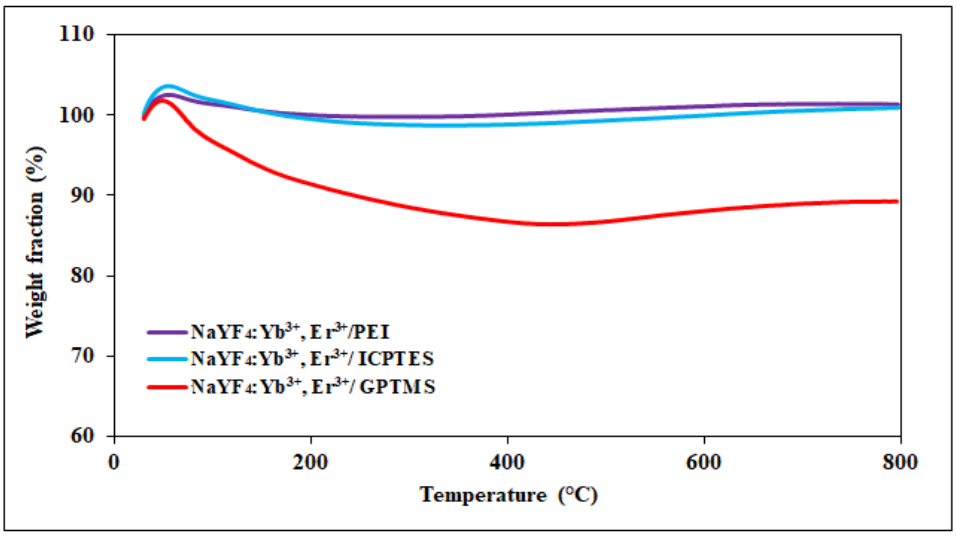

Figure 4.3: Thermograms of $NaYF_4$: Yb^{3+}, Er^{3+}/PEI, $NaYF_4$: Yb^{3+}, Er^{3+}/GPTMS, and $NaYF_4$: Yb^{3+}, Er^{3+}/ICPTES.

Table 4.1: Zeta potentials of $NaYF_4$: Yb^{3+}, Er^{3+} coated with PEI, GPTMS, and ICPTES.

Sample	Zeta potential (mV)
$NaYF_4$: Yb^{3+}, Er^{3+}/PEI	59.07 ± 0.42
$NaYF_4$: Yb^{3+}, Er^{3+}/GPTMS	37.4 ± 0.25
$NaYF_4$: Yb^{3+}, Er^{3+}/ICPTES	52.4 ± 1.48

4.1.1.4. X-Ray Photoelectron Spectroscopy (XPS)

The XPS spectrum of $NaYF_4$: Yb^{3+}, Er^{3+}/GPTMS and $NaYF_4$: Yb^{3+}, Er^{3+}/ICPTES UCNPs were examined, it is seen that there are peaks of all lanthanide cations and anions in the structure Figure 4.4. The presence of peaks of Si 2p and Si 2s bands in the structure was observed. The presence of silicon peaks indicates that the UCNPs surfaces were successfully coated with ICPTES and GPTMS.

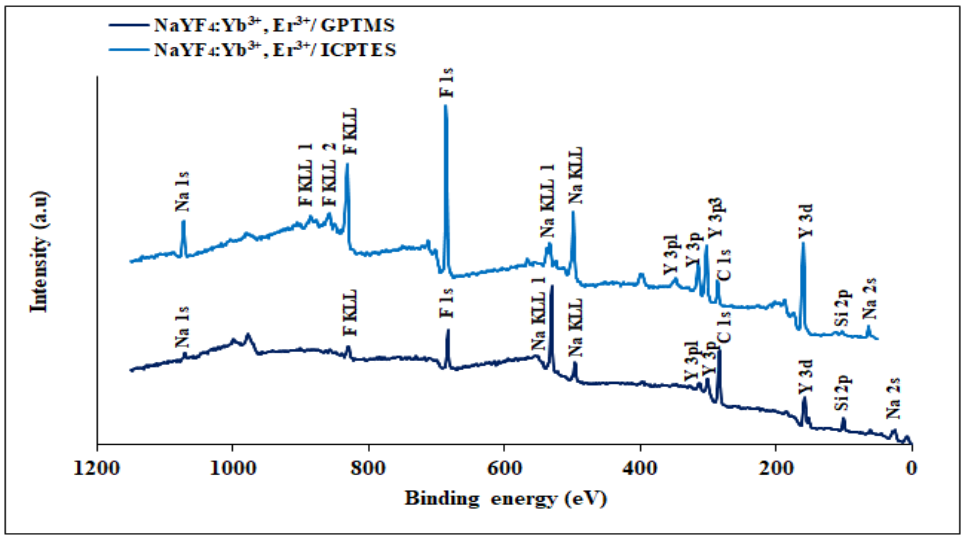

Figure 4.4: XPS spectra of $NaYF_4$: Yb^{3+}, Er^{3+}/GPTMS, and $NaYF_4$: Yb^{3+}, Er^{3+} /ICPTES.

4.1.1.5. Transmittance Electron Microscopy (TEM) and EDX

TEM images of $NaYF_4$: Yb^{3+}, Er^{3+}/PEI UCNPs synthesized by the hydrothermal method are given in Figure 4.5. Both rod and cubic structures were formed. Rod structures are generally 1000x50 nm in size, while Spherical structures are around 50 nm in size as seen in Figure 4.5.

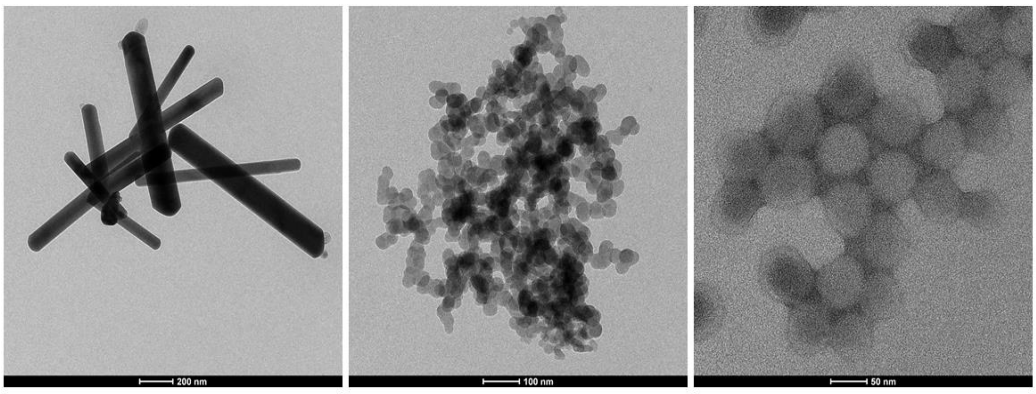

Figure 4.5: TEM images of $NaYF_4$: Yb^{3+}, Er^{3+}/PEI.

While in Figure 4.6, it was determined that the particle shape and size, the desired hexagonal crystal structure was formed from the SAED patterns and the elemental compositions determined theoretically from EDX spectra and the microscope images of the given $NaYF_4$: Yb^{3+}, Er^{3+}/GPTMS surfaces bare and silane-coated. Particle size growth after silane coatings is also evident from TEM images.

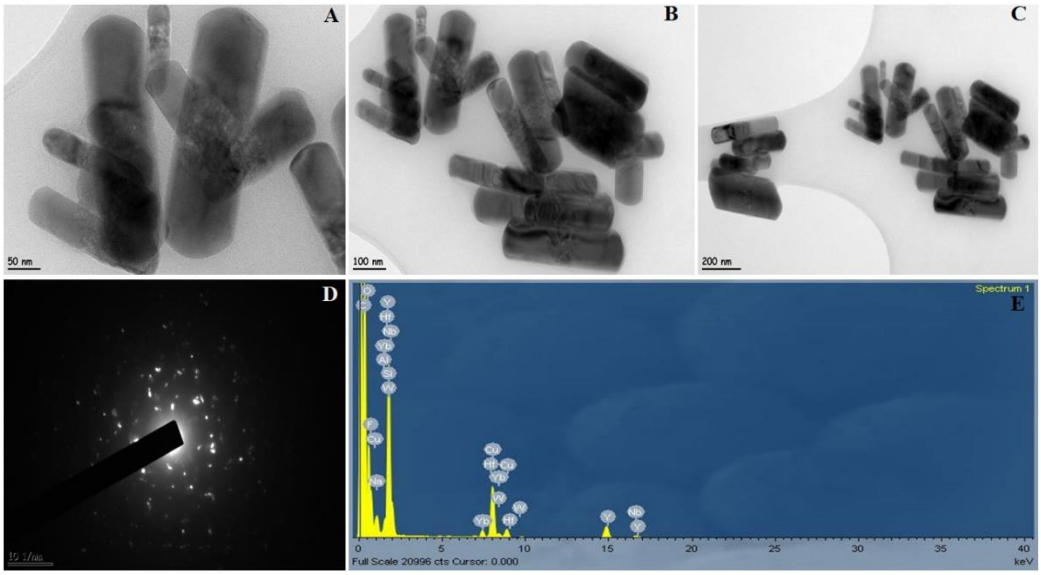

Figure 4.6: Surface bare (A), GPTMS coated (B) $NaYF_4$: Yb^{3+}, Er^{3+} UCNP's TEM image, SAED pattern (C) and EDX spectrum (D).

The Figure 4.7, EDX spectra were obtained from and the microscope images of $NaYF_4$: Yb^{3+}, Er^{3+}/ICPTES surfaces bare and silane-coated. Particle size growth after silane coatings is also evident from TEM images.

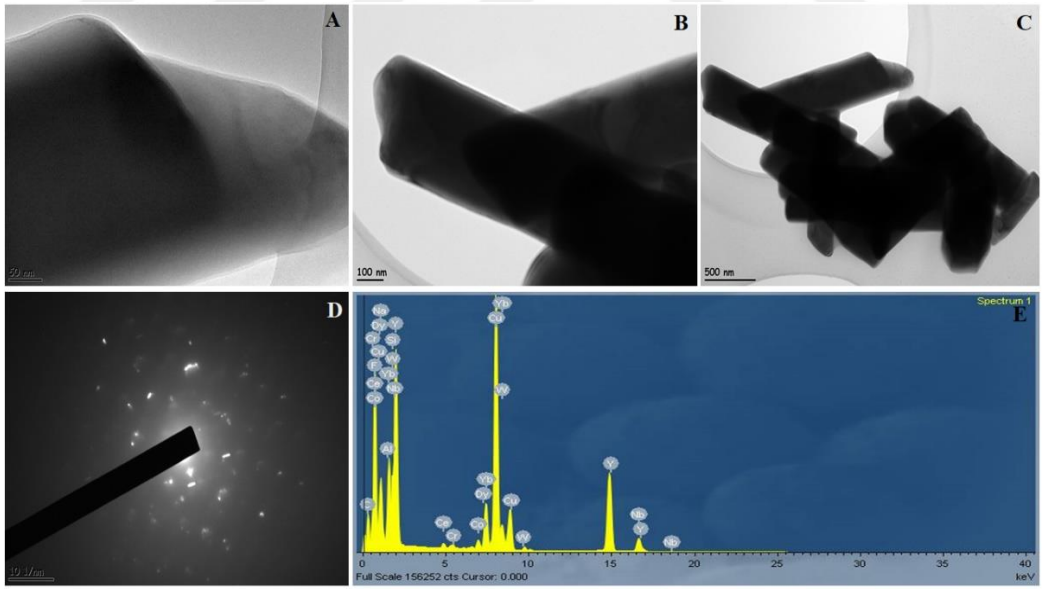

Figure 4.7: Surface bare (A), ICPTES coated (B) $NaYF_4$: Yb^{3+}, Er^{3+} UCNP's TEM image, SAED pattern (C) and EDX spectrum (D).

4.1.1.6. Fluorescence emission spectra

The luminescence properties of the synthesized UCNPs were characterized by fluorescence spectrometry under 980 nm laser excitation. Since Yb^{3+} has a wide

absorption peak at 980 nm, it is chosen as the activator of Er^{3+}, which enables energy transfer from Yb^{3+} to Er^{3+} [205]. As can be seen from the spectrum given in Figure 4.8, two characteristic peaks are observed in the spectrum of $NaYF_4$: Yb^{3+}, Er^{3+} UCNPs with bare surfaces and silane coated, red and strong around 650 nm, green and weak around 540 nm.

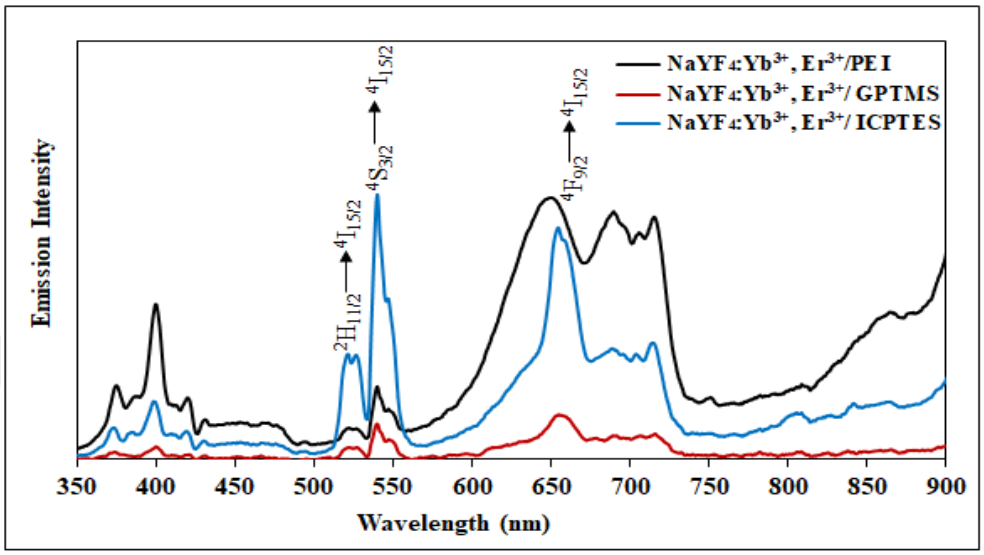

Figure 4.8: Fluorescence emission spectra of UCNPs.

4.1.2. Characterization of UCNPs radiating green at 808 nm ($NaYF_4$: Nd^{3+}, Yb^{3+}, Er^{3+})

4.1.2.1. X-Ray Diffraction (XRD)

During the synthesis of $NaYF_4$: Yb^{3+}, Er^{3+} based UCNPs, Nd^{3+} was added to the structure with laser excitation at a wavelength of 808 nm to produce ultraviolet and visible radiation particles. Figure 4.9 shows the XRD spectra of UCNPs synthesized for this purpose, bare surfaces, coated with PEI and silane compounds with different functional groups. The peaks observed in the spectrum at 2θ = 17.38, 30.48 °, 30.88 °, 34.19 °, 40.06 °, 43.75 °, 50.35 °, 54.65 °, 62.64 °, 64.34 ° belong to the hexagonal β-$NaYF_4$ crystal phase, respectively (100), (110) , (011), (200), (111), (201), (300), (102), (112) and (220) correspond to planes (JCPDS No. 16-0334) (Klier and Kumke 2015, Reddy et al. 2019). The addition of Nd^{3+} did not cause any change in the structure.

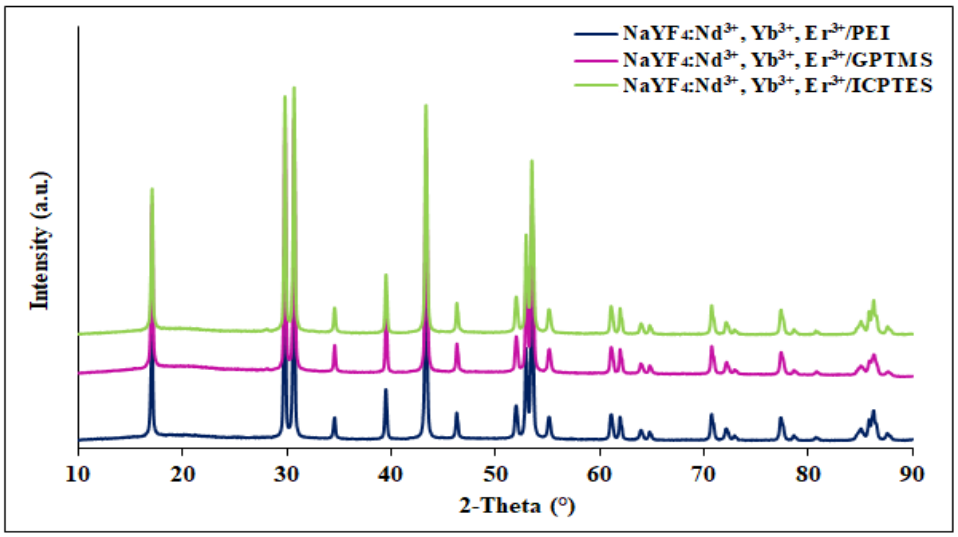

Figure 4.9: XRD spectra of $NaYF_4$:Nd^{3+}, Yb^{3+}, Er^{3+}/PEI, $NaYF_4$: Nd^{3+}, Yb^{3+}, Er^{3+}/GPTMS, and $NaYF_4$: Nd^{3+}, Yb^{3+}, Er^{3+}/ICPTES.

4.1.2.2. Fourier-Transform Infrared Spectroscopy (FTIR)

The presence of functional groups on the surfaces of the synthesized particles were evaluated by FTIR spectra. After the naked Nd/UCNP surfaces were coated with organic polymers, the changes in the types and intensities of the functional groups were followed through FTIR. In Figure 4.10, weak peaks between 3420-3320 cm^{-1} are due to the N-H stretching, and vibrations between 2960- 2870 cm^{-1} are due to the aliphatic C-H stretching of PEI. N-H in-plane bends, C-N bond stretching in PEI, N-H in-plane bending around 1600 cm^{-1}, vibrations between 1120 - 1050 cm^{-1} represent C-N bond stress in PEI, and peaks observed between 900-700 cm^{-1} represent N-H in-plane bending. The peak observed around 470 cm^{-1} is the stress vibrations of the PEI-Ln^{3+} bond. Furthermore, the modification of UCNP with epoxy functional group on the surface $NaYF_4$: Nd^{3+}, Yb^{3+}, Er^{3+}/GPTMS, typical aliphatic C-H stresses at 2988 and 2872 cm^{-1}, C = O at 1636 cm^{-1}, C = N at 1558 cm^{-1} and Si-O at 1088 cm^{-1}. -Si bond tensile vibrations are seen were included. When UCNPs are coated with GPTMS, in addition to the aliphatic C-H stresses at 2988 and 2872 cm^{-1}, the stresses of the epoxy ring came at 1739 cm^{-1} C-O, 1605 cm^{-1} C-C, and 1397 cm^{-1} C-H. The shear vibration of the methyl group is observed at 1194 cm^{-1}, and the stresses belonging to the methoxy group at 1103 and 1045 cm^{-1}. While the isocyanate functional $NaYF_4$: Nd^{3+}, Yb^{3+}, Er^{3+}/ICPTES, aliphatic C-H stresses at 2988 and 2872 cm^{-1}, C = O at 1636 cm^{-1}, C = N stresses at 1558 cm^{-1} and 1088 cm^{-1} shows the stress vibrations of the Si-O-Si bond.

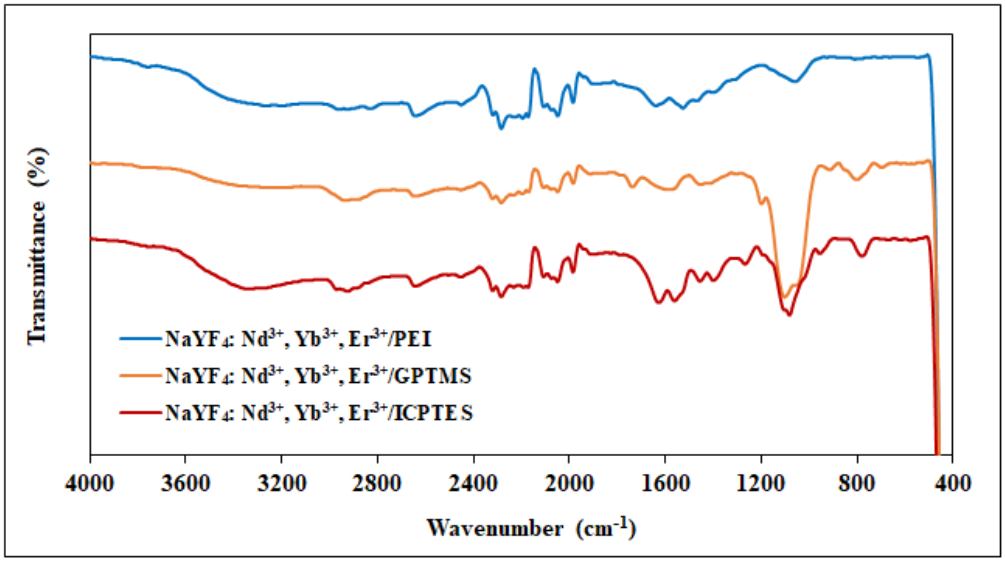

Figure 4.10: FTIR spectra of $NaYF_4$: Nd^{3+}, Yb^{3+}, Er^{3+}/PEI, $NaYF_4$: Nd^{3+}, Yb^{3+}, Er^{3+}/GPTMS and $NaYF_4$: Nd^{3+}, Yb^{3+}, Er^{3+}/ICPTES.

4.1.2.3. Thermogravimetric (TGA) and zeta potential

The thermogram is shown in Figure 4.11, when heat treatment is applied to UCNPs whose surfaces are coated with a silane compound, a mass loss in the range of 150-400 ° C is observed due to the burning of the aliphatic structure to which the OH groups of the silicon compounds and the functional ends are attached. The amount of mass loss allows us to make an estimate of the coating thickness on the surface. The change in mass fractions depending on the temperature is very low. In addition, after 400 ° C, a relatively mass increase is observed due to the crystal structure transformation. It was examined that mass loss decreases after silica coating. During the coating of Nd-UCNP surfaces, the hydrolysis of the alkoxy groups in ICPTES and GLYMO was completed and the thin PEI layer was used as an interface with silica, causing a change in mass loss. The very weak mass losses observed after the functional silica coating is due to the alkyl chain of the functional end.

Zeta potential results of UCNPs planned to be used for 808 nm laser stimulation are given In Table 4.2. The zeta potentials of $NaYF_4$: Nd^{3+}, Yb^{3+}, Er^{3+} coated PEI was founded over 50 mV. This is very important, as mentioned earlier, to ensure sufficient electrostatic attraction for both stable dispersion formation and physical interaction.

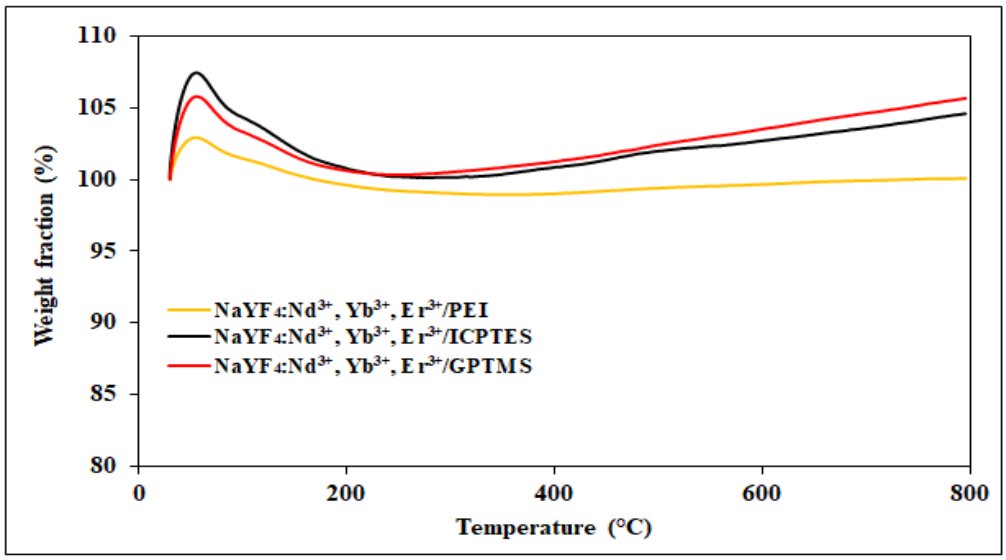

Figure 4.11: Thermograms of $NaYF_4$:Nd^{3+}, Yb^{3+}, Er^{3+}/PEI, $NaYF_4$: Nd^{3+}, Yb^{3+}, Er^{3+}/GPTMS, and $NaYF_4$: Nd^{3+}, Yb^{3+}, Er^{3+}/ICPTES.

Table 4.2: Zeta potentials of $NaYF_4$:Nd^{3+}, Yb^{3+}, Er^{3+} coated with PEI, GPTMS, and ICPTES.

Sample	Zeta potential (mV)
$NaYF_4$:Nd^{3+}, Yb^{3+}, Er^{3+}/PEI	51.5 ± 0.53
$NaYF_4$:Nd^{3+}, Yb^{3+}, Er^{3+}/GPTMS	41.9 ± 1.85
$NaYF_4$:Nd^{3+}, Yb^{3+}, Er^{3+}/ICPTES	42.7 ± 0.55

4.1.2.4. X-Ray Photoelectron Spectroscopy (XPS)

The XPS spectrum of $NaYF_4$: Nd^{3+}, Yb^{3+}, Er^{3+}/GPTMS and $NaYF_4$: Nd^{3+}, Yb^{3+}, Er^{3+} /ICPTES UCNPs were examined in Figure 4.12, the presence of silicon atoms on the surface and the oxidation step is aimed to be determined. The spectrum shows the oxidation states of all the elements in the structure. The peaks of Si 2s and Si 2p seen in the 110-140 eV region are evidence of the presence of silane groups on the surface.

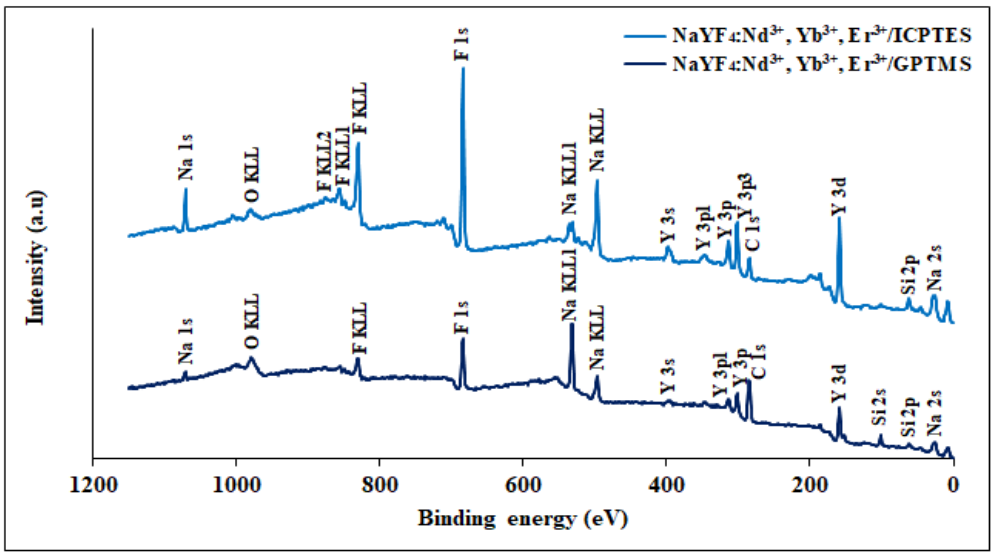

Figure 4.12: XPS spectra of $NaYF_4$: Nd^{3+}, Yb^{3+}, Er^{3+}/GPTMS, and $NaYF_4$: Nd^{3+}, Yb^{3+}, Er^{3+} /ICPTES.

4.1.2.5. Transmittance Electron Microscopy (TEM) and EDX

TEM images of UCNPs containing $NaYF_4$: Nd^{3+}, Yb^{3+}, Er^{3+}/PEI were given in Figure 4.13, which are accepted as optimized value, spherical particles smaller than 50 nm belong to the cubic structures observed in the XRD spectrum. It was seen Nd-UCNPs synthesized by the hydrothermal method are formed in rod structures, and UCNPs containing $NaYF_4$: Nd^{3+}, Yb^{3+}, Er^{3+}/PEI have an average length of 500 nm and a width of 100 nm. The rod structures obtained are in hexagonal crystal phase structure. Nanospheres were also found on TEM images. Such structures show that they formed in some cubic crystal phases. The observation of the peaks of the cubic phase in the XRD confirms that.

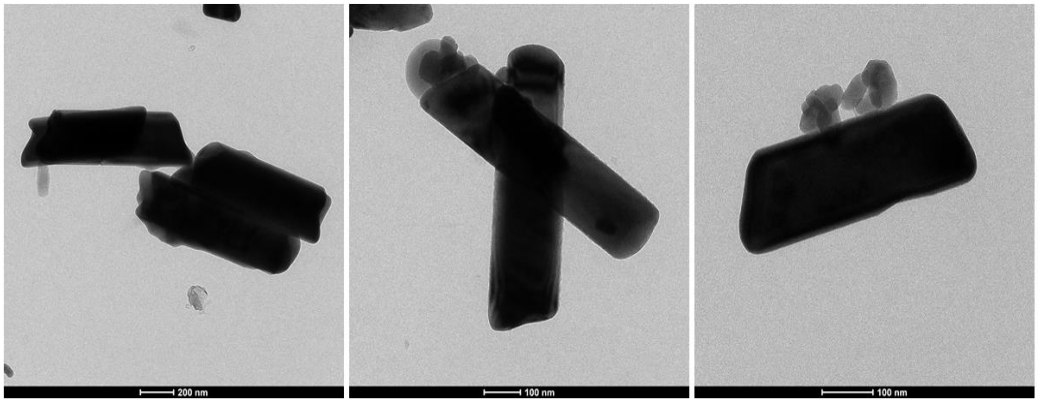

Figure 4.13: TEM images of $NaYF_4$: Nd^{3+}, Yb^{3+}, Er^{3+}/PEI.

The TEM image for the functionalized Nd-UCNPs with GPTMS were given in Figures 4.14. It is understood from the RTEM images that the particle surfaces are coated with GPTMS. The surface of UCNP containing $NaYF_4$: Nd^{3+}, Yb^{3+}, Er^{3+}/GPTMS have 150 nm thick.

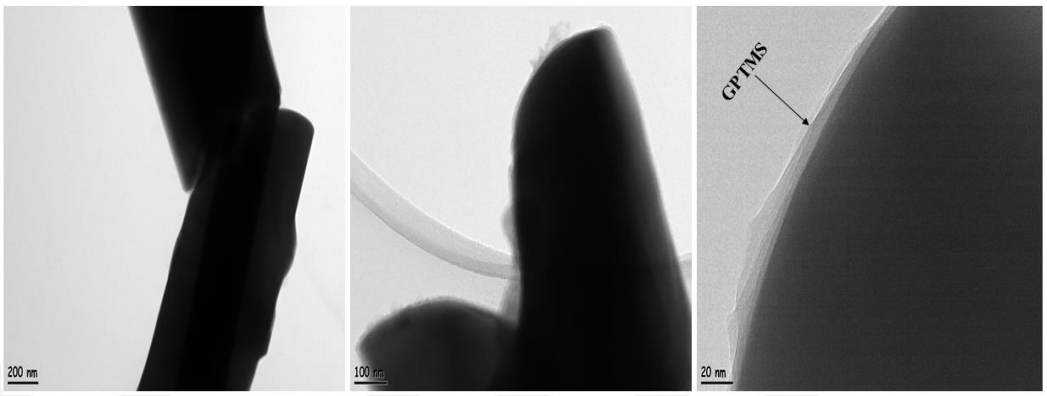

Figure 4.14: TEM images of $NaYF_4$: Nd^{3+}, Yb^{3+}, Er^{3+}/GPTMS.

Furthermore, it was determined that UCNPs containing $NaYF_4$: Nd^{3+}, Yb^{3+}, Er^{3+} /ICPTES are 300 x60 nm in size and the coating thickness is 10 nm. TEM-EDX analysis results show that the structure suitable for the desired elemental composition has been obtained. It is once again understood from the SAED pattern that the particles have high crystallinity. TEM images for the surfaces functionalized of Nd-UCNPs with ICPTES were given in Figures 4.15. It is understood from the RTEM, EDX spectrum, and SAED images that the $NaYF_4$: Nd^{3+}, Yb^{3+}, Er^{3+}/ICPTES particle were successfully coated with the isocyanate group. It has been determined that the particles are 300x60 nm in size and the ICPTES coating thickness is 10 nm. TEM-EDX analysis results show that the structure suitable for the desired elemental composition has been obtained. It is once again understood from the SAED pattern that the particles have high crystallinity.

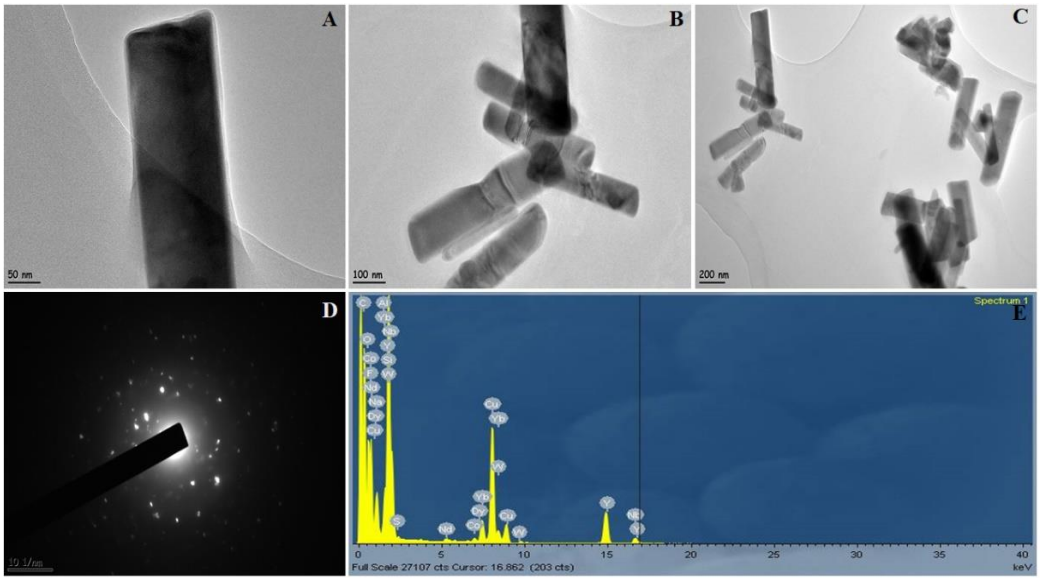

Figure 4.15. EDX spectrum and SAED pattern of UCNPs of $NaYF_4$: Nd $^{3+}$, Yb^{3+}, Er^{3+}/ICPTES.

4.1.2.6. Fluorescence emission spectra

The fluorescence spectra of $NaYF_4$: Nd^{3+}, Yb^{3+}, Er^{3+} UCNP, surfaces coated with PEI, GPTMS, and ICPTES are shown in Figure 4.16. Since the emissions under laser stimulation at this wavelength are low and not smooth, the spectrum appears to be more complex than at 980 nm excitation. $NaYF_4$: Nd^{3+}, Yb^{3+}, Er^{3+} based UCNPs have $^2H_{11/2} \rightarrow {}^4I_{15/2}$ at 525 nm and $^4S_{3/2} \rightarrow {}^4I_{15/2}$ transitions at 545 nm [206].

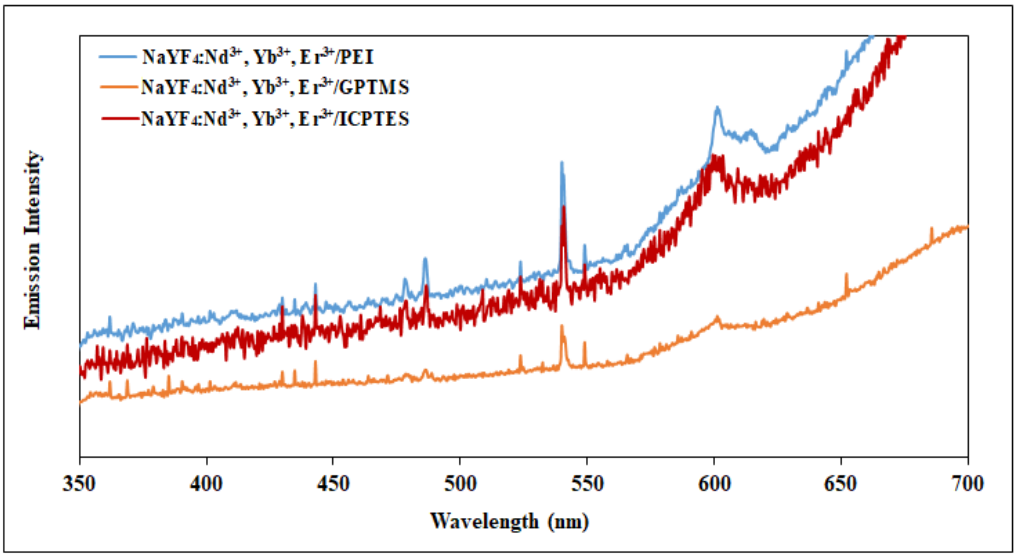

Figure 4.16: Fluorescence emission spectra of UCNPs.

4.1.3. Characterization of UCNP/PEG-L-ASNase

4.1.3.1. X-Ray Diffraction (XRD)

After PEG-L-ASNase immobilization, XRD analysis was performed to check the purity and crystallinity of the UCNPs. In Figure 4.17, XRD spectra of PEG-L-ASNase immobilized UCNPs are given. There is no significant change in XRD spectra compared to the non-immobilized PEG-L-ASNase. The sharp diffraction peaks are seen in all XRD spectra clearly prove that UCNPs retain their crystallinity after PEG-L-ASNase immobilization.

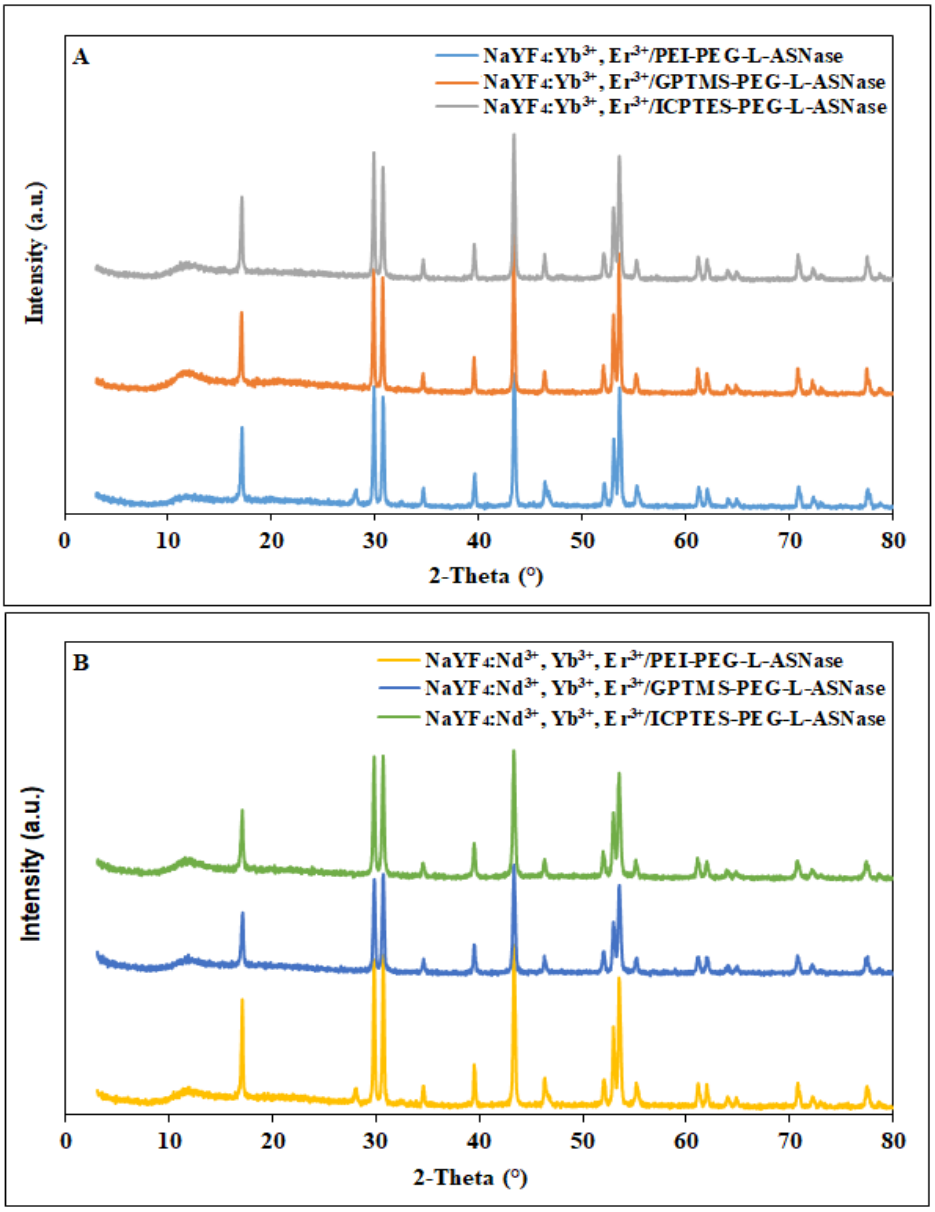

Figure 4.17: XRD spectra of PEG-L-ASNase immobilized UCNP particles, UCNPs 980 nm (A), and UCNPs 808 nm (B).

4.1.3.2. Fourier-Transform Infrared Spectroscopy (FTIR)

After enzyme immobilization, O-H stresses arising from the PEG structure and coming around 3400 cm^{-1} increased. In GPTMS and ICPTES coated UCNPs, it is observed that the peak intensities of the vibration of Si-OH bonds at 930 cm^{-1} and 1055 cm^{-1} decrease. This is an indication that the enzyme exists on the UCNP surface. In the spectrum, the C-O signal of the epoxy group at 1700 cm^{-1} in the GPTMS-coated UCNPs, the C = N peak at 1650 cm^{-1} of the isocyanate group, and the peaks of the N-H stresses observed at 1450 cm^{-1} in PEI-coated UCNPs are not visible due to binding as shown in Figure 4.18 A and B.

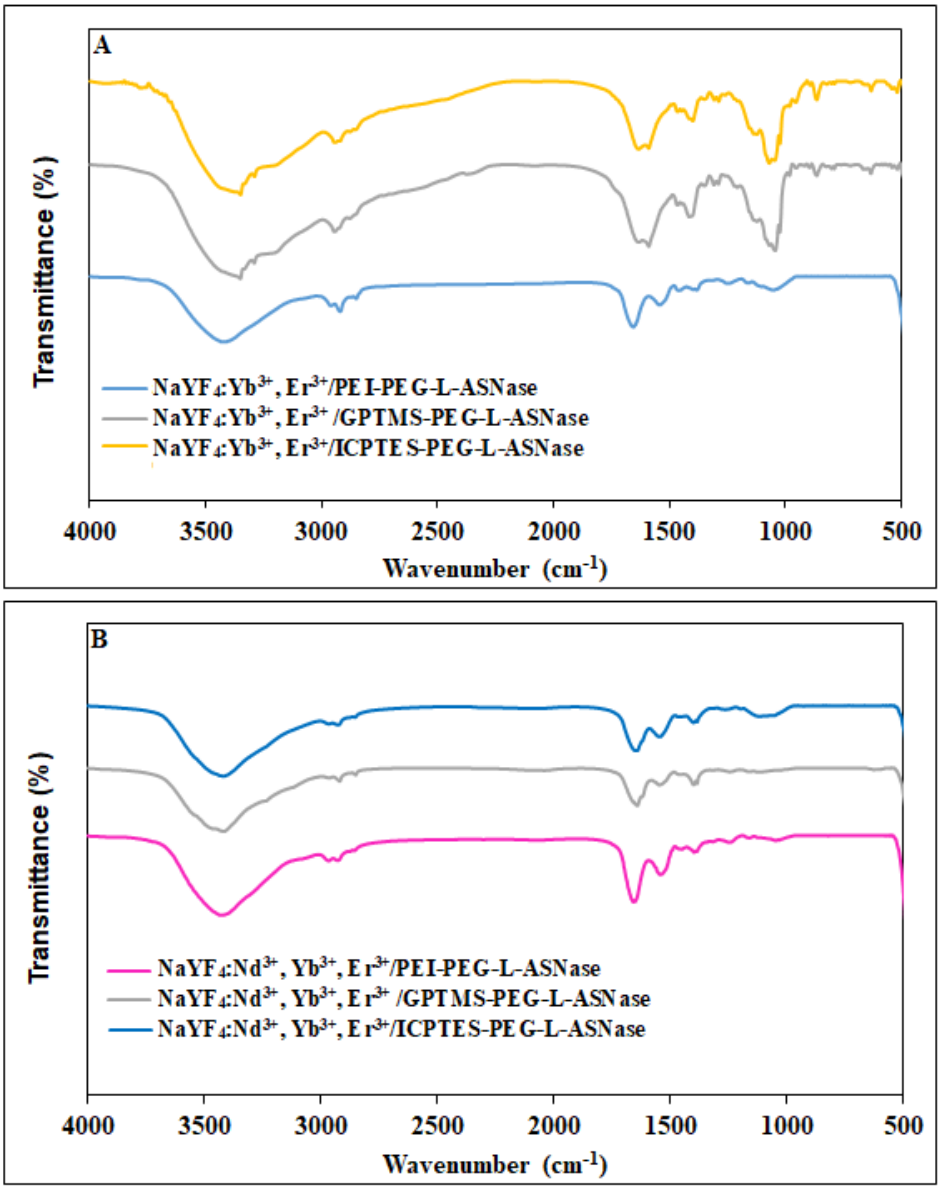

Figure 2.18: FTIR spectra of PEG-L-ASNase immobilized UCNPs, UCNPs 980 nm (A), and UCNPs 808 nm (B).

4.1.3.3. Transmittance Electron Microscopy (TEM)

Figure 4.19, CTEM and EDX images of PEG-L-ASNase loaded UCNPs that have the ability to radiate under 980 nm wavelength laser stimulation. Generally, particle sizes remain around 100 nm after enzyme loading.

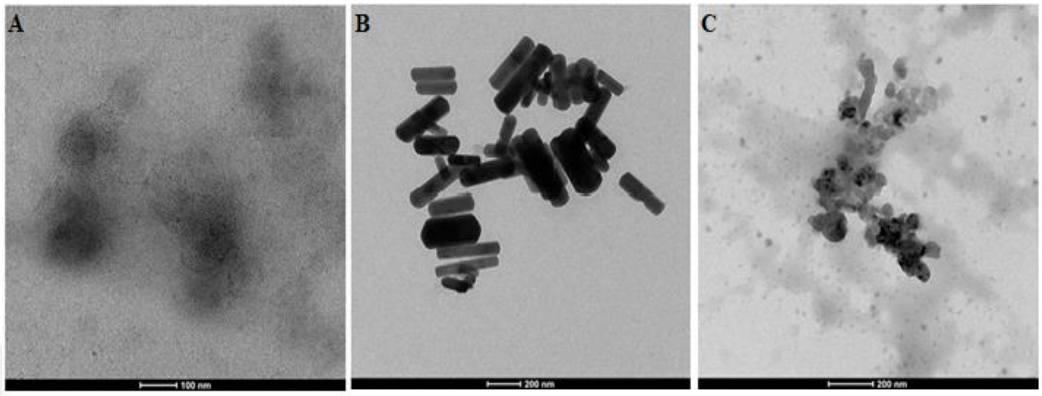

Figure 4.19: TEM images of $NaYF_4$:Yb^{3+}, Er^{3+}/PEI-PEG-L-ASNase (A), $NaYF_4$: Yb^{3+}, Er^{3+}/GPTMS-PEG- PEG-L-ASNase (B), and $NaYF_4$:Yb^{3+}, Er^{3+}/ICPTES-PEG-PEG-L-ASNase (C).

As a result of immobilization and stimulation with 808 nm laser, $NaYF_4$: Nd^{3+}, Yb^{3+}, Er^{3+}/PEI-PEG-L-ASNase, $NaYF_4$: Nd^{3+}, Yb^{3+}, Er^{3+}/GPTMS-PEG-L-ASNase, and $NaYF_4$: Nd^{3+}, Yb^{3+}, Er^{3+}/ICPTES-PEG-L-ASNase Electron microscope images of UCNPs were shown in Figure 4.20.

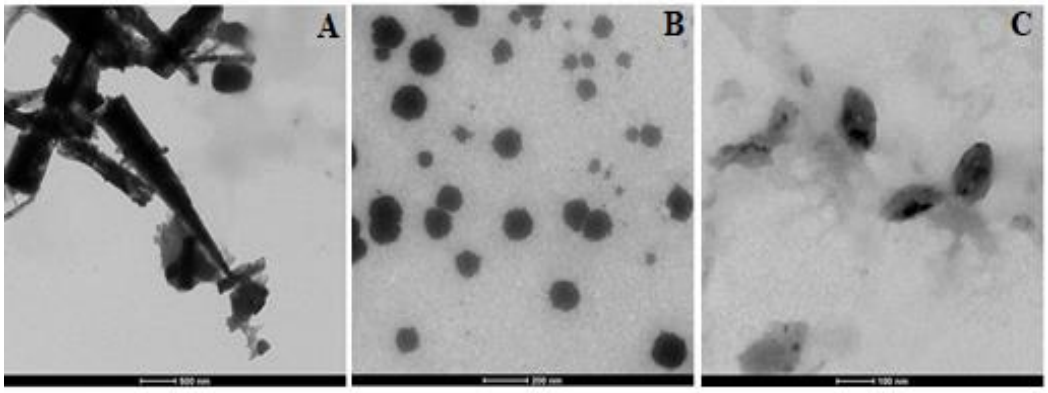

Figure 4.20: TEM images of $NaYF_4$: Nd^{3+}, Yb^{3+}, Er^{3+}/PEI-PEG-L-ASNase (A), $NaYF_4$:Nd^{3+},Yb^{3+},Er^{3+}/GPTMS-PEG-PEG-L-ASNase (B), and $NaYF_4$:Nd^{3+},Yb^{3+}, Er^{3+}/ICPTES-PEG-L-ASNase (C).

4.1.3.4. EDX analysis

Figure 4.21 and 4.22, show the EDX spectra of PEG-L-ASNase immobilized UCNPs. When the pure forms of UCNPs are compared with EDX spectra, the increase in C, N, and O peak intensities confirms that the PEG-L-ASNase enzyme has been successfully immobilized to UCNPs. In addition, the presence of a new S peak is another evidence supporting the success in immobilization.

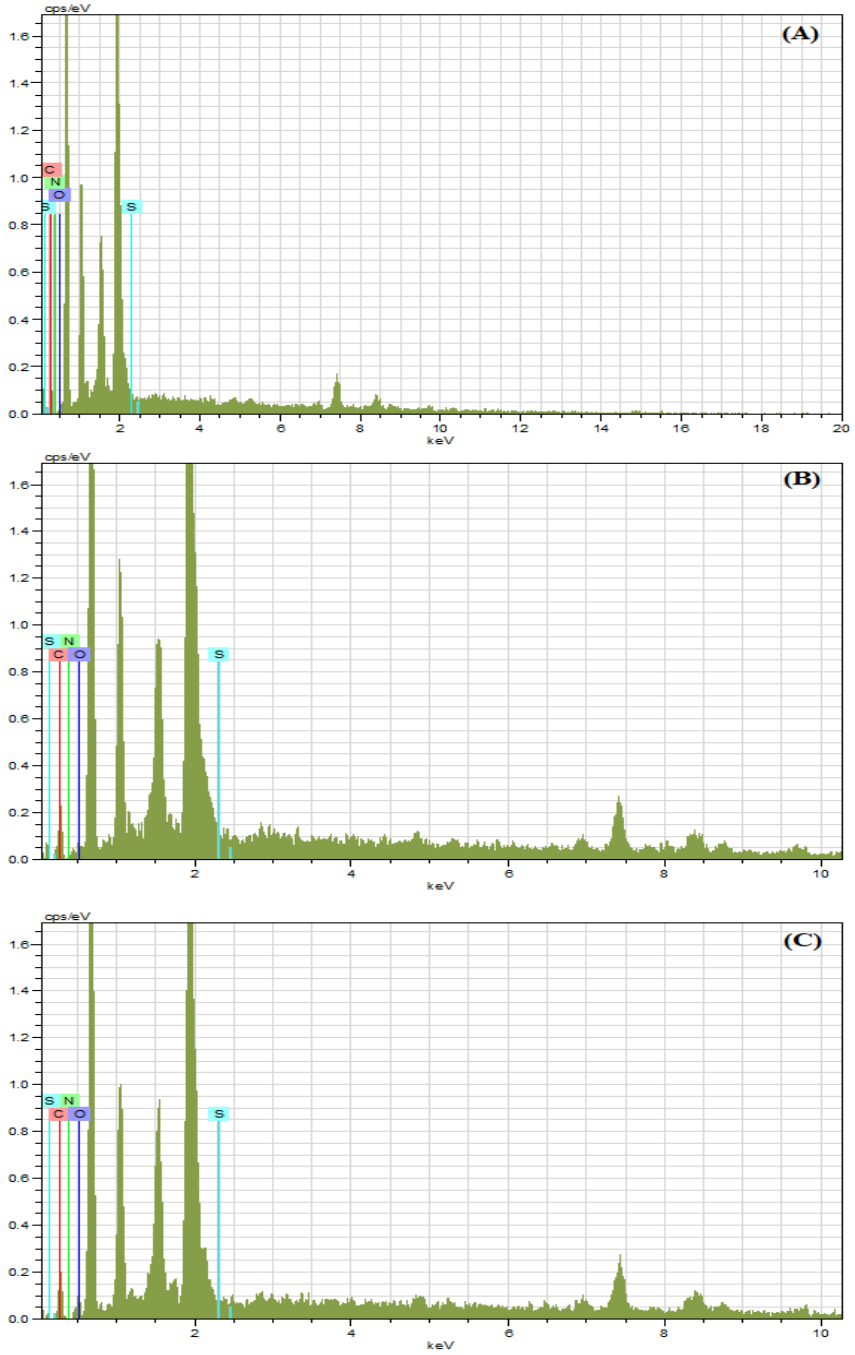

Figure 4.21: EDX for 980 nm UCNPs, $NaYF_4$: Yb^{3+}, Er^{3+}/PEI-PEG-L-ASNase (A), $NaYF_4$: Yb^{3+}, Er^{3+}/GPTMS-PEG-L-ASNase (B), and $NaYF_4$: Yb^{3+}, Er^{3+}/ICPTES-PEG-L-ASNase (C).

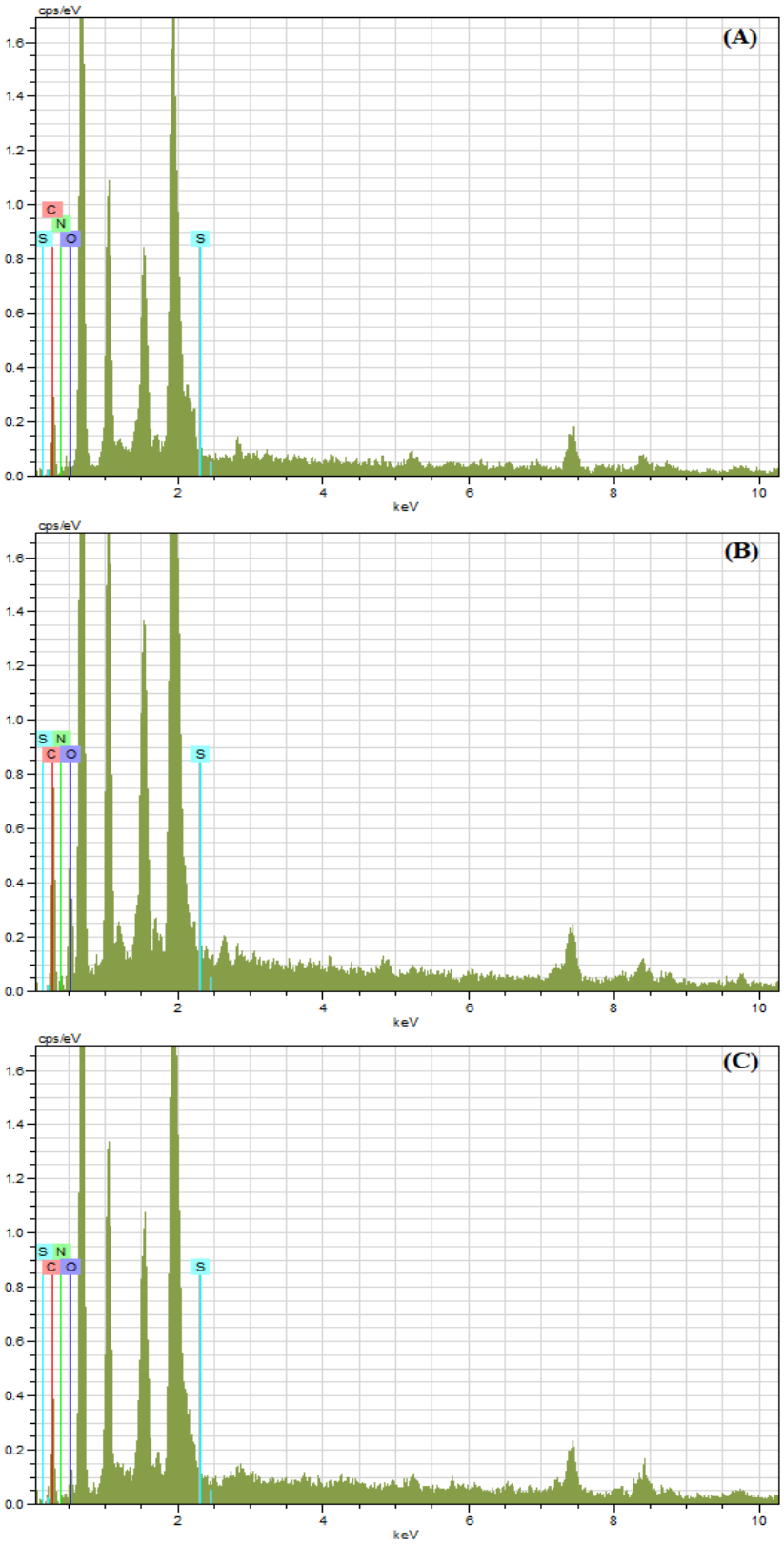

Figure 4.22: EDX for 808 nm UCNPs, $NaYF_4$: Nd^{3+}, Yb^{3+}, Er^{3+}/PEI-PEG-L-ASNase (A), $NaYF_4$: Nd^{3+}, Yb^{3+}, Er^{3+} /GPTMS-PEG-L-ASNase (B), and $NaYF_4$: Nd^{3+}, Yb^{3+}, Er^{3+}/ICPTES-PEG-L-ASNase (C).

4.1.3.5. Fluorescence emission spectra

In the Figure 4.23 A, fluorescence spectra of 980 nm laser excitation, the surface of the enzyme-loaded $NaYF_4$: Yb^{3+}, Er^{3+} UCNP's spectrum from $^4S_{3/2} \rightarrow {}^4I_{15/2}$ electronic transition around 540 nm and $^4F_{9/2} \rightarrow {}^4I_{15/2}$ around 650 nm. Emissions have occurred from the electronic transition [205]. The fluorescence spectrum of enzyme-loaded UCNPs under 808 nm laser excitation is shown in Figure 4.23B. Here, characteristic emission peaks originating from electronic transitions of $^2H_{11/2} \rightarrow {}^4I_{15/2}$ at 525 nm and $^4S_{3/2} \rightarrow {}^4I_{15/2}$ at 545 nm are seen [206]. Even after enzyme loading, the expected emissions indicate the presence of very strong energy.

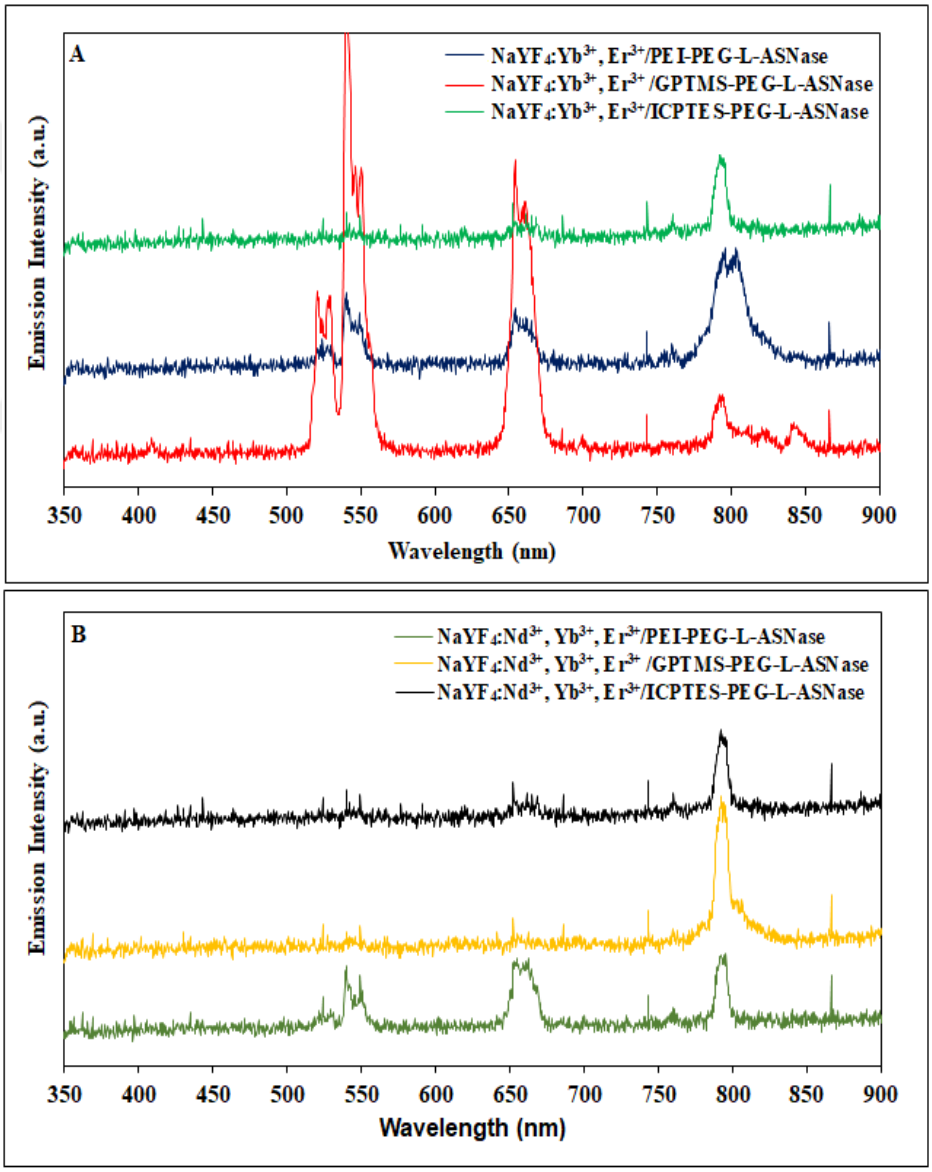

Figure 4.23: Fluorescence emission spectra of UCNPs at 980 nm (A), and 808 nm (B).

4.2. Immobilization Parameters

4.2.1. Immobilization parameters of $NaYF_4$: Yb^{3+}, Er^{3+}/PEI

4.2.1.1. Enzyme unit and incubation time

L-ASNAse immobilization yield and catalytic activity, and incubation time of $NaYF_4$:Yb^{3+}, Er^{3+}/PEI-PEG-L-ASNase were given in Figure 4.24 A. 75 U concentration was chosen as the amount of enzyme for immobilization. As seen in Figure 4.1 A, the immobilization yield decreased after 75 U, while in Figure 4.24 B, there was a sharp increase in the catalytic activity from 5-75 U. At the same time, 100 U only indicated either similar or small catalytic activity. Furthermore, the immobilization yield, activity yield, and immobilization efficiency for 75 Uwere founded as 89.6 ± 0.34 %, 85.69 ± 4.95 %, and 95.63 ± 3.56 %, respectively.

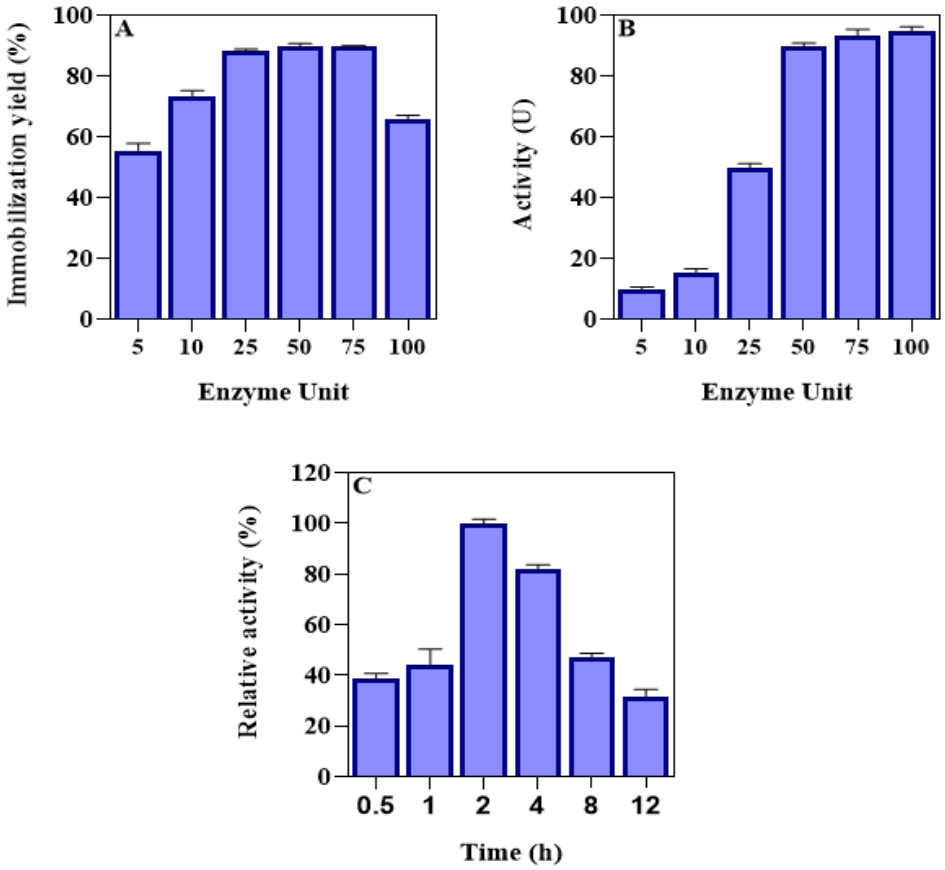

Figure 4.24: L-ASNAse immobilization yield (A), L-ASNase catalytic activity (B), and incubation time (C) of $NaYF_4$:Yb^{3+}, Er^{3+}/PEI-PEG-L-ASNase.

In order to determine the effect of immobilization time on enzyme activity, the time range between 30 min to 12 hours was examined. As can be seen from Figure

4.24 C, after two hours of immobilization, there was a marked increase in the relative activity of the enzyme. It was due to the amount of enzyme immobilized to UCNP has enough time to make chemical interactions between enzyme and UCNP. As a result of physical interaction between enzyme active site and UCNP, enzymatic activity diminished after 2 hours of immobilization. Owing to these results, 2 hours was selected as the optimum incubation time of immobilization.

4.2.1.2 Optimum pH and temperature

The enzymatic activities of PEG-L-ASNase and $NaYF_4:Yb^{3+}$, Er^{3+}/PEI-PEG-L-ASNase were measured between pH 4 and 10 to determine the optimum pH. As shown in Figure 4.25 A, the maximum activities of the PEG-L-ASNase and $NaYF_4:Yb^{3+}$, Er^{3+}/PEI-PEG-L-ASNase were obtained at pH 8.5 and 8.0, respectively. Generally, the changes in optimum pH induce enzymes conformational after immobilization. Also, the alteration of optimum pH value probably drives by a change in acidic or basic amino acid ionization surrounding the enzyme's active site. Apart from this, amine groups of PEIs, which is the main functional group on $NaYF_4:Yb^{3+}$, Er^{3+}/PEI, it regulates the shifting in pH. Meanwhile, this shifting is also important because of the similarity with human body pH. The relative activity of the $NaYF_4:Yb^{3+}$, Er^{3+}/PEI-PEG-L-ASNase was higher than free L-ASNase. It is noted that the main advantage of the immobilization process is higher stability of enzyme as well as alleviating effects environmental factors against the free enzyme.

The optimum temperature of PEG-L-ASNase and $NaYF_4:Yb^{3+}$, Er^{3+}/PEI-PEG-L-ASNase were tested within the range 20-70 °C and the obtained data were shown in Figure 4.25 B. Maximum relative activity of the PEG-L-ASNase was achieved at 40 °C. For $NaYF_4:Yb^{3+}$, Er^{3+}/PEI-PEG-L-ASNase, it was founded as 45 °C. Moreover, it remained above 56 % of its relative activity at 70 °C for immobilized and around 28 % for the free L-ASNase. These results showed that the $NaYF_4:Yb^{3+}$, Er^{3+}/PEI-PEG-L-ASNase had a significant higher thermal resistance as well as it affirmed the most prominent benefit of immobilization.

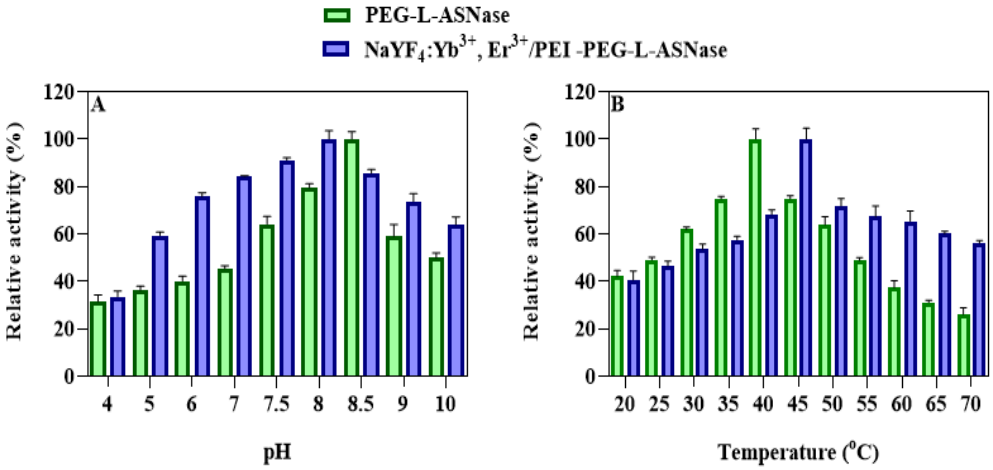

Figure 4.25: Optimum pH (A), and temperature (B) of PEG-L-ASNase and $NaYF_4$:Yb^{3+}, Er^{3+}/PEI-PEG-L-ASNase.

4.2.1.3. Thermal and pH stability

In comparison against free enzymes, thermal stability is also the most important benefit of immobilization. It is clearly displayed in Figure 4.26 A that the thermal stability PEG-L-ASNase and $NaYF_4$:Yb^{3+}, Er^{3+}/PEI-PEG-L-ASNase, were incubated at 50° C (which above the optimum degree by 5°C) for 6 hours. Afterward, the remained activity of PEG-L-ASNase was 28 % from its initial activity, while for $NaYF_4$:Yb^{3+}, Er^{3+}/PEI-PEG-L-ASNase remained 59 % from its initial activity. As a possible result of diminishing molecular mobility and conformational alterations of the enzyme, temperature resistance was emerged by immobilization of L-ASNase. Therefore, in accordance to the result immobilization significantly improved the thermal stability.

The pH stability is also an important parameter for enzyme immobilization. It is clearly noted that Figure 4.26 B and C displayed the pH stability of both PEG-L-ASNase and $NaYF_4$:Yb^{3+}, Er^{3+}/PEI-PEG-L-ASNase after 6 hours incubation at pH 4 and 9. After 6h, the relative activity for pH 4 was found above 21 % for free enzyme and 51 % for immobilized L-ASNase, while at pH 9 the activity was 40 % and 61 % for free and immobilized L-ASNase from initial activity. Owing to optimum pH in the alkaline range, it was clearly concluded that both PEG-L-ASNase and $NaYF_4$:Yb^{3+}, Er^{3+}/PEI-PEG-L-ASNase exhibited the higher enzymatic stability at pH 9 rather the pH 4.

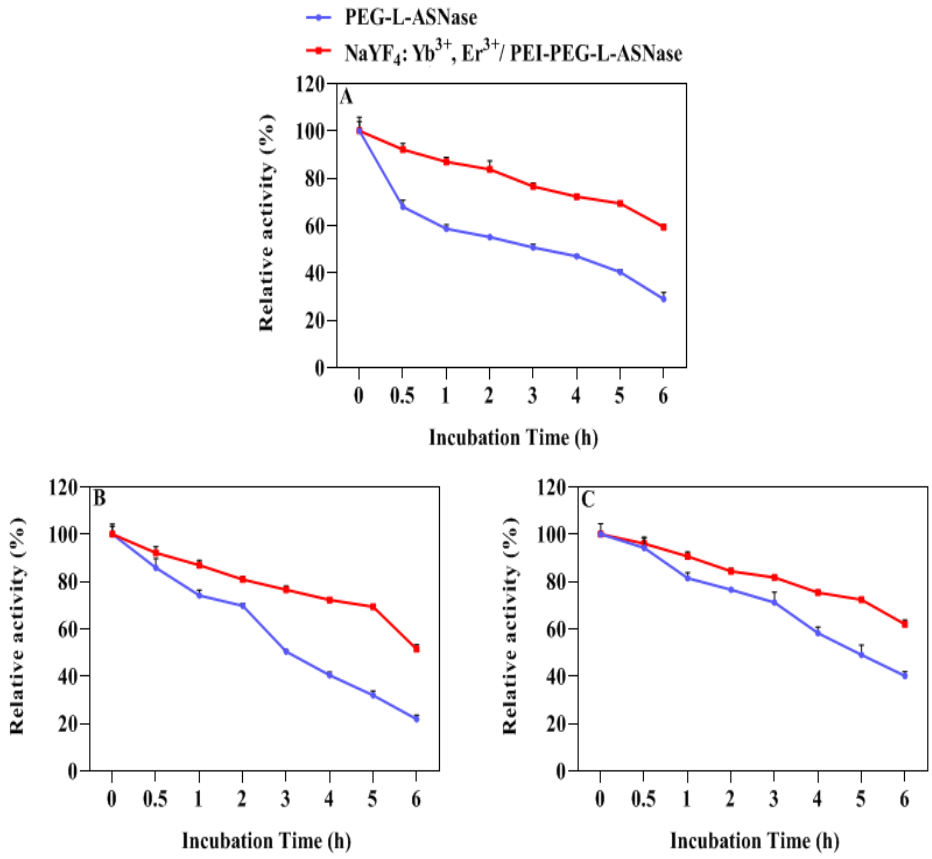

Figure 4.26: Thermal stability (A), pH stability at pH 4 (B), and pH stability at pH 9 (C) of PEG-L-ASNase and $NaYF_4$:Yb^{3+}, Er^{3+}/PEI-PEG-L-ASNase.

4.2.1.4. Effect metal ion and solvent

In order to determine the effect of metal ions on the activity of PEG-L-ASNase and NaYF4:Yb^{3+}, Er^{3+}/PEI-PEG-L-ASNase, samples were incubated with different metal ions. The results were shown in Figure 4.4 A. In comparison with the literature that monovalent cations such as K^{+}, and divalent cations Ca^{2+}, Co^{2+}, and Mg^{2+} increase L-ASNase activity [207]. In addition, it was reported that divalent metal cations for example Cu^{2+}, Fe^{2+}, Hg^{2+}, Zn^{2+}, and metal ions Cr^{3+} inhibit enzyme activity [208–210]. Owing to the result, Ag^{1+}, Ba^{2+}, Ca^{2+}, Co^{2+}, Mg^{2+}, Ni^{2+}, and Al^{3+} increased enzyme activity. In contrast, Na^{1+}, Cu^{2+}, Sr^{2+}, Zn^{2+}, and Cr^{3+} inhibited the enzyme activity. The activity of the immobilized enzyme was higher than the free enzyme counterpart it means that the immobilized enzyme was less affected by metal-based inhibition.

However, the solvent effect on of PEG-L-ASNase and $NaYF_4$:Yb^{3+}, Er^{3+}/PEI-PEG-L-ASNase were invested by application in different organic solvents or 24 hours in room temperature such as 1-pentanol, 2-propanol, acetonitrile, chloroform, ethanol,

ethyl acetate, *n*-hexane, isoamyl alcohol, DCM, DMF, DMSO, and THF, the activities were determined as shown in Figure 4.27 B. Owing to the result, the immobilized enzyme showed higher stability against organic solvent as compared free enzyme, except for acetonitrile and DMSO.

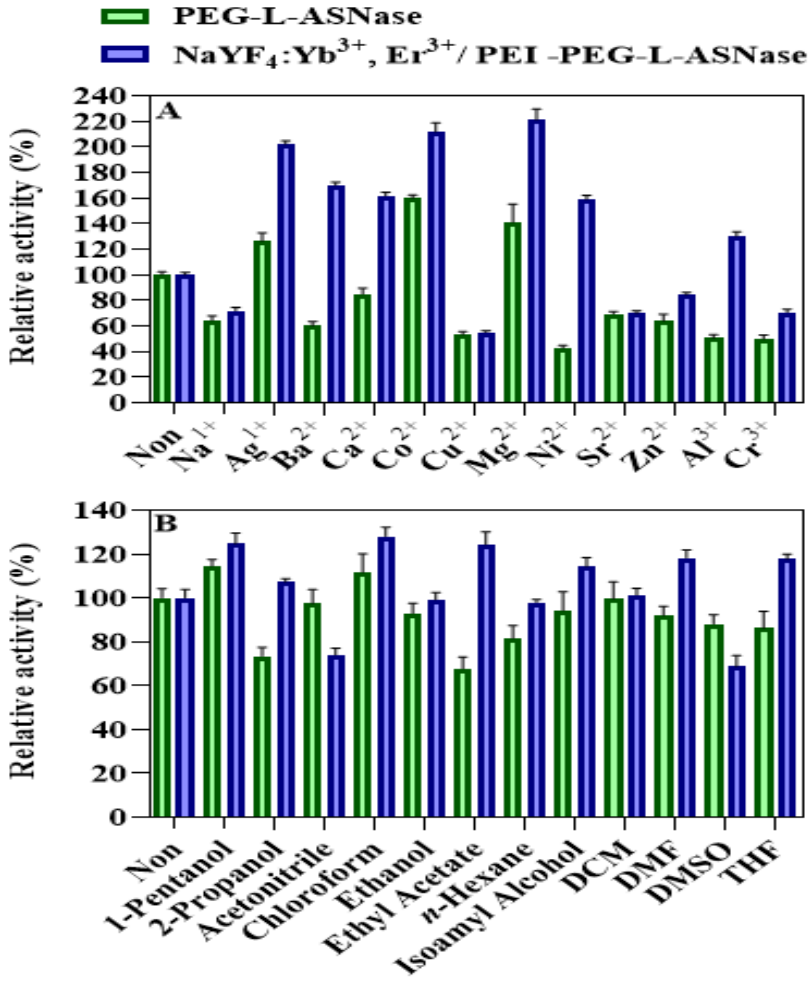

Figure 4.27: Stability of PEG-L-ASNase and $NaYF_4:Yb^{3+}$, Er^{3+}/PEI-PEG-L-ASNase on metal ions (A), and organic solvents (B).

4.2.1.5. Reusability

Reusability is one of the most important features of the immobilization process. The reusability of $NaYF_4:Yb^{3+}$, Er^{3+}/PEI-PEG-L-ASNase was shown in Figure 4 28. It was emphasized that 87 % was achieved after 5 cycles while 78 % has remained after 10 repetitions as well as 57 %, remained after 20 cycles. It was also noted that diminishing of enzymatic activity was driven by weaker bonds and subsequent enzyme leaks due to physical absorption of LASNases. In conclusion, one of main the advantages of immobilization is reusability due to easies separation of the enzyme

from the reaction mixture which leads the repetitive use. In contrast, the free enzyme is inseparable from the mixture.

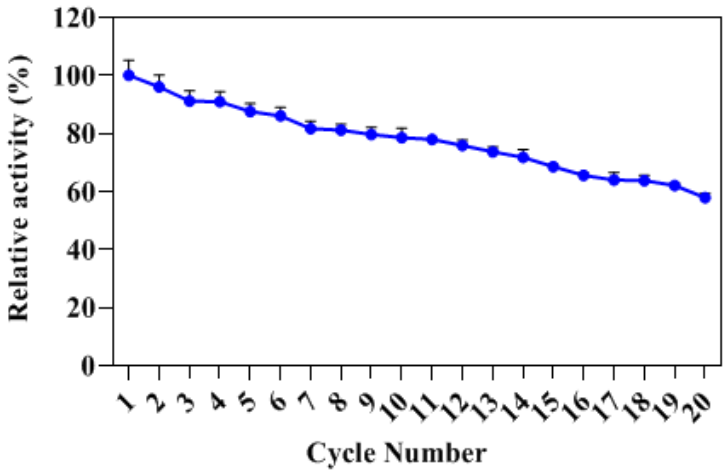

Figure 4.28: Reusability of $NaYF_4$:Yb^{3+}, Er^{3+}/PEI-PEG-L-ASNase.

4.2.1.6. Storage stability

Storage stability is a crucial parameter for commercial-scale application of an enzyme, while it has been recognized that enzyme activity continuously diminishes over time due to instability during storage. Therefore, the storage stability of both free PEG-L-ASNase and $NaYF_4$:Yb^{3+}, Er^{3+}/PEI-PEG-L-ASNase were investigated at 4 and 25 °C for 4 weeks with the weekly measurement result were shown in Figure 4.29. Under storage conditions, the free enzyme lost about 48 % and 75 % of its initial activity at 4 and 25 °C, respectively. In contrast, $NaYF_4$:Yb^{3+}, Er^{3+}/PEI-PEG-L-ASNase lost 33 % and 38 % of its initial activity at 4 and 25 °C in the same period. The loss of enzymatic activity is probably attributed to protein denaturation and degradation during long-term storage. These results showed that the storage stability of the $NaYF_4$:Yb^{3+}, Er^{3+}/ PEI-PEG-L-ASNase was better compared to the free enzyme at both 4 and 25 °C. It was also implied that the stability of immobilized enzyme was higher at 25°C with insignificant loss than the 4 °C counterparts. Owing to the result, $NaYF_4$:Yb^{3+}, Er^{3+}/ PEI-PEG-L-ASNase indicated its promising and alternative carrier matrix material due to its long-term storage stability.

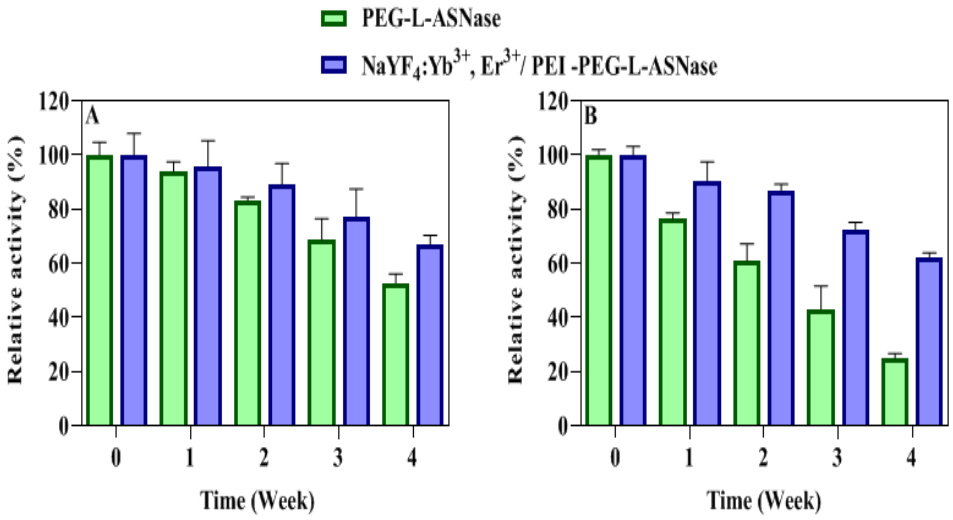

Figure 4.29: Storage stability of PEG-L-ASNase and $NaYF_4$:Yb^{3+}, Er^{3+}/PEI-PEG-L-ASNase at +4°C (A), and at +25 °C (B).

4.2.1.7. Trypsin resistance

One of the major problems of bacterial enzymes in the pharmaceutical application is the stability against proteolysis enzymes. Therefore, trypsin digestion was carried out to measure the resistance of PEG-L-ASNase and $NaYF_4$:Yb^{3+}, Er^{3+}/PEI-PEG-L-ASNase. The results showed that the resistance of immobilized enzyme to trypsin digestion was greatly improved compared to the free one (Figure 4.30). After 120 minutes from incubation with trypsin at +37 °C, free L-ASNase was almost completely hydrolyzed, while the activity of immobilized L-ASNase retained 33 % of its original activity.

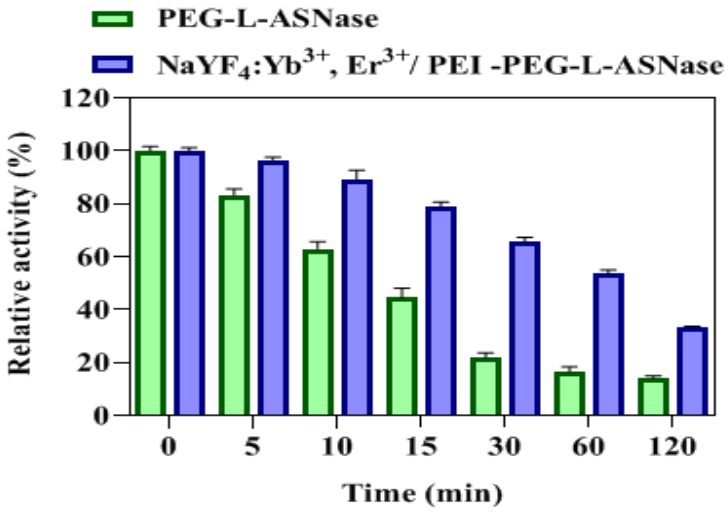

Figure 4.30: Trypsin resistance of PEG-L-ASNase and NaYF4:Yb^{3+}, Er^{3+}/PEI-PEG-L-ASNase.

4.2.1.8. Kinetic parameter

The kinetic parameters for both PEG-L-ASNase and $NaYF_4:Yb^{3+}$, Er^{3+}/PEI-PEG-L-ASNase were estimated and summarized in Table 4.3. Also, the Lineweaver–Burk plots were shown in Figure 4.31. As shown in Table 4.3, the obtained K*m* values for the free and immobilized were 2.31 and 1.56 mM, respectively. After immobilization, the K*m* value decreases. It is obviously shown that low Km value enzyme indicated high catalytic efficiency as it achieved the maximum catalytic efficiency in low substrate concentration. Therefore, the decrease of K*m* value after immobilization represents the high affinity of the enzyme to its substrate. Meanwhile, an increase in the *Vmax* was observed value after enzyme immobilization. The apparent *Vmax* value increased from 140.85 to 138.89 µmol/min. The obtained results are in accordance with the values reported previously.

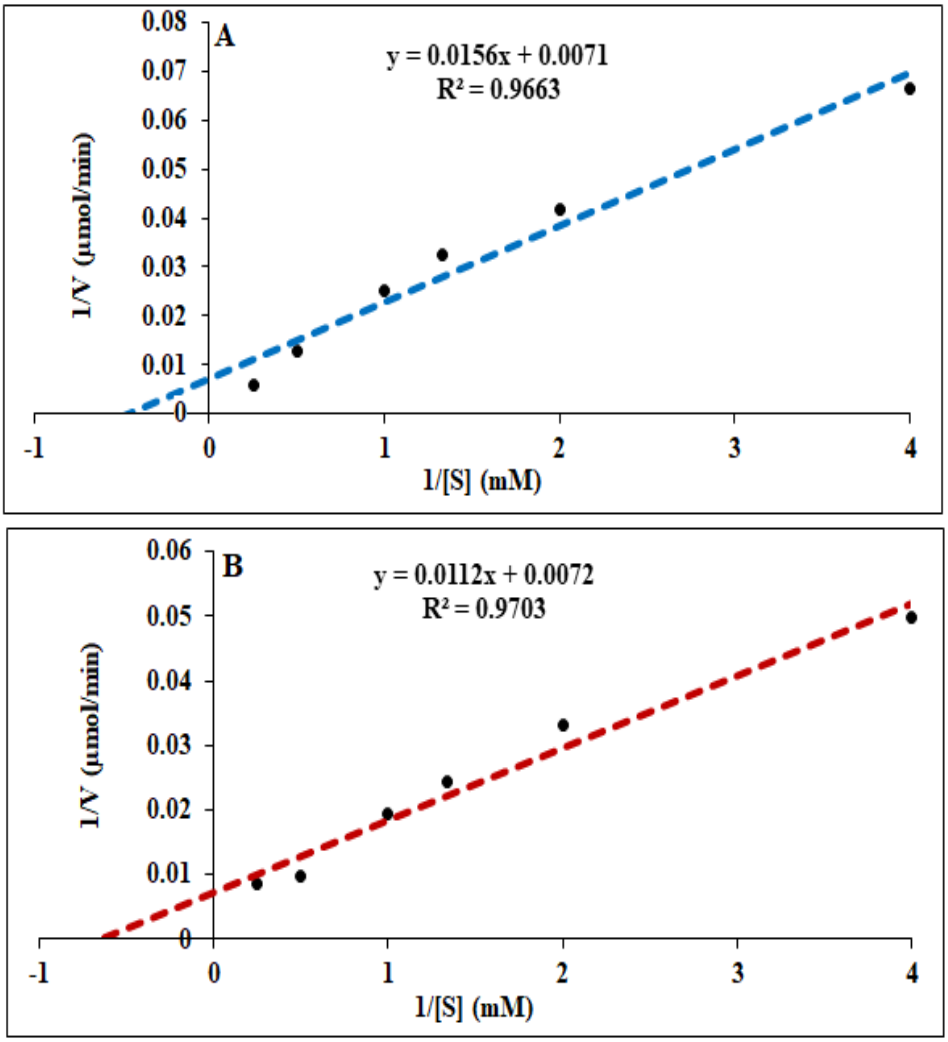

Figure 4.31: Kinetic parameters of PEG-L-ASNase (A), and $NaYF_4:Yb^{3+}$, Er^{3+}/PEI-PEG-L-ASNase (B).

Table 4.3: Kinetic parameters of PEG-L-ASNase and $NaYF_4:Yb^{3+}$, Er^{3+}/PEI-PEG-L-ASNase.

Sample	K*m* (mM)	*Vmax* (µmol/min)	R^2
PEG-L-ASNase	2.31 ± 0.042	140.85 ± 3.235	0.9663
$NaYF_4:Yb^{3+}$, Er^{3+}/PEI-PEG-L-ASNase	1.56 ± 0.064	138.89 ± 1.66	0.9703

4.2.1.9. Activation energy

The activation energy (*Ea*) was determined by the Arrhenius equation for both PEG-L-ASNase and $NaYF_4:Yb^{3+}$, Er^{3+}/PEI-PEG-L-ASNase. The Ea values were calculated from the slope of log (% relative activity) versus 1000/T, while *Ea* values were determined as 17.13 kJ/mol for PEG-L-ASNase and 10.97 kJ/mol for the $NaYF_4:Yb^{3+}$, Er^{3+}/PEI-PEG-L-ASNase as seen in Figure 4.32. The low *Ea* value was reported beneficial also for enzyme immobilization. This implied that the immobilized enzymes have less temperature-sensitive. This reduction in *Ea* value demonstrated that the immobilized enzyme required less energy than the free one to overcome the conversion barrier to transform the substrate into a product. The results implied immobilized enzyme higher stability and advantages than the free counterpart.

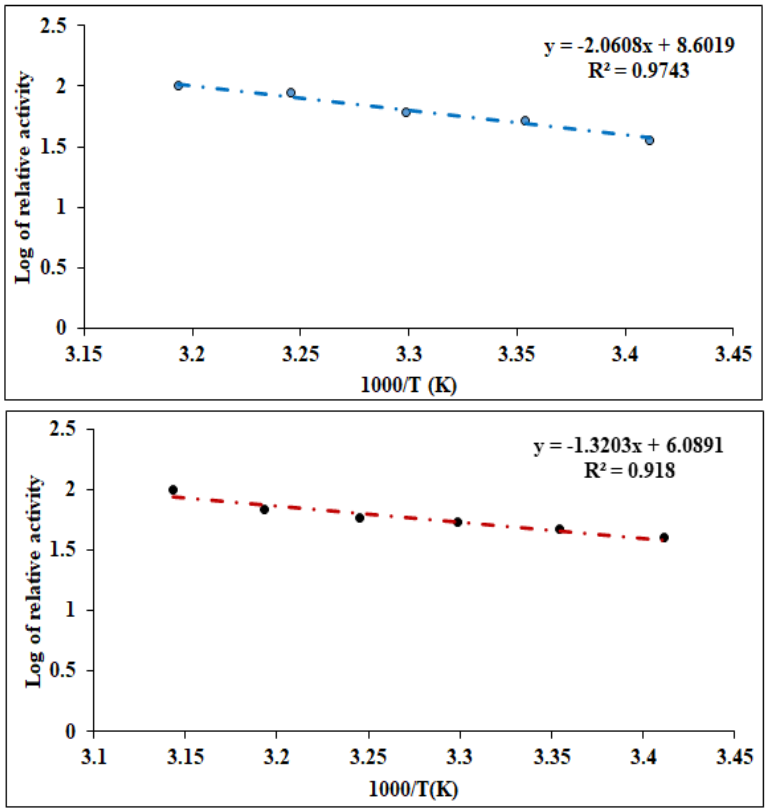

Figure 4.32: The activation energy of PEG-L-ASNase (A), and $NaYF_4:Yb^{3+}$, Er^{3+}/ PEI-PEG-L-ASNase (B).

4.2.1.10. Laser power, laser distance, and laser exposure time

To determine the optimum laser power for $NaYF_4$:Yb^{3+}, Er^{3+}/PEI-PEG-L-ASNase, NIR light was induced to immobilize the enzyme on UCNP. Different milliwatts (mW) were scanned to find out the optimum power of UCNP by applying a constant amount of UCNP with a fixed distance between nanoparticles and NIR light. Owing to the result, the optimum laser power was founded 800 mW and the enzyme activity was increased from 100 % to 206 % as shown in Figure 4.33 A. In accordance to the result, diminishing enzyme activity took place coincidently with increasing NIR light power, it was assumed that the NIR generated heat probable affected the three-dimensional structure of enzyme or weak interaction between enzyme and UCNP.

After the maximum NIR light power was found, the right distance between $NaYF_4$:Yb^{3+}, Er^{3+}/PEI-PEG-L-ASNase and laser power was optimized. In this experiment the NIR light was arranged at 800 mW with a fixed amount of enzyme immobilized on UCNP and different distances were scanned (0 – 5 cm) with the optimum activity was found at 1 cm between NIR and UCNP immobilized enzyme as seen in (Figure 4.33 B). Owing to the result, diminishing enzyme activity was inversely proportional to the increasing in the distance due to decreasing the effect of NIR light on UCNP nanoparticles.

NIR exposure time was investigated by keeping constant laser power, distance, and the amount of $NaYF_4$:Yb^{3+}, Er^{3+}/PEI-PEG-L-ASNase, while the activity was also determined in the absence of NIR radiation. As shown in Figure 4.33 C, there was a sharp increase in the activity due to the exposure to NIR light until 60 min, thereafter a slight decrease in the activity that may be due to the heat become from NIR laser led to effect on enzyme and decrease in activity occurred.

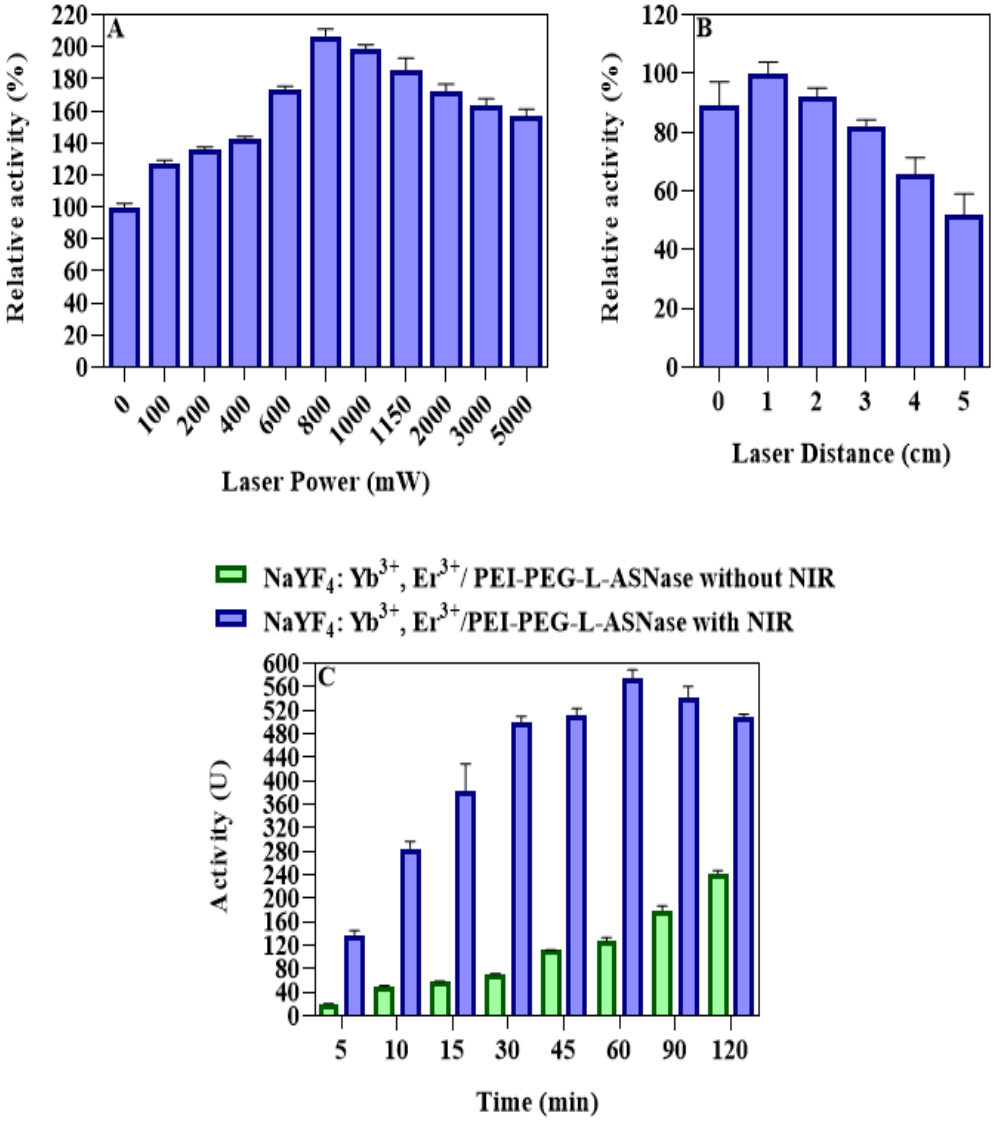

Figure 4.33: Induce of $NaYF_4$:Yb^{3+}, Er^{3+}/PEI-PEG-L-ASNase, NIR light power (A), NIR distance (B), and NIR time (C).

4.2.1.11. Stability of $NaYF_4$:Yb^{3+}, Er^{3+}/PEI-PEG-L-ASNase

To measure the stability of $NaYF_4$:Yb^{3+}, Er^{3+}/PEI-PEG-L-ASNase and the effect of NIR after storage. Different samples of $NaYF_4$:Yb^{3+}, Er^{3+}/PEI-PEG-L-ASNase were incubated with PBS (50 mM, pH 7.4) at +37 °C, and the activity was measured every single day by exposure to NIR light at optimum conditions the activity measured. After one week from incubation, the activity was above 51 % from the initial activity as shown in (Figure 4.34).

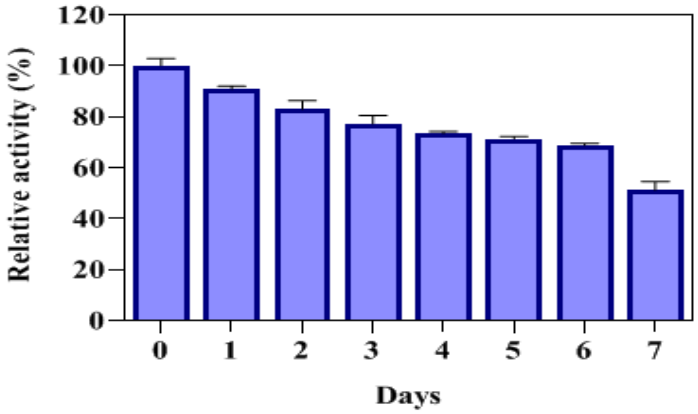

Figure 4.34: Stability of $NaYF_4$:Yb^{3+}, Er^{3+}/PEI-PEG-L-ASNase in PBS by NIR light.

4.2.1.12. *In vitro* half-life

In vitro half-life of were determined for both free PEG-L-ASNase and immobilized $NaYF_4$:Yb^{3+}, Er^{3+}/PEI-PEG-L-ASNase enzyme. The samples and rat blood serum were incubated for 1 week at +37 °C. Thereafter, the activity of the free and immobilized enzyme was measured with optimum conditions, and their *in vitro* half-life was calculated by comparing with the initial activity as we can see in (Figure 4.35).

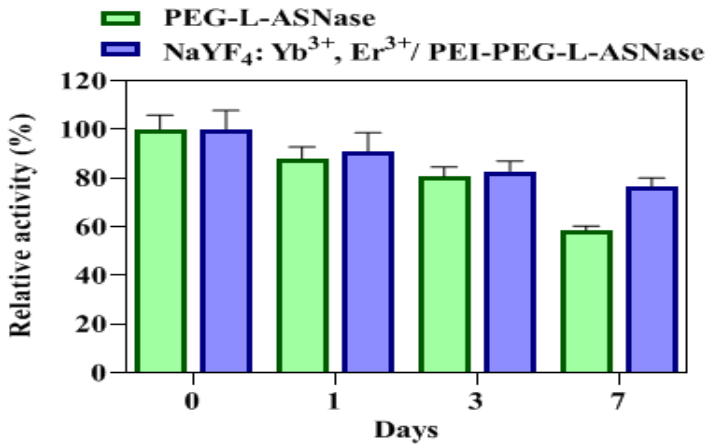

Figure 4.35: *In vitro* half-life of PEG-L-ASNase and immobilized $NaYF_4$:Yb^{3+}, Er^{3+}/ PEI-PEG-L-ASNase.

4.2.1.13. Plasma coagulation

The prothrombin time (PT) and the activated partial thromboplastin time (APTT), reflect the effect of $NaYF_4$:Yb^{3+}, Er^{3+}/PEI and $NaYF_4$:Yb^{3+}, Er^{3+}/PEI-PEG-L-ASNase on the intrinsic and extrinsic pathways of the blood coagulation cascade. They were

determined by incubating both in platelet-poor plasma (Figure 4.36). It is clearly indicated that the absence of coagulation occurred when UCNPs were added. These findings indicate that both $NaYF_4:Yb^{3+}$, Er^{3+}/PEI and $NaYF_4:Yb^{3+}$, Er^{3+}/PEI-PEG-L-ASNase are hemocompatible, which may be related to the hydrophilicity and surface area charge of these particles.

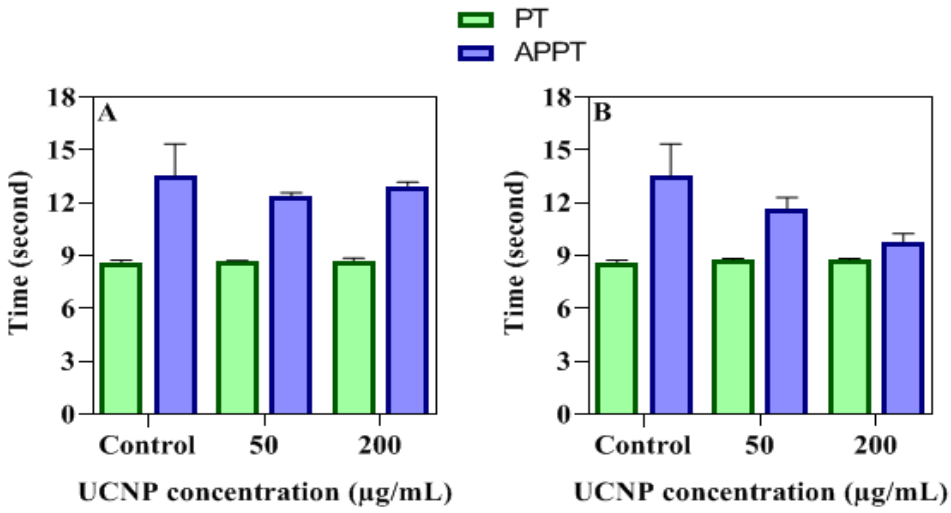

Figure 4.36: Plasma coagulation of $NaYF_4:Yb^{3+}$, Er^{3+}/PEI (A), and $NaYF_4:Yb^{3+}$, Er^{3+}/PEI-PEG-L-ASNase (B).

4.2.1.14. *In vitro* cytotoxicity

The *in vitro* cytotoxicity of the prepared UCNP was tested calorimetrically by employing the MTT test and the results were shown in Figure 4.37 A and B. Owing to cell viability classification of cytotoxicity it is widely recognized that 50 % as toxic, 51 to 70 % as mildly toxic and less than 71 % non-cytotoxic [211]. Different concentration (12.5, 25, 50, 100, and 200 µg/mL) of $NaYF_4:Yb^{3+}$, Er^{3+}/PEI and $NaYF_4:Yb^{3+}$, Er^{3+}/ PEI-PEG-L-ASNase were tested against mouse fibroblast (L-929). In addition, the morphology of the cells treated with $NaYF_4:Yb^{3+}$, Er^{3+}/PEI and NaYF4:Yb^{3+}, Er^{3+}/PEI-PEG-L-ASNase were given in Figure 4.37 C, after 24, 48, and 72 h form incubation. As a result, the morphological alteration was absent that the synthesized UCNP did not indicate *in vitro* toxicity in accordance to cell viability.

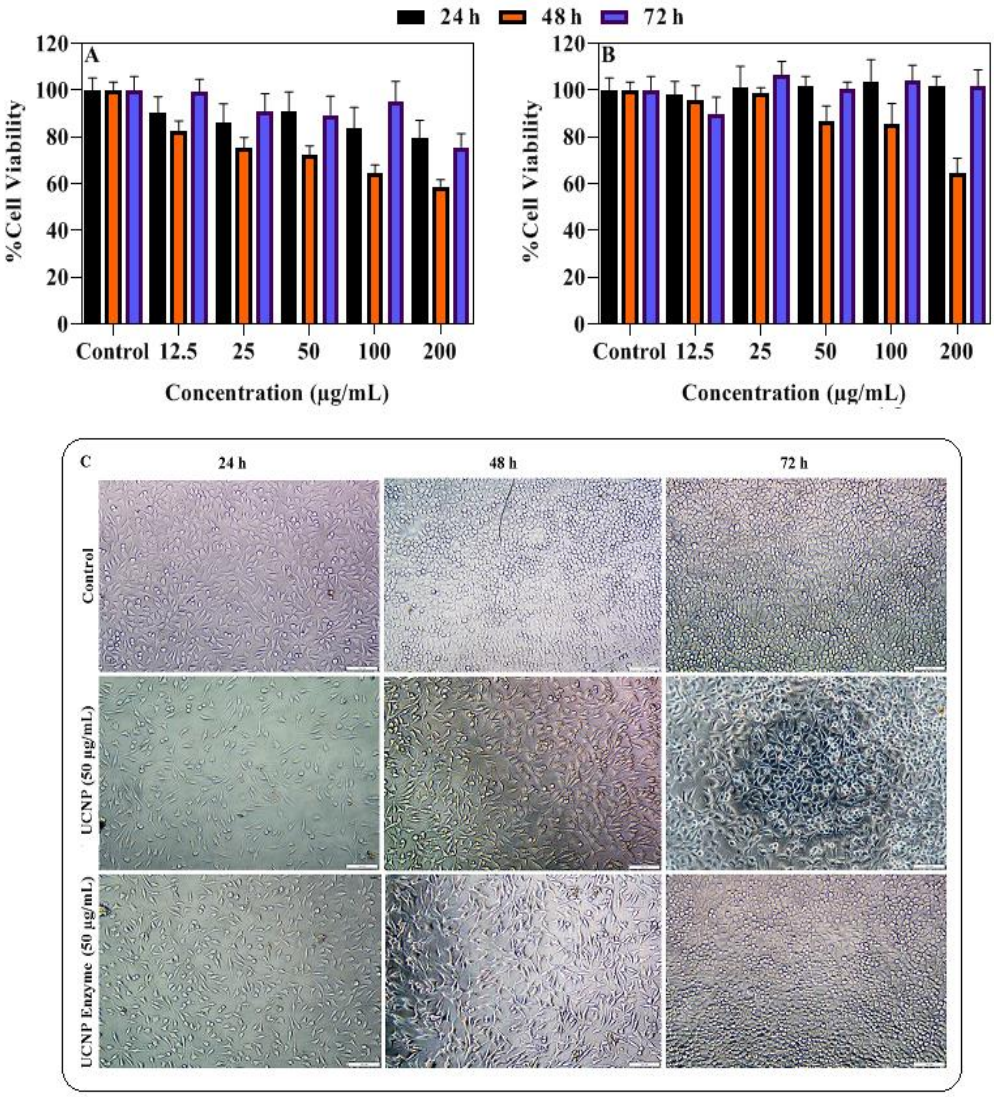

Figure 4. 37: Cell viability results after incubation 24, 48, and 72 hours of L-929 with $NaYF_4$:Yb^{3+}, Er^{3+}/PEI (A), $NaYF_4$:Yb^{3+}, Er^{3+}/PEI-PEG-L-ASNase (B), and morphological image of L-929 fibroblast cells (C).

4.2.2. Immobilization parameters of $NaYF_4$: Yb^{3+}, Er^{3+}/GPTMS

4.2.2.1. Enzyme unit and incubation time

20 U concentration was chosen as the amount of enzyme for immobilization. As seen in Figure 4.38 A, the immobilization yield decreased after 20 U, while in Figure 4.38 B, there is was a sharp increase in the catalytic activity from 5-20 U. In the same time, 25 U and 50 U only indicated either similar or small increased in catalytic activity. Furthermore, the immobilization yield, activity yield, and immobilization efficiency for 20 U were as founded as 90.19 ± 0.82 %, and the activity yield 74.12 ± 3.76 %, while immobilization efficiency 82.12 ± 4.58 %, respectively.

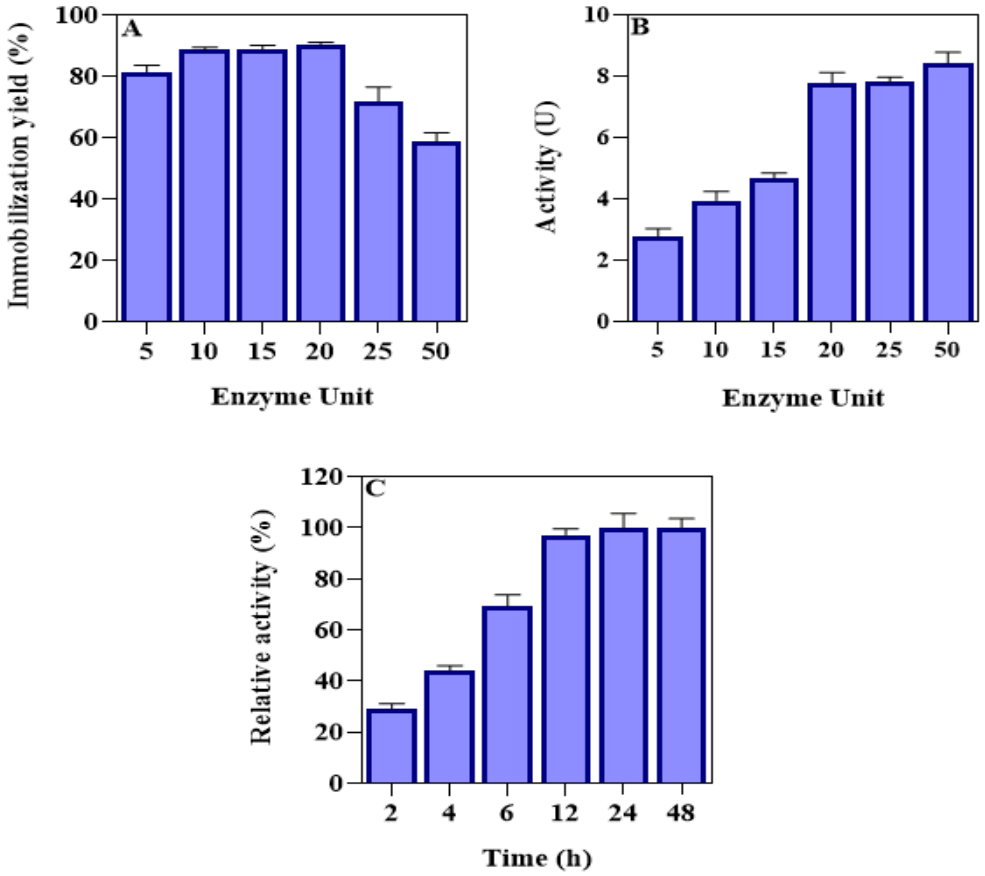

Figure 4.38: L-ASNase immobilization yield (A), L-ASNase catalytic activity (B), and incubation time (C) of $NaYF_4:Yb^{3+}$, Er^{3+}/GPTMS-PEG-L-ASNase.

In order to determine the effect of immobilization time on enzyme activity, the time range between 2 min to 48 hours was examined. As can be seen from Figure 4.38 C, after twelve hours of immobilization, there was a marked increase in the relative activity of the enzyme. It was due to the amount of enzyme immobilized to UCNP has enough time to make chemical interactions between enzyme and UCNP. As a result of covalent interaction between enzyme active site and UCNP. Owing to these results, 12 hours was elected as the optimum incubation time of immobilization.

4.2.2.2. Optimum pH and temperature

The enzymatic activities of PEG-L-ASNase and $NaYF_4:Yb^{3+}$, Er^{3+}/GPTMS-PEG-L-ASNase were measured between pH 4 and 10 to determine the optimum pH. The maximum activities of PEG-L-ASNase were obtained at pH 8.5, while the optimum pH value for $NaYF_4:Yb^{3+}$, Er^{3+}/GPTMS increased to 9.0 as shown in Figure 4.39 A. The reason for this alteration is attributed to structural conformational changes in the

enzyme resulting from covalent interactions between the enzyme and UCNPs. Compared to the free enzyme, the high pH resistance of the immobilized enzyme is probably regulated by the strong binding between the enzyme and UCNP. The relative activity of the $NaYF_4:Yb^{3+}$, Er^{3+}/GPTMS-PEG-L-ASNase higher than that L-ASNase, even at pH 10 the activity of immobilized still above 90 % while for L-ASNase above 53 %.

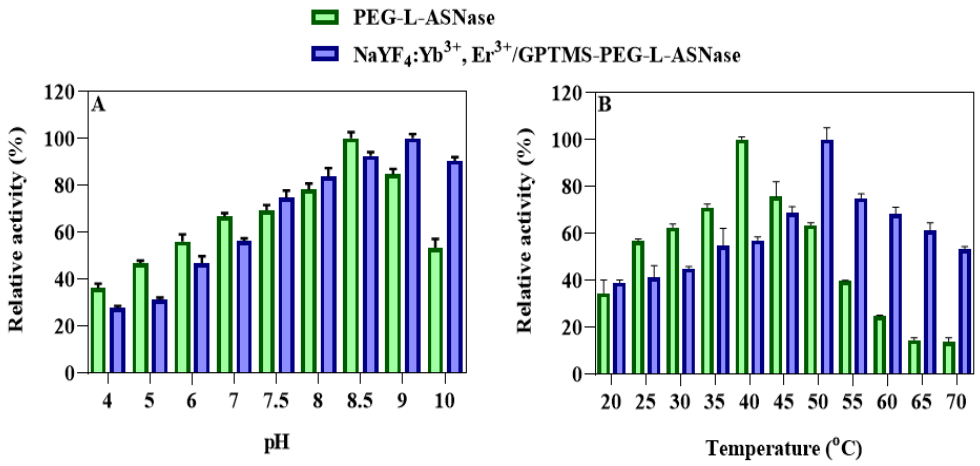

Figure 4.39: Optimum pH (A), and temperature (B) of PEG-L-ASNase and $NaYF_4:Yb^{3+}$, Er^{3+}/GPTMS-PEG-L-ASNase.

The optimum temperature of PEG-L-ASNase and $NaYF_4:Yb^{3+}$, Er^{3+}/GPTMS - PEG-L-ASNase were tested within the range 20-70 °C and the obtained data were shown in Figure 4.39 B. Maximum relative activity of the PEG-L-ASNase was achieved at 40 °C. For $NaYF_4:Yb^{3+}$, Er^{3+}/GPTMS-PEG-L-ASNase, it was was founded as 50 °C. Moreover, it remained above 53 % of its relative activity at 70 °C for immobilized and around 13 % for the free one. These results showed that the $NaYF_4:Yb^{3+}$, Er^{3+}/GPTMS-PEG-L-ASNase had a significantly higher thermal resistance as well as it affirmed the most prominent benefit of immobilization.

4.2.2.3. Thermal and pH stability

Thermal stability is also an important advantage of immobilized enzymes compared to free L-ASNase. The thermal stability results shown in Figure 4.40 A for both PEG-L-ASNase and $NaYF_4:Yb^{3+}$, Er^{3+}/GPTMS-PEG-L-ASNase were incubated at 50° C for 6 hours. After 6 hours, the remained activity for L-ASNase was founded above 26 % while $NaYF_4:Yb^{3+}$, Er^{3+}/GPTMS-PEG-L-ASNase the activity retained 59

% from its initial. As a possible result of diminishing molecular mobility and conformational alterations of the enzyme, temperature resistance was emerged by immobilization of L-ASNase. Therefore, in accordance to result immobilization significantly improves thermal stability.

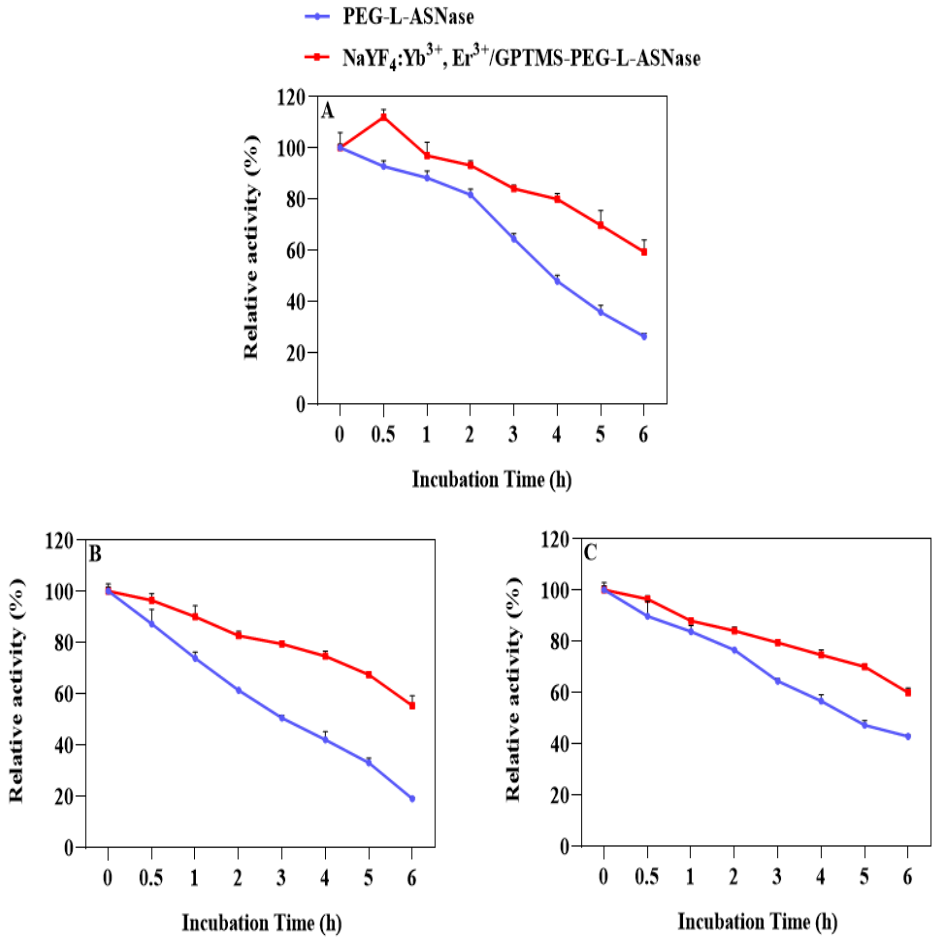

Figure 4.40: Thermal stability (A), pH stability at pH 4 (B), and pH stability at pH 9 (C) of PEG-L-ASNase and $NaYF_4:Yb^{3+}$, Er^{3+}/GPTMS-PEG-L-ASNase.

It is clearly noted that Figure 4.40 B and C displayed the pH stability of both PEG-L-ASNase and $NaYF_4:Yb^{3+}$, Er^{3+}/GPTMS-PEG-L-ASNase after 6 hours incubation at pH 4 and 9. After 6h, the relative activity for pH 4 was found above 19 % for free L-ASNase and 55 % for immobilized L-ASNase, while at pH 9 the activity was 42 % and 59 % for free and immobilized LASNase from initial activity, respectively. Owing to optimum pH in the alkaline range, it was clearly concluded that both PEG-L-ASNase and $NaYF_4:Yb^{3+}$, Er^{3+}/GPTMS-PEG-L-ASNase exhibited the higher enzymatic stability at pH 9 rather the pH 4.

4.2.2.4. Effect metal ion and solvent

The effect of both metal ions and organic solvents were measured on free PEG-L-ASNase and immobilized $NaYF_4:Yb^{3+}$, Er^{3+}/GPTMS-PEG-L-ASNase, samples were incubated with different metal ions. The results were shown in Figure 4.41 A. It has been reported in the literature that monovalent cations such as Na^{+}, and divalent cations Ca^{2+}, $Co^{2+,}$ and Mg^{2+} increase L-ASNase activity [207]. In comparison to other studies, divalent cations such as Cu^{2+}, Fe^{2+}, Hg^{2+}, Zn^{2+}, and metal ions Cr^{3+} inhibit enzyme activity [208–210]. Owing to experiment, Na^{1+}, Ag^{1+}, Ba^{2+}, Ca^{2+}, Co^{2+} , Mg^{2+}, Ni^{2+} , and Al^{3+} increased enzyme activity. In contrast, Cu^{2+}, Sr^{2+}, Zn^{2+}, and Cr^{3+} inhibited the enzyme activity. The activity of the immobilized enzyme is higher compare to the free enzyme with less metal ion effect than its free enzyme counterpart.

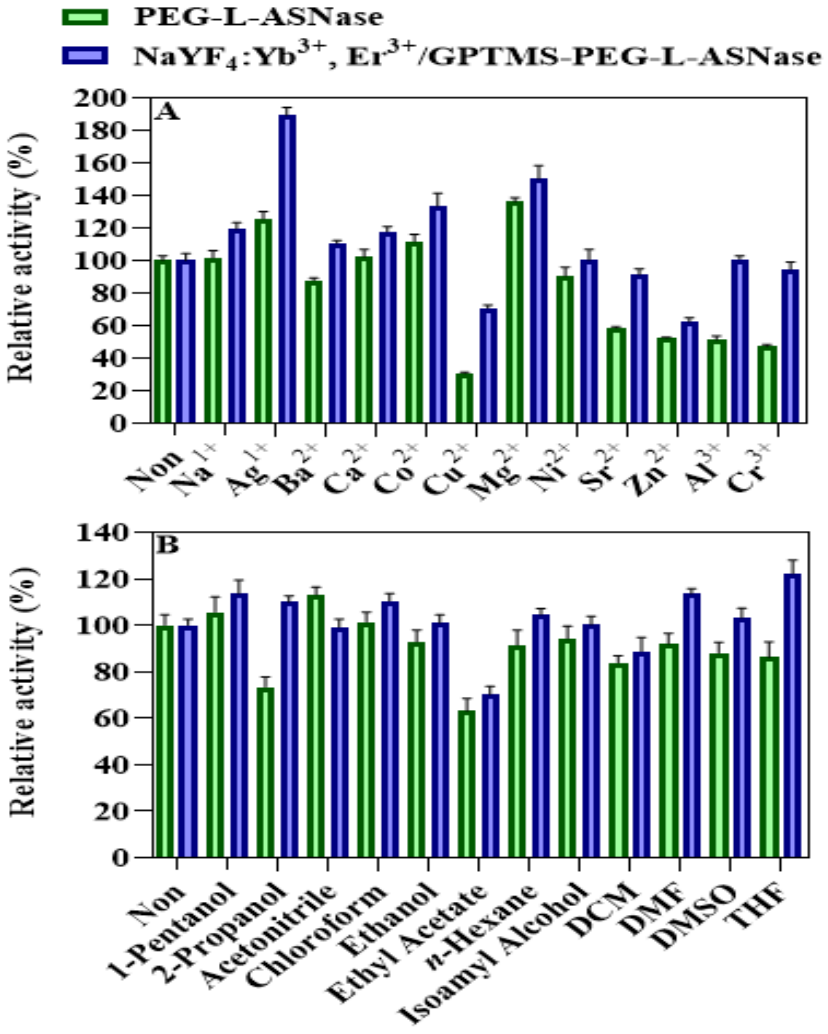

Figure 4.41: Stability of PEG-L-ASNase and NaYF4:Yb^{3+}, Er^{3+}/GPTMS-PEG-L-ASNase on metal ions (A), and organic solvents (B).

However, the solvent effect on the activity of PEG-L-ASNase and $NaYF_4:Yb^{3+}$, Er^{3+}/GPTMS-PEG-L-ASNase as shown in figure 4.41 B were determined by 24 h incubation at room temperature by various organic solvents such as 1-pentanol, 2-propanol, acetonitrile, chloroform, ethanol, ethyl acetate, *n*-hexane, isoamyl alcohol, DCM, DMF, DMSO, and THF. Owing to the result, the immobilized L-ASNase showed higher stability against organic solvent except for acetonitrile which the free L-ASNase showed higher activity than immobilized L-ASNase.

4.2.2.5. Reusability

Reusability is one of the most important features of the immobilization process. The reusability of covalent immobilization of $NaYF_4:Yb^{3+}$, Er^{3+}/GPTMS-PEG-L-ASNase was shown in Figure 4.42. It was emphasized that the activity after 10 cycles was above 80 %, while 20 cycles retained 62 %. In comparison with the literature, covalent immobilization improves the reusability of enzymes higher than the physical one. Reusability is one of the advantages of immobilization, in accordance to easiness separation of the immobilized enzyme from the reaction mixture as well as repeating use while the free enzyme is inseparable from the reaction medium.

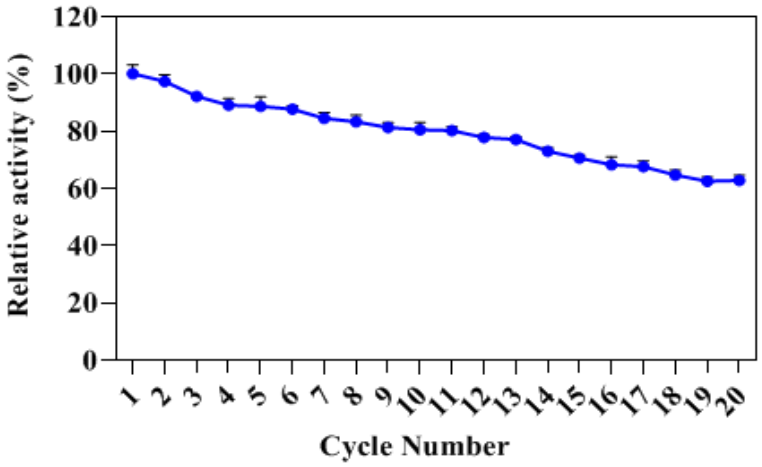

Figure 4.42: Reusability of $NaYF_4:Yb^{3+}$, Er^{3+}/GPTMS-PEG-L-ASNase.

4.2.2.6. Storage stability

Storage stability is a crucial parameter for commercial-scale application of an enzyme, while it has been recognized that enzyme activity continuously diminishes over time due to instability during storage. Therefore, the storage stability of both free

PEG-L-ASNase and $NaYF_4:Yb^{3+}$, Er^{3+}/GPTMS-PEG-L-ASNase were investigated at 4 and 25 °C for 4 weeks with the weekly measurement results were shown in Figure 4.43. After 4 weeks of storage, the activity of immobilized L-ASNase still above 69 % and 59 % of their initial activities at 4 and 25 °C, respectively. Free L-ASNase preserved 49 % and 27 % of its initial activity, respectively. These results showed that the storage stability of the $NaYF_4:Yb^{3+}$, Er^{3+}/GPTMS-PEG-L-ASNase was better compared to the free L-ASNase at both 4 and 25 °C. It was also implied that the stability of immobilized L-ASNase was higher at 25°C with insignificant loss than the 4 °C counterparts.

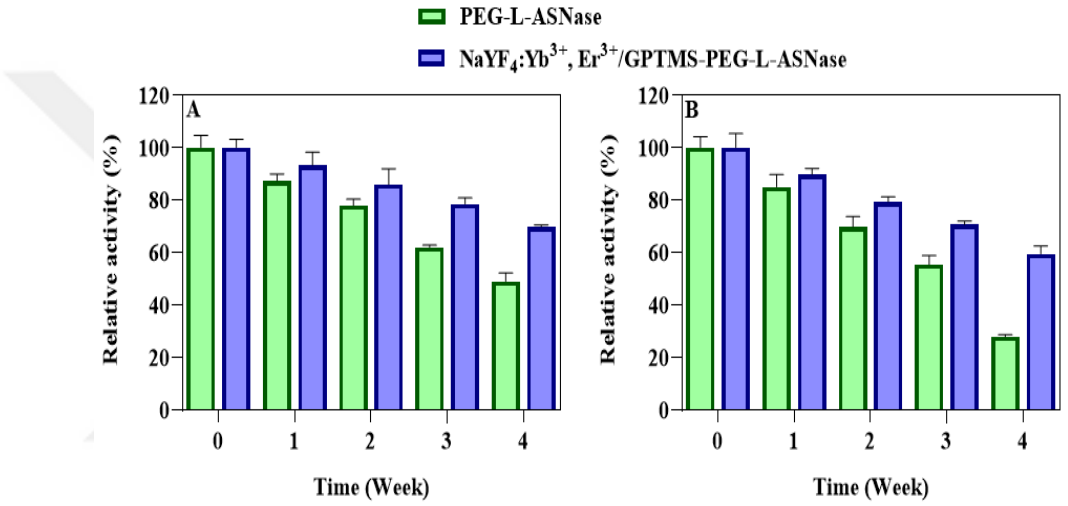

Figure 4.43: Storage stability of PEG-L-ASNase and $NaYF_4:Yb^{3+}$, Er^{3+}/GPTMS-PEG-L-ASNase at +4°C (A), and at +25 °C (B).

4.2.2.7. Trypsin resistance

One of the major problems of bacterial enzymes in the pharmaceutical application is the stability against proteolysis enzymes. Therefore, trypsin digestion was carried out to measure the resistance of the free L-ASNase and $NaYF_4:Yb^{3+}$, Er^{3+}/GPTMS-PEG-L-ASNase against trypsin digestion was shown in Figure 4.44, which implied that the resistance of immobilized to trypsin digestion was significantly improved compared to the free L-ASNase. After 120 minutes from incubation with trypsin at +37 °C, PEG-L-ASNase was almost completely hydrolyzed, while the activity of $NaYF_4:Yb^{3+}$, Er^{3+}/GPTMS-PEG-L-ASNase retained about 41 % of its original activity.

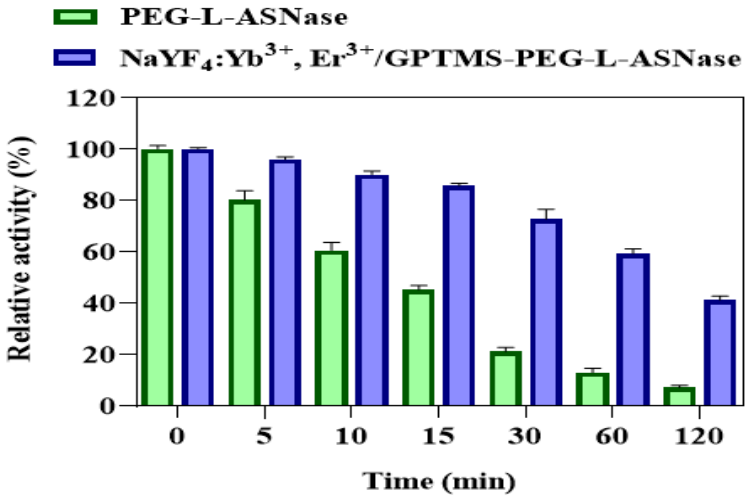

Figure 4.44: Trypsin resistance of PEG-L-ASNase and $NaYF_4$:Yb^{3+}, Er^{3+}/GPTMS-PEG-L-ASNase.

4.2.2.8. Kinetic parameter

The kinetic parameters for both PEG-L-ASNase and $NaYF_4$:Yb^{3+}, Er^{3+}/GPTMS-PEG-L-ASNase were measured and summarized in Table 4.4. The obtained K*m* values for the free and immobilized were 2.31 and 1.791 mM, respectively. After immobilization, the K*m* value decreased. It is obviously shown that low Km value enzyme indicated high catalytic efficiency as it achieved the maximum catalytic efficiency in low substrate concentration. Therefore, the decrease of K*m* value after immobilization represents the high affinity of the enzyme to its substrate. Besides, the Lineweaver–Burk plots were shown in Figure 4.45. It is widely noted that a lower K*m* value implies maximum catalytic efficiency at low substrate concentration. Meanwhile, a decrease in the V*max* was observed value after enzyme immobilization. The apparent *Vmax* value increased from 140.85 to 116.28 µmol/min.

Table 4.4: Kinetic parameters of PEG-L-ASNase and NaYF4:Yb^{3+}, Er^{3+}/GPTMS-PEG-L-ASNase.

Sample	**K*m* (mM)**	***Vmax* (µmol/min)**	**R^2**
PEG-L-ASNase	2.31 ± 0.042	140.85 ± 3.235	0.9663
$NaYF_4$:Yb^{3+},Er^{3+}/GPTMS-PEG-L-ASNase	1.791 ± 0.05	116.28 ± 2.362	0.9741

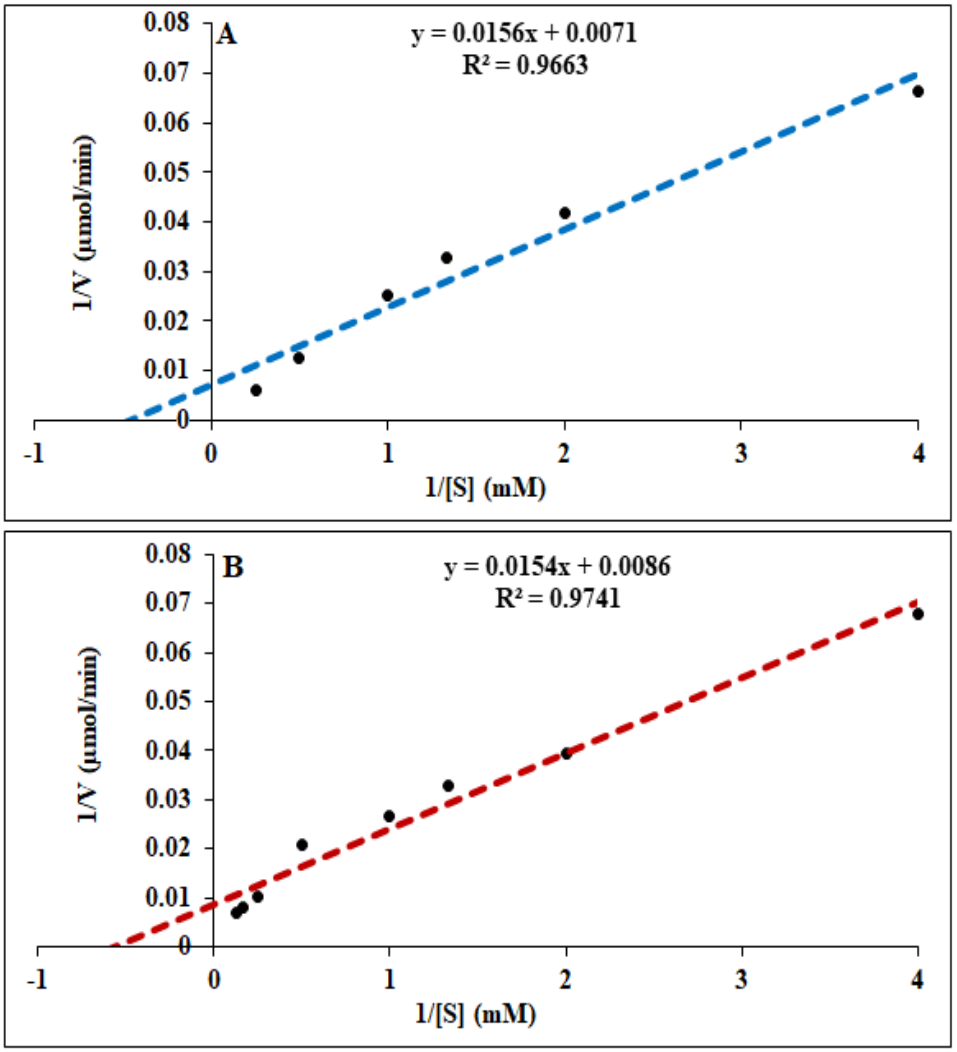

Figure 4.45: Kinetic parameters of PEG-L-ASNase (A), and $NaYF_4:Yb^{3+}$, Er^{3+}/GPTMS-PEG-L-ASNase (B).

4.2.2.9. Activation energy

The activation energy (*Ea*) values calculated by the Arrhenius equation for both PEG-L-ASNase and $NaYF_4:Yb^{3+}$, Er^{3+}/GPTMS-PEG-L-ASNase. The Ea values which were calculated from the slope of log (% relative activity) versus 1000/T. The *Ea* was founded for free L-ASNase as 17.13 kJ/mol, while for immobilized L-ASNase 9.93 kJ/mol as seen in Figure 4.46. The *Ea* value decreased after immobilization, which is another advantage of immobilization as it implied that the diminishing temperature sensitivity of the immobilized enzyme. This reduction in *Ea* value demonstrated that the immobilized enzyme required less energy than the free one to overcome the conversion barrier to transform the substrate into a product. The results

indicate that the immobilized L-ASNase more stable and advantageous than the free counterpart.

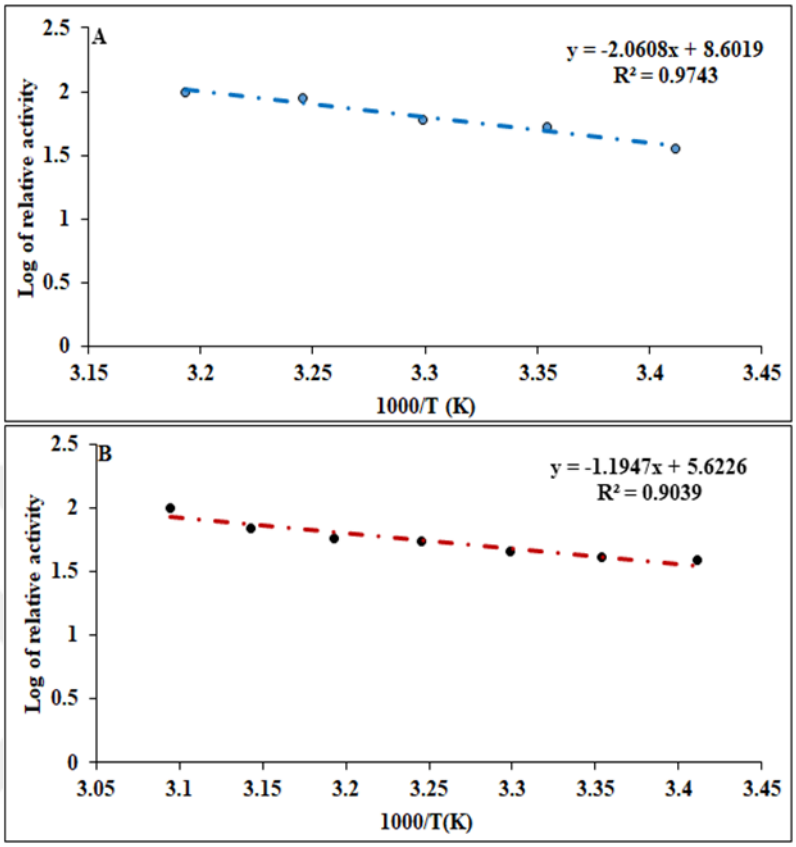

Figure 4.46: The activation energy of PEG-L-ASNase (A), and $NaYF_4:Yb^{3+}$, Er^{3+}/ GPTMS-PEG-L-ASNase (B).

4.2.2.10. Laser power, laser distance, and laser exposure time

The optimum power of $NaYF_4:Yb^{3+}$, Er^{3+}/GPTMS-PEG-L-ASNase was determined by the induced different power of NIR light to immobilize enzyme on UCNP. Different milliwatts (mW) were scanned to find out the optimum power of UCNP by applying the constant amount of UCNP with a fixed distance between nanoparticles and NIR light. The obtained optimum power was 600 mW, the enzyme activity was an increase from 100 % to 195 % as shown in Figure 4.47 A. After increasing the NIR power decrease in enzyme activity took place coincidentally, it was assumed that the NIR generated heat probable affected on the three-dimensional structure of the enzyme or due to less enzyme immobilized to this type of UCNP.

After the maximum NIR light power was found, the right distance between $NaYF_4:Yb^{3+}$, Er^{3+}/GPTMS-PEG-L-ASNase and laser power was optimized. In this

experiment, the NIR light was arranged at 400 mW with a fixed amount of enzyme immobilized on UCNP and different distances were scanned (0 – 5 cm). The optimum activity was founded at a 2 cm distance between NIR light and UCNP enzyme immobilized as seen in Figure 4.47 B. It was determined that decreasing the enzyme activity by increasing the distance, due to decreasing the effect of NIR light on UCNP nanoparticles.

NIR exposure time of $NaYF_4:Yb^{3+}$, Er^{3+}/GPTMS-PEG-L-ASNase, on the other hand, the activity affected by time was also determined without exposure to NIR light. As it is shown in Figure 4.47 C, there was a sharp increase in the activity the exposure to NIR light until 90 min, after that small decrease in the activity that may be due to the heat from NIR laser leads to an effect on enzyme and decrease in activity occurred.

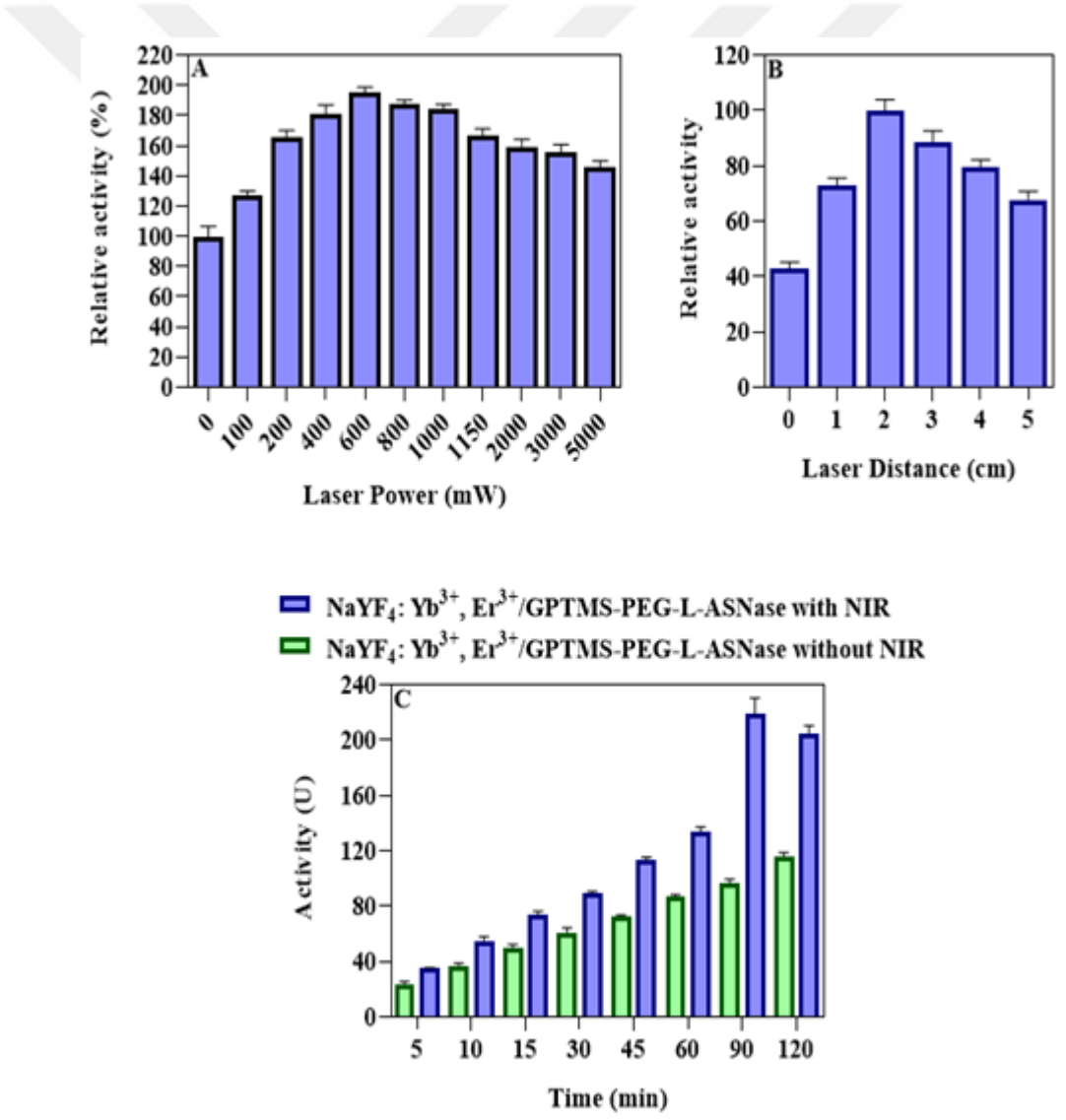

Figure 4.47: Induce of $NaYF_4:Yb^{3+}$, Er^{3+}/GPTMS-PEG-L-ASNase, NIR light power (A), NIR distance (B), and NIR time (C).

4.2.2.11. Stability of $NaYF_4:Yb^{3+}$, Er^{3+}/GPTMS-PEG-L-ASNase

The stability of $NaYF_4:Yb^{3+}$, Er^{3+}/GPTMS-PEG-L-ASNase and the effect of NIR after storage. Different samples of immobilized enzyme were incubated with PBS (50 mM, pH 7.4) at +37 °C for one week, and the activity was measured every single day by first exposure to NIR light at optimum conditions then measured. After one week the activity was above 54 % from the initial activity as shown in Figure 4.48.

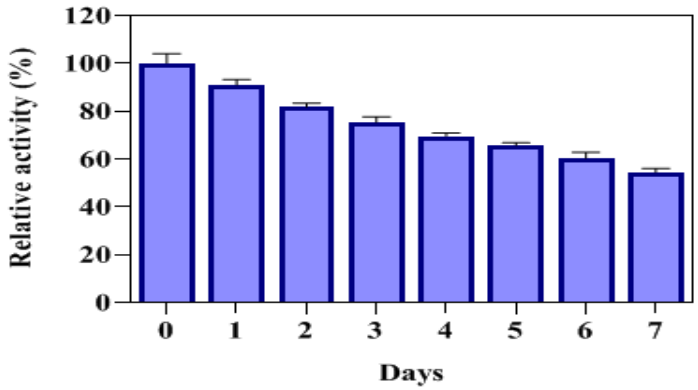

Figure 4.48: Stability of $NaYF_4:Yb^{3+}$, Er^{3+}/GPTMS-PEG-L-ASNase in PBS by NIR light.

4.2.2.12. *In vitro* half-life

PEG-L-ASNase and $NaYF_4:Yb^{3+}$, Er^{3+}/GPTMS-PEG-L-ASNas, were incubated with rat blood serum for 1 week at +37 °C, to investigate *in vitro* half-life of the enzyme. Then, the activity of the free L-ASNase and immobilized L-ASNase was measured at optimum conditions and their *in vitro* half-life was calculated by comparing with the initial activity as shown in Figure 4.49.

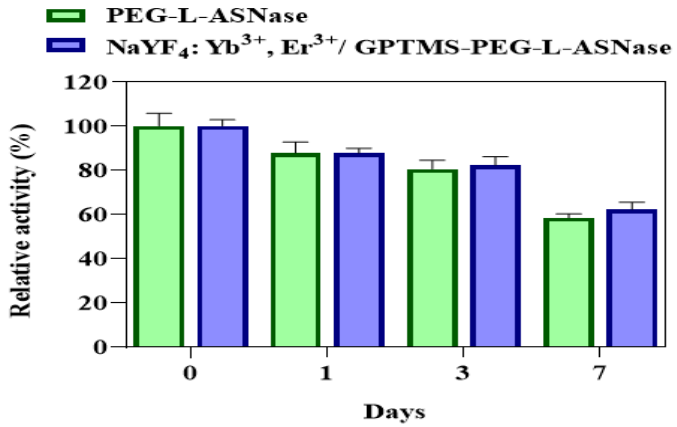

Figure 4.49: *In vitro* half-life of PEG-L-ASNase and immobilized $NaYF_4:Yb^{3+}$, Er^{3+}/ GPTMS-PEG-L-ASNase.

4.2.2.13. Plasma coagulation

The prothrombin time (PT) and the activated partial thromboplastin time (APTT), the reflective effect of $NaYF_4:Yb^{3+}$, Er^{3+}/GPTMS and $NaYF_4:Yb^{3+}$, Er^{3+}/GPTMS-PEG-L-ASNase on intrinsic and extrinsic pathways of the blood coagulation cascade. They were determined by incubating in platelet-poor plasma as seen in Figure 4.50. The results suggested there no coagulation occurred when UCNPs were added these findings indicate that both $NaYF_4:Yb^{3+}$, Er^{3+}/GPTMS and $NaYF_4:Yb^{3+}$, Er^{3+}/ GPTMS-PEG-L-ASNase are hemocompatible which may be related to the hydrophilicity and surface area charge of these particles.

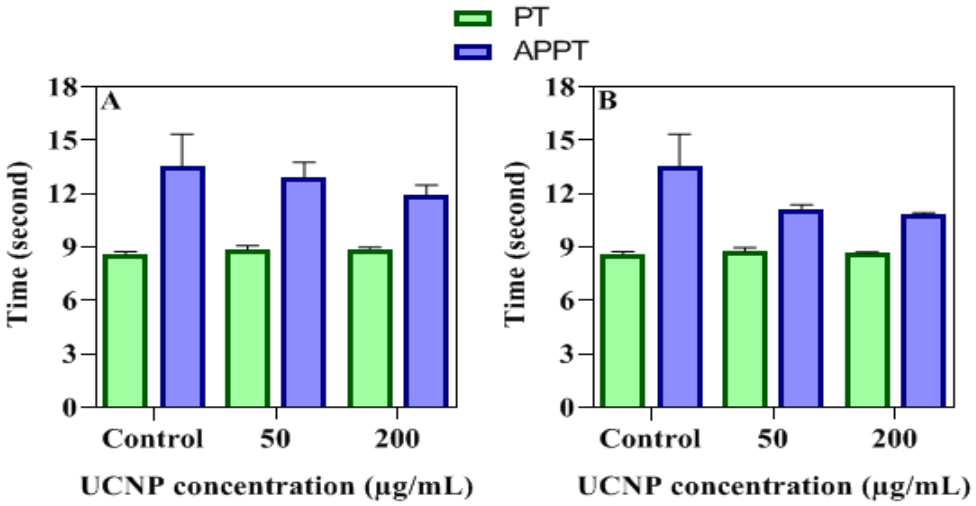

Figure 4.50: Plasma coagulation of $NaYF_4:Yb^{3+}$, Er^{3+}/GPTMS (A), and $NaYF_4:Yb^{3+}$, Er^{3+}/GPTMS-PEG-L-ASNase (B).

4.2.2.14. *In vitro* cytotoxicity

The *in vitro* cytotoxicity of the prepared UCNP was tested calorimetrically by using the MTT test and the results were shown in Figure 4.51 A and B. In cytotoxicity studies, cell viability is classified as more than 50 % toxic, from 51 to 70 % mildly cytotoxic, less than 71% non-cytotoxic [211]. Different concentration (12.5, 25, 50, 100, and 200 µg/mL) of $NaYF_4:Yb^{3+}$, Er^{3+}/GPTMS and $NaYF_4:Yb^{3+}$, Er^{3+}/GPTMS-PEG-L-ASNase were tested against mouse fibroblast (L-929). Also, the morphology of the cells treated with UCNPs and UCNPs-PEG-L-ASNase were given in (Figure 4.28 C), after 24, 48, and 72 h form incubation, as a result, there was no change in the morphological structure of the cells. As a result, it was observed that the synthesized UCNP nanoparticles had no *in vitro* toxic effects on cell viability.

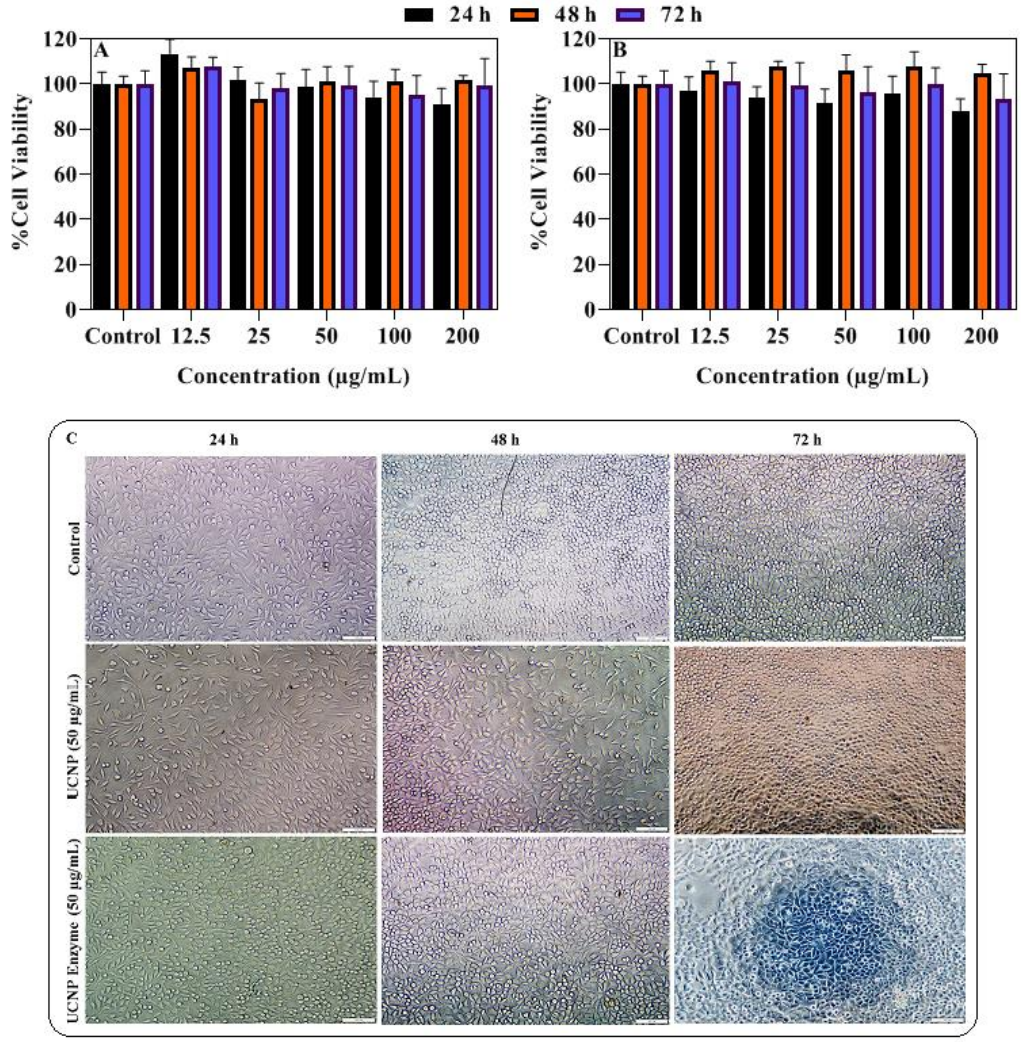

Figure 4. 51: Cell viability results after incubation 24, 48, and 72 hours of L-929 with $NaYF_4$:Yb^{3+}, Er^{3+}/GPTMS (A), $NaYF_4$:Yb^{3+}, Er^{3+}/GPTMS-PEG-L-ASNase (B), and morphological image of L-929 fibroblast cells (C).

4.2.3. Immobilization parameters of $NaYF_4$: Yb^{3+}, Er^{3+}/ICPTES

4.2.3.1. Enzyme unit and incubation time

The enzyme unit of covalent immobilization for $NaYF_4$:Yb^{3+}, Er^{3+}/ICPTES PEG-L-ASNase was determined as 35 U and chosen as the amount of enzyme for immobilization. As seen in (Figure 4.52 A), the immobilization yield decreased after 35 U, while in Figure 4.52 B there was a sharp increase in the catalytic activity from 5-35 U. In the same time, 50 U and 75 U only indicated either similar or small increased in the catalytic activity. Furthermore, the immobilization yield, activity yield, and immobilization efficiency for 35 U were founded as 98.74 ± 0.60 %, 75.02 ± 3.86 %, and 76.08 ± 3.42 %, respectively.

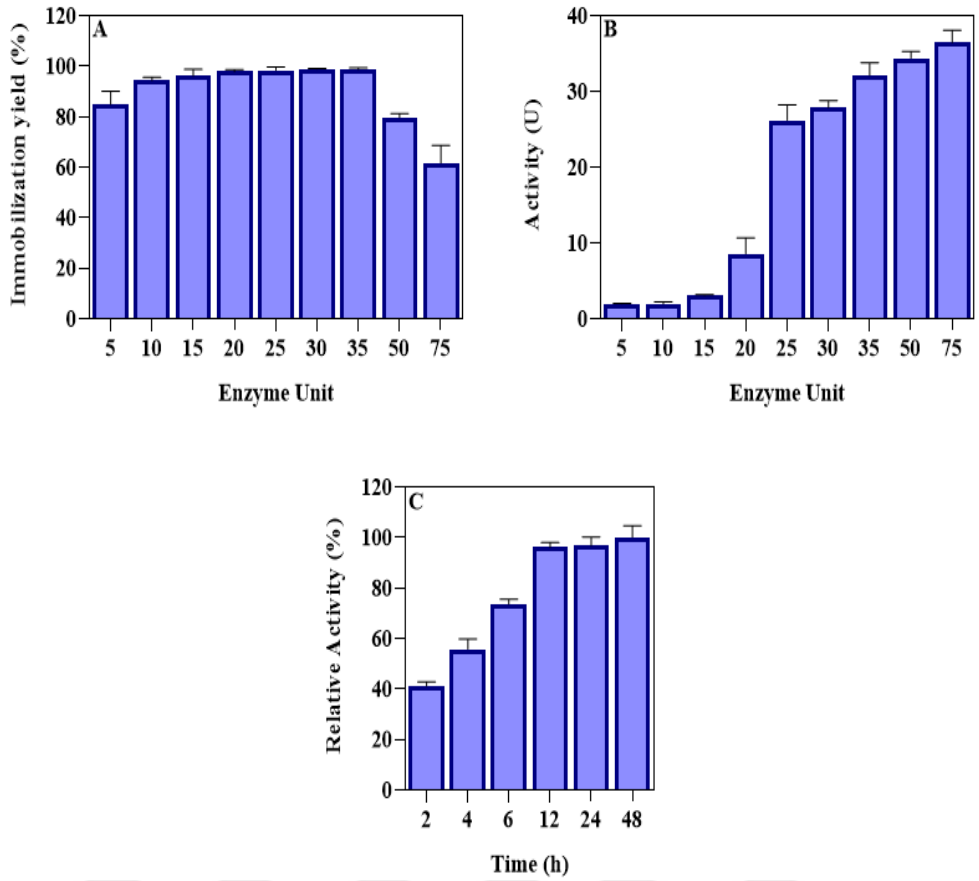

Figure 4.52: L-ASNase immobilization yield (A), L-ASNase catalytic activity (B), and incubation time (C) of $NaYF_4$:Yb^{3+}, Er^{3+}/ICPTES-PEG-L-ASNase.

The immobilization times were taken place between 2 to 48 hours. A long duration of immobilization means it difficult to bind the enzyme to the carrier material, which decreases the activity of the enzymes. As can be seen in Figure 4.52 C, after 12 hours from immobilization, there is a marked increase in the relative activity of the enzyme. As the immobilization time increased, the relative activity of the immobilized enzyme approximately stays constant, due to the covalently bond between the enzyme and UCNP after 12 hours of immobilization don't have a free group anymore on UCNP even if we increase the enzyme concentrations. Based on these results, the ideal time of 12 hours as the immobilization time was taken as the optimum value.

4.2.3.2. Optimum pH and temperature

The enzymatic activities of PEG-L-ASNase and $NaYF_4$:Yb^{3+}, Er^{3+}/ICPTES-PEG-L-ASNase were measured between pH 4 and 10 to determine the optimum pH. As shown in Figure 4.53 A, the maximum activities of the PEG-L-ASNase and

$NaYF_4:Yb^{3+}$, Er^{3+}/ICPTES-PEG-L-ASNase were obtained at pH 8.5 and 7.5, respectively. Generally, the changes in optimum pH induce enzymes conformational after immobilization. Also, the alteration of optimum pH value probably drives the change in acidic or basic amino acid ionization surrounding the enzyme's active site. Apart from this, amine groups of PEIs, which is the main functional group on $NaYF_4:Yb^{3+}$, Er^{3+}/ICPTES, it regulates the shifting in pH. Meanwhile, this shifting is also important because of the similarity with human body pH. The relative activity of the $NaYF_4:Yb^{3+}$, Er^{3+}/ICPTES-PEG-L-ASNase was higher than that L-ASNase. The relative activity of the $NaYF_4:Yb^{3+}$, Er^{3+}/ICPTES-PEG-L-ASNase higher than that L-ASNase even at pH 10, the activity of immobilized still above 66 % while the free one above 41 %. It is noted that the main advantage of immobilization process is higher stability of enzyme as well as alleviating effects environmental factors against enzyme.

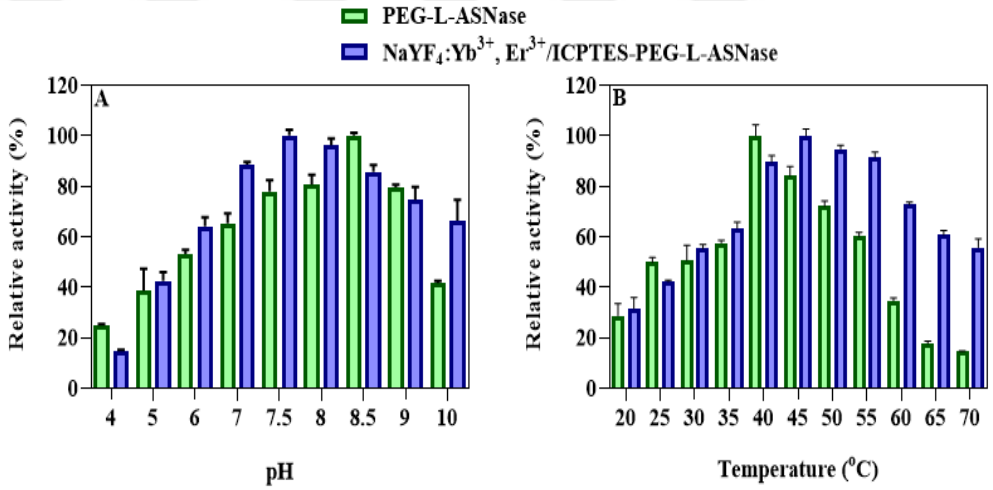

Figure 4.53: Optimum pH (A), and temperature (B) of PEG-L-ASNase and $NaYF_4:Yb^{3+}$, Er^{3+}/ICPTES-PEG-L-ASNase.

The optimum temperature for free L-ASNase was found at 40 °C, while this value increased to 45 °C after immobilization on $NaYF_4:Yb^{3+}$, Er^{3+}/ICPTES-PEG-L-ASNase as shown in Figure 4.53 B. The increase in optimum temperature may be due to the increased affinity of the enzyme to the substrate and the change in the conformational integrity of the enzyme structure due to covalent interactions between the enzyme and the prepared UCNP.

4.2.3.3. Thermal and pH stability

In comparison against the free enzyme, thermal stability is also the most important benefit of immobilization. The results show in Figure 4.54 A, that the thermal stability of PEG-L-ASNase and $NaYF_4:Yb^{3+}$, Er^{3+}/ICPTES-PEG-L-ASNase were incubated at 50 °C for 6 hours. After 6 hours, the remained activity of PEG-L-ASNase was 24% from its initial activity, while for $NaYF_4:Yb^{3+}$, Er^{3+}/ICPTES-PEG-L-ASNase remained 54 % from its initial activity. As a possible result of diminishing molecular mobility and conformational alterations of the enzyme, temperature resistance was emerged by immobilization of L-ASNase. Therefore, in accordance to result immobilization significantly improves thermal stability.

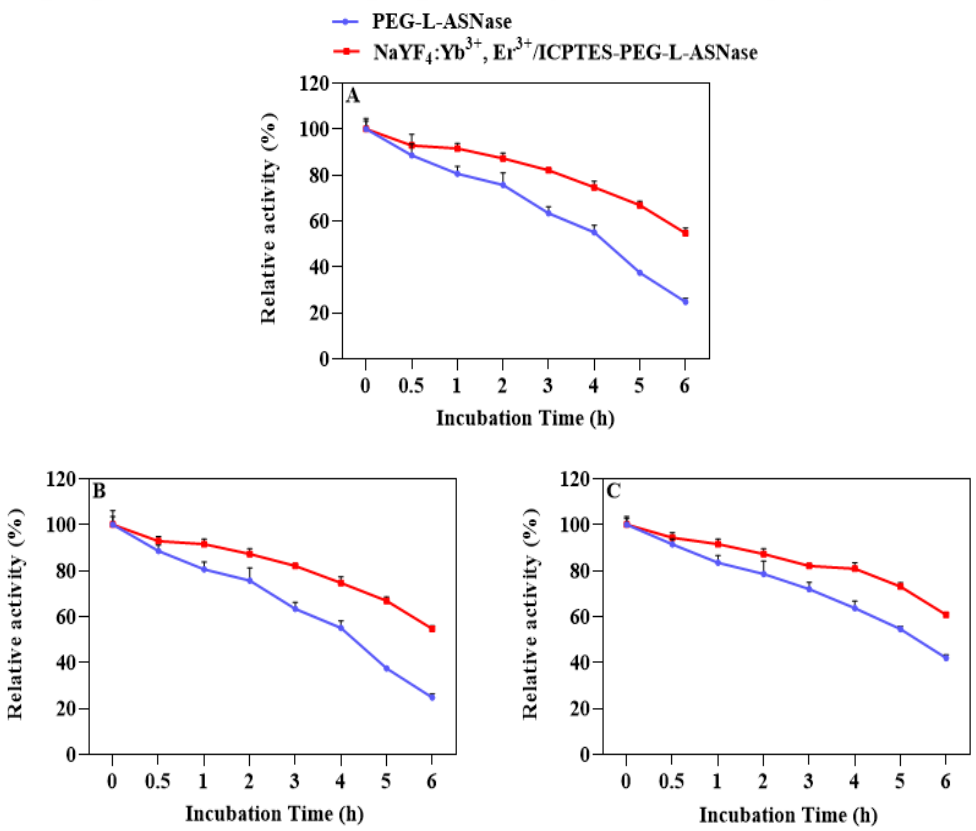

Figure 4.54: Thermal stability (A), pH stability at pH 4 (B), and pH stability at pH 9 (C) of PEG-L-ASNase and $NaYF_4:Yb^{3+}$, Er^{3+}/ICPTES-PEG-L-ASNase.

pH stability is also an important parameter for enzyme immobilization. The pH stability was determined by incubation PEG-L-ASNase and $NaYF_4:Yb^{3+}$, Er^{3+}/ ICPTES-PEG-L-ASNase at pH 4 and 9 for 6 hours as shown in Figure 4.54 B and C. After 6h, the relative activity for pH 4 were found above 24 % for free enzyme and 54 % for immobilized one, while at pH 9 the activity was 41 % and 60 % for free and

immobilized LASNase from initial activity, respectively. Owing to optimum pH in the alkaline range, it was clearly concluded that both PEG-L-ASNase and $NaYF_4$:Yb^{3+}, Er^{3+}/ICPTES-PEG-L-ASNase exhibited the higher enzymatic stability at pH 9 rather the pH 4.

4.2.3.4. Effect of metal ion and solvent

The effect of both metal ions and organic solvents were determined on the free PEG-L-ASNase and immobilized $NaYF_4$:Yb^{3+}, Er^{3+}/ICPTES-PEG-L-ASNase were incubated with different metal ions. In our study, Na^{1+}, Ag^{1+}, Ba^{2+}, Ca^{2+}, Co^{2+} , Mg^{2+}, Ni^{2+} , and Al^{3+} increased enzyme activity. On the other hand, Cu^{2+}, Sr^{2+}, Zn^{2+}, and Cr^{3+} inhibited the enzyme activity as shown in Figure 4.55 A. The activity of the immobilized enzyme is better compared with the free enzyme. However, immobilized enzymes have been affected by metal ions that inhibit activity less than as much as free enzymes.

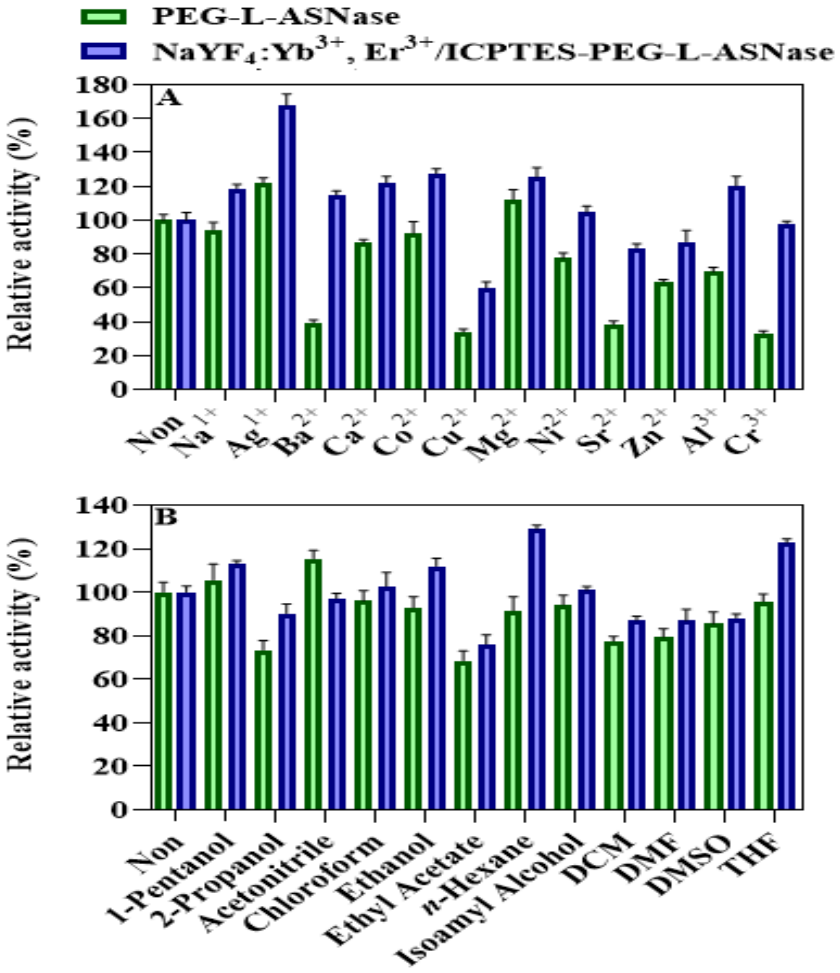

Figure 4.55: Stability of PEG-L-ASNase and $NaYF_4$:Yb^{3+}, Er^{3+}/ICPTES-PEG-L-ASNase on metal ions (A), and organic solvents (B).

However, the solvent effect on of PEG-L-ASNase and $NaYF_4:Yb^{3+}$, Er^{3+}/ICPTES-PEG-L-ASNase were invested by using different organic solvents like (1-pentanol, 2-propanol, acetonitrile, chloroform, ethanol, ethyl acetate, *n*-hexane, isoamyl alcohol, DCM, DMF, DMSO, and THF after incubation for 24 h at room temperature, the activities were determined as shown in figure 4.55 B. The results were indicated that the immobilization enzyme has better stability against organic solvent even in some of the solvents the activity immobilization enzyme was increased, except for acetonitrile the activity for the free enzyme was higher than the immobilized one.

4.2.3.5. Reusability

The reusability of $NaYF_4:Yb^{3+}$, Er^{3+}/ICPTES-PEG-L-ASNase was shown in Figure 4.56. The remaining relative activity after a cycle was still above 91 % from its initial activity, while the activity still retained more than 82 % of its starting activity even after 20 cycles. Covalent immobilization improves the reusability of the enzyme compared to the physical one. Reusability is one of the advantages of immobilization, due to the easy separation of the immobilized enzyme from the reaction mixture and reused for several times, unlike the free enzyme that can not separate from the reaction medium.

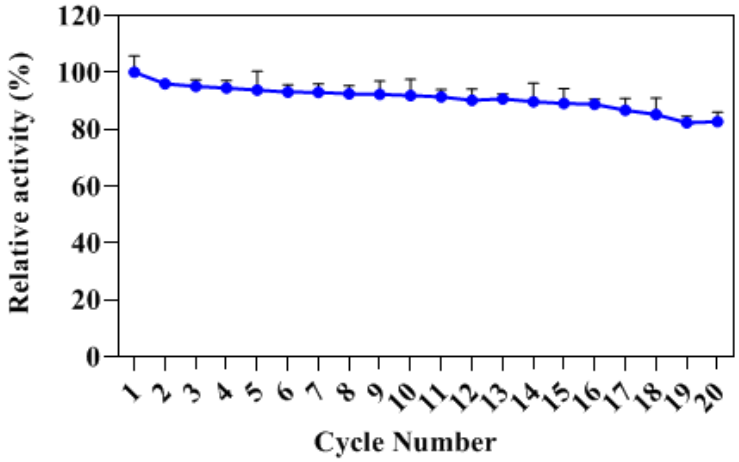

Figure 4.56: Reusability of $NaYF_4:Yb^{3+}$, Er^{3+}/ICPTES-PEG-L-ASNase.

4.2.3.6. Storage stability

Storage stability is a crucial parameter for commercial-scale application of an enzyme, while it has been recognized that enzyme activity continuously diminishes over time due to instability during storage. Therefore, the storage stability of both free

PEG-L-ASNase and $NaYF_4:Yb^{3+}$, Er^{3+}/ICPTES-PEG-L-ASNase were investigated at 4 and 25 °C for 4 weeks with the weekly measurement results were shown in Figure 4.57. The activity $NaYF_4:Yb^{3+}$, Er^{3+}/ICPTES-PEG-L-ASNase still above 71 % and 61 % of their initial activities at 4 and 25 °C, respectively. Free L-ASNase preserved 52 % and 43 % of its initial activity, respectively. The loss of enzymatic activity is probably attributed to protein denaturation and degradation during long-term storage. These results showed that the storage stability of the $NaYF_4:Yb^{3+}$, Er^{3+}/ICPTES-PEG-L-ASNase was better compared to the free enzyme at both 4 and 25 °C. It was also implied that the stability of immobilized enzyme was higher at 25°C with insignificant loss than the 4 °C counterparts. Owing to the result, $NaYF_4:Yb^{3+}$, Er^{3+}/ICPTES-PEG-L-ASNase indicated its promising and alternative carrier matrix material due to its long-term storage stability.

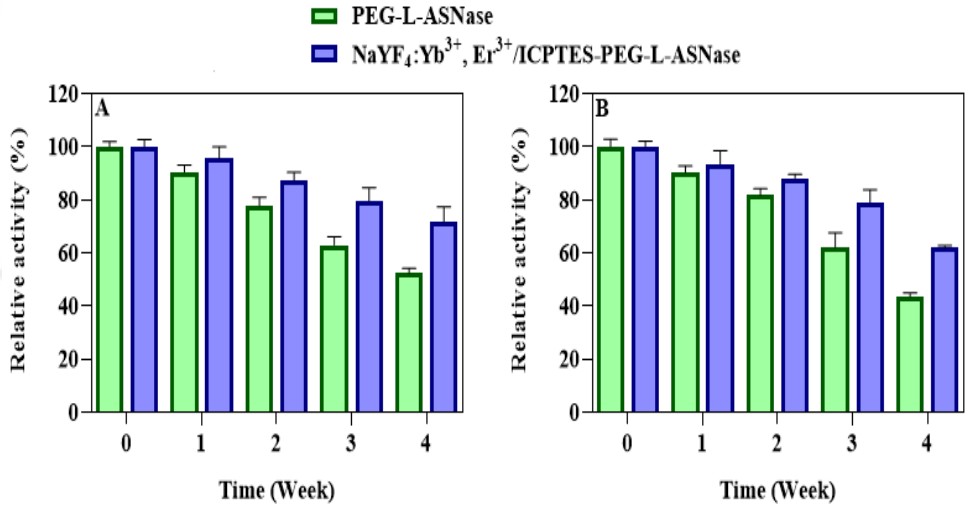

Figure 4.57: Storage stability of PEG-L-ASNase and $NaYF_4:Yb^{3+}$, Er^{3+}/ICPTES-PEG-L-ASNase at +4°C (A), and at +25 °C (B).

4.2.3.7. Trypsin resistance

The resistance of both free PEG-L-ASNase and $NaYF_4:Yb^{3+}$, Er^{3+}/ICPTES-PEG-L-ASNase against trypsin digestion is shown in Figure 4.58. After 120 minutes from incubation with trypsin at +37 °C, free L-ASNase was almost completely hydrolyzed, while the activity of immobilized LASNases retained 52 % of its original activity. The results showed that the resistance of immobilized enzyme to trypsin digestion was greatly improved compared to the free one.

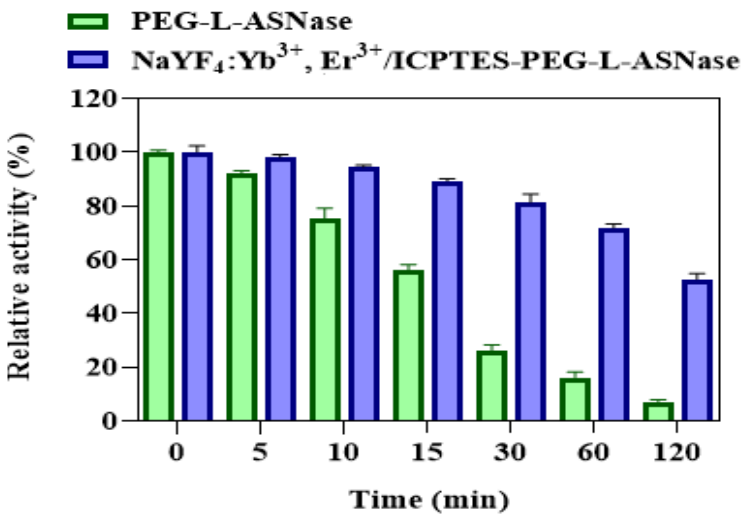

Figure 4.58: Trypsin resistance of PEG-L-ASNase and $NaYF_4$:Yb^{3+}, Er^{3+}/ICPTES-PEG-L-ASNase.

4.2.3.8. Kinetic parameter

The kinetic parameters of free PEG-L-ASNase and $NaYF_4$:Yb^{3+}, Er^{3+}/ICPTES-PEG-L-ASNase were estimated and summarized in Table 4.5. The obtained K*m* values for the free L-ASNase and immobilized L-ASNase were 2.31 and 1.651 mM, respectively. Besides, the Lineweaver–Burk plots were shown in Figure 4.59. When the enzyme has a small K*m* value, it achieves maximum catalytic efficiency at a low substrate concentration. Meanwhile, a decrease in the Vmax was observed value after enzyme immobilization. The apparent *Vmax* value increased from 140.85 to 112.36 µmol/min. The obtained results are in accordance with the values reported previously.

Table 4.5: Kinetic parameters of PEG-L-ASNase and $NaYF_4$:Yb^{3+}, Er^{3+}/ICPTES-PEG-L-ASNase.

Sample	**K*m* (mM)**	***Vmax* (µmol/min)**	**R^2**
PEG-L-ASNase	2.31 ± 0.042	140.85 ± 3.235	0.9663
$NaYF_4$:Yb^{3+},Er^{3+}/ICPTES-PEG-L-ASNase	1.651 ± 0.05	112.36 ± 4.123	0.9269

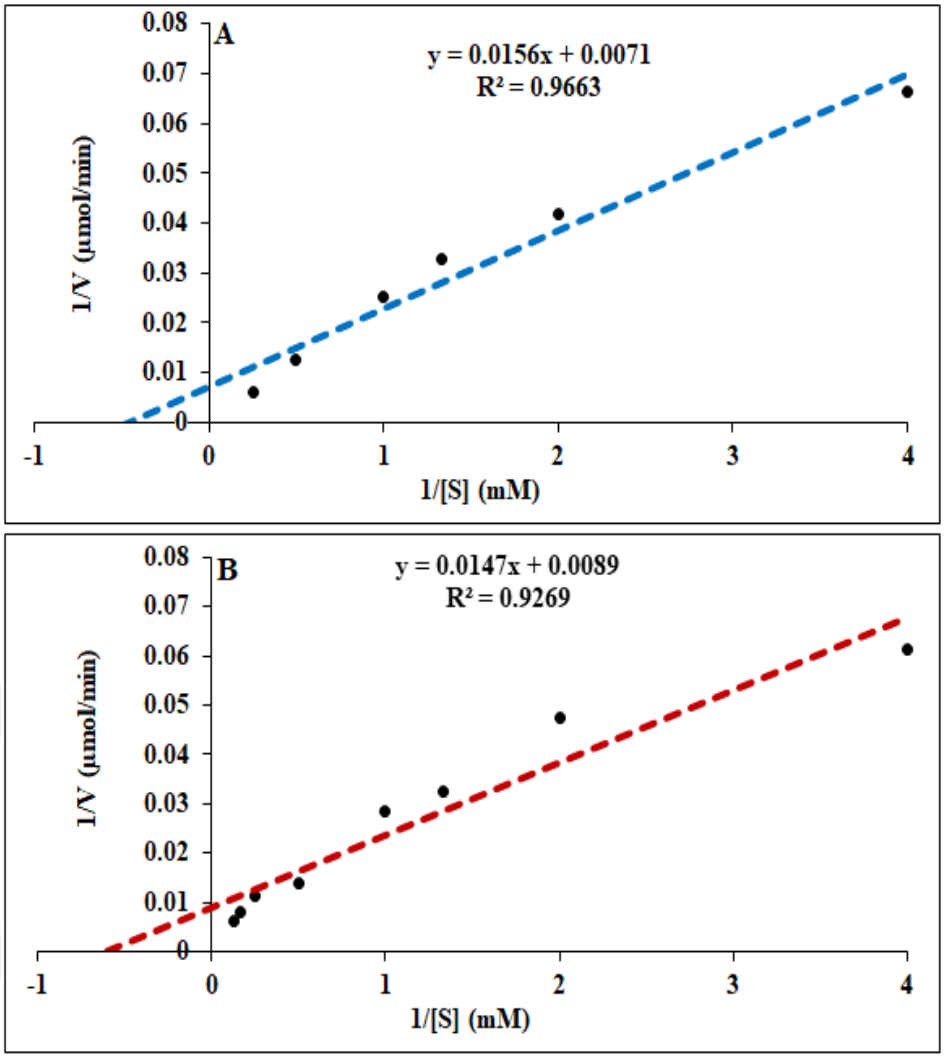

Figure 4.59: Kinetic parameters of PEG-L-ASNase (A), and $NaYF_4:Yb^{3+}$, Er^{3+}/ICPTES-PEG-L-ASNase (B).

4.2.3.9. Activation energy

The activation energy (*Ea*) values were calculated by the Arrhenius equation for both PEG-L-ASNase and $NaYF_4:Yb^{3+}$, Er^{3+}/ICPTES-PEG-L-ASNase. The *Ea* values which were calculated from the slope of log (% relative activity) versus 1000/T, while *Ea* values were founded for free L-ASNase as 17.13 kJ/mol, while for immobilized L-ASNase 18.1 kJ/mol as seen in Figure 4.60. The *Ea* value was increased after immobilization, this type of immobilization has higher temperature sensitivity. This increased in *Ea* value demonstrated that immobilized L-ASNase requires more energy than the free L-ASNase to overcome the conversion barrier to transform the substrate into a product.

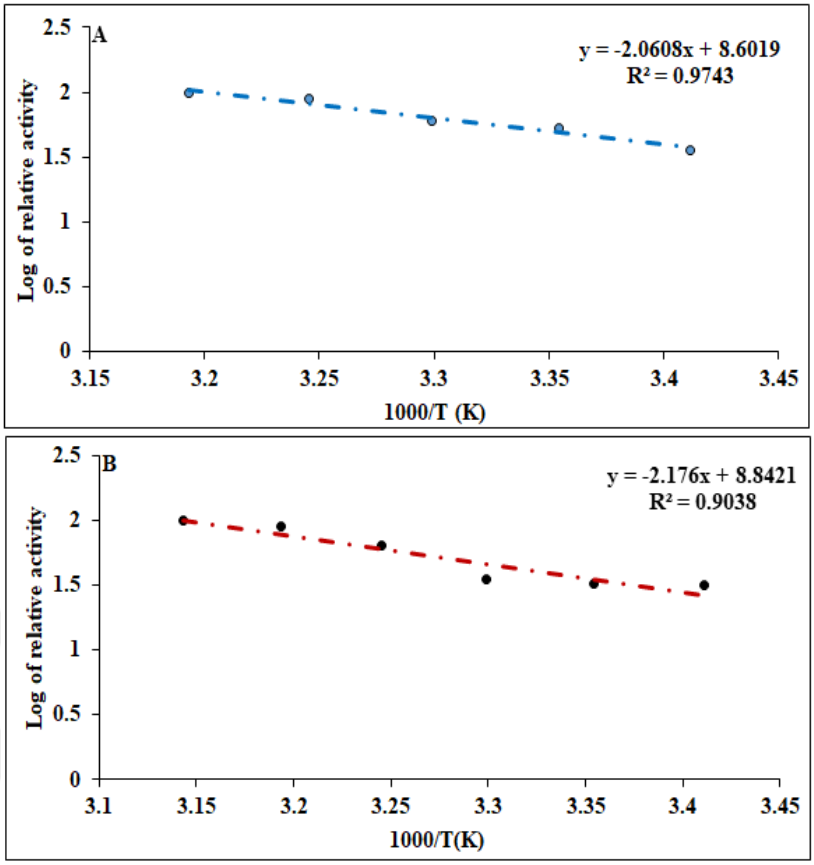

Figure 4.60: The activation energy of PEG-L-ASNase (A), and $NaYF_4:Yb^{3+}$, Er^{3+}/ ICPTES-PEG-L-ASNase (B).

4.2.3.10. Laser power, laser distance, and laser exposure time

The optimum laser power for $NaYF_4:Yb^{3+}$, Er^{3+}/ICPTES-PEG-L-ASNase was determined by the induced NIR light to immobilize enzyme on UCNP. Different milliwatts (mW) were scanned to find out the optimum power of UCNP by applying the constant amount of UCNP with a fixed distance between nanoparticles and NIR light. According to the result, the obtained optimum power was 600 mW, with an increase in L-ASNase activity from 100 % to 238 % as shown in Figure 4.61. In accordance to the result, diminishing enzyme activity took place coincidently with increasing NIR light power, it was assumed that the NIR generated heat probable affected on the three-dimensional structure of the enzyme or due to less enzyme bounded to this type of UCNP.

After the maximum NIR light power was found, the optimum distance between $NaYF_4:Yb^{3+}$, Er^{3+}/ICPTES-PEG-L-ASNase and laser power was optimized. In this experiment, the NIR light was fixed arranged at 600 mW with a fixed amount of

enzyme immobilized on UCNP and different distances were scanned (0–5 cm). The optimum activity was founded at a 2 cm distance between NIR light and UCNP immobilized enzyme as seen in Figure 4.61 B. Due to the result, the decrease in enzyme activity was inversely proportional against the increasing distance due to decreasing the effect of NIR light on UCNP nanoparticles.

NIR exposure time was investigated by keeping constant laser power, distance, and the amount of $NaYF_4$:Yb^{3+}, Er^{3+}/ICPTES-PEG-L-ASNase, while the activity was also determined in the absence of NIR radiation. As shown in Figure 4.61 C there was a sharp increase in the activity due to the exposure of NIR light until 90 min, thereafter a slight decrease in the activity that may be due to the heat become from the NIR laser led to effect on enzyme and decrease in activity occurred.

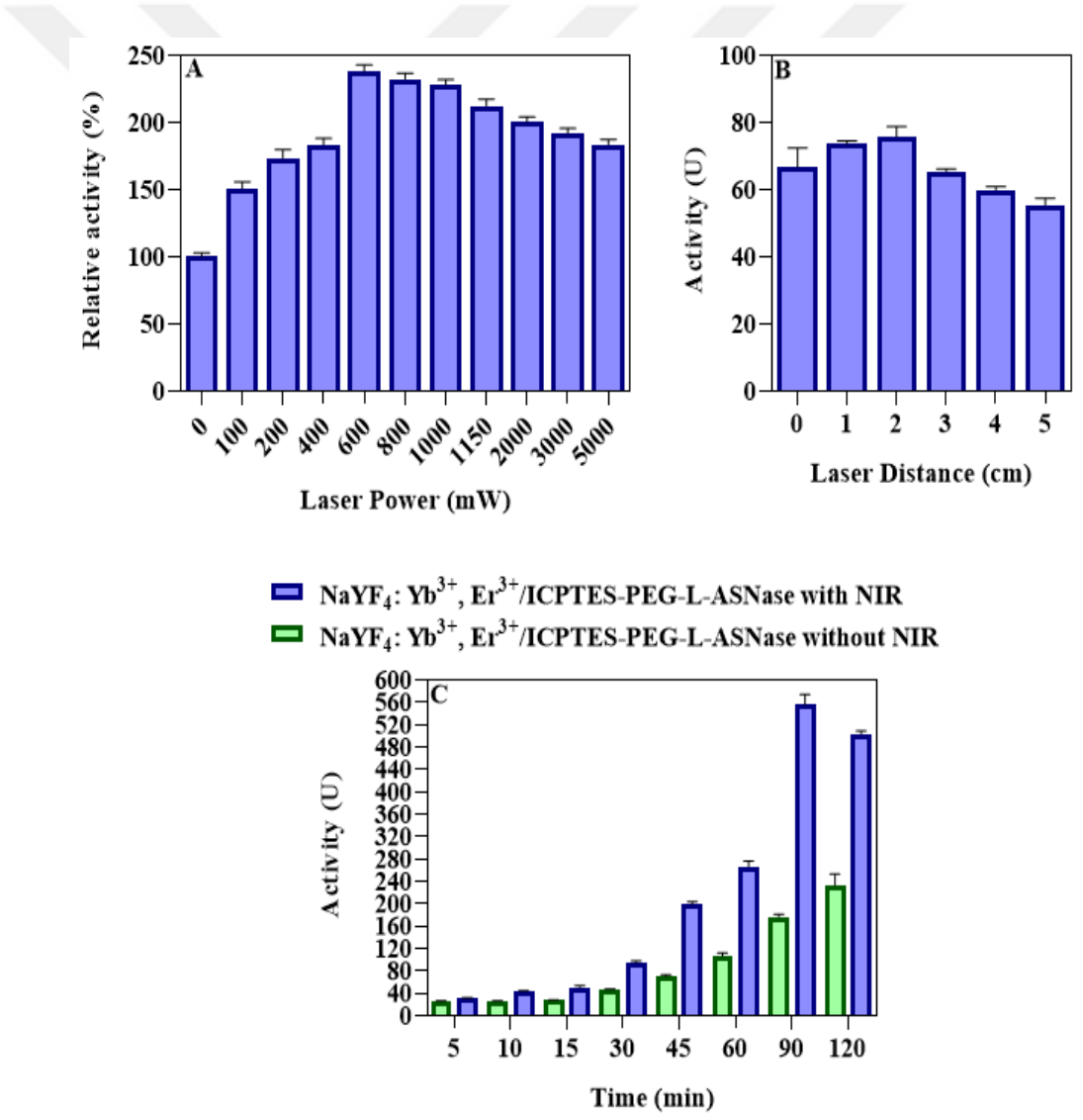

Figure 4.61: Induce of $NaYF_4$:Yb^{3+}, Er^{3+}/ICPTES-PEG-L-ASNase, NIR light power (A), NIR distance (B), and NIR time (C).

4.2.3.11. Stability of $NaYF_4:Yb^{3+}$, Er^{3+}/ICPTES-PEG-L-ASNase

The stability of $NaYF_4:Yb^{3+}$, Er^{3+}/ICPTES-PEG-L-ASNase and the effect of NIR after storage. Different samples of $NaYF_4:Yb^{3+}$, Er^{3+}/ICPTES-PEG-L-ASNase were incubated with PBS (50 mM, pH 7.4) at +37 °C for one week, and the activity was measured every single day by first exposure to NIR light at optimum conditions then the activity was measured. After one week the activity was above 67 % from the initial activity as shown in (Figure 4.62).

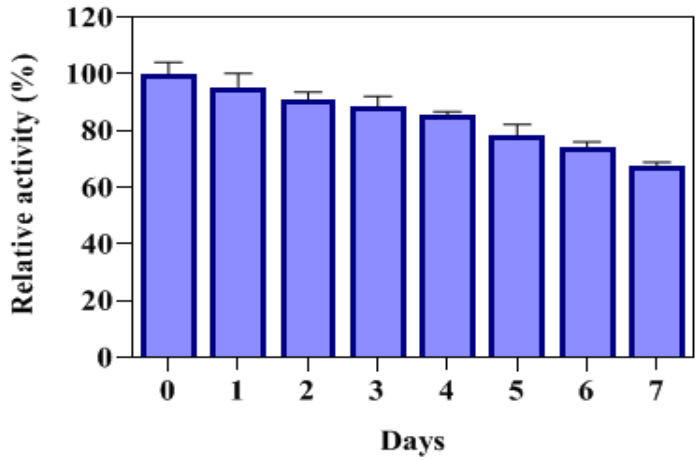

Figure 4.62: Stability of $NaYF_4:Yb^{3+}$, Er^{3+}/ICPTES-PEG-L-ASNase in PBS by NIR light.

4.2.3.12. *In vitro* half-life

In vitro half-life of were determined for both free PEG-L-ASNase and $NaYF_4:Yb^{3+}$, Er^{3+}/ICPTES -PEG-L-ASNas. The samples and rat blood serum were incubated with rat blood serum for 1 week at +37 °C. Then, the activity of the free and immobilized enzyme was measured at optimum conditions and their *in vitro* half-life was calculated by compare with the initial activity as shown in (Figure 4.63).

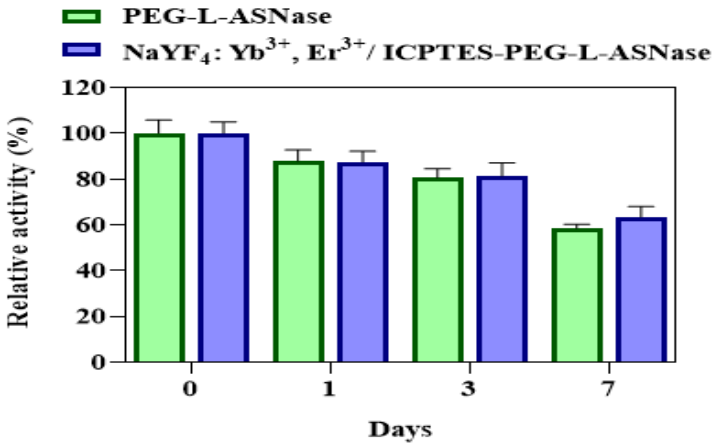

Figure 4.63: *In vitro* half-life of PEG-L-ASNase and immobilized $NaYF_4$:Yb^{3+}, Er^{3+}/ ICPTES-PEG-L-ASNase.

4.2.3.13. Plasma coagulation

The prothrombin time (PT) and the activated partial thromboplastin time (APTT), reflect the effect of $NaYF_4$:Yb^{3+}, Er^{3+}/ICPTES and $NaYF_4$:Yb^{3+}, Er^{3+}/ICPTES-PEG-L-ASNase on intrinsic and extrinsic pathways of the blood coagulation. They were determined by incubating in platelet-poor plasma as seen in Figure 4.64. The results suggested there is no coagulation occurred when UCNPs were added, which is probably related to the hydrophilicity and surface area charge of these particles.

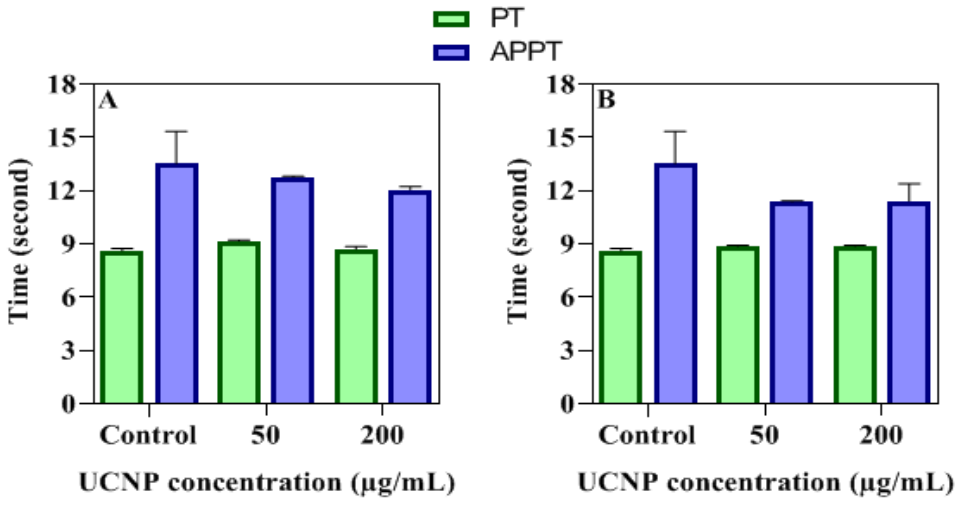

Figure 4.64: Plasma coagulation of $NaYF_4$:Yb^{3+}, Er^{3+}/ICPTES (A), and $NaYF_4$:Yb^{3+}, Er^{3+}/ICPTES-PEG-L-ASNase (B).

4.2.3.14. *In vitro* cytotoxicity

The *in vitro* cytotoxicity of the synthesized UCNP was tested calorimetrically by using the MTT test and the results were shown in Figure 4.65 A and B. Owing to the cell viability classification in cytotoxicity studies, 50 %, 51–70 %, and 71 % are consecutively classified as toxic, mildly cytotoxic and non-cytotoxic [211]. Different concentration (12.5, 25, 50, 100, and 200 µg/mL) of $NaYF_4:Yb^{3+}$, Er^{3+}/ICPTES and $NaYF_4:Yb^{3+}$, Er^{3+}/ICPTES-PEG-L-ASNase were tested against mouse fibroblast (L-929). In addition, the morphology of the cells treated with UCNPs and UCNPs-PEG-L-ASNase were given in (Figure 4.65 C), after 24, 48, and 72 h form incubation. As a result, the morphological alteration was absent, which due to the synthesized UCNP did not indicate *in vitro* toxicity in accordance to cell viability.

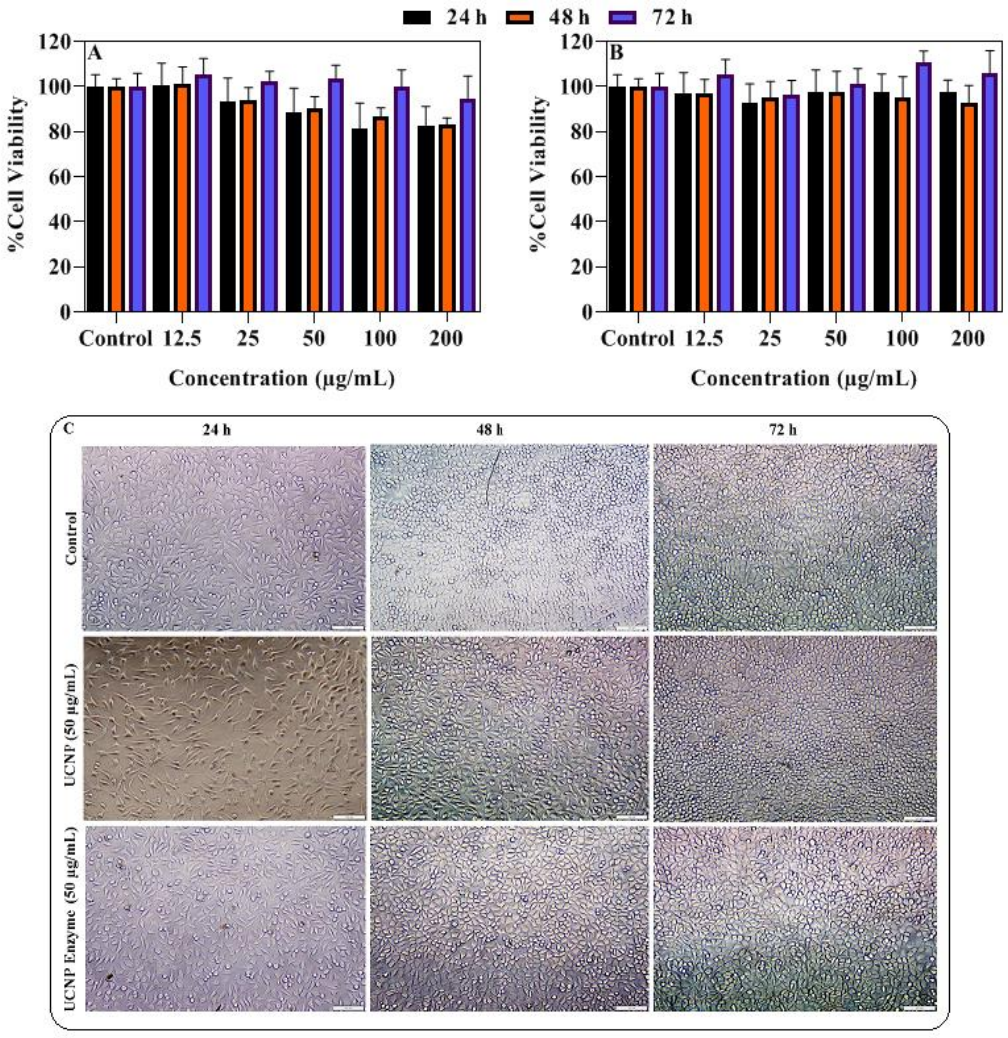

Figure 4. 65: Cell viability results after incubation 24, 48, and 72 hours of L-929 with $NaYF_4:Yb^{3+}$, Er^{3+}/ICPTES (A), $NaYF_4:Yb^{3+}$,Er^{3+}/ICPTES-PEG-L-ASNase (B), and morphological image of L-929 Fibroblast cells (C).

4.2.4. Immobilization parameters of $NaYF_4$: Nd^{3+}, Yb^{3+}, Er^{3+}/PEI

4.2.4.1. Enzyme unit and incubation time

The optimum enzyme concentration was chosen as 75 U the right amount of enzyme for immobilization. As seen in (Figure 4.66 A), the immobilization yield decreased after 75 U, while in (Figure 4.66 B) there was a sharp increase in the catalytic activity from 5-75 U. Later, relative activity decreased as the enzyme unit was increased. This decrease in enzyme activity can be explained by the enzyme is overloaded into the formulation with a higher enzyme concentration, which will cover the active site and cause a decrease in enzyme activity, and the loading capacity of 25 mg of UCNP immobilized physically 75 U all the function group bounded to enzyme so there is no more free function group. In the same time, 100 U only indicated either a similar or small increase in the catalytic activity. Furthermore, the immobilization yield (IY), activity yield (AY), and immobilization efficiency (IE) for 75 Uwere founded as 98.17 ± 0.13 %, 86.78 ±1.58 %, and 95.63 ± 3.56 %.

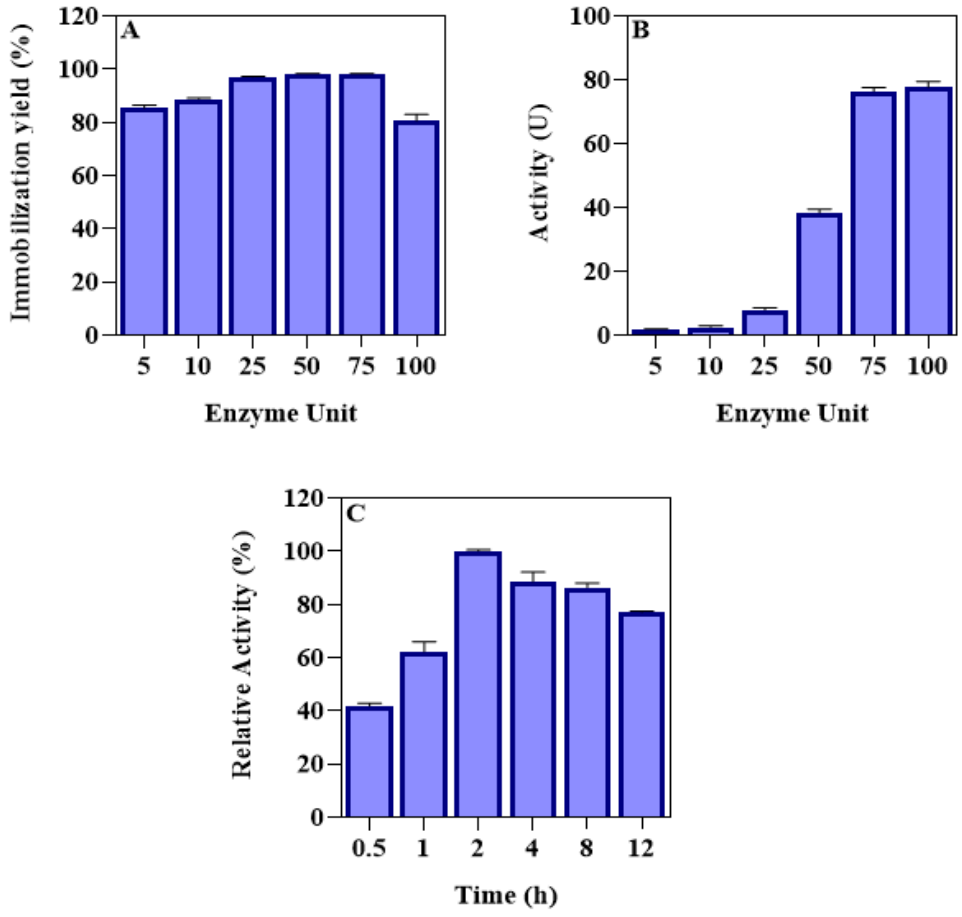

Figure 4.66: L-ASNase immobilization yield (A), L-ASNase catalytic activity (B), and incubation time (C) of $NaYF_4$: Nd^{3+}, Yb^{3+}, Er^{3+}/PEI-PEG-L-ASNase.

In order to determine the effect of immobilization time on enzyme activity, the time range between 30 min to 12 hours was examined. As can be seen from Figure 4.66 C, after two hours of immobilization, there was a marked increase in the relative activity of the enzyme. It was due to the amount of enzyme immobilized to UCNP has enough time to make chemical interactions between enzyme and UCNP. A short immobilization time means that most of the enzyme molecules have enough time to binding to the carrier material. A long immobilization time makes the binding between enzyme with carrier material difficult and this causes a decrease in enzyme activity. As a result of physical interaction between enzyme active site and UCNP, enzymatic activity diminished after 2 hours of immobilization. Owing to these results, 2 hours was selected as the optimum incubation time of immobilization.

4.2.4.2. Optimum pH and temperature

To determine the optimum pH, enzymatic activities of PEG-L-ASNase and $NaYF_4$: Nd^{3+}, Yb^{3+}, Er^{3+}/PEI-PEG-L-ASNase were measured between pH 4 and 10. As shown in Figure 4.67 A, the maximum activities of the PEG-L-ASNase and $NaYF_4$: Nd^{3+}, Yb^{3+}, Er^{3+}/PEI-PEG-L-ASNase were obtained at pH 8.5 and 8.0, respectively. Generally, the changes in optimum pH depending on changes in enzymes conformational after immobilization. This change in the optimum pH value may be caused by a change in acidic or basic amino acid ionization surrounding the enzyme's active site. Also, amine groups of PEI, which is the main function group on $NaYF_4$: Nd^{3+}, Yb^{3+}, Er^{3+}/PEI, and it's the responsibility to cause shifting in pH, the shifting is important because of the optimum pH near to pH of the human body. Due to immobilization, the enzyme becomes more stable and less affected by environmental factors than the free enzyme. This is the main advantage of the immobilization process. The optimum temperature of PEG-L-ASNase and $NaYF_4$: Nd^{3+}, Yb^{3+}, Er^{3+}/PEI-PEG-L-ASNase were also investigated between 20-70 °C and the obtained data were shown in Figure 4.67 B. Maximum relative activity of the PEG-L-ASNase was achieved at 40 °C, while for $NaYF_4$: Nd^{3+}, Yb^{3+}, Er^{3+}/PEI-PEG-L-ASNase was founded 50 °C. Moreover, it remained above 59 % of its relative activity at 70 ° C for immobilization L-ASNase and around 29 % for free L-ASNase. These results showed that the UCNP had a much higher thermal resistance and this one of the most important advantages of immobilization.

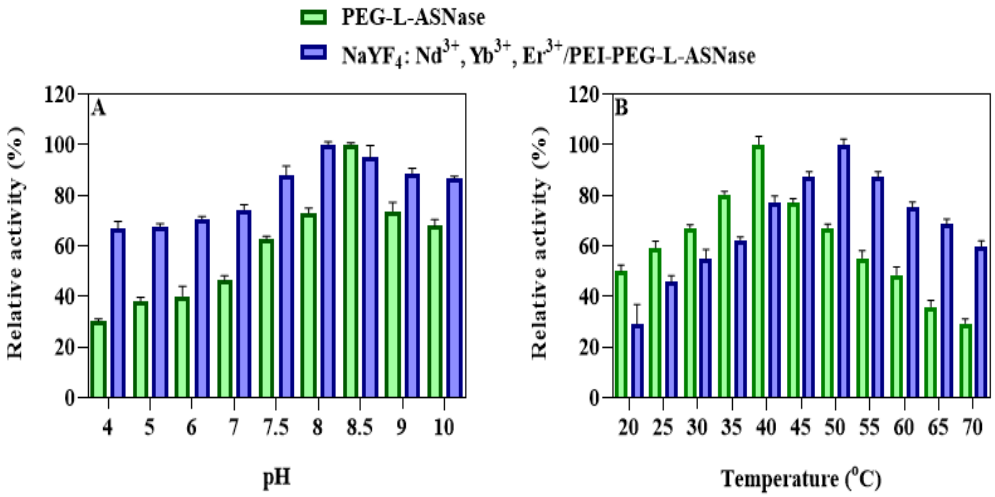

Figure 4.67: Optimum pH (A), and temperature (B) of PEG-L-ASNase and $NaYF_4$: Nd^{3+}, Yb^{3+}, Er^{3+}/PEI-PEG-L-ASNase.

4.2.4.3. Thermal and pH stability

Thermal stability results show in Figure 4.68 A of both PEG-L-ASNase and $NaYF_4$: Nd^{3+}, Yb^{3+}, Er^{3+}/PEI-PEG-L-ASNase were incubated at 50 °C for 6 hours. After 6 hours, the remained activity for PEG-L-ASNase was above 38 % from its initial activity, while for immobilized PEG-L-ASNase the activity still 62 % from its initial activity. This improvement in resistance to temperature may have resulted from the decrease in the molecular mobility and conformational changes of the enzyme due to the immobilization of L-ASNase. These results were showed that immobilization significantly improves thermal stability.

The pH stability was investigated by incubating both PEG-L-ASNase and $NaYF_4$: Nd^{3+}, Yb^{3+}, Er^{3+}/PEI-PEG-L-ASNase at pH 4 and 9 for 6 hours as shown in Figure 4.45 B and C. After 6 h, the relative activity for pH 4 were found above 19 % for PEG-L-ASNase and 55 % for immobilized PEG-L-ASNase, while at pH 9 the activity were 42 % and 59 % for PEG-L-ASNase and immobilized PEG-L-ASNase respectively, form initial activity. Owing to optimum pH in the alkaline range, it was clearly concluded that both PEG-L-ASNase and $NaYF_4$:Yb^{3+}, Er^{3+}/PEI-PEG-L-ASNase exhibited the higher enzymatic stability at pH 9 rather the pH 4.

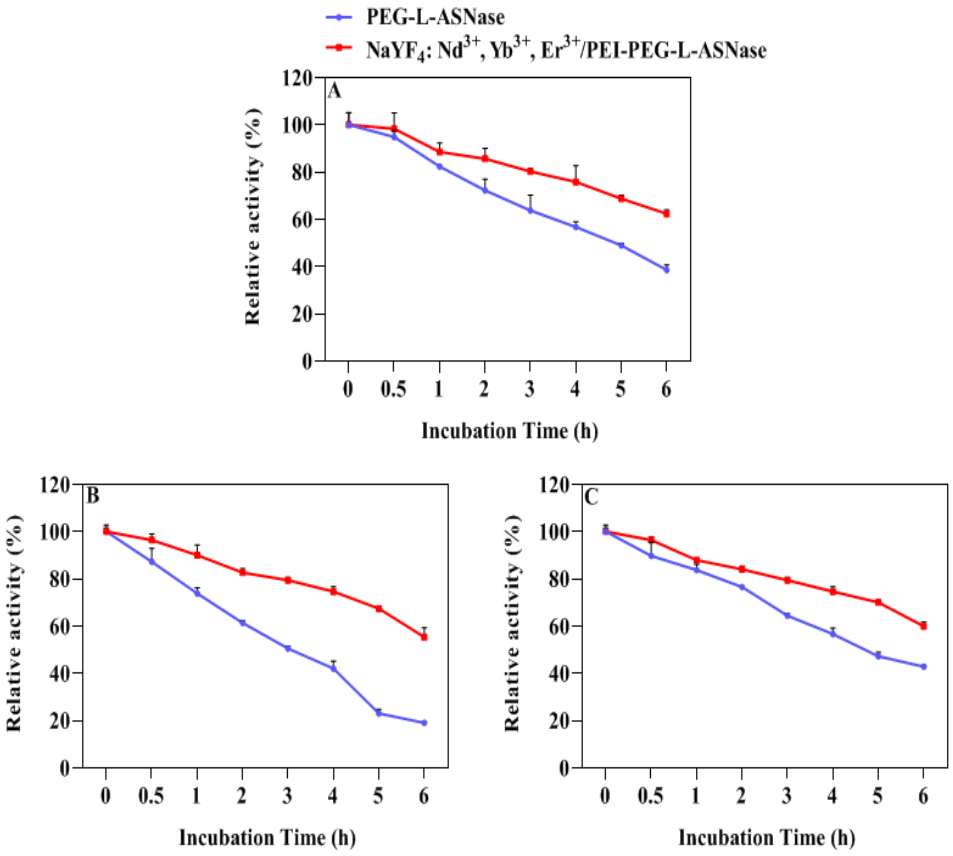

Figure 4.68: Thermal stability (A), pH stability at pH 4 (B), and pH stability at pH 9 (C) of PEG-L-ASNase and $NaYF_4$: Nd^{3+}, Yb^{3+}, Er^{3+}/PEI-PEG-L-ASNase.

4.2.4.4. Effect metal ion and solvent

To determine the effect of metal ions on the activity of PEG-L-ASNase and $NaYF_4$: Nd^{3+}, Yb^{3+}, Er^{3+}/PEI-PEG-L-ASNase, samples were incubated with different metal ions. The remaining activity was measured at optimum conditions. The obtained results were shown in Figure 4.69 A. It has been reported in the literature that monovalent cations such as Na^{+}, K^{+}, and divalent cations Ca^{2+}, Co^{2+}, and Mg^{2+} increase L-ASNase activity [207]. Studies were showing that divalent cations such as Cu^{2+}, Zn^{2+}, and metal ions Cr^{3+} inhibit enzyme activity [208–210]. In our study, Na^{1+}, Ag^{1+}, Ba^{2+}, Ca^{2+}, Co^{2+} , Mg^{2+}, Ni^{2+} , Sr^{2+}, $Zn^{2+}$and Al^{3+} increased enzyme activity. In contrast, Cu^{2+} and Cr^{3+} inhibited the enzyme activity. The activity of the immobilized L-ASNase was higher compared to the free L-ASNase. As a result, the activity of the immobilized L-ASNase enzyme is greater than that L-ASNase.

However, the solvent effect on of PEG-L-ASNase and $NaYF_4$: Nd^{3+}, Yb^{3+}, Er^{3+}/PEI-PEG-L-ASNase were determined by used different organic solvents such as

1-pentanol, 2-propanol, acetonitrile, chloroform, ethanol, ethyl acetate, *n*-hexane, isoamyl alcohol, DCM, DMF, DMSO, and THF after incubation for 24 h at room temperature, the activities were determined as shown in figure 4.69 B. The results were indicated that the immobilization enzyme has better stability against organic solvent even in some solvents the activity immobilization enzyme was increased. The results showed that immobilization protected the enzyme against the inhibitory effects of some chemicals.

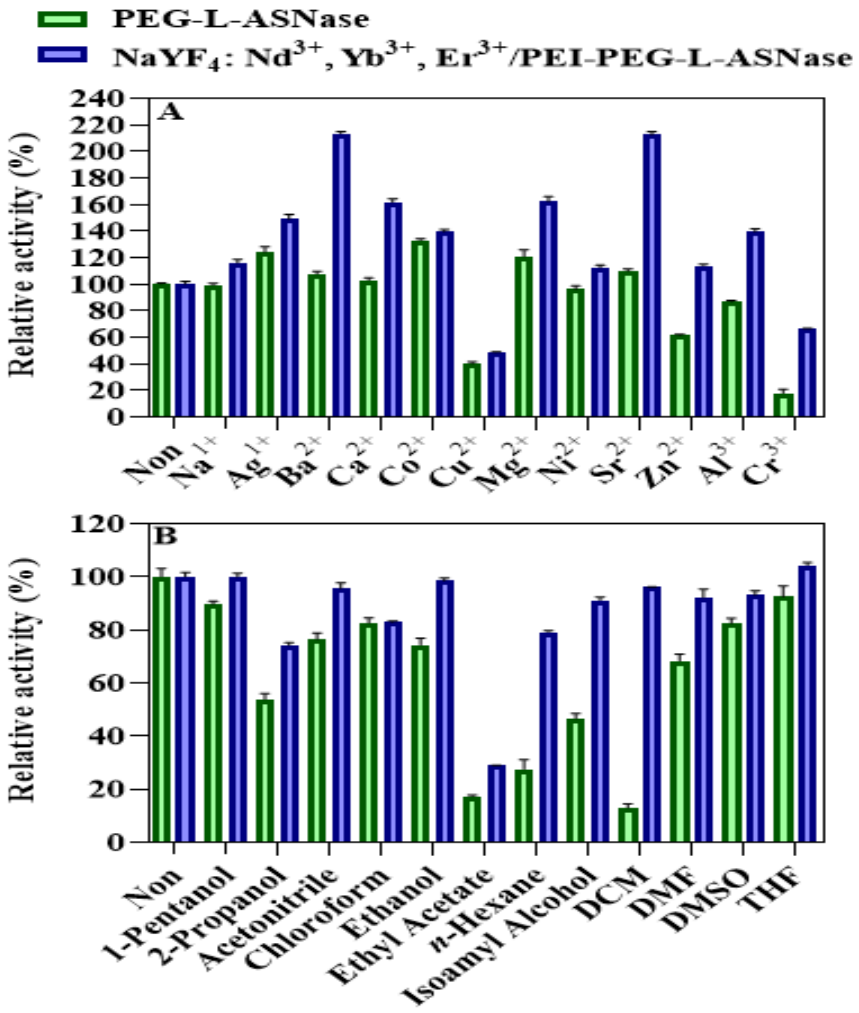

Figure 4.69: Stability of PEG-L-ASNase and $NaYF_4$: Nd^{3+}, Yb^{3+}, Er^{3+}/PEI-PEG-L-ASNase on metal ions (A), and organic solvents (B).

4.2.4.5. Reusability

Reusability is one of the most important features of immobilization. The reusability of $NaYF_4$: Nd^{3+}, Yb^{3+}, Er^{3+}/PEI-PEG-L-ASNase was shown in Figure 4.70. It was emphasized that the activity after 5 cycles was still above 97 %, and after 10 cycles

the activity was 83 % remaining from the initial activity, the retained activity still more than 56 % of its starting activity even after 20 cycles. It was also noted that diminishing of enzymatic activity was driven by weaker bonds and subsequent enzyme leak due to physical absorption of LASNases. In conclusion, one of the main advantages of immobilization is reusability due to easies separation of the enzyme from the reaction mixture which leads the repetitive use. In contrast, the free enzyme is inseparable from the mixture.

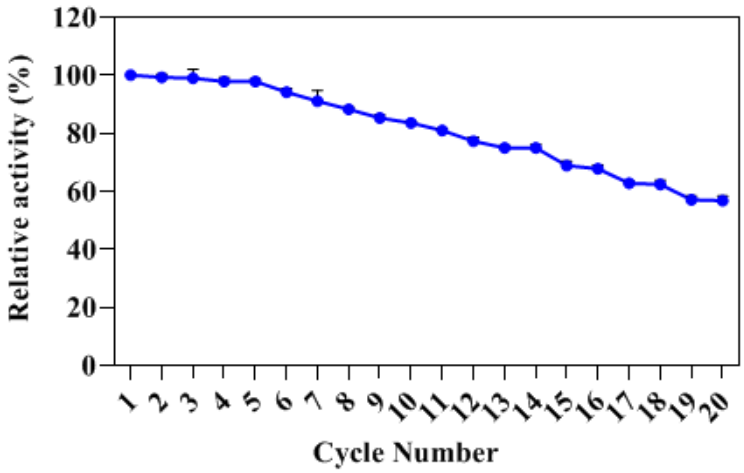

Figure 4.70: Reusability of $NaYF_4$: Nd^{3+}, Yb^{3+}, Er^{3+}/PEI-PEG-L-ASNase.

4.2.4.6. Storage stability

Storage stability is a crucial parameter for commercial-scale application of an enzyme, while it has been recognized that enzyme activity continuously diminishes over time due to instability during storage. The storage stability of both PEG-L-ASNase and $NaYF_4$: Nd^{3+}, Yb^{3+}, Er^{3+}/PEI-PEG-L-ASNase were investigated at 4 and 25 °C for 4 weeks to be measured every week and the results were given in Figure 4.71. Under storage conditions, the free L-ASNase lost about 49 % and 65 % of its initial activity at 4 and 25 °C, respectively. $NaYF_4$:Yb^{3+}, Er^{3+}/PEI-PEG-L-ASNase lost 37 % and 41 % of its initial activity at 4 and 25 °C, over the same period. The loss of enzymatic activity during this period can be attributed to protein denaturation and degradation during long-term storage. These results showed that the storage stability of $NaYF_4$: Nd^{3+}, Yb^{3+}, Er^{3+}/PEI-PEG-L-ASNase has better compared to the free L-ASNase at both 4 and 25 °C. The results showed also the stability of immobilized L-ASNase at 25 °C was no much loss in activity compared to 4 °C.

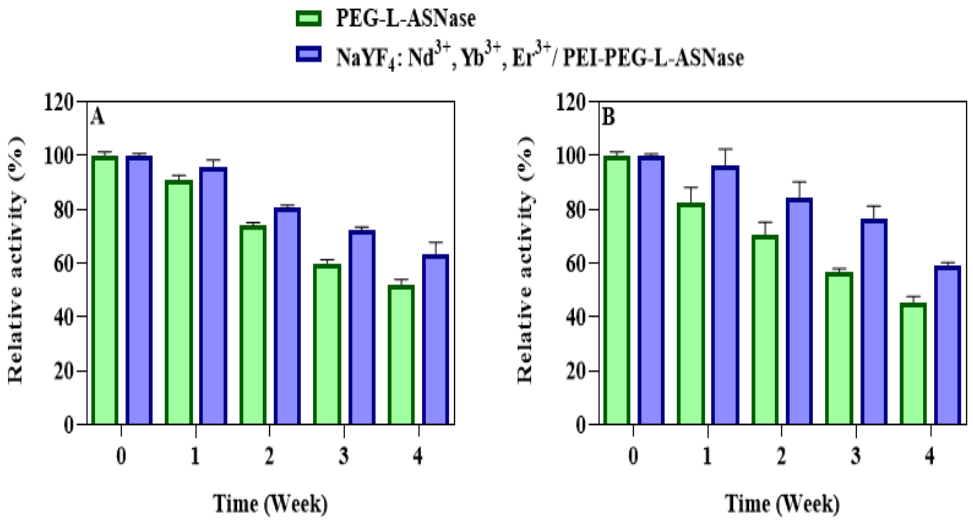

Figure 4.71: Storage stability of PEG-L-ASNase and $NaYF_4$: Nd^{3+}, Yb^{3+}, Er^{3+}/PEI-PEG-L-ASNase at +4°C (A), and at +25 °C (B).

4.2.4.7. Trypsin resistance

The biggest problem of bacterial enzymes used as pharmaceuticals is their low stability against proteolysis enzymes. Therefore, to measure the resistance of PEG-L-ASNase and $NaYF_4$: Nd^{3+}, Yb^{3+}, Er^{3+}/PEI-PEG-L-ASNase against trypsin digestion is shown in Figure 4.72. The results showed that the resistance of immobilized L-ASNase to trypsin digestion was greatly improved compared to the free L-ASNase. After 120 minutes from incubation both with trypsin at +37 °C, free L-ASNase was almost completely hydrolyzed, while immobilized L-ASNase the activity is still above 31 % of its original activity.

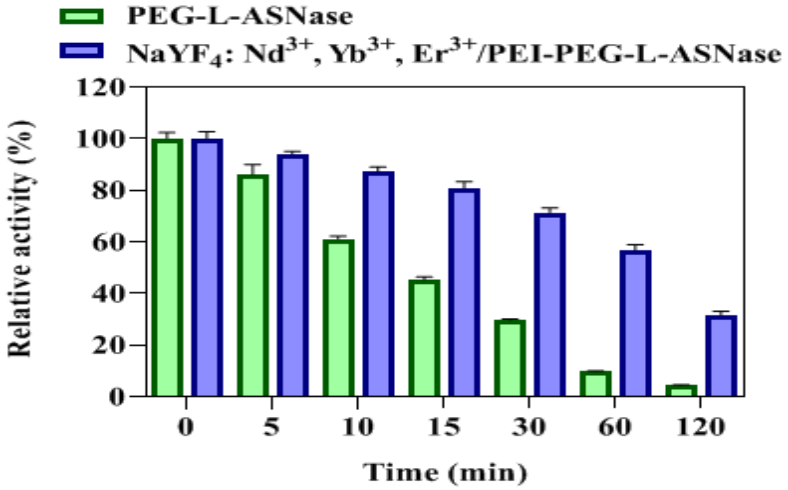

Figure 4.72: Trypsin resistance of PEG-L-ASNase and $NaYF_4$: Nd^{3+}, Yb^{3+}, Er^{3+}/PEI-PEG-L-ASNase.

4.2.4.8. Kinetic parameter

The kinetic parameters for both PEG-L-ASNase and $NaYF_4$: Nd^{3+}, Yb^{3+}, Er^{3+}/PEI-PEG-L-ASNase were estimated and summarized in Table 4.6. Also, the Lineweaver–Burk plots were shown in Figure 4.73. As shown in Table 4.6, the obtained K*m* values for the free and immobilized were 2.31 and 1.95 mM, respectively. After immobilization, the K*m* value decreased. It is obvious that when the enzyme has a small K*m* value, it achieves maximum catalytic efficiency at a low substrate concentration, which means that the enzyme has high catalytic efficiency. Therefore, the decrease of K*m* value after immobilization represents the high affinity of the enzyme to its substrate. Meanwhile, the decrease in the *Vmax* was observed value after enzyme immobilization. The apparent *Vmax* value decrease from 140.85 to 126.58 µmol/min. The obtained results are in accordance with the values reported previously.

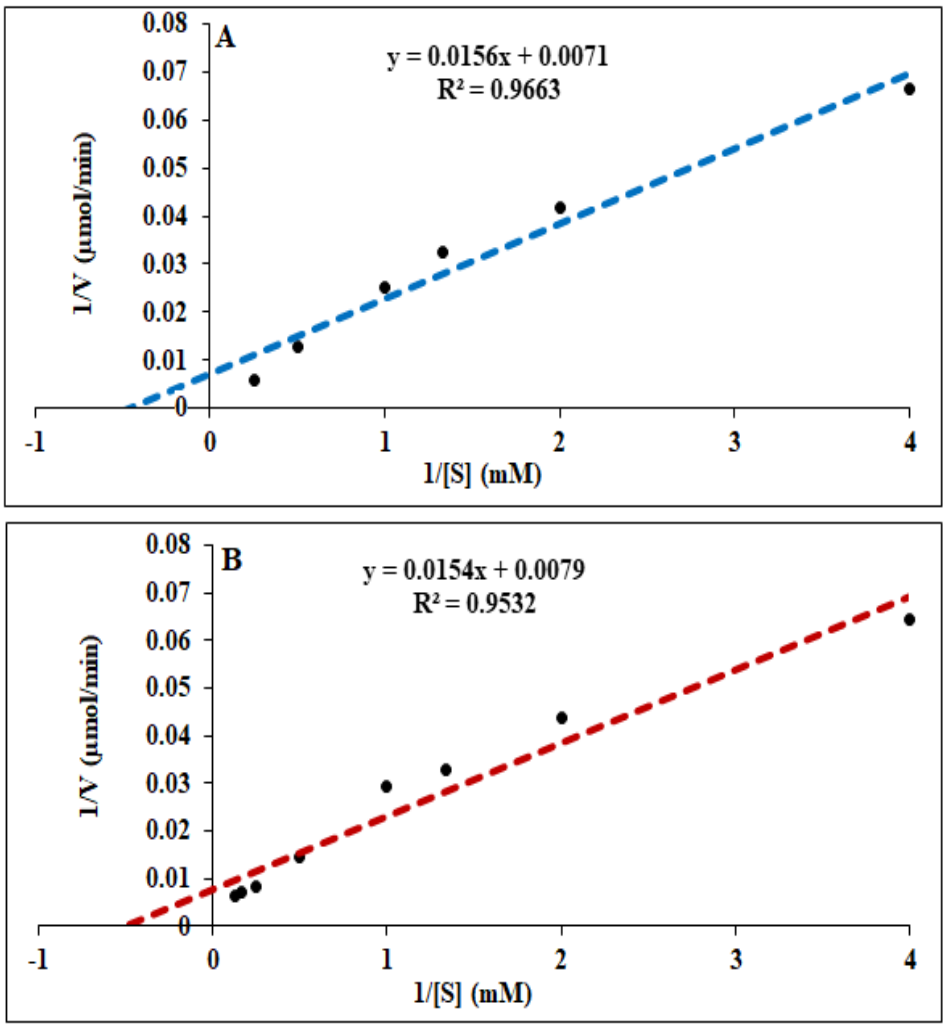

Figure 4.73: Kinetic parameters of PEG-L-ASNase (A), and $NaYF_4$: Nd^{3+}, Yb^{3+}, Er^{3+}/PEI-PEG-L-ASNase (B).

Table 4.6: Kinetic parameters of PEG-L-ASNase and $NaYF_4$: Nd^{3+}, Yb^{3+}, Er^{3+}/PEI-PEG-L-ASNase.

Sample	K*m* (mM)	*Vmax* (µmol/min)	R^2
PEG-L-ASNase	2.31 ± 0.042	140.85 ± 3.235	0.9663
$NaYF_4$: Nd^{3+}, Yb^{3+}, Er^{3+}/ PEI -PEG-L-ASNase	1.95 ± 0.061	126.58 ± 2.836	0.9532

4.2.4.9. Activation energy

The activation energy (*Ea*) values calculated by the Arrhenius equation for both PEG-L-ASNase and $NaYF_4$: Nd^{3+}, Yb^{3+}, Er^{3+}/PEI-PEG-L-ASNase. The *Ea* values calculated from the slope of log (% relative activity) versus 1000/T, Ea values were determined as 17.13 kJ/mol for free enzyme and 11.008 kJ/mol for immobilized one as seen in (Figure 4.74). The low *Ea* value was reported beneficial also for enzyme immobilization. This implied that the immobilized enzymes are less temperature-sensitive. This reduction in *Ea* value demonstrated that immobilized enzyme requires less energy than the free one to overcome the conversion barrier to transform the substrate into a product. It makes the immobilized enzyme more stable and advantageous than the free counterpart.

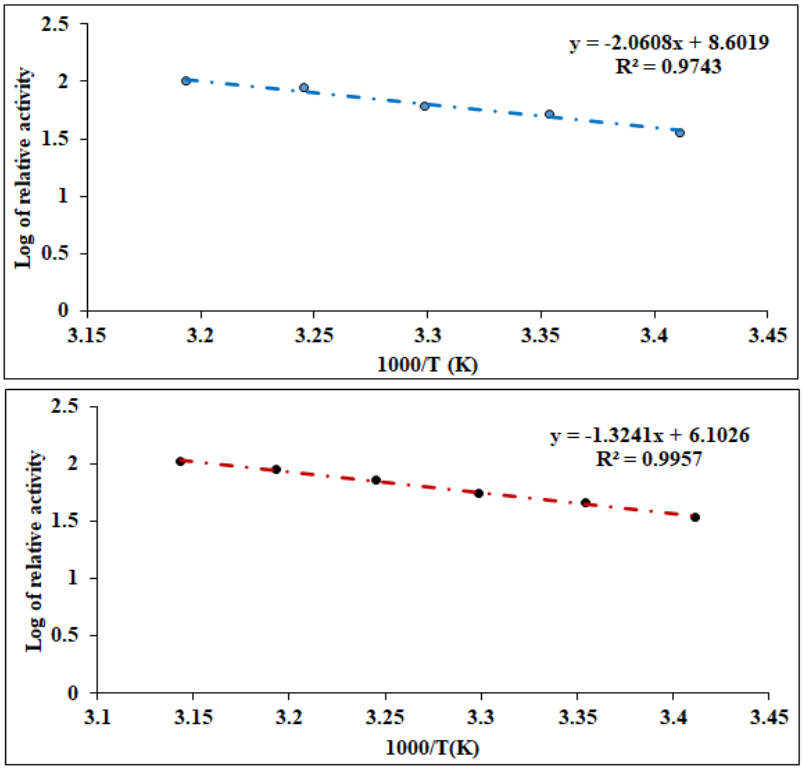

Figure 4.74: The activation energy of PEG-L-ASNase (A), and $NaYF_4$: Nd^{3+}, Yb^{3+}, Er^{3+}/PEI-PEG-L-ASNase (B).

4.2.4.10. Laser power, laser distance, and laser exposure time

To determine the optimum laser power for $NaYF_4$: Nd^{3+}, Yb^{3+}, Er^{3+}/PEI-PEG-L-ASNase, NIR (808 nm) light was induced to immobilize the enzyme on UCNP. Different milliwatts (mW) were scanned to find out the optimum power of UCNP by applying a constant amount of UCNP with a fixed distance between nanoparticles and NIR light. The obtained optimum power was 400 mW and the enzyme activity was increased from 100 % to 323 % as shown in Figure 4.75 A, with increasing the NIR light power decrease in enzyme activity took place, it was assumed that the NIR generated heat probable affected on enzyme three-dimensional structure of enzyme active center or weak interaction between enzyme and UCNP.

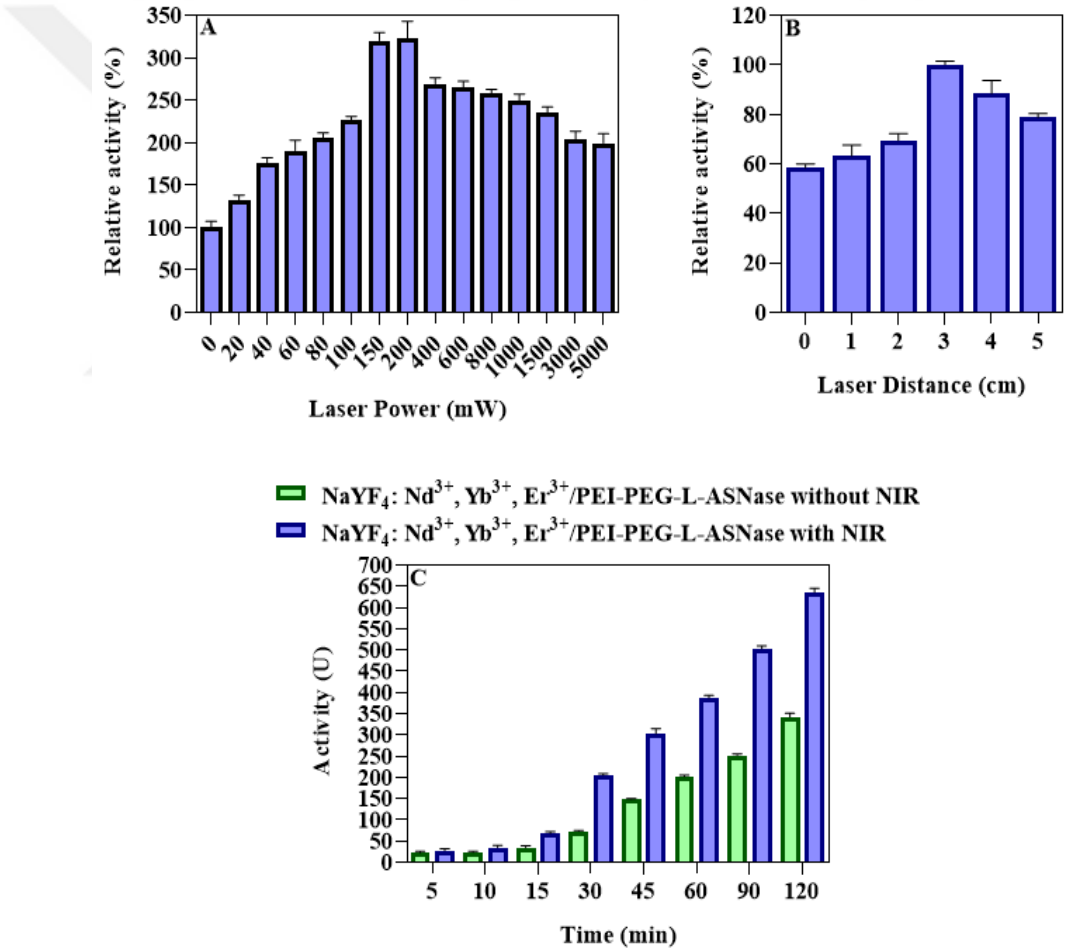

Figure 4.75: Induce of $NaYF_4$: Nd^{3+}, Yb^{3+}, Er^{3+}/PEI-PEG-L-ASNase, NIR light power (A), NIR distance (B), and NIR time (C).

After the maximum NIR light power was found, the optimum distance between $NaYF_4$: Nd^{3+}, Yb^{3+}, Er^{3+}/PEI-PEG-L-ASNase and laser powers were determined. In this experiment, the NIR light was arranged at 400 mW with a fixed amount of enzyme

immobilized on UCNP and different distances were scanned (0 – 5 cm). The optimum activity was founded at a 3 cm distance between NIR light and UCNP immobilized enzyme as seen in Figure 4. 75 B. It was determined that decreasing in enzyme activity by increasing the distance, this due to decrease the effect of NIR light on UCNP nanoparticles.

NIR exposure time was investigated by keeping constant laser power, distance, and the amount of $NaYF_4$: Nd^{3+}, Yb^{3+}, Er^{3+}/PEI-PEG-L-ASNase, while the activity affected by time was also determined in the absence of NIR radiation. As it is shown in Figure 4.75 C there was a sharp increase in the activity the exposure to NIR light until 120 min.

4.2.4.11. Stability of $NaYF_4$: Nd^{3+}, Yb^{3+}, Er^{3+}/PEI-PEG-L-ASNase

To measure the stability of $NaYF_4$: Nd^{3+}, Yb^{3+}, Er^{3+}/PEI-PEG-L-ASNase and the effect of NIR after storage. Different samples of immobilized enzyme were incubated with PBS (50 mM, pH 7.4) at +37 °C, and the activity was measured every single day by first exposure to NIR light at optimum conditions then the activity was measured. After one week from incubation, the activity was above 55 % from the initial activity as shown in (Figure 4.76).

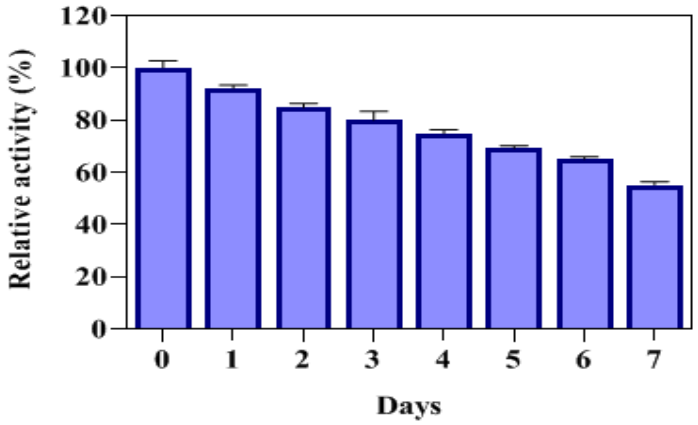

Figure 4.76: Stability of $NaYF_4$: Nd^{3+}, Yb^{3+}, Er^{3+}/PEI-PEG-L-ASNase in PBS by NIR light.

4.2.4.12. *In vitro* half-life

In vitro half-life was determined for both free PEG-L-ASNase and immobilized $NaYF_4$: Nd^{3+}, Yb^{3+}, Er^{3+}/PEI-PEG-L-ASNase enzyme. The samples were incubated in

rat blood serum for 1 week at +37 °C. Then, the activity of the L-ASNase and immobilized L-ASNase were measured with optimum conditions and their *in vitro* half-life was calculated by comparing with the initial activity as we can see in (Figure 4.77).

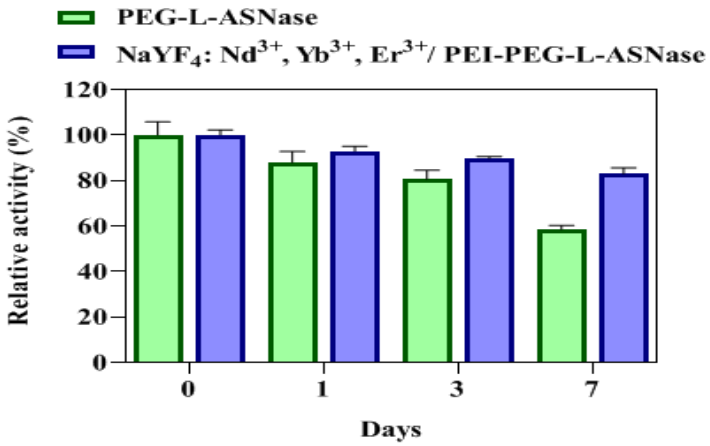

Figure 4.77: *In vitro* half-life of PEG-L-ASNase and immobilized $NaYF_4$: Nd^{3+}, Yb^{3+}, Er^{3+}/PEI-PEG-L-ASNase.

4.2.4.13. Plasma coagulation

The prothrombin time (PT) and the activated partial thromboplastin time (APTT), reflect the effect of $NaYF_4$: Nd^{3+}, Yb^{3+}, Er^{3+}/PEI and $NaYF_4$: Nd^{3+}, Yb^{3+}, Er^{3+}/ PEI-PEG-L-ASNase on the intrinsic and extrinsic pathways of the blood coagulation cascade. They were determined by incubating both in platelet-poor plasma Figure as shown in 4.78, suggesting that no coagulation occurred when UCNPs were added. These findings indicate that both $NaYF_4$: Nd^{3+}, Yb^{3+}, Er^{3+}/PEI and $NaYF_4$: Nd^{3+}, Yb^{3+}, Er^{3+}/PEI-PEG-L-ASNase are hemocompatible, which may be related to the hydrophilicity and surface area charge of these particles.

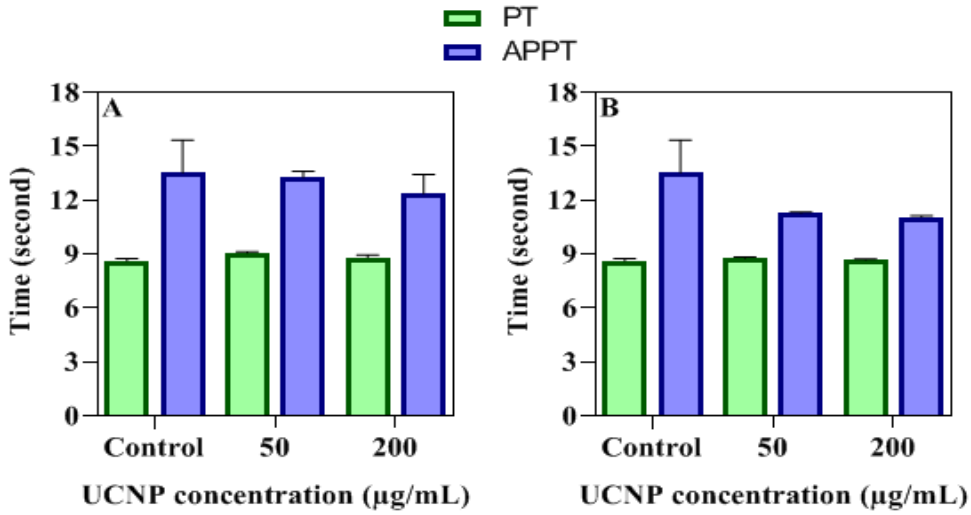

Figure 4.78: Plasma coagulation of $NaYF_4$: Nd^{3+}, Yb^{3+}, Er^{3+}/PEI (A), and $NaYF_4$: Nd^{3+}, Yb^{3+}, Er^{3+}/PEI-PEG-L-ASNase (B).

4.2.4.14. *In vitro* cytotoxicity

The *in vitro* cytotoxicity of the prepared UCNP was tested calorimetrically by using the MTT test and the results were shown in Figure 4.79 A and B. In cytotoxicity studies, cell viability is classified as more than 50 % toxic, from 51 to 70% mildly cytotoxic, less than 71% non-cytotoxic [211]. Different concentration (12.5, 25, 50, 100, and 200 µg/mL) of $NaYF_4$: Nd^{3+}, Yb^{3+}, Er^{3+}/PEI and $NaYF_4$: Nd^{3+}, Yb^{3+}, Er^{3+}/PEI-PEG-L-ASNase were tested against mouse fibroblast (L-929). Besides, the morphology of the cells treated with $NaYF_4$: Nd^{3+}, Yb^{3+}, Er^{3+}/PEI and NaYF4: Nd^{3+}, Yb^{3+}, Er^{3+}/PEI-PEG-L-ASNase were given in Figure 4.79 C, after to 24, 48, and 72 h form incubation. As a result, there was no change in the morphological structure of the cells. It was observed that the synthesized UCNP nanoparticles had no *in vitro* toxic effects on cell viability.

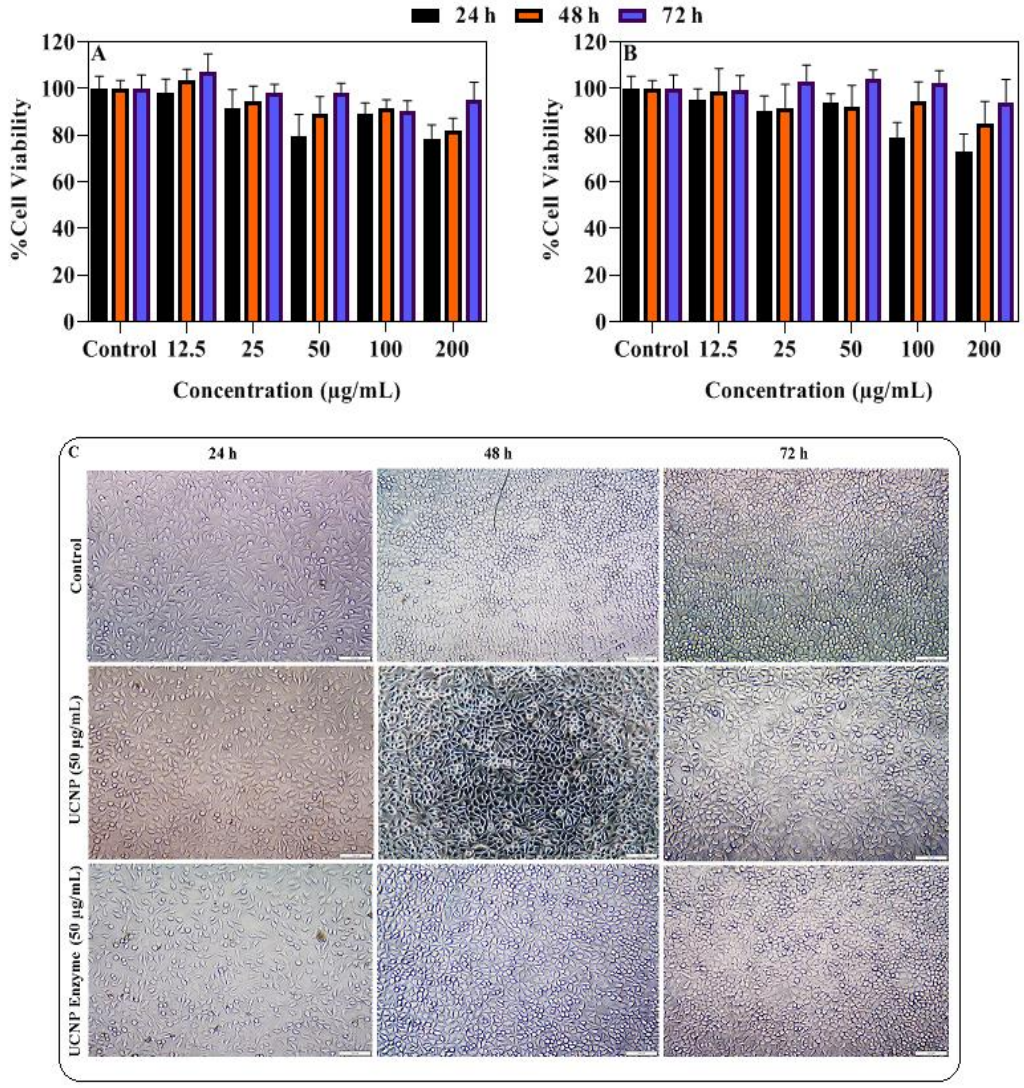

Figure 4. 79: Cell viability results after incubation 24, 48, and 72 hours of L-929 with $NaYF_4$: Nd^{3+}, Yb^{3+},Er^{3+}/PEI (A), $NaYF_4$: Nd^{3+}, Yb^{3+},Er^{3+}/PEI-PEG-L-ASNase (B), and morphological image of L-929 fibroblast cells (C).

4.2.5. Immobilization parameters of NaYF4: Nd^{3+}, Yb^{3+}, Er^{3+}/GPTMS

4.2.5.1. Enzyme unit and incubation time

The optimum enzyme unit of $NaYF_4$: Nd^{3+}, Yb^{3+}, Er^{3+}/GPTMS was determined as 25 U concentration was chosen as the amount of enzyme for immobilization. As seen in (Figure 4.80 A), the immobilization yield decreased after 25 U the decrease in immobilization yield due to loading capacity of 25 U can covalently immobilize all UCNP by cover all the function group was bounded to the enzyme, while in (Figure 4.80 B), there was a sharp increase in the catalytic activity from 5-25 U. In the same

time, 50 U only indicated either similar or small catalytic activity. Furthermore, the immobilization yield, activity yield, and immobilization efficiency for 25 U were founded as 97.31 ± 0.05 %, 74.26 ± 1.95 %, and 76.31 ± 2.23 %, respectively.

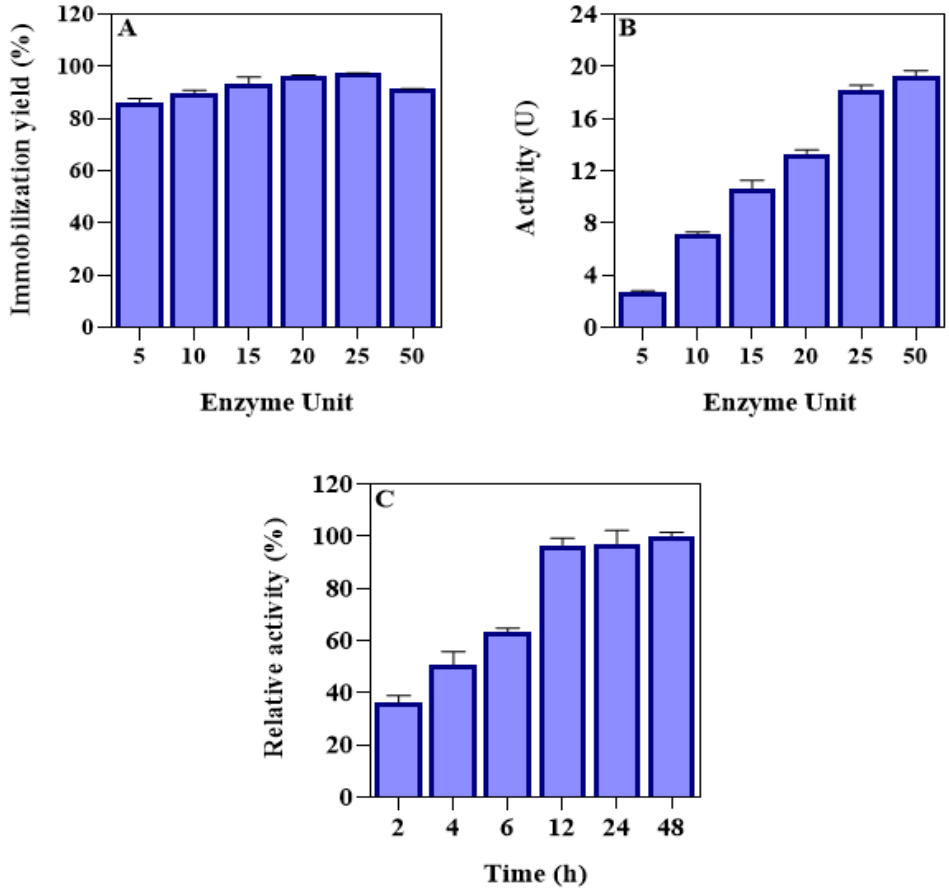

Figure 4.80: L-ASNase immobilization yield (A), L-ASNase catalytic activity (B), and incubation time (C) of $NaYF_4$: Nd^{3+}, Yb^{3+}, Er^{3+}/GPTMS-PEG-L-ASNase.

In order to determine the effect of immobilization time on enzyme activity, the time immobilization was taken place between 2 to 48 hours. A brief duration of immobilization means that most molecules of the enzyme have time to bind to the carrier material. In contrast, a long duration of immobilization indicated the binding obstacle between enzyme and material, which diminishes the activity of the enzymes. As can be seen in (Figure 4.80 C), after 12 hours from immobilization, there is a marked increase in the relative activity of the enzyme. As the immobilization time increased, the relative activity of the immobilized enzyme approximately stayed constant, due to covalently bond between the enzyme and UCNP after 12 hours of immobilization that there is no anymore free group on UCNP even if we increase the

enzyme concentrations. Based on these results, the ideal time of 12 hours as the immobilization time was taken as the optimum value.

4.2.5.2. Optimum pH and temperature

Optimum pH for both PEG-L-ASNase and $NaYF_4$: Nd^{3+}, Yb^{3+}, Er^{3+}/GPTMS-PEG-L-ASNase founded at pH 8.5, it was observed that there is no change in the optimum pH value as shown in Figure 4.81 A. Compared to the free enzyme, the high pH resistance of the immobilized enzyme may have caused by the strong binding between the enzyme and UCNP. The relative activity of the $NaYF_4$: Nd^{3+}, Yb^{3+}, Er^{3+}/GPTMS-PEG-L-ASNase higher than that L-ASNase, even at pH 10 the activity of immobilized still above 75 % while the free one above 58 %.

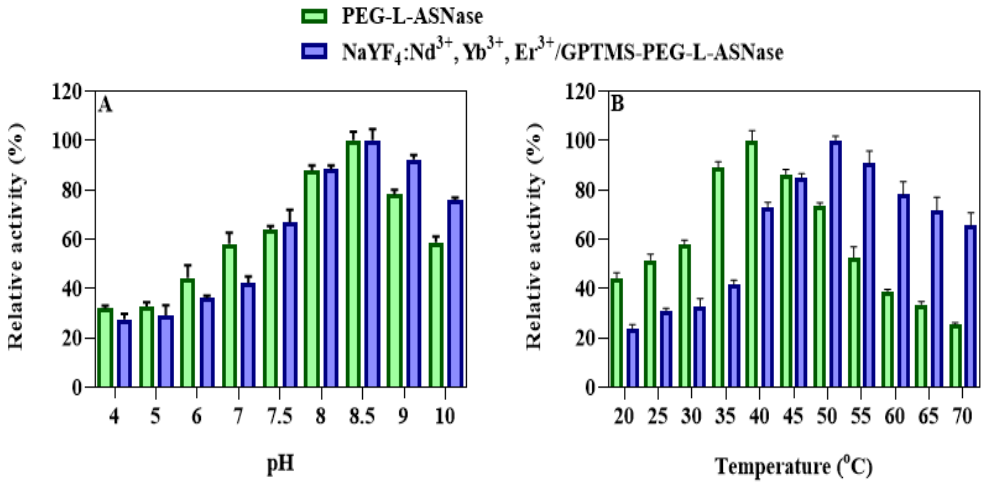

Figure 4.81: Optimum pH (A), and temperature (B) of PEG-L-ASNase and $NaYF_4$: Nd^{3+}, Yb^{3+}, Er^{3+}/GPTMS-PEG-L-ASNase.

The optimum temperature for PEG-L-ASNase and $NaYF_4$: Nd^{3+}, Yb^{3+}, Er^{3+}/GPTMS-PEG-L-ASNase were shown in Figure 4.81 B. The optimum temperature for the free enzyme was 40 °C, this value increased to 50 °C after immobilization. Moreover, it remained above 65 % of its relative activity at 70 °C for immobilized and around 25 for the free one. This result shows that immobilization makes conformational integrity and increases the stability against temperature. The increase in optimum temperature may be due to the increased affinity of the enzyme to the substrate and the change in the conformational integrity of the enzyme structure due to covalent interactions between the enzyme and the prepared UCNP.

4.2.5.3. Thermal and pH stability

Thermal stability is one of the most important advantages of immobilized enzymes. Thermal stability results show in Figure 4.82 A, both PEG-L-ASNase and $NaYF_4$: Nd^{3+}, Yb^{3+}, Er^{3+}/GPTMS-PEG-L-ASNase were incubated at 50 °C for 6 hours. After 6 hours, the activity of the free enzyme remained above 37 % from its initial activity, while for $NaYF_4$: Nd^{3+}, Yb^{3+}, Er^{3+}/GPTMS-PEG-L-ASNase the activity still 68 % from its initial activity. This improvement in resistance to temperature may have resulted from the decrease in the molecular mobility and conformational changes of the enzyme due to the immobilization of L-ASNase. These results were showed that immobilization significantly improves thermal stability.

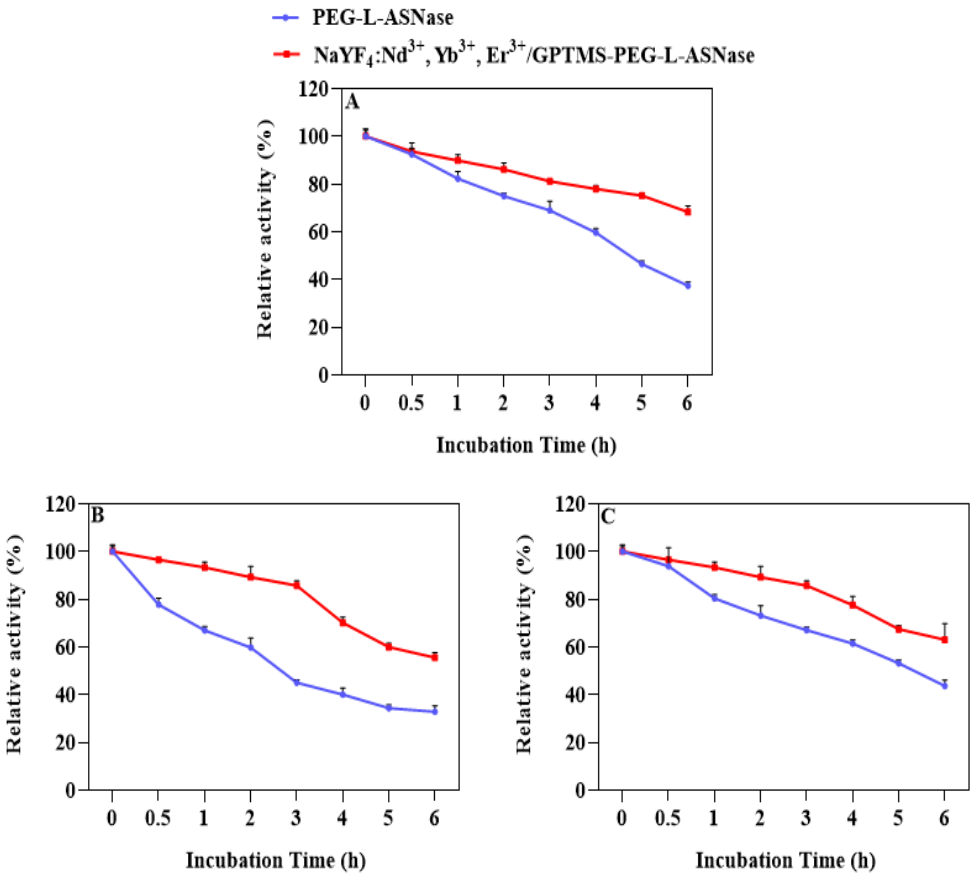

Figure 4.82: Thermal stability (A), pH stability at pH 4 (B), and pH stability at pH 9 (C), of PEG-L-ASNase and $NaYF_4$: Nd^{3+}, Yb^{3+}, Er^{3+}/GPTMS-PEG-L-ASNase.

The pH stability is an important parameter for enzyme immobilization. pH stability was determined by incubation PEG-L-ASNase and $NaYF_4$: Nd^{3+}, Yb^{3+}, Er^{3+}/GPTMS -PEG-L-ASNase at pH 4 and 9 for 6 hours as shown in Figure 4.82 B and C. After 6h, the relative activity for pH 4 were found above 32 % for free enzyme and 55% for

immobilized one, while at pH 9 the activity was 43 % and 63% for free and immobilized LASNase from initial activity, respectively. Owing to optimum pH in the alkaline range, it was clearly concluded that both PEG-L-ASNase and $NaYF_4$: Nd^{3+}, Yb^{3+}, Er^{3+}/GPTMS-PEG-L-ASNase exhibited the higher enzymatic stability at pH 9 rather the pH 4.

4.2.5.4. Effect metal ion and solvent

The effect of metal ions was investigated for both free PEG-L-ASNase and immobilized $NaYF_4$: Nd^{3+}, Yb^{3+}, Er^{3+}/GPTMS-PEG-L-ASNase, samples were incubated with different metal ions. The results were shown in Figure 4.83 A. It has been reported in the literature that monovalent cations such as Na^{+}, and divalent cations Ca^{2+}, $Co^{2+,}$ and Mg^{2+} increase L-ASNase activity [207]. In addition, it was reported that the divalent cations such as Cu^{2+}, Fe^{2+}, Hg^{2+}, Zn^{2+}, and metal ions Cr^{3+} inhibit enzyme activity [208–210]. In our study, Na^{1+}, Ag^{1+}, Ba^{2+}, Ca^{2+}, Co^{2+} , Mg^{2+}, Ni^{2+} , and Al^{3+} increased enzyme activity. In contrast, Cu^{2+}, Sr^{2+}, Zn^{2+}, and Cr^{3+} inhibited the enzyme activity counterpart. Nevertheless, the immobilized enzyme is higher than the free enzyme. However, immobilized enzymes have been affected by metal ions that inhibit activity less than as much as the free enzyme.

In contrast, the solvent effect on PEG-L-ASNase and $NaYF_4$: Nd^{3+}, Yb^{3+}, Er^{3+}/GPTMS-PEG-L-ASNase were invested by using different organic solvents such as 1-pentanol, 2-propanol, acetonitrile, chloroform, ethanol, ethyl acetate, *n*-hexane, isoamyl alcohol, DCM, DMF, DMSO, and THF after incubation for 24 h at room temperature, the activity was determined as shown in figure 4.83 B. The results were indicated that the immobilization enzyme has better stability against organic solvent even in some solvents the activity immobilization enzyme was increased, except for acetonitrile the activity for the enzyme was higher than the immobilized one.

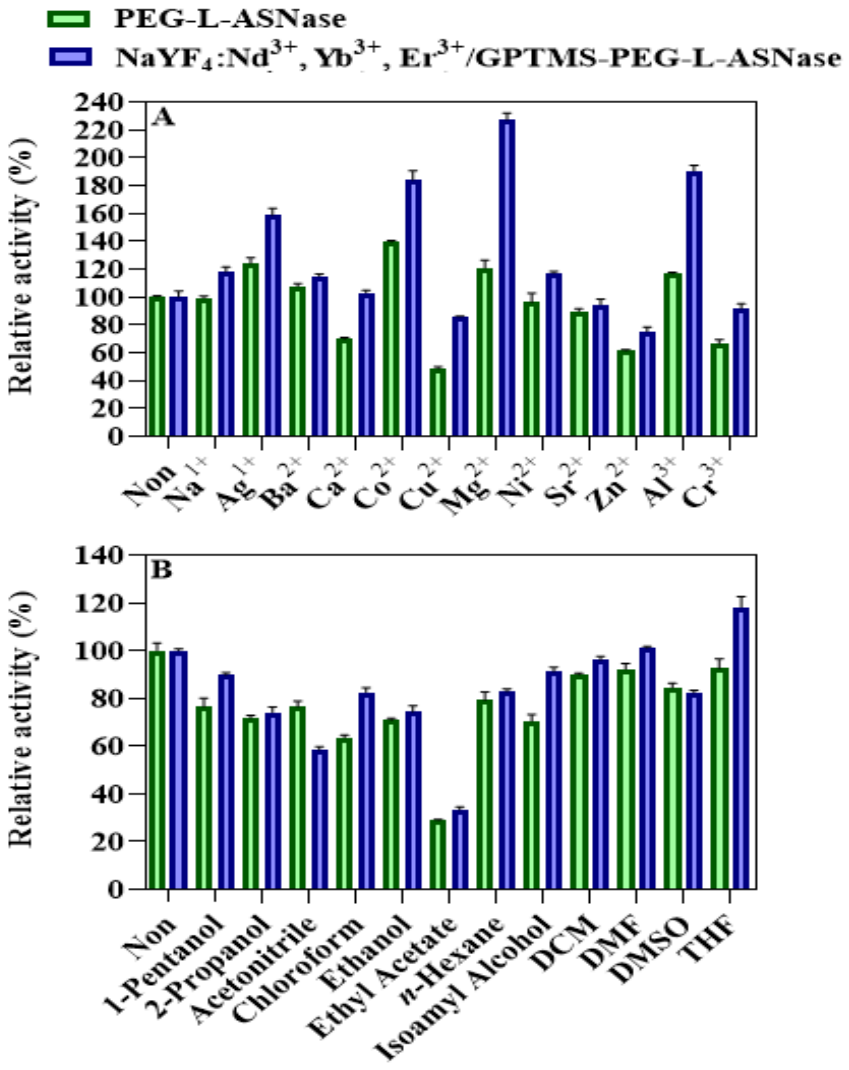

Figure 4.83: Stability of PEG-L-ASNase and $NaYF_4$: Nd^{3+}, Yb^{3+}, Er^{3+}/GPTMS-PEG-L-ASNase on metal ions (A), and organic solvents (B).

4.2.5.5. Reusability

The reusability of $NaYF_4$: Nd^{3+}, Yb^{3+}, Er^{3+}/GPTMS-PEG-L-ASNase was measured as shown in Figure 4.84. The remaining relative activity after 5 cycles was still above 92% from its initial activity, while the activity still retained more than 80 % of its starting activity after 10 cycles, even after 20 cycles the activity still above 63 % from the initial activity. Covalent immobilization improves the reusability of enzymes compared to the physical one. Reusability is one of the advantages of immobilization, due to the easy separation of the immobilized enzyme from the reaction mixture and reused for several times. In contrast, the free enzyme is inseparable from the mixture.

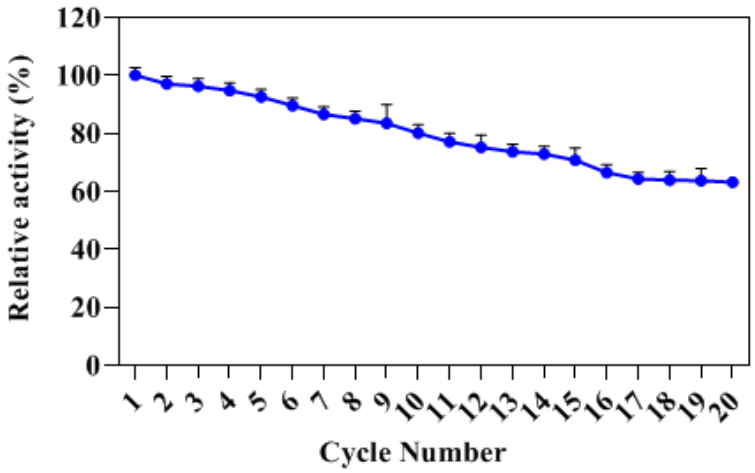

Figure 4.84: Reusability of $NaYF_4$: Nd^{3+}, Yb^{3+}, Er^{3+}/GPTMS-PEG-L-ASNase.

4.2.5.6. Storage stability

Storage stability is a crucial parameter for commercial-scale application of an enzyme, while it has been recognized that enzyme activity continuously diminishes over time due to instability during storage. The storage stability of both PEG-L-ASNase and NaYF4: Nd^{3+}, Yb^{3+}, Er^{3+}/GPTMS-PEG-L-ASNase, enzymes were stored at +4 and +25 °C and residual activities were measured. As shown in Figure 4.85 after 4 weeks of storage, the activity of immobilized enzymes still above 68 % and 59 % of their initial activities at +4 and +25 °C, respectively. Free enzyme preserved 49 % and 38 % of its initial activity, respectively. These results showed that the storage stability of the $NaYF_4$: Nd^{3+}, Yb^{3+}, Er^{3+}/GPTMS-PEG-L-ASNase was better compared to the free enzyme at both 4 and 25 °C. It was also implied that the stability of immobilized enzyme was higher at 25°C with insignificant loss than the 4 °C counterparts. Owing to the result, $NaYF_4$: Nd^{3+}, Yb^{3+}, Er^{3+}/GPTMS-PEG-L-ASNase indicated its promising and alternative carrier matrix material due to its long-term storage stability.

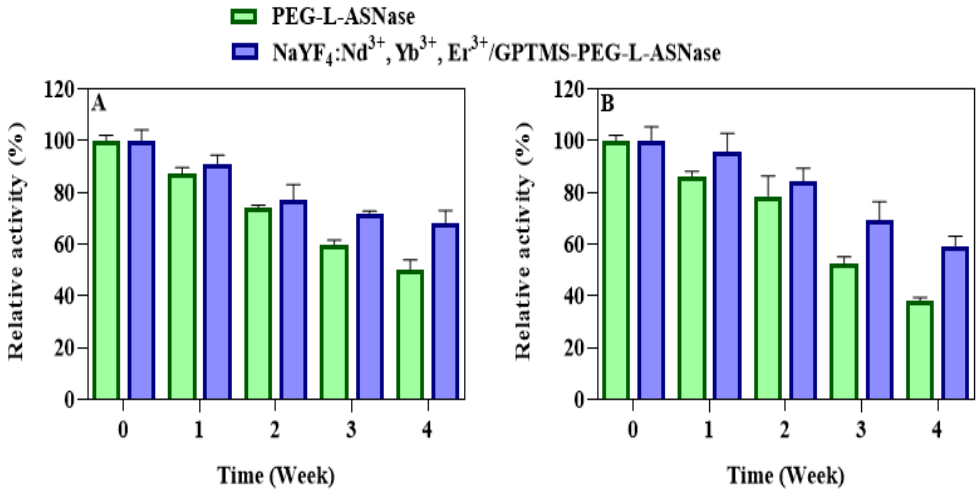

Figure 4.85: Storage stability of PEG-L-ASNase and $NaYF_4$: Nd^{3+}, Yb^{3+}, Er^{3+}/GPTMS-PEG-L-ASNase at +4°C (A), and at +25 °C (B).

4.2.5.7. Trypsin resistance

One of the major problems of bacterial enzymes in the pharmaceutical application is the stability against proteolysis enzymes. The resistance of both free enzyme and $NaYF_4$: Nd^{3+}, Yb^{3+}, Er^{3+}/GPTMS-PEG-L-ASNase against trypsin digestion is shown in Figure 4.86. The results showed that the resistance of immobilized to trypsin digestion is greatly improved compared to the free form. After 120 minutes of hydrolysis with the addition of trypsin, PEG-L-ASNase is almost completely hydrolyzed, while $NaYF_4$: Nd^{3+}, Yb^{3+}, Er^{3+}/GPTMS-PEG-L-ASNase retained about 45 % of its original activity.

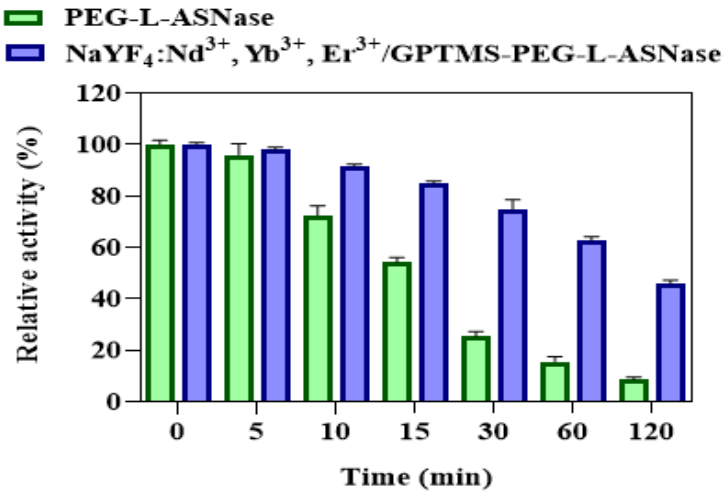

Figure 4.86: Trypsin resistance of PEG-L-ASNase and $NaYF_4$: Nd^{3+}, Yb^{3+}, Er^{3+} /GPTMS-PEG-L-ASNase.

4.2.5.8. Kinetic parameter

The kinetic parameters for both PEG-L-ASNase and $NaYF_4$: Nd^{3+}, Yb^{3+}, Er^{3+}/GPTMS -PEG-L-ASNase were measured. The obtained K*m* values for L-ASNase and immobilized L-ASNase were 3.15 and 0.284 mM, respectively summarized in Table 4.7. Also, the Lineweaver–Burk plots were shown in Figure 4.87. When the enzyme has a small K*m* value, it achieves maximum catalytic efficiency at a low substrate concentration. Meanwhile, a decrease in the Vmax was observed value after enzyme immobilization. The apparent V*max* value increased from 192.31 to 30.96 µmol/min. The obtained results are in accordance with the values reported previously.

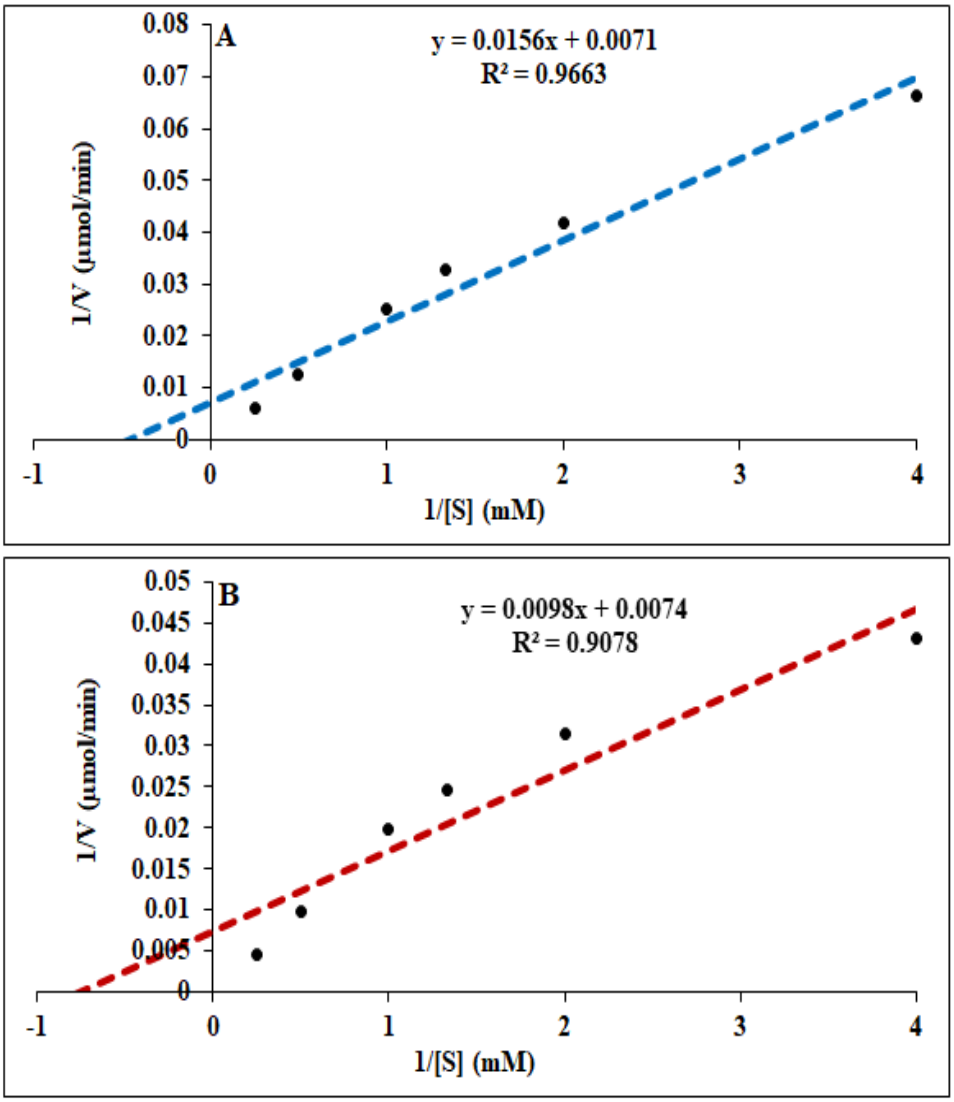

Figure 4.87: Kinetic parameters of PEG-L-ASNase (A), and $NaYF_4$: Nd^{3+}, Yb^{3+}, Er^{3+}/ GPTMS-PEG-L-ASNase (B).

Table 4.7: Kinetic parameters of PEG-L-ASNase and $NaYF_4$: Nd^{3+}, Yb^{3+}, Er^{3+}/ GPTMS-PEG-L-ASNase.

Sample	K*m* (mM)	*Vmax* (µmol/min)	R^2
PEG-L-ASNase	2.31± 0.04	140.85 ± 3.23	0.9663
$NaYF_4$: Nd^{3+}, Yb^{3+}, Er^{3+}/ GPTMS-PEG-L-ASNase	1.324 ± 0.062	135.14 ± 4.74	0.9078

4.2.5.9. Activation energy

The activation energy (*Ea*) values calculated by the Arrhenius equation for both PEG-L-ASNase and $NaYF_4$: Nd^{3+}, Yb^{3+}, Er^{3+}/GPTMS-PEG-L-ASNase. The *Ea* values were founded for L-ASNase as 17.31 kJ/mol, while for immobilized L-ASNase and 17.44 kJ/mol as seen in Figure 4.88. The *Ea* value was an increase after immobilization. This increase in *Ea* value demonstrated that immobilized enzyme requires more energy than the free one to overcome the conversion barrier to transform the substrate into a product.

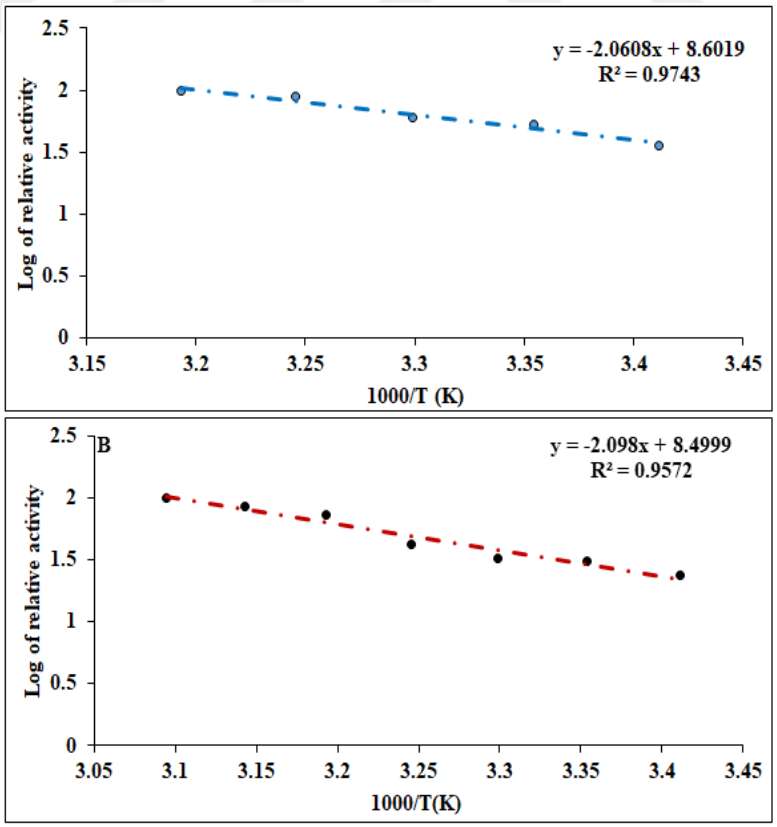

Figure 4.88: The activation energy of PEG-L-ASNase (A), and $NaYF_4$: Nd^{3+}, Yb^{3+}, Er^{3+}/GPTMS-PEG-L-ASNase (B).

4.2.5.10. Laser power, laser distance, and laser exposure time

The optimum laser power of $NaYF_4$: Nd^{3+}, Yb^{3+}, Er^{3+}/GPTMS-PEG-L-ASNase was determined by induced NIR power to immobilize on UCNP. Different milliwatts (mW) were scanned to find out the optimum power of UCNP by applying a constant amount of UCNP with a fixed distance between nanoparticles and NIR light. Owing to the result, the optimum laser power was founded 100 mW and the enzyme activity was increased from 100 % to 456 % as shown in Figure 4.89 A. After increasing the NIR power decrease in enzyme activity was recognized, due to NIR generated heat probable affected on the enzyme three-dimensional structure of enzyme active center or weak interaction between enzyme and UCNP.

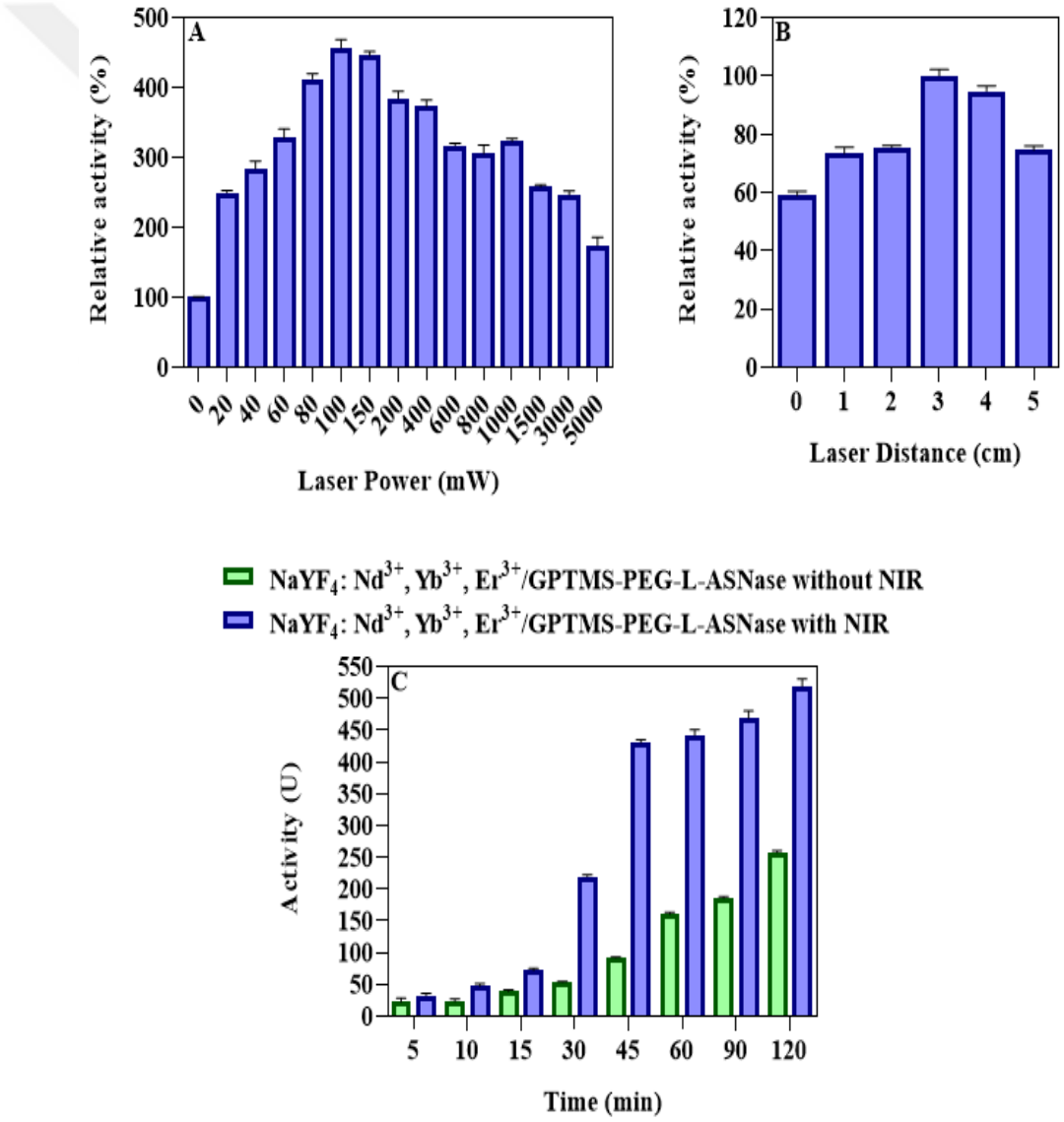

Figure 4.89: Induce of $NaYF_4$: Nd^{3+}, Yb^{3+}, Er^{3+}/GPTMS-PEG-L-ASNase, NIR light power (A), NIR distance (B), and NIR time (C).

After the maximum NIR light power was found, the right distance between $NaYF_4$: Nd^{3+}, Yb^{3+}, Er^{3+}/GPTMS-PEG-L-ASNase and laser power was optimized. In this experiment, the NIR light was arranged at 100mW with a constant amount of UCNP and different distances were scanned (0–5 cm). The optimum activity was founded at a 3 cm distance between NIR light and UCNP immobilized enzyme as seen in Figure 4.89 B. It was determined that decreasing the enzyme activity by increasing the distance, this due to decrease the effect of NIR light on UCNP nanoparticles.

NIR exposure time was investigated by keeping constant laser power, distance, and the amount of of $NaYF_4$: Nd^{3+}, Yb^{3+}, Er^{3+}/GPTMS-PEG-L-ASNase, while the activity was also determined in the absence of NIR radiation. As it is shown in Figure 4.89 C there was a sharp increase in the activity due to the exposure to NIR light.

4.2.5.11. Stability of $NaYF_4$: Nd^{3+}, Yb^{3+}, Er^{3+}/GPTMS-PEG-L-ASNase

The stability of $NaYF_4$: Nd^{3+}, Yb^{3+}, Er^{3+}/GPTMS-PEG-L-ASNase and the effect of NIR after storage. Different samples of $NaYF_4$: Nd^{3+}, Yb^{3+}, Er^{3+}/GPTMS-PEG-L-ASNase were incubated with PBS (50 mM, pH 7.4) at +37 °C for one week, and the activity was measured every single day by first exposure to NIR light at optimum conditions then the activity was measured. After one week the activity was above 57 % from the initial activity as shown in (Figure 4.90).

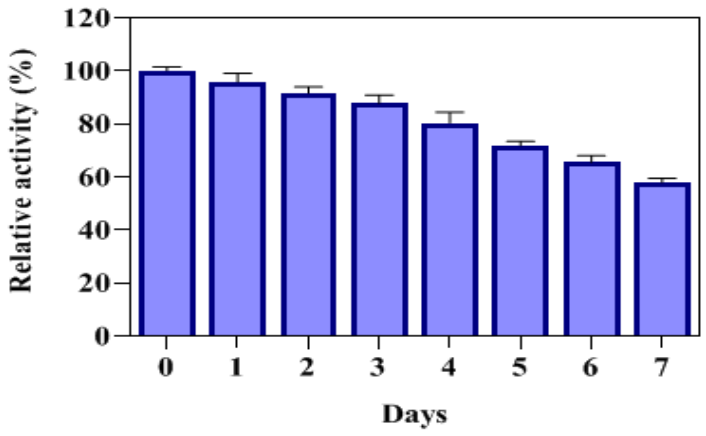

Figure 4.90: Stability of $NaYF_4$: Nd^{3+}, Yb^{3+}, Er^{3+}/GPTMS-PEG-L-ASNase in PBS by NIR light.

4.2.5.12. *In vitro* half-life

In vitro half-life of were determined for both PEG-L-ASNase and $NaYF_4$: Nd^{3+}, Yb^{3+}, Er^{3+}/GPTMS-PEG-L-ASNase. The samples were incubated with rat blood serum for 1 week at +37 °C. Then, the activity of the free and immobilized enzyme was measured at optimum conditions and their *in vitro* half-life was calculated by compare with the initial activity as shown in (Figure 4.91).

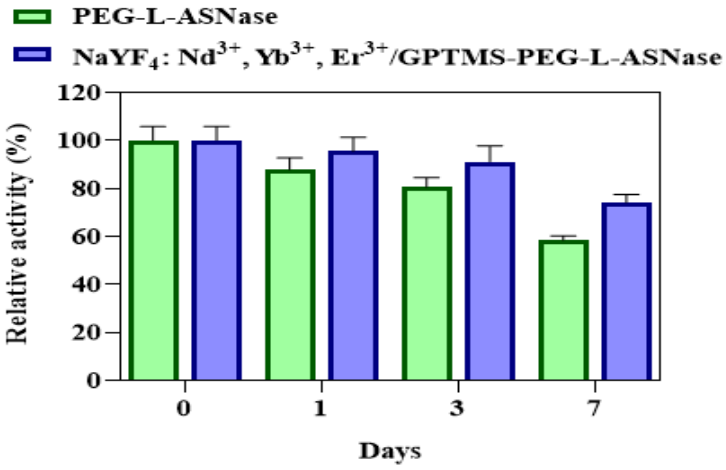

Figure 4.91: *In vitro* half-life of PEG-L-ASNase and immobilized $NaYF_4$: Nd^{3+}, Yb^{3+}, Er^{3+}/GPTMS-PEG-L-ASNase.

4.2.5.13. Plasma coagulation

The prothrombin time (PT) and the activated partial thromboplastin time (APTT), the reflective effect of $NaYF_4$: Nd^{3+}, Yb^{3+}, Er^{3+}/GPTMS and $NaYF_4$: Nd^{3+}, Yb^{3+}, Er^{3+}/ GPTMS-PEG-L-ASNase on intrinsic and extrinsic pathways of the blood coagulation. They were determined by incubating in platelet-poor plasma as seen in Figure 4.92. The results suggested there no coagulation occurred when UCNPs were added. These findings indicate that both reflect the effect of $NaYF_4$: $Nd^{3+,}$ Yb^{3+}, Er^{3+}/GPTMS and $NaYF_4$: Nd^{3+}, Yb^{3+}, Er^{3+}/GPTMS-PEG-L-ASNase, which may be related to the hydrophilicity and surface area charge of these particles.

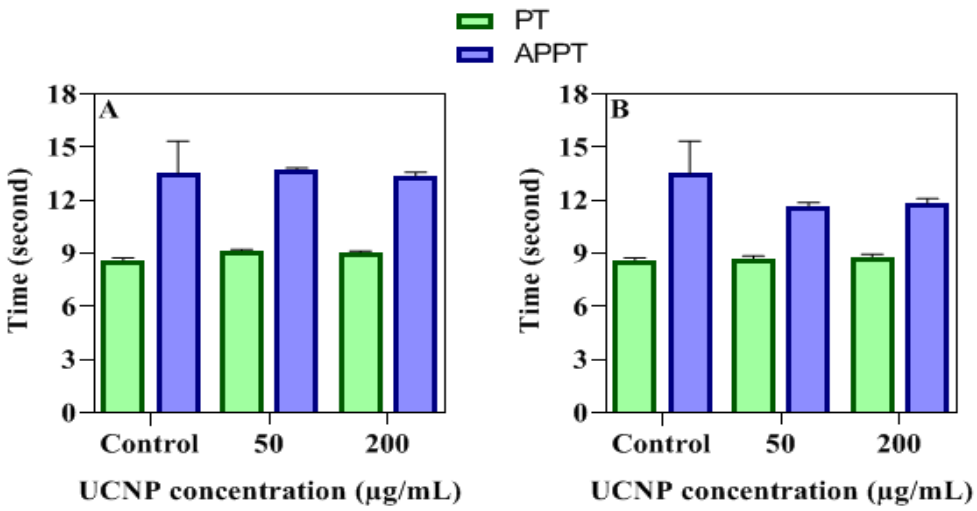

Figure 4.92: Plasma coagulation of $NaYF_4$: Nd^{3+}, Yb^{3+}, Er^{3+}/GPTMS (A), and $NaYF_4$: Nd^{3+}, Yb^{3+}, Er^{3+}/GPTMS-PEG-L-ASNase (B).

4.2.5.14. *In vitro* cytotoxicity

The *in vitro* cytotoxicity of the prepared UCNP was tested calorimetrically by using the MTT test and the results were shown in Figure 4.93 A and B. In cytotoxicity studies, cell viability is classified as more than 50 % toxic, from 51 to 70% mildly cytotoxic, less than 71% non-cytotoxic [211]. Different concentration (12.5, 25, 50, 100, and 200 µg/mL) of $NaYF_4$: Nd^{3+}, Yb^{3+}, Er^{3+}/GPTMS and $NaYF_4$: Nd^{3+}, Yb^{3+}, Er^{3+}/GPTMS-PEG-L-ASNase were tested against mouse fibroblast (L-929). In addition, the morphology of the cells treated with UCNPs and UCNPs-PEG-L-ASNase were given in Figure 4.93 C, after to 24, 48, and 72 h form incubation. As a result, it was observed that the synthesized UCNP nanoparticles had no *in vitro* toxic effects on cell viability.

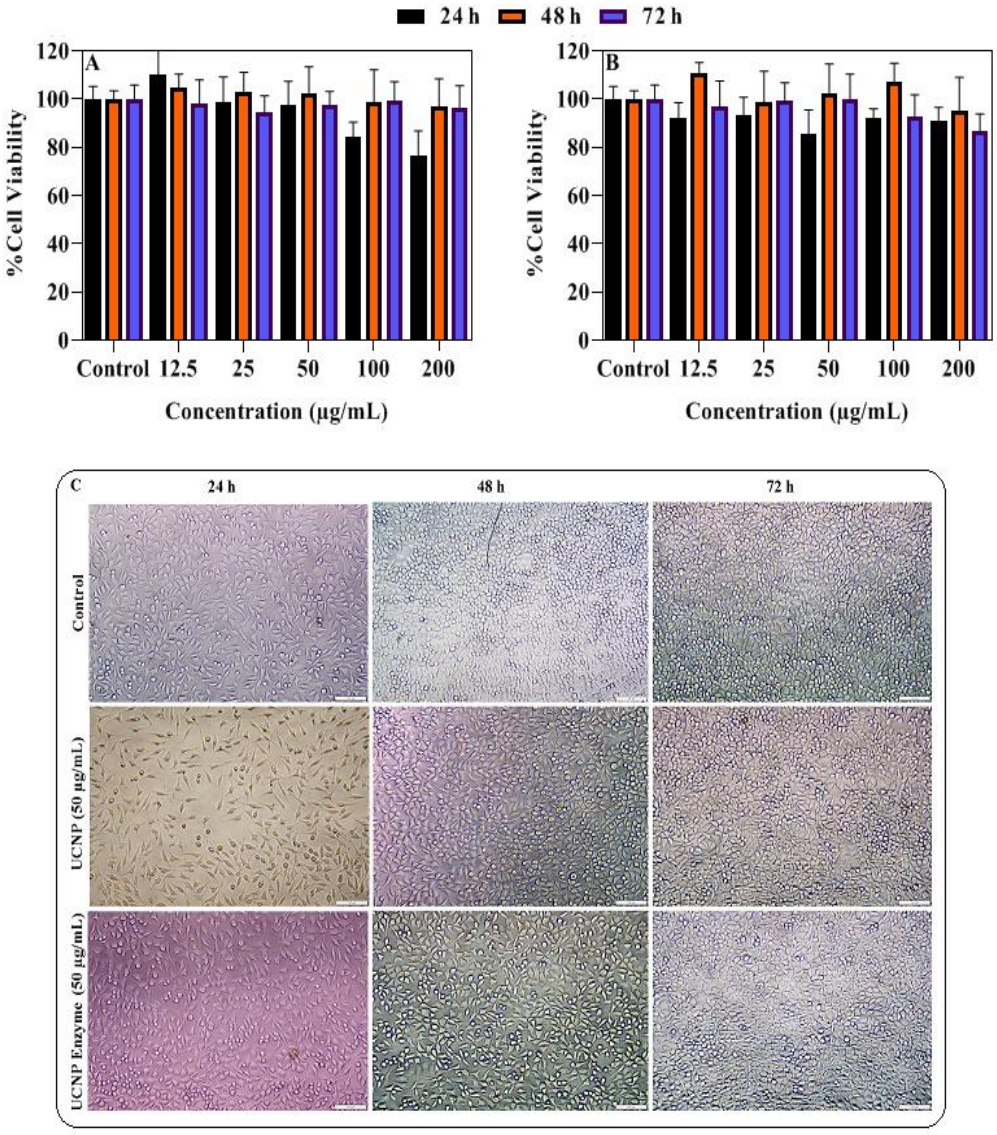

Figure 4. 93: Cell viability results after incubation 24, 48, and 72 hours of L-929 with $NaYF_4$: Nd^{3+},Yb^{3+},Er^{3+}/GPTMS (A), $NaYF_4$: Nd^{3+}, Yb^{3+},Er^{3+}/GPTMS-PEG-L-ASNase (B), and morphological image of L-929 fibroblast cells (C).

4.2.6. Immobilization parameters of $NaYF_4$: Nd^{3+}, Yb^{3+}, Er^{3+}/ICPTES

4.2.6.1. Enzyme unit and incubation time

35 U concentration was chosen as the amount of enzyme for $NaYF_4$: Nd^{3+}, Yb^{3+}, Er^{3+}/ ICPTES. As seen in (Figure 4.94 A), the immobilization yield decreased after 35 U, while in (Figure 4.94 B), there was a sharp increase in the catalytic activity from 5-35 U. In the same time, 50 U only indicated either similar or small catalytic activity. The activity nearly stays constant, this due covalent function group cannot attach more than 35 U on their surface area. Furthermore, the immobilization yield, activity yield,

and immobilization efficiency for 35 U were founded as 96.81 ± 0.47 %, 78.47 ± 2.03 %, and 80.59 ± 1.69 %, respectively.

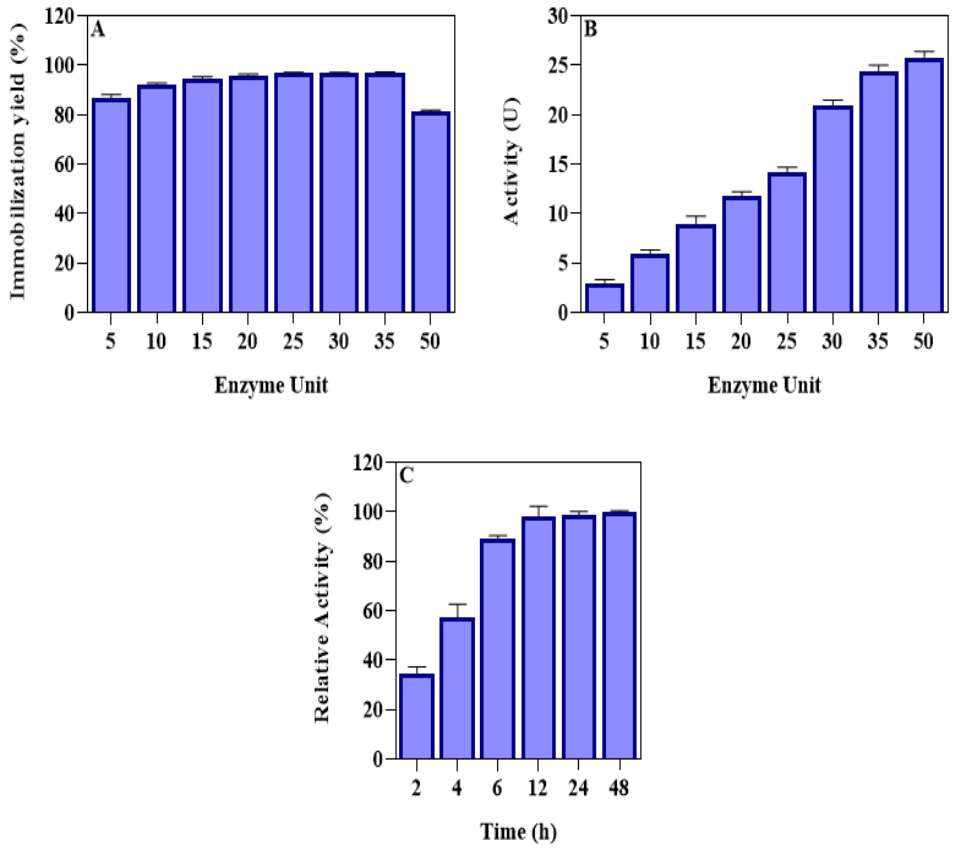

Figure 4.94: L-ASNase immobilization yield (A), L-ASNase catalytic activity (B), and incubation time (C) of $NaYF_4$: Nd^{3+}, Yb^{3+}, Er^{3+}/ICPTES-PEG-L-ASNase.

In order to determine the effect of immobilization time on enzyme activity, the immobilization times were taken place between 2 to 48 hours. As seen in Figure 4.94 C, from 2 -12 hours from immobilization there was a marked increase in the relative activity of the enzyme. After 12 hours from the immobilization, the relative activity of the immobilized enzyme approximately stays constant, due to the amount of enzyme immobilized to UCNP has enough time to make covalent interactions between enzyme and UCNP. Based on these results, 12 hours was selected as the optimum incubation time of immobilization.

4.2.6.2. Optimum pH and temperature

The enzymatic activities of PEG-L-ASNase and $NaYF_4$: Nd^{3+}, Yb^{3+}, Er^{3+}/ICPTES were measured between pH 4 and 10 to determine the optimum pH. As shown in

Figure 4.95 A**,** the optimum pH of PEG-L-ASNase was founded at pH 8.5, while the optimum pH value for $NaYF_4$: Nd^{3+}, Yb^{3+}, Er^{3+}/ICPTES decreased to pH 8. The reason for this change can be attributed to structural conformational changes in the enzyme resulting from covalent interactions between the enzyme and UCNP. The relative activity of immobilized enzyme higher than that free one, even at pH 10 the activity of immobilized still above 87 % while the free 43 %. Generally, the changes in optimum pH induce enzymes conformational after immobilization. Also, the alteration of optimum pH value probably drives the change in acidic or basic amino acid ionization surrounding the enzyme's active site. Meanwhile, this shifting is also important because the similarity with pH with the human body is required pH. The relative activity of the $NaYF_4$: Nd^{3+}, Yb^{3+}, Er^{3+}/ICPTES-PEG-L-ASNase was higher than that L-ASNase. It is noted that the main advantage of immobilization process is higher stability of enzyme as well as alleviating effects environmental factors against enzyme.

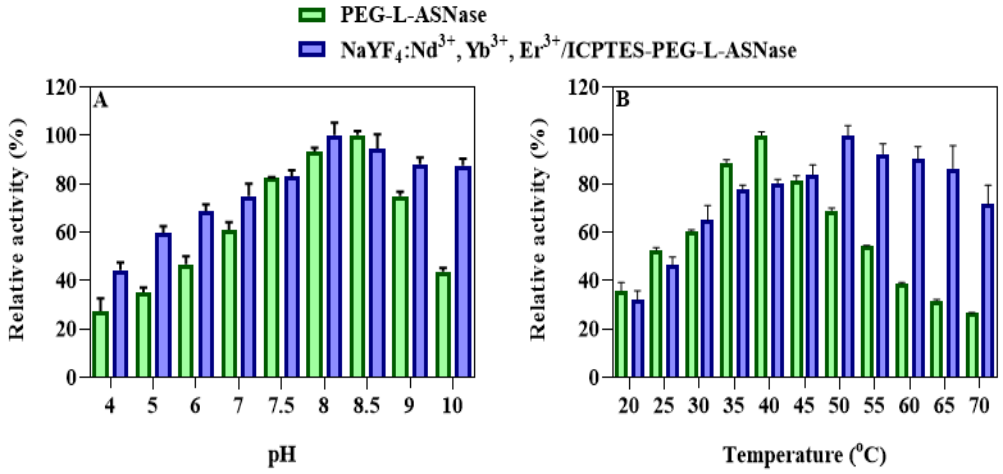

Figure 4.95: Optimum pH (A), and temperature (B), of PEG-L-ASNase and $NaYF_4$: Nd^{3+}, Yb^{3+}, Er^{3+}/ICPTES-PEG-L-ASNase.

The optimum temperature of PEG-L-ASNase and $NaYF_4$: Nd^{3+}, Yb^{3+}, Er^{3+}/ICPTES-PEG-L-ASNase were tested within the range 20-70 °C. The optimum temperature for PEG-L-ASNase was found at 40 °C, while this value increased to 50 °C after immobilized as shown in Figure 4.95 B. Moreover, it remained above 71 % of its relative activity at 70 ° C for immobilized and around 26 for the free one. The increase in optimum temperature due to $NaYF_4$: Nd^{3+}, Yb^{3+}, Er^{3+}/ICPTES-PEG-L-ASNase hada significantly higher thermal resistance due to covalent interactions between enzyme and UCNP.

4.2.6.3. Thermal and pH stability

In comparison against the free enzymes, thermal stability is also the most important benefit of immobilization. Thermal stability results were shown in Figure 4.96 A, for both PEG-L-ASNase and $NaYF_4$: Nd^{3+}, Yb^{3+}, Er^{3+}/ICPTES-PEG-L-ASNase were incubated at 50° C for 6 hours. The activity was measured after 6 hours, the remained activity of PEG-L-ASNase was 49 % from its initial activity, while for immobilized PEG-L-ASNase the activity still above 76 %. This resistance in temperature due to a decrease in the molecular mobility and conformational changes of the enzyme that because of the immobilization of L-ASNase. Therefore, in accordance to result immobilization significantly improves thermal stability.

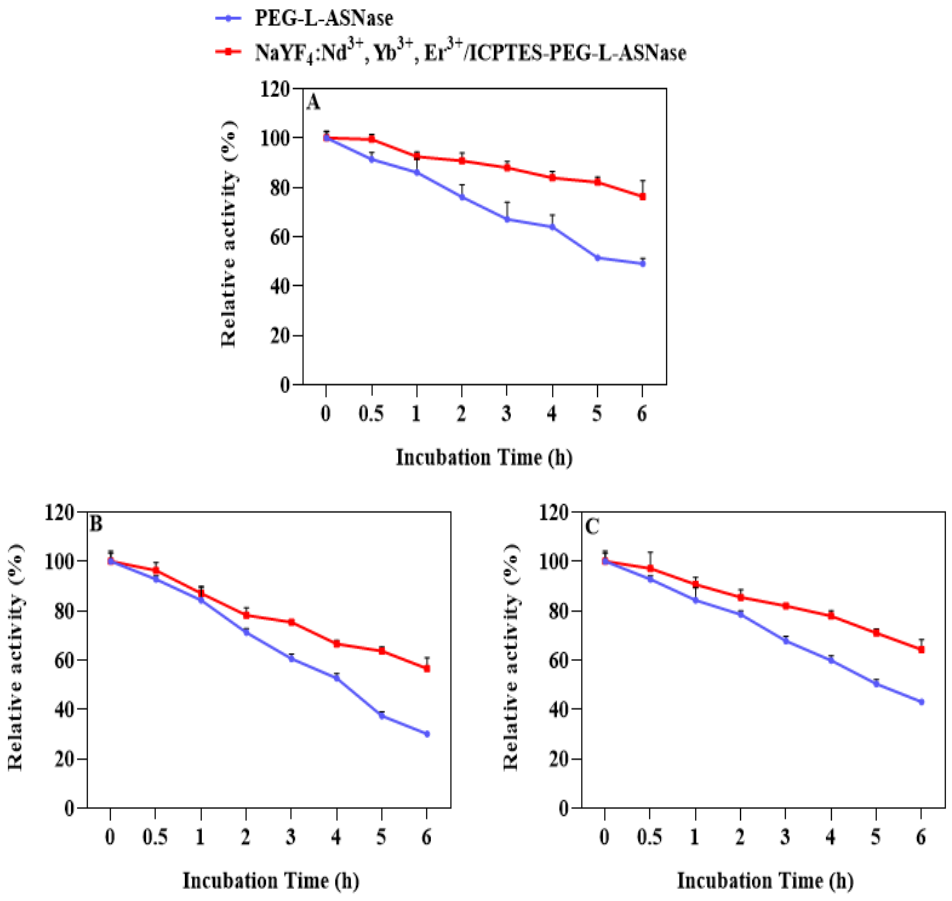

Figure 4.96: Thermal stability (A), pH stability at pH 4 (B), and pH stability at pH 9 (C) of PEG-L-ASNase and $NaYF_4$:Yb^{3+}, Er^{3+}/ICPTES-PEG-L-ASNase.

4.2.6.4. Effect metal ion and solvent

The effect of both metal ions and organic solvents were determined on the free PEG-L-ASNase and immobilized $NaYF_4$: Nd^{3+}, Yb^{3+}, Er^{3+}/ICPTES-PEG-L-ASNase,

samples were incubated with different metal ions. In our study, Na^{1+}, Ag^{1+}, Ba^{2+}, Ca^{2+}, Co^{2+} , Mg^{2+}, Ni^{2+} , and Al^{3+} increased enzyme activity. On the other hand, Cu^{2+}, Sr^{2+}, Zn^{2+}, and Cr^{3+} inhibited the enzyme activity as shown in (Figure 4.97 A). The activity of the immobilized enzyme is better to compare with the free enzyme. However, immobilized enzymes have been affected by metal ions that inhibit activity less than as much as the free enzyme. However, the solvent effect on of PEG-L-ASNase and $NaYF_4$: Nd^{3+}, Yb^{3+}, Er^{3+}/ICPTES-PEG-L-ASNase were invested by using different organic solvents such as 1-pentanol, 2-propanol, acetonitrile, chloroform, ethanol, ethyl acetate, *n*-hexane, isoamyl alcohol, DCM, DMF, DMSO, and THF after incubation for 24 h at room temperature, the activities were determined as shown in figure 4.97 B. The results were indicated that the immobilization enzyme has better stability against organic solvent even in some solvents the activity immobilization enzyme was increased, except for acetonitrile and DMSO the activity for the free enzyme was higher than the immobilized one.

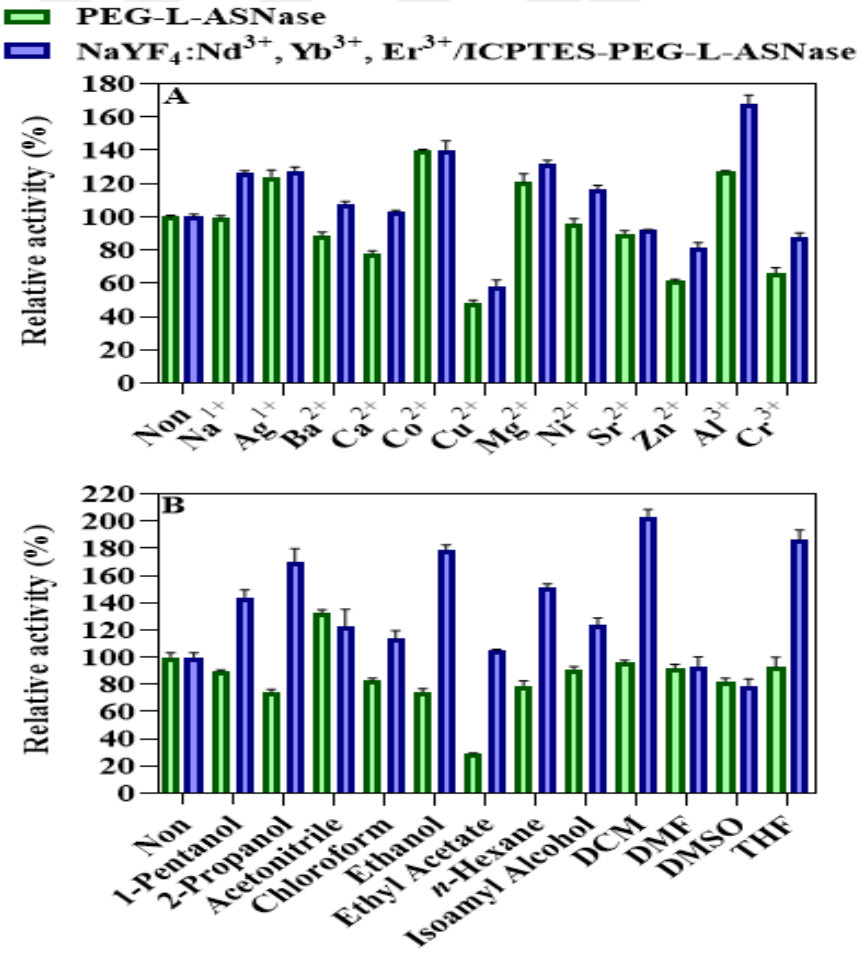

Figure 4.97: Stability of PEG-L-ASNase and $NaYF_4$: Nd^{3+}, Yb^{3+}, Er^{3+}/ICPTES-PEG-L-ASNase on metal ions (A), and organic solvents (B).

4.2.6.5. Reusability

The reusability of covalent immobilization of $NaYF_4$: Nd^{3+}, Yb^{3+}, Er^{3+}/ICPTES-PEG-L-ASNase was measured as shown in (Figure 4.98). The remaining relative activity after 10 cycles was still above 80 % from its initial activity, while the activity still retained more than 66 % of its starting activity even after 20 cycles. Covalent immobilization improves the reusability of the enzyme to compare with the physical one. Reusability is one of the advantages of immobilization, due to the simple separation of the immobilized enzyme from the reaction mixture and reused for several times, unlike the free enzyme that can not separate from the reaction medium.

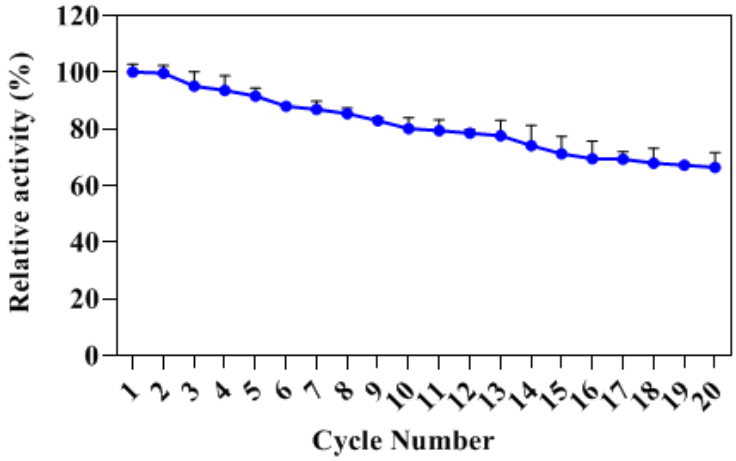

Figure 4.98: Reusability of $NaYF_4$: Nd^{3+}, Yb^{3+}, Er^{3+}/ICPTES-PEG-L-ASNase.

4.2.6.6. Storage stability

Storage stability is a crucial parameter for commercial-scale application of an enzyme, while it has been recognized that enzyme activity continuously diminishes over time due to instability during storage. Therefore, the storage stability of both PEG-L-ASNase and $NaYF_4$: Nd^{3+}, Yb^{3+}, Er^{3+}/ICPTES-PEG-L-ASNase were investigated at +4 and +25 °C for 4 weeks with the weekly measurement results were showed in Figure 4.99. After 4 weeks, the relative activity of immobilized L-ASNase was still above 70 % and 60% from initial activities at 4 and 25 °C, respectively. While for Free L-ASNase preserved 50 % and 43 % at 4 and 25 °C of, respectively. In particular, the enzyme immobilized at 4 °C showed higher storage stability. The loss of enzymatic activity is probably attributed to protein denaturation and degradation during long-term storage. These results showed that the storage stability of $NaYF_4$:

Nd^{3+}, Yb^{3+}, Er^{3+}/ICPTES-PEG-L-ASNase was better compared to the free enzyme at both 4 and 25 °C. It was also implied that the stability of immobilized enzyme was higher at 25°C with insignificant loss than the 4 °C counterparts. Owing to the result, $NaYF_4$: Nd^{3+}, Yb^{3+}, Er^{3+}/ICPTES-PEG-L-ASNase indicated its promising and alternative carrier matrix material due to its long-term storage stability.

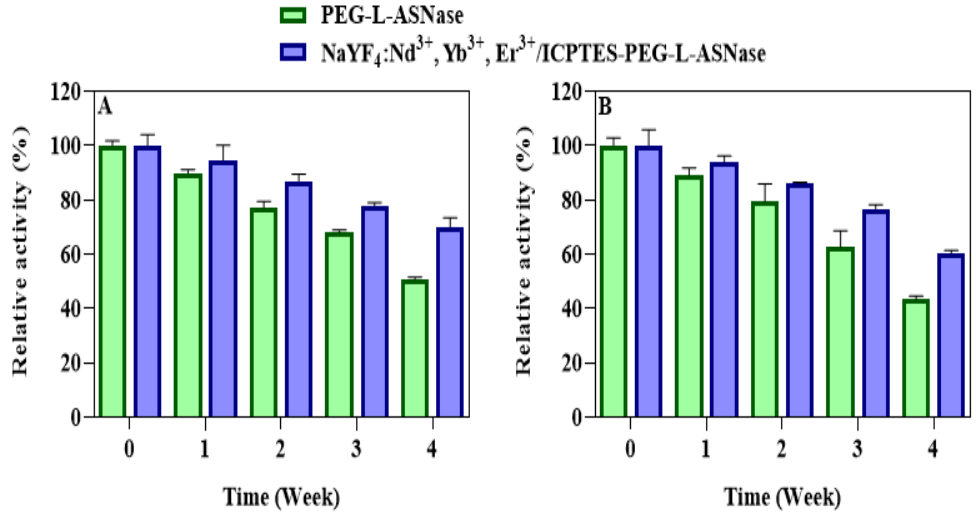

Figure 4.99: Storage stability of PEG-L-ASNase and $NaYF_4$: Nd^{3+}, Yb^{3+}, Er^{3+}/ICPTES-PEG-L-ASNase at +4°C (A), and at +25 °C (B).

4.2.6.7. Trypsin resistance

One of the major problems of bacterial enzymes in the pharmaceutical application is the stability against proteolysis enzymes. The resistance of both free enzyme and $NaYF_4$: Nd^{3+}, Yb^{3+}, Er^{3+}/ICPTES-PEG-L-ASNase against trypsin digestion is shown in Figure 4.100. After 120 minutes After 120 minutes from incubation with trypsin at +37 °C, PEG-L-ASNase was almost completely hydrolyzed, while the immobilized L-ASNase retained about 59 % of its original activity. The results showed that the resistance of immobilized L-ASNase aginst trypsin digestion was greatly improved compared to the free PEG-L-ASNase.

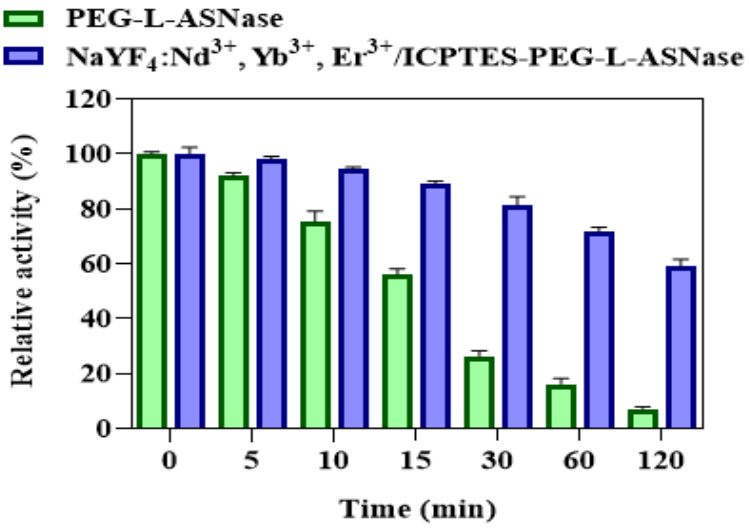

Figure 4.100: Trypsin resistance of PEG-L-ASNase and $NaYF_4$: Nd^{3+}, Yb^{3+}, Er^{3+}/ ICPTES-PEG-L-ASNase.

4.2.6.8. Kinetic parameter

The kinetic parameters for both PEG-L-ASNase and $NaYF_4$: Nd^{3+}, Yb^{3+}, Er^{3+}/ ICPTES-PEG-L-ASNase were estimated and summarized in Table 4.8. Also, the Lineweaver–Burk plots were shown in Figure 4.101. As shown in Table 4.8, the obtained K*m* values for the free and immobilized were 2.43 and 0.182 mM, respectively. After immobilization, the K*m* value decreased. It is obviously shown that low Km value enzyme indicated high catalytic efficiency as it achieved the maximum catalytic efficiency in low substrate concentration. Therefore, the decrease of K*m* value after immobilization represents the high affinity of the enzyme to its substrate. Meanwhile, an increase in the *Vmax* was observed value after enzyme immobilization. The apparent *Vmax* value increased from 166.67 to 22.72. The obtained results are in accordance with the values reported previously.

Table 4.8: Kinetic parameters of PEG-L-ASNase and $NaYF_4$: Nd^{3+}, Yb^{3+}, Er^{3+}/ICPTES-PEG-L-ASNase.

Sample	K*m* (mM)	*Vmax* (µmol/min)	R^2
PEG-L-ASNase	2.31 ± 0.042	140.85 ± 3.235	0.9663
$NaYF_4$: Nd^{3+}, Yb^{3+}, Er^{3+} /ICPTES-PEG-L-ASNase	2.27 ± 0.054	123.45 ± 2.87	0.9862

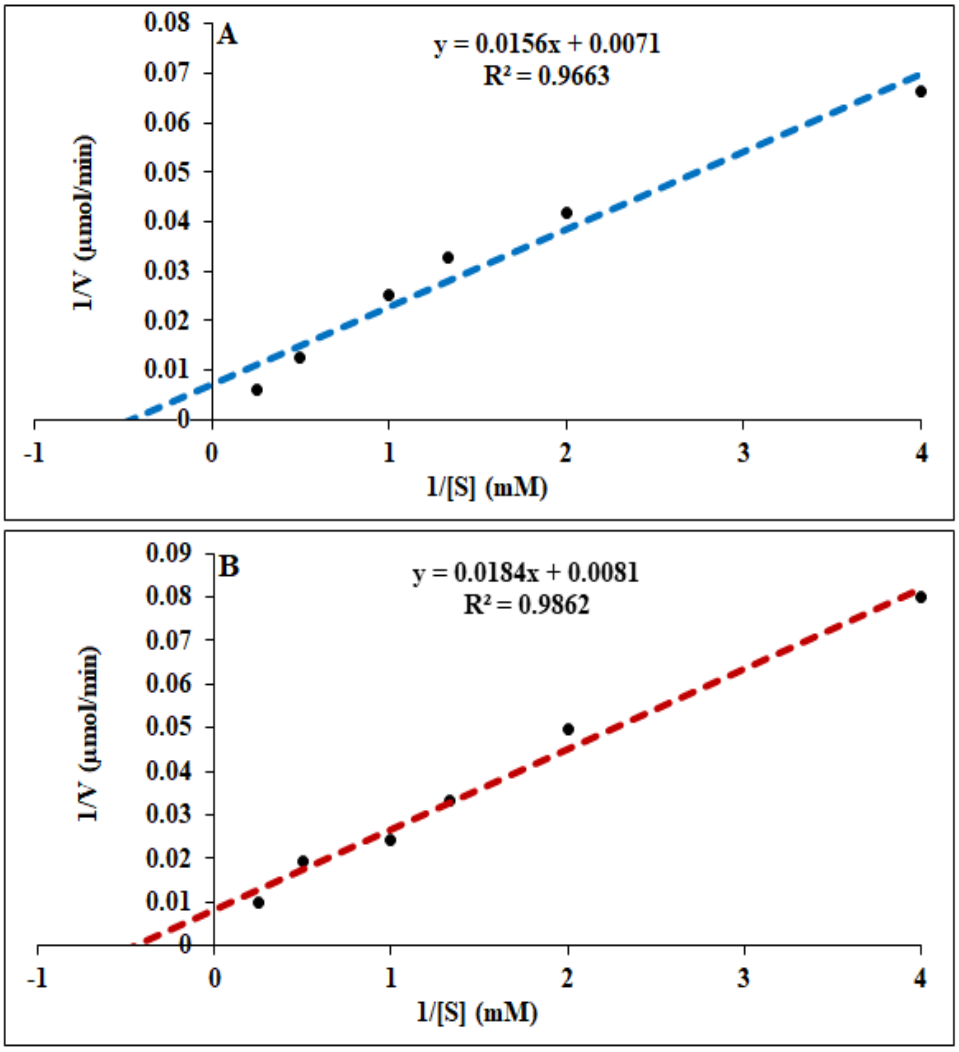

Figure 4.101: Kinetic parameters of PEG-L-ASNase (A), and $NaYF_4$: Nd^{3+}, Yb^{3+}, Er^{3+}/ICPTES-PEG-L-ASNase (B).

4.2.6.9. Activation energy

The activation energy (*Ea*) was determined by the Arrhenius equation for both PEG-L-ASNase and $NaYF_4$: Nd^{3+}, Yb^{3+}, Er^{3+}/ICPTES-PEG-L-ASNase. The *Ea* values which were calculated from the slope of log (% relative activity) versus 1000/T, while Ea values were determined as 17.13 kJ/mol for PEG-L-ASNase and 12.29 kJ/mol for the $NaYF_4$:Yb^{3+}, Er^{3+}/PEI-PEG-L-ASNase as seen in Figure 4.102. The low Ea value was reported beneficial also for enzyme immobilization. This implied that the immobilized enzymes were less temperature-sensitive. This reduction in *Ea* value demonstrated that the immobilized enzyme required less energy than the free one to overcome the conversion barrier to transform the substrate into a product. The results implied immobilized enzyme higher stability and advantages than the free counterpart.

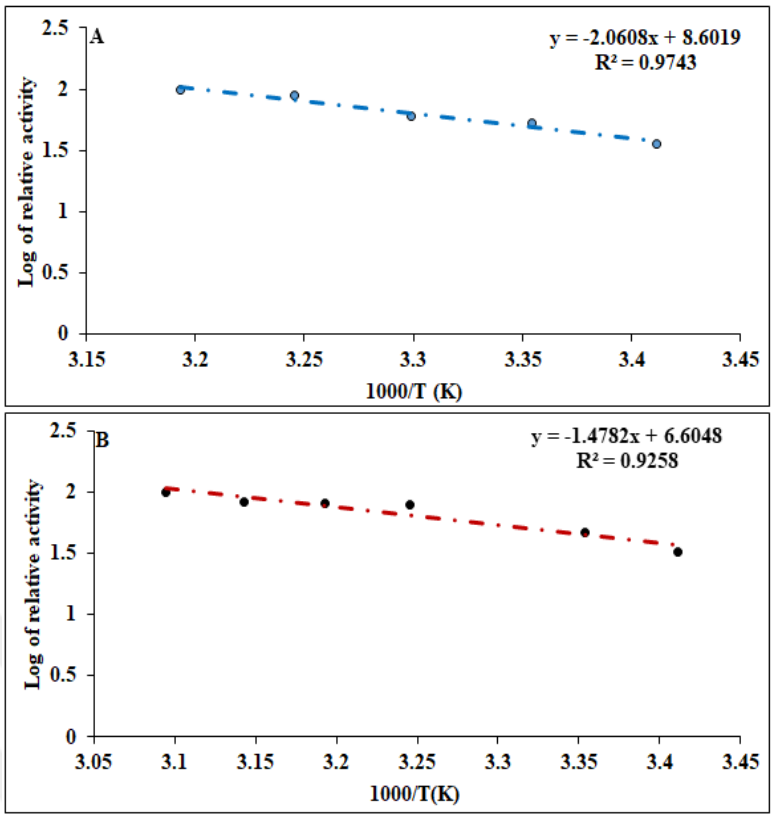

Figure 4.102: The activation energy of PEG-L-ASNase (A), and $NaYF_4$: Nd^{3+}, Yb^{3+}, Er^{3+}/ICPTES-PEG-L-ASNase (B).

4.2.6.10. Laser power, laser distance, and laser exposure time

To determine the optimum laser power for $NaYF_4$: Nd^{3+}, Yb^{3+}, Er^{3+}/ICPTES-PEG-L-ASNase, NIR light was induced to immobilize enzyme on UCNP. Different milliwatts (mW) were scanned to find out the optimum power of UCNP by applying a constant amount of UCNP with a fixed distance between nanoparticles and NIR light. Owing to the result, the optimum was founded 150 mW, and enzyme activity was increased from 100 % to 547 % as shown in Figure 4.103 A. In accordance to the result, diminishing enzyme activity took place coincidently with increasing NIR light power, it was assumed that the NIR generated heat probably affected the three-dimensional structure of enzyme or less enzyme interaction between enzyme and UCNP.

After the maximum NIR light power was found, it's from the right distance between $NaYF_4$: Nd^{3+}, Yb^{3+}, Er^{3+}/ICPTES-PEG-L-ASNaseand laser power was to optimizing the right distance of $NaYF_4$: Nd^{3+}, Yb^{3+}, Er^{3+}/ICPTES-PEG-L-ASNase and laser power. In this experiment, the NIR light was fixed arranged at 150 mW with a

fixed amount of enzyme immobilized on UCNP, and different distances were scanning scanned (0 – 5 cm) with the optimum activity was found at 3 cm between NIR and UCNP immobilized enzyme as seen in (Figure 4.103 B). Owing to the result, diminishing enzyme activity was inversely proportional against the increasing distance due to decreasing the effect of NIR light on UCNP nanoparticles.

NIR exposure time was investigated by keeping constant laser power, distance, and the amount of $NaYF_4$: Nd^{3+}, Yb^{3+}, Er^{3+}/ICPTES-PEG-L-ASNase, while the activity was also determined in the absence of NIR radiation. As it is shown in Figure 4.103 C there was a sharp increase in the activity due to the exposure to NIR light until 120 min. NIR exposure time of $NaYF_4$: Nd^{3+}, Yb^{3+}, Er^{3+}/ICPTES-PEG-L-ASNase, on the other hand, the activity affected by time was also determined without exposure to NIR light. As it is shown in (Figure 4.103 C) there was a sharp increase in the activity of the exposure to NIR light until 120 min.

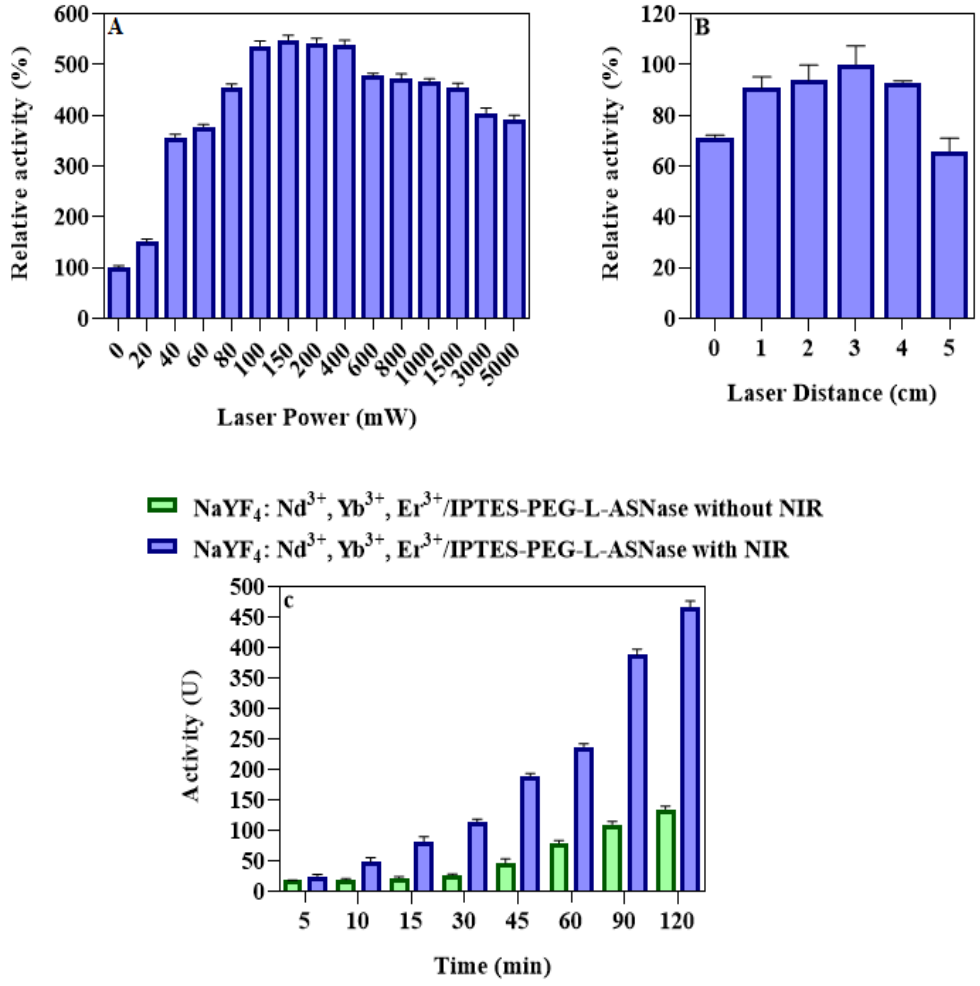

Figure 4.103: Induce of $NaYF_4$: Nd^{3+}, Yb^{3+}, Er^{3+}/ICPTES-PEG-L-ASNase, NIR light power (A), NIR distance (B), and NIR time (C).

4.2.6.11. Stability of $NaYF_4$:Yb^{3+}, Er^{3+}/ICPTES-PEG-L-ASNase

To measure the stability of $NaYF_4$: Nd^{3+}, Yb^{3+}, Er^{3+}/ICPTES-PEG-L-ASNase and the effect of NIR after storage. Different samples of $NaYF_4$: Nd^{3+}, Yb^{3+}, Er^{3+}/ICPTES-PEG-L-ASNase were incubated with PBS (50 mM, pH 7.4) at +37 °C for one week, and the activity was measured every single day by first exposure to NIR light at optimum conditions then the activity was measured. After one week the activity was above 67 % from the initial activity as shown in (Figure 4.104).

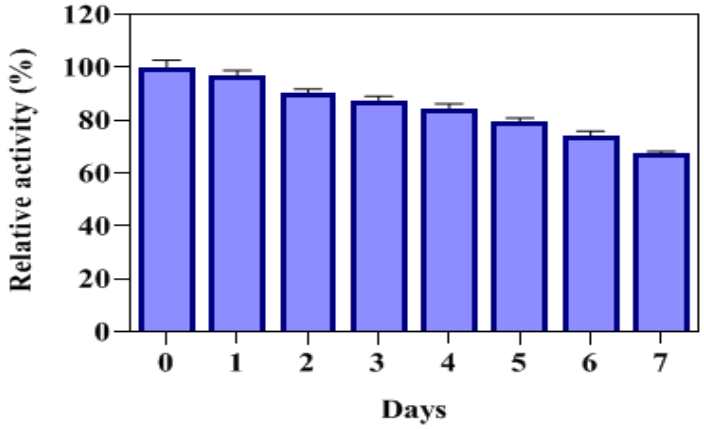

Figure 4.104: Stability of $NaYF_4$: Nd^{3+}, Yb^{3+}, Er^{3+}/ICPTES-PEG-L-ASNase in PBS by NIR light.

4.2.6.12. *In vitro* half-life

In vitro half-life of were determined for both free PEG-L-ASNase and $NaYF_4$: Nd^{3+}, Yb^{3+}, Er^{3+}/ICPTES-PEG-L-ASNase. The samples and rat blood serum were incubated for 1 week at +37 °C. The activity of the free and immobilized enzyme was measured at optimum conditions and their *in vitro* half-life was calculated by comparing with the initial activity as shown in (Figure 4.105).

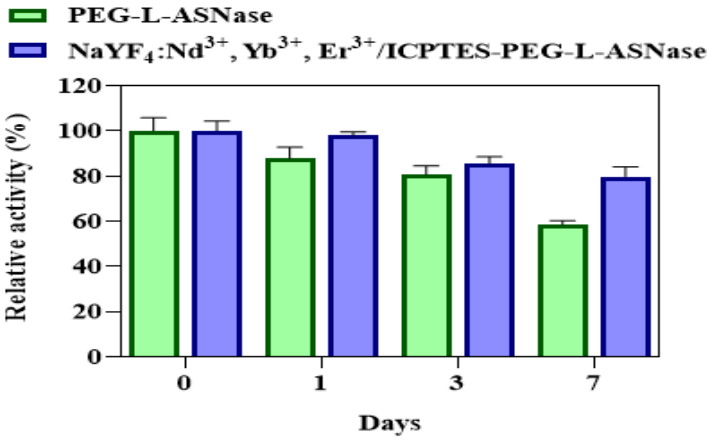

Figure 4.105: *In vitro* half-life of PEG-L-ASNase and immobilized $NaYF_4$: Nd^{3+}, Yb^{3+}, Er^{3+}/ICPTES-PEG-L-ASNase.

4.2.6.13. Plasma coagulation

The prothrombin time (PT) and the activated partial thromboplastin time (APTT), reflect the effect of $NaYF_4$: Nd^{3+}, Yb^{3+}, Er^{3+}/ICPTES and $NaYF_4$: Nd^{3+}, Yb^{3+}, Er^{3+}/ ICPTES-PEG-L-ASNase on the intrinsic and extrinsic pathways of the blood coagulation cascade. They were determined by incubating both in platelet-poor plasma (Figure 4.106). It is clearly indicated that the absence of coagulation occurred when UCNPs were added. These findings indicate that both $NaYF_4$: Nd^{3+}, Yb^{3+}, Er^{3+}/ICPTES and $NaYF_4$: Nd^{3+}, Yb^{3+}, Er^{3+}/ICPTES-PEG-L-ASNase are hemocompatible, which may be related to the hydrophilicity and surface area charge of these particles.

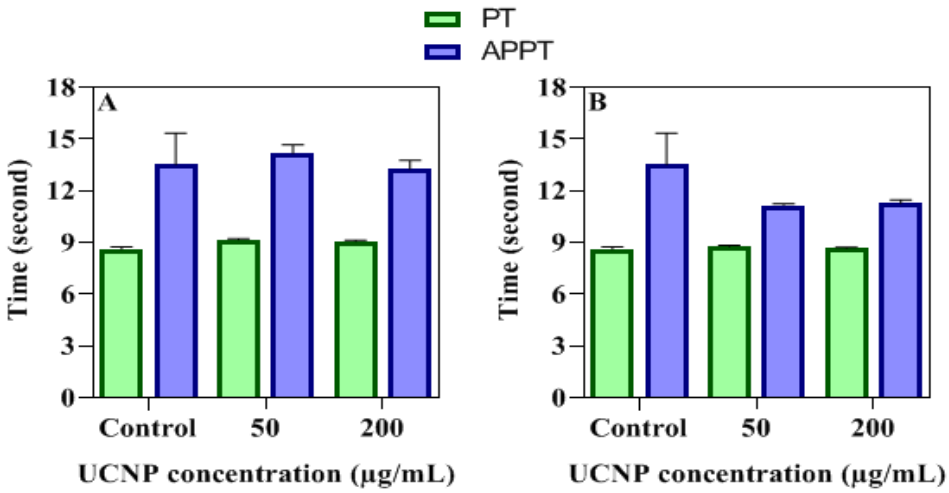

Figure 4.106: Plasma coagulation of $NaYF_4$: Nd^{3+}, Yb^{3+}, Er^{3+}/ICPTES (A), and $NaYF_4$: Nd^{3+}, Yb^{3+}, Er^{3+}/ICPTES-PEG-L-ASNase (B).

4.2.6.14. *In vitro* cytotoxicity

The *in vitro* cytotoxicity of the synthesized UCNP was tested calorimetrically by using the MTT test and the results were shown in Figure 4.107 A and B. In cytotoxicity studies, cell viability is classified as more than 50 % toxic, between 51 and 70 % mildly cytotoxic, less than 71 % non-cytotoxic [211]. Different concentration (12.5, 25, 50, 100, and 200 µg/mL) of $NaYF_4$: Nd^{3+}, Yb^{3+}, Er^{3+}/ICPTES and $NaYF_4$: Nd^{3+}, Yb^{3+},Er^{3+}/ICPTES-PEG-L-ASNase were tested against mouse fibroblast (L-929). In addition, the morphology of the cells treated with UCNPs and UCNPs-PEG-L-ASNase were given in Figure 4.107 C, after 24, 48, and 72 h form incubation. Owing to the result, the morphological alteration was absent took place while that the synthesized UCNP did not indicate *in vitro* toxicity in accordance to cell viability.

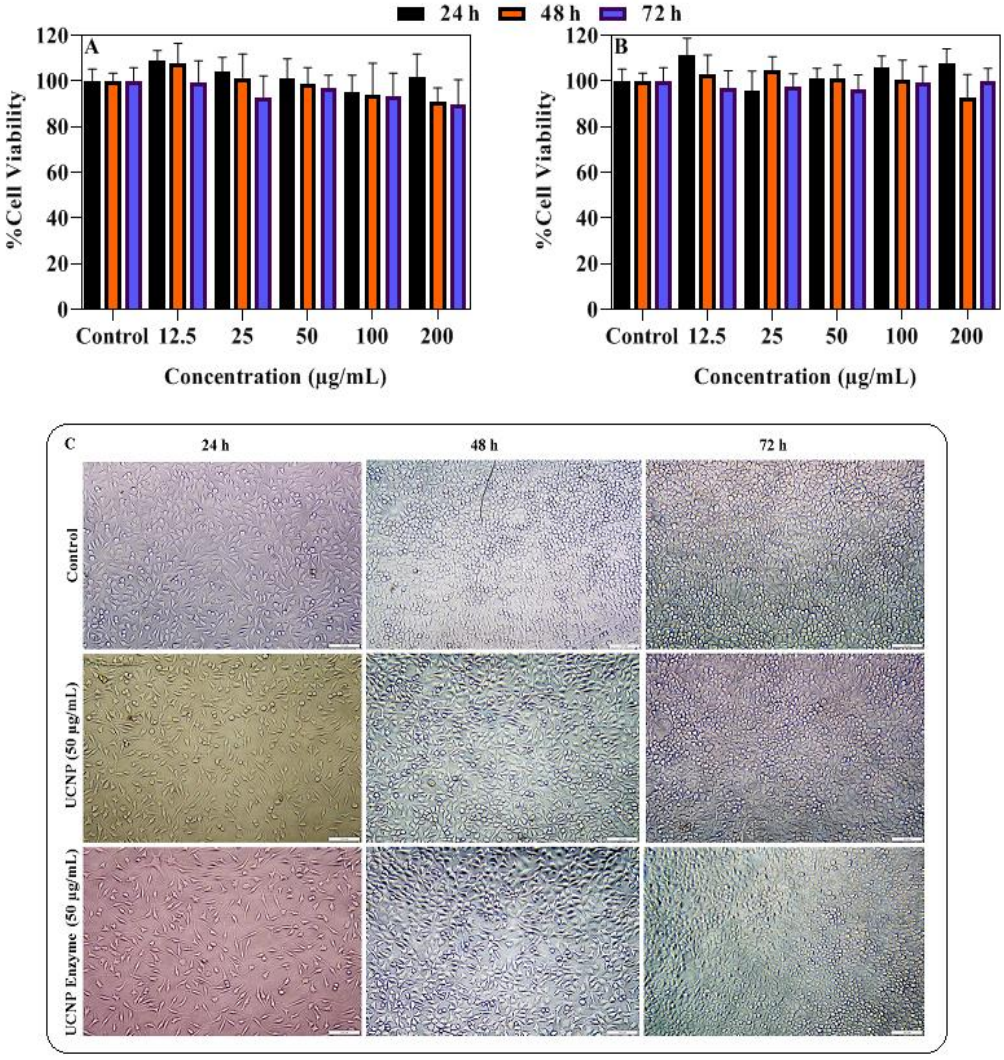

Figure 4.107: Cell viability results after incubation 24, 48, and 72 hours of L-929 with $NaYF_4$: Nd^{3+}, Yb^{3+} Er^{3+}/ICPTES (A), $NaYF_4$: Nd^{3+}, Yb^{3+}, Er^{3+}/ICPTES-PEG-L-ASNase (B), and morphological image of L-929 fibroblast cells (C).

4.2.6.15. *In vitro* catalytic activity

From the *in vitro* catalytic activity experiment, $NaYF_4:Nd^{3+}$, Yb^{3+}, Er^{3+}/ICPTES, PEG-L-ASNase, NIR, $NaYF_4:Nd^{3+}$, Yb^{3+}, Er^{3+}/ICPTES+NIR, $NaYF_4:Nd^{3+}$,Yb^{3+}, Er^{3+}/ICPTES-PEG-L-ASNase, and $NaYF_4:Nd^{3+}$, Yb^{3+}, Er^{3+}/ICPTES-PEG-L-ASNase + NIR groups exhibited 11.3 %, 13.8 %, 15.1 %, 20.9 %, 24.5 %, and 70.2% as HL-60 cell growth inhibition (%), respectively. The results showed that toxicities of NIR light and nanoparticles were in the acceptable limits according to ASTM standards. In addition, $NaYF_4:Nd^{3+}$, Yb^{3+}, Er^{3+}/ICPTES-PEG-L-ASNase has almost 3 times more activity after NIR inducement.

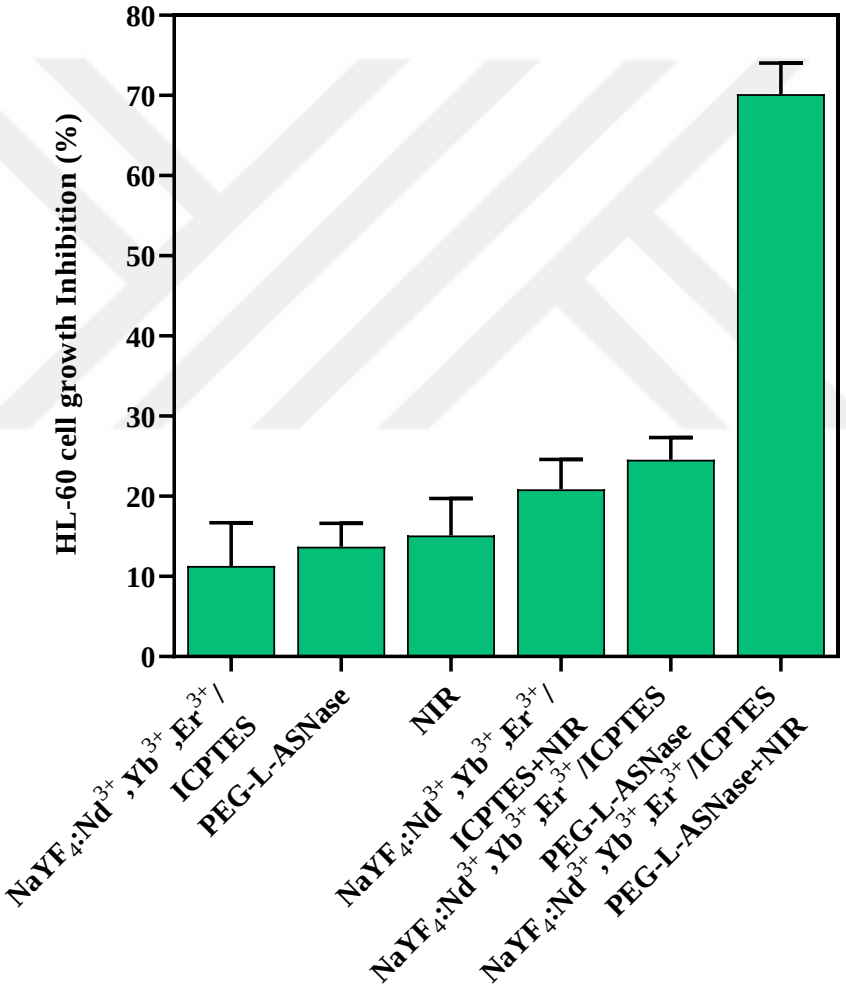

Figure 4.108: Cell growth inhibition (%) results of $NaYF_4:Nd^{3+}$, Yb^{3+}, Er^{3+}/ICPTES-PEG-L-ASNase against HL-60 cell lines after NIR inducement.

5. DISCUSSION

In this thesis, 6 different types of UCNPs nanoparticles were synthesized and crystal structures, particle size distribution and particle hydrodynamic diameter in the polar solvent environment, particle surface charge, particle shapes and sizes, organic and inorganic surface modifications of the synthesized products were characterized by using X-Ray Diffraction (XRD), Dynamic Light Scattering (DLS), Zetameter, Transmittance Electron Microscopy (TEM), FTIR, Thermal Analysis (TGA) and X-ray Photoelectron Spectroscopy (XPS) techniques, respectively. The photophysical properties of pure and modified UCNPs at the relevant wavelength (980 and 808 nm) under laser stimulation were determined by Fluorescence Spectroscopy. Furthermore, the synthesized UCNPs; $NaYF_4$: Yb^{3+}, Er^{3+}/PEI, $NaYF_4$: Yb^{3+}, Er^{3+}/GPTMS, $NaYF_4$:Yb^{3+}, Er^{3+}/ICPTES, $NaYF_4$: Nd^{3+}, Yb^{3+}, Er^{3+}/PEI, $NaYF_4$: Nd^{3+}, Yb^{3+}, Er^{3+}/ GPTMS and $NaYF_4$:Nd^{3+}, Yb^{3+}, Er^{3+}/ICPTES were used for immobilization PEG-L-ASNase. Thereafter, the immobilization parameters and biocompatibility of UCNPs-PEG-L-ASNase were investigated and NIR radiation was used to increase L-ASNase activity.

For physical immobilization of L-ASNase on 25 mg of $NaYF_4$: Yb^{3+}, Er^{3+}/PEI and $NaYF_4$: Nd^{3+}, Yb^{3+}, Er^{3+}/PEI, the optimum enzyme unit was determined as 75 U and immobilization time was 2 hours. However, for covalent immobilization of L-ASNase on 25 mg of $NaYF_4$:Yb^{3+}, Er^{3+}/ICPTES, $NaYF_4$:Nd^{3+}, Yb^{3+}, Er^{3+}/ICPTES, $NaYF_4$: Yb^{3+}, Er^{3+}/GPTMS and $NaYF_4$: Nd^{3+}, Yb^{3+}, Er^{3+}/GPTMS, the optimum enzyme unit was determined as 35 U, 35U, 20 U and 25 U, respectively. The optimum enzyme unit for covalent immobilizations was less than the physical one. Therefore, it may arise from the less functional group or interaction. On the other hand, the immobilization time for all covalent binding was 12 hours because the interaction between UCNPs and enzymes needs more time as compared with physical interaction. The optimum pHs for $NaYF_4$:Yb^{3+}, Er^{3+}/PEI-PEG-L-ASNase and $NaYF_4$:Nd^{3+}, Yb^{3+}, Er^{3+}/PEI-PEG-L-ASNase was founded as 8 in the physical immobilization and optimum pHs for $NaYF_4$:Yb^{3+}, Er^{3+}/GPTMS-PEG-L-ASNase, $NaYF_4$: Nd^{3+}, Yb^{3+}, Er^{3+}/GPTMS-PEG-L-ASNase, $NaYF_4$:Yb^{3+}, Er^{3+}/ICPTES-PEG-L-ASNase, and $NaYF_4$:Nd^{3+}, Yb^{3+}, Er^{3+}/ICPTES-PEG-L-ASNase were in the range from 7.5 and 9 in the chemical immobilization.

The optimum temperatures for UCNPs-PEG-L-ASNase were in the range from 45 and 50 °C and the relative activities of covalent immobilization were generally higher than the physical immobilization above 50 °C. The thermal stability was amazingly improved after immobilization and Nd/UCNP showed high thermal stability, especially, the relative activity of, $NaYF_4$:Nd^{3+}, Yb^{3+}, Er^{3+}/ICPTES-PEG-L-ASNase was still above 76 % from initial activity. The pH stability at pH 4 and 9 were investigated and the relative activities of immobilized PEG-L-ASNase were higher than free PEG-L-ASNase. Besides, immobilized L-ASNase against metal ions and solvents showed higher stability than free L-ASNase.

Reusability is one of the most important features of the immobilization process and the remained activities for $NaYF_4$:Yb^{3+}, Er^{3+}/PEI-PEG-L-ASNase, $NaYF_4$:Yb^{3+}, Er^{3+}/GPTMS-PEG-L-ASNase, $NaYF_4$:Yb^{3+}, Er^{3+}/ICPTES-PEG-L-ASNase, $NaYF_4$:Nd^{3+}, Yb^{3+}, Er^{3+}/PEI-PEG-L-ASNase, $NaYF_4$: Nd^{3+}, Yb^{3+}, Er^{3+}/GPTMS-PEG-L-ASNase, and $NaYF_4$:Nd^{3+}, Yb^{3+}, Er^{3+}/ICPTES-PEG-L-ASNase were still above 57 %, 62 %, 82 %, 56 %, 63 %, and 66 %, respectively. Covalent immobilization showed better reusability than physical immobilization due to the strong interaction between UCNP and PEG-L-ASNase. The ICPTES group showed preferable reusable stability than the GPTMS group.

The storage stability at +4 C and + 25 C of immobilized L-ASNase were remarkably increased, especially in ICPTES functional group. Trypsin degradation was also investigated for free PEG-L-ASNase and immobilized PEG-L-ASNase. The remained activity for $NaYF_4$:Yb^{3+}, Er^{3+}/PEI-PEG-L-ASNase, $NaYF_4$:Yb^{3+}, Er^{3+}/GPTMS-PEG-L-ASNase, $NaYF_4$:Yb^{3+}, Er^{3+}/ICPTES-PEG-L-ASNase, $NaYF_4$:Nd^{3+}, Yb^{3+}, Er^{3+}/PEI-PEG-L-ASNase, $NaYF_4$: Nd^{3+}, Yb^{3+}, Er^{3+}/GPTMS-PEG-L-ASNase, and $NaYF_4$:Nd^{3+}, Yb^{3+}, Er^{3+}/ICPTES-PEG-L-ASNase were still above 33 %, 41 %, 52 %, 31 %, 45 %, and 59 %, respectively, While free PEG-L-ASNase was almost completely hydrolyzed. Covalent immobilization showed the highest resistance against trypsin degradation, especially in ICPTES functional group. The K*m* value for L-ASNase was deceased after immobilization.

Furthermore, the innovator parameter in this thesis is to increase the L-ASNase activity by exposure the immobilized L-ASNase on UCNPs to NIR light. The enzyme activities for $NaYF_4$:Yb^{3+}, Er^{3+}/PEI-PEG-L-ASNase, $NaYF_4$:Yb^{3+}, Er^{3+}/GPTMS-PEG-L-ASNase, $NaYF_4$:Yb^{3+}, Er^{3+}/ICPTES-PEG-L-ASNase, $NaYF_4$:Nd^{3+}, Yb^{3+}, Er^{3+}/PEI-PEG-L-ASNase, $NaYF_4$: Nd^{3+}, Yb^{3+}, Er^{3+}/GPTMS-PEG-L-ASNase, and

$NaYF_4$:Nd^{3+}, Yb^{3+}, Er^{3+}/ICPTES-PEG-L-ASNase were increased by 206 %, 195 %, 238 %, 323 %, 456 %, and 547 %, respectively. *In vitro* half-life of UCNPs in rat blood serum for one week was determined and $NaYF_4$:Yb^{3+}, Er^{3+}/PEI-PEG-L-ASNase, $NaYF_4$:Yb^{3+}, Er^{3+}/GPTMS-PEG-L-ASNase, $NaYF_4$:Yb^{3+}, Er^{3+}/ICPTES-PEG-L-ASNase, $NaYF_4$:Nd^{3+}, Yb^{3+}, Er^{3+}/PEI-PEG-L-ASNase, $NaYF_4$: Nd^{3+}, Yb^{3+}, Er^{3+}/GPTMS-PEG-L-ASNase, and $NaYF_4$:Nd^{3+}, Yb^{3+}, Er^{3+}/ICPTES-PEG-L-ASNas were exhibited 76.27 %, 62.37 %, 63.37 %, 83.82 %, 74.03 %, and 79.75 % as remaining activities, respectively.

The prothrombin time (PT) and the activated partial thromboplastin time (APTT) of immobilized L-ASNase and UCNPs were investigated and the results showed no increase in time of AP and APTT. This data means that immobilized L-ASNase and UCNPs have not any coagulation effect. Finally, the *in vitro* cytotoxicities were also investigated for all UCNPs and the results showed there was no toxic effect against the L-929 cell line.

Finally, cell growth inhibition of $NaYF_4$:Nd^{3+}, Yb^{3+}, Er^{3+}/ICPTES-PEG-L-ASNase sample was 70.2 % as against HL-60 cell line after NIR inducement.

In the literature it was only two studies were found related to L-ASNase inducement enzyme activity methods in the last few years.

The first study was reported by Uygun et al. (2017) which immobilized L-ASNase enzyme to Au/ Ni/Au/PEDOT-PPy-COOH nanowires by ultrasonic induction, which concluded that free L-ASNase inhibited the growth of EL4 lymphoma cells by 17.3 %, while ultrasonically stimulated (5V, 2.83 MHz) counterpart inhibited 22.9 %. In addition, the immobilized enzyme inhibited the growth of lymphoma cells by 28 %, while the ultrasonically stimulated counterpart inhibited at a rate of 92 %. Therefore, it was noted that higher activity by ultrasonic stimulation reached 1.32 fold for free enzyme while the immobilized counterpart reached 3.28 fold [173]. The second study of L-ASNase by Ates et al., (2018), which relied on Fe_3O_4-chitosan magnetic nanoparticles immobilization of L-ASNase with the main purpose of magnetic and frequency inducement of L-ASNase activity. At the end of the study, it was distinguished that the relative activity of the L-ASNase increased approximately 300% at 3Hz and 30 mT magnetic field conditions [174]. The drawback of these two methods it's not possible to apply this technique to humans. Therefore, it is necessary to develop new carrier platform which is applicable to human and increase L-ASNase activity. UCNPs are one of the most promising platforms for drug delivery and enzyme

immobilization due to NIR light. NIR light has also a harmlessness effect on the human body and can enter deep tissues without giving any toxicity or harm to organs.

Some studies from the literature were used NIR light for enzyme control. In a study reported by Zhang et al., PE-E/Pt was prepared for switching of enzyme activity by near-infrared light-induced. They used glucoamylase (GA), proteinase K (ProK), and deoxyribonuclease I (DNase I) acting on starch, proteins, and DNA plasmids, respectively, into poly (AAmco-AN)-engineered E/Pt (PE-E/Pt) and investigate the optical control of their enzyme activities [212].

In addition, Yin et al., they developed a biocompatible antibacterial system based on polyethylene glycol functionalized molybdenum disulfide nanoflowers (PEG-MoS2 NFs). The PEG-MoS_2NFs have high near-infrared (NIR) absorption and peroxidase-like activity. The peroxidase-like activity used for killing bacteria *in vitro* for Gram-negative *Escherichia coli* and Gram-positive *Bacillus subtilis* after using NIR light and almost all the bacteria were died [213].

Furthermore, Wang et al., developed PtNP for immobilization of glucoamylase (GA), glucose oxidase (GOD), catalase (CAT), and proteinase K (ProK) and increase their activity by NIR radiation. The enzyme activities were increased by 38 % for GA, nearly 2.5 times more for GOD, 173 % for CAT, and 312% for proK due to local heating from the photothermal effect of PtNP [214].

In the conclusion, L-asparaginase was immobilized to UCNPs that can be induced at 980 and 808 nm for the first time within the scope of this thesis, and it has been shown that the enzyme can be induced with the FRET mechanism by NIR, independently from heating. A better carrier system ($NaYF_4$:Nd^{3+}, Yb^{3+}, Er^{3+}/ICPTES) than existing systems has been developed by reaching approximately 547 % in the induction rates of L-ASNase enzyme activity with NIR. In addition, $NaYF_4$:Nd^{3+}, Yb^{3+}, Er^{3+}/ICPTES-PEG-L-ASNase has almost 3 times more activity after NIR inducement against HL-60 cell lines in the catalytic activity experiment. As a result, this carrier system appears to be a promising system for biotechnological enzyme drugs due to no toxicity to humans.

REFERENCES

[1] Pui, C. H., Robison, L. L., & Look, A. T. (2008). Acute lymphoblastic leukemia. *The Lancet*, *371*(9617), 1030-1043.

[2] Batool, T., Makky, E. A., Jalal, M., & Yusoff, M. M. (2016). A comprehensive review on L-asparaginase and its applications. *Applied biochemistry and biotechnology*, 178(5), 900-923.

[3] Swain, A. L., Jaskólski, M., Housset, D., Rao, J. K., & Wlodawer, A. (1993). Crystal structure of Escherichia coli L-asparaginase, an enzyme used in cancer therapy. *Proceedings of the National Academy of Sciences*, 90(4), 1474-1478.

[4] Wriston Jr, J. C. (1985). [79] Asparaginase. *Methods in enzymology*, *113*, 608-618.

[5] Kumar, K., Kaur, J., Walia, S., Pathak, T., & Aggarwal, D. (2014). L-asparaginase: an effective agent in the treatment of acute lymphoblastic leukemia. *Leukemia & lymphoma*, 55(2), 256-262.

[6] Marini, B. L., Perissinotti, A. J., Bixby, D. L., Brown, J., & Burke, P. W. (2017). Catalyzing improvements in ALL therapy with asparaginase. *Blood reviews*, 31(5), 328-338.

[7] Kidd, J. G. (1953). Regression of transplanted lymphomas induced in vivo by means of normal guinea pig serum I. Course of transplanted cancers of various kinds in mice and rats given guinea pig serum, horse serum, or rabbit serum. *Journal of Experimental Medicine*, *98*(6), 565-582.

[8] Clementi, A. (1922). La désamidation enzymatique de l'asparagine chez les différentes espéces animales et la signification physio logique de sa presence dans l'organisme. *Archives Internationales de Physiologie*, 19(4), 369-398.

[9] Broome, J. D. (1963). Evidence that the L-asparaginase of guinea pig serum is responsible for its anti-lymphoma effects: I. Properties of the L-asparaginase of guinea pig serum in relation to those of the anti-lymphoma substance. *The Journal of experimental medicine*, *118*(1), 99.

[10] Dolowy, W. C., Henson, D., Cornet, J., & Sellin, H. (1966). Toxic and antineoplastic effects of l-asparaginase: Study of mice with lymphoma and normal monkeys and report on a child with leukemia. *Cancer*, 19(12), 1813-1819.

[11] Boice Jr, J. D., Mandel, J. S., Doody, M. M., Yoder, R. C., & Bsrt, R. M. (1992). A health survey of radiologic technologists. *Cancer*, 69(2), 586-598.

[12] McCredie, K. B., Ho, D. H. W., & Freireich, E. J. (1973). L-asparaginase for the treatment of cancer. *CA: a cancer journal for clinicians*, 23(4), 220-227.

[13] Ramya, L. N., Doble, M., Rekha, V. P. B., & Pulicherla, K. K. (2011). In silico engineering of L-asparaginase to have reduced glutaminase side activity for effective treatment of acute lymphoblastic leukemia. *Journal of pediatric hematology/oncology*, 33(8), 617-621.

[14] Lubkowski, J., Dauter, M., Aghaiypour, K., Wlodawer, A., & Dauter, Z. (2003). Atomic resolution structure of Erwinia chrysanthemi L-asparaginase. *Acta Crystallographica Section D: Biological Crystallography*, 59(1), 84-92.

[15] Swain, A. L., Jaskólski, M., Housset, D., Rao, J. K., & Wlodawer, A. (1993). Crystal structure of Escherichia coli L-asparaginase, an enzyme used in cancer therapy. *Proceedings of the National Academy of Sciences*, 90(4), 1474-1478.

[16] MAITA, T., MOROKUMA, K., & MATSUDA, G. (1979). Amino acid sequences of the tryptic peptides from carboxymethylated L-asparaginase from Escherichia coli. *Hoppe-Seyler´ s Zeitschrift für physiologische Chemie*, 360(2), 1483-1496.

[17] Illarionova, N. G., Petrov, L. N., Olennikova, L. V., Roshchin, S. N., Pasechnik, A., Khalyapin, B. D., Polotskii, A. E., Voinova, N. E., & Shtukina, T. B. T. B. (1980). Study of L-asparaginase EC-3.5. 1.1 secondary structure in a wide pH region. *Molekulyamaya Biologiya* (Moscow), 14(4), 951-955.

[18] Lubkowski, J., Palm, G. J., Gilliland, G. L., Derst, C., Röhm, K. H., & Wlodawer, A. (1996). Crystal structure and amino acid sequence of Wolinella succinogenesl-asparaginase. *European journal of biochemistry*, 241(1), 201-207.

[19] Aghaiypour, K., Wlodawer, A., & Lubkowski, J. (2001). Structural basis for the activity and substrate specificity of Erwinia chrysanthemi L-asparaginase. *Biochemistry*, 40(19), 5655-5664.

[20] Kozak, M., Jaskólski, M., & Röhm, K. H. (2000). Preliminary crystallographic studies of Y25F mutant of periplasmic Escherichia coli L-asparaginase. *Acta Biochimica Polonica*, 47(3), 807-814.

[21] Narta, U. K., Kanwar, S. S., & Azmi, W. (2007). Pharmacological and clinical evaluation of L-asparaginase in the treatment of leukemia. *Critical reviews in oncology/hematology*, 61(3), 208-221.

[22] Janin, J., Rodier, F., Chakrabarti, P., & Bahadur, R. P. (2007). Macromolecular recognition in the protein data bank. *Acta Crystallographica Section D: Biological Crystallography*, 63(1), 1-8.

[23] Yun, M. K., Nourse, A., White, S. W., Rock, C. O., & Heath, R. J. (2007). Crystal structure and allosteric regulation of the cytoplasmic Escherichia coli L-asparaginase I. *Journal of molecular biology*, 369(3), 794-811.

[24] Kotzia, G. A., Lappa, K., & Labrou, N. E. (2007). Tailoring structure-function properties of L-asparaginase: engineering resistance to trypsin cleavage. *Biochemical Journal*, 404(2), 337-343.

[25] Batool, T., Makky, E. A., Jalal, M., & Yusoff, M. M. (2016). A comprehensive review on L-asparaginase and its applications. *Applied biochemistry and biotechnology*, 178(5), 900-923.

[26] Cachumba, J. J. M., Antunes, F. A. F., Peres, G. F. D., Brumano, L. P., Dos Santos, J. C., & Da Silva, S. S. (2016). Current applications and different approaches for microbial L-asparaginase production.*Brazilian journal of microbiology*, 47, 77-85.

[27] Pastuszak, I., & Szymona, M. (1976). Purification and properties of L-asparaginase from Mycobacterium phlei. *Acta Biochimica Polonica*, 23(1), 37-44.

[28] Tiul'panova, E. S., & Eremenko, V. V. (1976). Amino acid regulation of L-asparaginase formation in Bacillus mesentericus. *Mikrobiologiia*, 45(2), 259-265.

[29] Mikucki, J., Szarapińska-Kwaszewska, J., & Krzemiński, Z. (1977). Factors influencing L-asparaginase production by Staphylococci. Zentralblatt für Bakteriologie, Parasitenkunde, Infektionskrankheiten und Hygiene. *Zweite Naturwissenschaftliche Abteilung: Allgemeine, Landwirtschaftliche und Technische Mikrobiologie*, 132(2), 135-142.

[30] Nefelova, M. V., Ignatov, S. G., Chigalenchik, A. G., Vinogradov, B. D., & Egorov, N. S. (1978). Biosynthesis of L-asparaginase-2 by cultures of Bacillus polymyxa var. Ross. *Prikladnaia biokhimiia i mikrobiologiia*, 14(4), 510-514.

[31] Golden, K. J., & Bernlohr, R. W. (1985). Nitrogen catabolite repression of the L-asparaginase of Bacillus licheniformis. *Journal of bacteriology*, 164(2), 938-940.

[32] Rozalska, M., & Mikucki, J. (1992). Staphylococcal L-asparaginase: catabolic repression of synthesis. *Acta Microbiologica Polonica*, 41(3-4), 145-150.

[33] Mohapatra, B. R., Sani, R. K., & Banerjee, U. C. (1995). Characterization of L-asparaginase from Bacillus sp. isolated from an intertidal marine alga (Sargassum sp.*). Letters in applied microbiology*, 21(6), 380-383.

[34] Fisher, S. H., & Wray, L. V. (2002). Bacillus subtilis 168 contains two differentially regulated genes encoding L-asparaginase. *Journal of Bacteriology*, 184(8), 2148-2154.

[35] Wriston, J. C., & Yellin, T. O. (1973). L-asparaginase: a review. *Adv Enzymol Relat Areas Mol Biol*, 39, 185-248.

[36] Hymavathi, M., Sathish, T., Rao, C. S., & Prakasham, R. S. (2009). Enhancement of L-asparaginase production by isolated Bacillus circulans (MTCC 8574) using response surface methodology. *Applied biochemistry and biotechnology*, 159(1), 191-198.

[37] Prakasham, R. S., Hymavathi, M., Rao, C. S., Arepalli, S. K., Rao, J. V., Kennady, P. K., Nasaruddin, K., Vijayakumar, J.B., & Sarma, P. N. (2010). Evaluation of antineoplastic activity of extracellular asparaginase produced by isolated Bacillus circulans. *Applied biochemistry and biotechnology*, 160(1), 72-80.

[38] Ahmad, N., Pandit, N. P., & Maheshwari, S. K. (2012). L-asparaginase gene a therapeutic approach towards drugs for cancer cell. *Int J Biosci*, 2(4), 1-11.

[39] Tarafdar, J. C., Sharma, S., & Raliya, R. (2013). Nanotechnology: Interdisciplinary science of applications. *African Journal of Biotechnology*, 12(3).

[40] Batool, T., Makky, E. A., Jalal, M., & Yusoff, M. M. (2016). A comprehensive review on L-asparaginase and its applications. *Applied biochemistry and biotechnology*, 178(5), 900-923.

[41] Zhang, S. R., Hao, Z. M., Wang, L. H., Shen, S., Cao, Z. Y., Xin, Y. Y., Hou, M. L., Gu, S. Q., Han, J. M., & Dong, J. G. (2012). StRas2 regulates morphogenesis, conidiation and appressorium development in Setosphaeria turcica. *Microbiological research*, 167(8), 478-486.

[42] Tosa, T., Sano, R., Yamamoto, K., Nakamura, M., & Chibata, I. (1972). L-Asparaginase form Proteus vulgaris. Purification, crystallization, and enzymic properties. *Biochemistry*, 11(2), 217-222.

[43] Bascomb, S., Banks, G. T., Skarstedt, M. T., Fleming, A., Bettelheim, K. A., & Connors, T. A. (1975). The properties and large-scale production of L-asparaginase from Citrobacter. *Microbiology*, 91(1), 1-16.

[44] Joner, P. E. (1976). Purification and properties of l-asparaginase B from Acinetobacter calcoaceticus. *Biochimica et Biophysica Acta (BBA)-Enzymology*, 438(1), 287-295.

[45] Distasio, J. A., Niederman, R. A., Kafkewitz, D., & Goodman, D. (1976). Purification and characterization of L-asparaginase with anti-lymphoma activity from Vibrio succinogenes. *Journal of Biological Chemistry*, 251(22), 6929-6933.

[46] Netrval, J. (1977). Stimulation of L-asparaginase production in *Escherichia coli* by organic and amino acids. *Folia microbiologica*, 22(2), 106-116.

[47] Curran, M. P., Daniel, R. M., Guy, G. R., & Morgan, H. W. (1985). A specific L-asparaginase from Thermus aquaticus. *Archives of biochemistry and biophysics*, 241(2), 571-576.

[48] Maladkar, N. K., Singh, V. K., & Naik, S. R. (1993). Fermentative production and isolation of L-asparaginase from Erwinia carotovora, EC-113. *Hindustan Antibiotics Bulletin*, 35(1-2), 77-86.

[49] Moola, Z. B., Scawen, M. D., Atkinson, T., & Nicholls, D. J. (1994). Erwinia chrysanthemil asparaginase: epitope mapping and production of antigenically modified enzymes. *Biochemical Journal*, 302(3), 921-927.

[50] Manna, S., Sinha, A., Sadhukhan, R., & Chakrabarty, S. L. (1995). Purification, characterization and antitumor activity of L-asparaginase isolated from Pseudomonas stutzeri MB-405. *Current microbiology*, 30(5), 291-298.

[51] Stark, R. M., Suleiman, M. S., Hassan, I. J., Greenman, J., & Millar, M. R. (1997). Amino acid utilisation and deamination of glutamine and asparagine by Helicobacter pylori. *Journal of medical microbiology*, 46(9), 793-800.

[52] Nawaz, M. S., Zhang, D., Khan, A. A., & Cerniglia, C. E. (1998). Isolation and characterization of Enterobacter cloacae capable of metabolizing asparagine. *Applied microbiology and biotechnology*, 50(5), 568-572.

[53] Pritsa, A. A., & Kyriakidis, D. A. (2001). L-asparaginase of Thermus thermophilus: Purification, properties and identificaation of essential amino acids for its catalytic activity. *Molecular and cellular Biochemistry*, 216(1), 93-101.

[54] Agarwal, A., Kumar, S., & Veeranki, V. D. (2011). Effect of chemical and physical parameters on the production of l-asparaginase from a newly isolated Serratia marcescens SK-07. *Letters in applied microbiology*, *52*(4), 307-313.

[55] Kamble, K. D., Bidwe, P. R., Muley, V. Y., Kamble, L. H., Bhadange, D. G., & Musaddiq, M. (2012). Characterization of L-asparaginase producing bacteria from water, farm and saline soil. *Bioscience discovery*, 3(1), 116-119.

[56] Muslim, S. N. (2014). Production, purification and characterization of a novel l-asparaginase from Acinetobacter baumannii with anticancerous activity. *Int. J. Curr. Eng. Technol.*, 4(1).

[57] Nakahama, K., Imada, A., Igarasi, S., & Tubaki, K. (1973). Formation of L-asparaginase by Fusarium species. *Microbiology*, 75(2), 269-273.

[58] Raha, S. K., Dey, S. K., Roy, S. K., Chaudhuri, S., & Chakrabarty, S. L. (1990). Antitumor activity of L-asparaginase from Cylindrocarpon obtusisporum MB-10 and its effect on the immune system. *Biochemistry International*, 21(6), 1001-1011.

[59] Mohapatra, B. R., Bapuji, M., & Banerjee, U. C. (1997). Production and properties of L-asparaginase from Mucor species associated with a marine sponge (Spirastrella sp.). *Cytobios*, 92(370-371), 165-173.

[60] Sarquis, M. I. D. M., Oliveira, E. M. M., Santos, A. S., & Costa, G. L. D. (2004). Production of L-asparaginase by filamentous fungi. *Memorias do Instituto Oswaldo Cruz*, 99(5), 489-492.

[61] Mishra, A. (2006). Production of L-asparaginase, an anticancer agent, from Aspergillus niger using agricultural waste in solid state fermentation. *Applied biochemistry and biotechnology*, 135(1), 33-42.

[62] Hendriksen, H. V., Kornbrust, B. A., Østergaard, P. R., & Stringer, M. A. (2009). Evaluating the potential for enzymatic acrylamide mitigation in a range of food products using an asparaginase from Aspergillus oryzae. *Journal of agricultural and food chemistry*, 57(10), 4168-4176.

[63] Gupta, N., Dash, S. J., & Basak, U. C. (2009). L-asparaginases from fungi of Bhitarkanika mangrove ecosystem. *AsPac J. Mol. Biol. Biotech*, 17(1), 27-30.

[64] Volpe, M., Goldfarb, J. L., & Fiori, L. (2018). Hydrothermal carbonization of Opuntia ficus-indica cladodes: Role of process parameters on hydrochar properties. *Bioresource technology*, 247, 310-318.

[65] Patro, K. R., & Gupta, N. (2012). Extraction, purification and characterization of L-asparaginase from Penicillium sp. by submerged fermentation. *International Journal of Biotechnology and Molecular Biology Research*, 3(3), 30-34.

[66] Vandermaesen, J., Horemans, B., Bers, K., Vandermeeren, P., Herrmann, S., Sekhar, A., Seuntjens, P., & Springael, D. (2016). Application of biodegradation in mitigating and remediating pesticide contamination of freshwater resources: state of the art and challenges for optimization. *Applied microbiology and biotechnology*, 100(17), 7361-7376.

[67] Chow, Y., & Ting, A. S. (2015). Endophytic L-asparaginase-producing fungi from plants associated with anticancer properties. *Journal of advanced research*, 6(6), 869-876.

[68] Muneer, F., Siddique, M. H., Azeem, F., Rasul, I., Muzammil, S., Zubair, M., Afzal, M., & Nadeem, H. (2020). Microbial L-asparaginase: purification, characterization and applications. *Archives of microbiology*, 1-15.

[69] Gonçalves, A. B., Maia, A. C. F., Rueda, J. A., & Vanzela, A. P. D. F. C. (2016). < b> Fungal production of the anti-leukemic enzyme L-asparaginase: from screening to medium development. *Acta Scientiarum. Biological Sciences*, 38(4), 387-394.

[70] Benchamin, D., Sreejai, R., Sujitha, S., Jensy Roshan, F., Albert, C., & Rishad, K. (2019). Anti-proliferative activity of L-Asparaginase enzyme from fungi on breast cancer. *J Pharmacogn Phytochem*, 8(1), 407-410.

[71] Nakahama, K., Imada, A., Igarasi, S., & Tubaki, K. (1973). Formation of L-asparaginase by Fusarium species. *Microbiology*, 75(2), 269-273.

[72] Dunlop, P. C., & Roon, R. J. (1975). L-Asparaginase of Saccharomyces cerevisiae: an extracellular Enzyme. *Journal of bacteriology*, 122(3), 1017-1024.

[73] Foda, M. S., Zedan, H. H., & Hashem, S. A. (1980). Formation and properties of L-glutaminase and L-asparaginase activities in Pichia polymorpha. *Acta Microbiologica Polonica*, *29*(4), 343-352.

[74] SAXENA, R. K. (1981). L-asparaginase and glutaminase activities in the culture filtrates of Aspergillus nidulans.

[75] Raha, S. K., Roy, S. K., Dey, S. K., & Chakrabarty, S. L. (1990). Purification and properties of an L-asparaginase from Cylindrocarpon obtusisporum MB-10. *Biochemistry International,* 21(6), 987-1000.

[76] Kil, J. O., Kim, G. N., & Park, I. (1995). Extraction of extracellular L-asparaginase from Candida utilis. *Bioscience, biotechnology, and biochemistry*, 59(4), 749-750.

[77] Ramakrishnan, M. S., & Joseph, R. (1996). Characterization of an extracellular asparaginase of Rhodosporidium toruloides CBS14 exhibiting unique physicochemical properties. *Canadian Journal of microbiology*, 42(4), 316-325.

[78] Mohapatra, B. R., Bapuji, M., & Banerjee, U. C. (1997). Production and properties of L-asparaginase from Mucor species associated with a marine sponge (Spirastrella sp.). *Cytobios*, 92(370-371), 165-173.

[79] Sarquis, M. I. D. M., Oliveira, E. M. M., Santos, A. S., & Costa, G. L. D. (2004). Production of L-asparaginase by filamentous fungi. *Memorias do Instituto Oswaldo Cruz*, 99(5), 489-492.

[80] Mishra, A. (2006). Production of L-asparaginase, an anticancer agent, from Aspergillus Niger using agricultural waste in solid state fermentation. *Applied biochemistry and biotechnology*, 135(1), 33-42.

[81] Hendriksen, H. V., Kornbrust, B. A., Østergaard, P. R., & Stringer, M. A. (2009). Evaluating the potential for enzymatic acrylamide mitigation in a range of food products using an asparaginase from Aspergillus oryzae. *Journal of agricultural and food chemistry*, 57(10), 4168-4176.

[82] Daverey, A., & Pakshirajan, K. (2010). Kinetics of growth and enhanced sophorolipids production by Candida bombicola using a low-cost fermentative medium. *Applied biochemistry and biotechnology*, 160(7), 2090-2101.

[83] Nagarajan, A., Thirunavukkarasu, N., Suryanarayanan, T. S., & Gummadi, S. N. (2014). Screening and isolation of novel glutaminase free L-asparaginase from fungal endophytes. *Research Journal of Microbiology*, 9(4), 163.

[84] Batool, T., Makky, E. A., Jalal, M., & Yusoff, M. M. (2016). A comprehensive review on L-asparaginase and its applications. *Applied biochemistry and biotechnology*, 178(5), 900-923.

[85] Dejong, P. J. (1972). L-Asparaginase production by Streptomyces griseus. *Applied microbiology*, 23(6), 1163-1164.

[86] Mostafa, S. A., & Salama, M. S. (1979). L-asparaginase-producing Streptomyces from the soil of Kuwait. Zentralblatt für Bakteriologie, Parasitenkunde, Infektionskrankheiten und Hygiene. *Zweite Naturwissenschaftliche Abteilung: Mikrobiologie der Landwirtschaft, der Technologie und des Umweltschutzes*, 134(4), 325-334.

[87] Mostafa, S. A., & Ali, O. K. A. (1983). L-asparaginase activity in cell-free extracts of Thermoactinomyces vulgaris 13 MES. *Zentralblatt für Mikrobiologie*, 138(5), 397-404.

[88] Koshy, A., Dhevendaran, K., Georgekutty, M. I., & Natarajan, P. (1997). L-asparaginase in Streptomyces plicatus isolated from the alimentary canal of the fish, Gerres filamentosus (Cuvier). *Journal of Marine Biotechnology*, 5(2-3), 0181-0185.

[89] Abdel-Fattah, Y. R., & Olama, Z. A. (2002). L-asparaginase production by Pseudomonas aeruginosa in solid-state culture: evaluation and optimization of culture conditions using factorial designs. *Process Biochemistry*, 38(1), 115-122.

[90] Gupta, N., Mishra, S., & Basak, U. C. (2007). Occurrence of Streptomyces aurantiacus in mangroves of Bhitarkanika. *Malaysian J Microbiol*, 3, 7-14.

[91] Narayana, K. J. P., Kumar, K. G., & Vijayalakshmi, M. (2008). L-asparaginase production by Streptomyces albidoflavus. *Indian Journal of Microbiology*, 48(3), 331-336.

[92] Gupta, N., Mishra, S., & Basak, U. C. (2009). Diversity of Streptomyces in mangrove ecosystem of Bhitarkanika. *Iranian Journal of Microbiology*, 37-42.

[93] Kavitha, A., & Vijayalakshmi, M. (2010). Optimization and Purification of L-Asparaginase Produced by Streptomyces tendae TK-VL_333. *Zeitschrift für Naturforschung C*, 65(7-8), 528-531.

[94] Kavitha, A., & Vijayalakshmi, M. (2012). A study on L-asparaginase of Nocardia Levis MK-VL_113. *The Scientific World Journal*, 2012.

[95] Szymanska, B., Wilczynska-Kalak, U., Kang, M. H., Liem, N. L., Carol, H., Boehm, I., & Lock, R. B. (2012). Pharmacokinetic modeling of an induction regimen for in vivo combined testing of novel drugs against pediatric acute lymphoblastic leukemia xenografts. *PloS one*, 7(3), e33894.

[96] Shakambari, G., Ashokkumar, B., & Varalakshmi, P. (2019). L-asparaginase–A promising biocatalyst for industrial and clinical applications. *Biocatalysis and Agricultural Biotechnology*, 17, 213-224.

[97] Duval, M., Suciu, S., Ferster, A., Rialland, X., Nelken, B., Lutz, P., Benoit, Y., Robert, A., Manel, A. M., Vilmer, E., Otten, J., & Philippe, N. (2002). Comparison of Escherichia coli–asparaginase with Erwinia-asparaginase in the treatment of childhood lymphoid malignancies: results of a randomized European Organisation for Research and Treatment of Cancer—Children's Leukemia Group phase 3 trial. *Blood, the Journal of the American Society of Hematology*, 99(8), 2734-2739.

[98] Radulović, S., Golubović, Z., Jovanović, B., & Pejanović, J. (2004). Surgery for complication of neutropenic enterocolitisin a patient with acute lymfoblast leukemia. *Srpski arhiv za celokupno lekarstvo*, 132(suppl. 1), 119-121.

[99] Chen, C. H., Lu, M. Y., Lin, K. H., Lin, D. T., Peng, S. F., & Jou, S. T. (2004). Ureteral obstruction caused by L-asparaginase-induced pancreatitis in a child with acute lymphoblastic leukemia. *Journal of the Formosan Medical Association= Taiwan yi zhi*, 103(5), 380-384.

[100] Moola, Z. B., Scawen, M. D., Atkinson, T., & Nicholls, D. J. (1994). Erwinia chrysanthemil-asparaginase: epitope mapping and production of antigenically modified enzymes. *Biochemical Journal*, 302(3), 921-927.

[101] Pochedly, C. (1977). Neurotoxicity due to CNS therapy for leukemia. *Medical and pediatric oncology*, 3(1), 101-115.

[102] Nowak-Göttl, U., Ahlke, E., Fleischhack, G., Schwabe, D., Schobess, R., Schumann, C., & Junker, R. (2003). Thromboembolic events in children with acute lymphoblastic leukemia (BFM protocols): prednisone versus dexamethasone administration. *Blood*, 101(7), 2529-2533.

[103] Hernández-Espinosa, D., Minano, A., Martínez, C., Pérez-Ceballos, E., Heras, I., Fuster, J. L., Vicente, V., & Corral, J. (2006). L-asparaginase-induced antithrombin type I deficiency: implications for conformational diseases. *The American journal of pathology*, 169(1), 142-153.

[104] Athale, U. H., & Chan, A. K. (2003). Thrombosis in children with acute lymphoblastic leukemia: part I. Epidemiology of thrombosis in children with acute lymphoblastic leukemia. *Thrombosis research*, 111(3), 125-131.

[105] Avramis, V. I., & Tiwari, P. N. (2006). Asparaginase (native ASNase or pegylated ASNase) in the treatment of acute lymphoblastic leukemia. *International journal of nanomedicine*, 1(3), 241.

[106] Pieters, R., Hunger, S. P., Boos, J., Rizzari, C., Silverman, L., Baruchel, A., Nicola Goekbuget, N., Martin Schrappe, M., & Pui, C. H. (2011). L-asparaginase treatment in acute lymphoblastic leukemia: a focus on Erwinia asparaginase. *Cancer*, 117(2), 238-249.

[107] Bodmer, M., Sulz, M., Stadlmann, S., Droll, A., Terracciano, L., & Krähenbühl, S. (2006). Fatal liver failure in an adult patient with acute lymphoblastic leukemia following treatment with L-asparaginase. *Digestion*, 74(1), 28-32.

[108] Fromenty, B., & Pessayre, D. (1997). Impaired mitochondrial function in microvesicular steatosis effects of drugs, ethanol, hormones and cytokines. *Journal of hepatology*, 26, 43-53.

[109] Raja, R. A., Schmiegelow, K., & Frandsen, T. L. (2012). Asparaginase-associated pancreatitis in children. *British journal of haematology*, 159(1), 18-27.

[110] Fu, C. H., & Sakamoto, K. M. (2007). PEG-asparaginase. *Expert opinion on pharmacotherapy*, 8(12), 1977-1984.

[111] Wada, H., Imamura, I., Sako, M., Katagiri, S., Tarui, S., Nishimura, H., & Inada, Y. (1990). Antitumor enzyme: polyethylene glycol–modified asparaginase. *Annals of the New York Academy of Sciences*, 613(1), 95-108.

[112] Hak, L. J., Relling, M. V., Cheng, C., Pei, D., Wang, B., Sandlund, J. T., Rubnitz, J., & Pui, C. H. (2004). Asparaginase pharmacodynamics differ by formulation among children with newly diagnosed acute lymphoblastic leukemia. *Leukemia*, 18(6), 1072-1077.

[113] Zeidan, A., Wang, E. S., & Wetzler, M. (2009). Pegasparaginase: where do we stand. *Expert opinion on biological therapy*, 9(1), 111-119.

[114] Cox, M. M., & Nelson, D. L. (2008). *Lehninger principles of biochemistry* (Vol. 5). New York: Wh Freeman. [115] Berg, J. M., Tymoczko, J. L., & Stryer, L. (2002). Biochemistry.

[116] Armstrong, E. F. (1933). Enzymes: A Discovery and its Consequences.

[117] Liu, D. M., Chen, J., & Shi, Y. P. (2018). Advances on methods and easy separated support materials for enzymes immobilization. *TrAC Trends in Analytical Chemistry*, 102, 332-342.

[118] Zhang, D. H., Yuwen, L. X., & Peng, L. J. (2013). Parameters affecting the performance of immobilized enzyme. *Journal of chemistry*, 2013.

[119] Zhou, Z., & Hartmann, M. (2013). Progress in enzyme immobilization in ordered mesoporous materials and related applications. *Chemical Society Reviews*, 42(9), 3894-3912.

[120] Hudson, S., Cooney, J., & Magner, E. (2008). Proteins in mesoporous silicates. *Angewandte chemie international edition*, *47*(45), 8582-8594.

[121] Carlsson, N., Gustafsson, H., Thörn, C., Olsson, L., Holmberg, K., & Åkerman, B. (2014). Enzymes immobilized in mesoporous silica: a physical–chemical perspective. *Advances in colloid and interface science*, 205, 339-360.

[122] Nguyen, H. H., & Kim, M. (2017). An overview of techniques in enzyme immobilization. *Applied Science and Convergence Technology*, 26(6), 157-163.

[123] Hanefeld, U., Gardossi, L., & Magner, E. (2009). Understanding enzyme immobilization. *Chemical Society Reviews*, 38(2), 453-468.

[124] Sheldon, R. A. (2007). Enzyme immobilization: the quest for optimum performance. *Advanced Synthesis & Catalysis*, 349(8-9), 1289-1307.

[125] Cirillo, G., Nicoletta, F. P., Curcio, M., Spizzirri, U. G., Picci, N., & Iemma, F. (2014). Enzyme immobilization on smart polymers: Catalysis on demand. *Reactive and Functional Polymers*, 83, 62-69.

[126] Jia, F., Narasimhan, B., & Mallapragada, S. (2014). Materials-based strategies for multi-enzyme immobilization and co-localization: a review. *Biotechnology and bioengineering*, *111*(2), 209-222.

[127] D'souza, S. F. (1999). Immobilized enzymes in bioprocess. *Current Science*, 69-79.

[128] Mohamad, N. R., Marzuki, N. H. C., Buang, N. A., Huyop, F., & Wahab, R. A. (2015). An overview of technologies for immobilization of enzymes and surface analysis techniques for immobilized enzymes. *Biotechnology & Biotechnological Equipment*, 29(2), 205-220.

[129] Tran, D. N., & Balkus Jr, K. J. (2011). Perspective of recent progress in immobilization of enzymes. *Acs Catalysis*, 1(8), 956-968.

[130] Cabral, J. M., & Kennedy, J. F. (1991). Covalent and coordination immobilization of proteins. *Bioprocess technology*, 14, 73-138.

[131] Bilal, M., Iqbal, H. M., Hu, H., Wang, W., & Zhang, X. (2017). Development of horseradish peroxidase-based cross-linked enzyme aggregates and their environmental exploitation for bioremediation purposes. *Journal of environmental management*, 188, 137-143.

[132] Hartmann, M., & Kostrov, X. (2013). Immobilization of enzymes on porous silicas–benefits and challenges. *Chemical Society Reviews*, 42(15), 6277-6289.

[133] Qiu, Y., Tong, S., Zhang, L., Sakurai, Y., Myers, D. R., Hong, L., Lam, W. A., & Bao, G. (2017). Magnetic forces enable controlled drug delivery by disrupting endothelial cell-cell junctions. *Nature communications*, 8(1), 1-10.

[134] Rocha-Santos, T. A. (2014). Sensors and biosensors based on magnetic nanoparticles. *TrAC Trends in Analytical Chemistry*, 62, 28-36.

[135] Guibert, C., Dupuis, V., Peyre, V., & Fresnais, J. (2015). Hyperthermia of magnetic nanoparticles: experimental study of the role of aggregation. *The Journal of Physical Chemistry C*, 119(50), 28148-28154.

[136] Dobson, J. (2006). Gene therapy progress and prospects: magnetic nanoparticle-based gene delivery. *Gene therapy*, 13(4), 283-287.

[137] Shylesh, S., Schuenemann, V., & Thiel, W. R. (2010). Magnetically separable nanocatalysts: bridges between homogeneous and heterogeneous catalysis. *Angewandte Chemie International Edition*, 49(20), 3428-3459.

[138] Basavegowda, N., Mishra, K., & Lee, Y. R. (2014). Sonochemically synthesized ferromagnetic Fe 3 O 4 nanoparticles as a recyclable catalyst for the preparation of pyrrolo [3, 4-c] quinoline-1, 3-dione derivatives. *RSC Advances*, 4(106), 61660-61666.

[139] Bezerra, C. S., de Farias Lemos, C. M. G., de Sousa, M., & Gonçalves, L. R. B. (2015). Enzyme immobilization onto renewable polymeric matrixes: Past, present, and future trends. *Journal of Applied Polymer Science*, 132(26).

[140] Hartmann, M., & Kostrov, X. (2013). Immobilization of enzymes on porous silicas–benefits and challenges. *Chemical Society Reviews*, 42(15), 6277-6289.

[141] Babaki, M., Yousefi, M., Habibi, Z., Brask, J., & Mohammadi, M. (2015). Preparation of highly reusable biocatalysts by immobilization of lipases on epoxy-functionalized silica for production of biodiesel from canola oil. *Biochemical Engineering Journal*, 101, 23-31.

[142] Wang, X. Y., Jiang, X. P., Li, Y., Zeng, S., & Zhang, Y. W. (2015). Preparation Fe3O4@ chitosan magnetic particles for covalent immobilization of lipase from Thermomyces lanuginosus. *International journal of biological macromolecules*, *75*, 44-50.

[143] Fan, J., & Gao, Y. (2006). Nanoparticle-supported catalysts and catalytic reactions–a mini-review. *Journal of Experimental Nanoscience*, *1*(4), 457-475.

[144] Zhang, Z., Duan, H., Li, S., & Lin, Y. (2010). Assembly of magnetic nanospheres into one-dimensional nanostructured carbon hybrid materials. *Langmuir*, *26*(9), 6676-6680.

[145] Adams, S. A., Hauser, J. L., Allen, A. L. C., Lindquist, K. P., Ramirez, A. P., Oliver, S., & Zhang, J. Z. (2018). Fe3O4@ SiO2 nanoparticles functionalized with gold and poly (vinylpyrrolidone) for bio-separation and sensing applications. *ACS Applied Nano Materials*, 1(3), 1406-1412.

[146] Ulu, A., Ozcan, I., Koytepe, S., & Ates, B. (2018). Design of epoxy-functionalized Fe3O4@ MCM-41 core–shell nanoparticles for enzyme immobilization. *International journal of biological macromolecules*, *115*, 1122-1130.

[147] Manna, K., & Srivastava, S. K. (2017). Fe3O4@ carbon@ polyaniline trilaminar core–shell composites as superior microwave absorber in shielding of electromagnetic pollution. *ACS Sustainable Chemistry & Engineering*, *5*(11), 10710-10721.

[148] Wang, S., Humphreys, E. S., Chung, S. Y., Delduco, D. F., Lustig, S. R., Wang, H., Parker, K. N., Rizzo, N. W., Subramoney, S., Chiang, Y. M., & Jagota, A. (2003). Peptides with selective affinity for carbon nanotubes. *Nature materials*, 2(3), 196-200.

[149] Geim, A. K., & Novoselov, K. S. (2010). *The rise of graphene*. In Nanoscience and technology: a collection of reviews from nature journals (pp. 11-19).

[150] Jeong, J., Ha, T. H., & Chung, B. H. (2006). Enhanced reusability of hexa-arginine-tagged esterase immobilized on gold-coated magnetic nanoparticles. *Analytica Chimica Acta*, 569(1-2), 203-209.

[151] Shoabargh, S., Karimi, A., Dehghan, G., & Khataee, A. (2014). A hybrid photocatalytic and enzymatic process using glucose oxidase immobilized on TiO2/polyurethane for removal of a dye. *Journal of Industrial and Engineering Chemistry*, 20(5), 3150-3156.

[152] Li, J., Li, X., Zhao, Q., Jiang, Z., Tadé, M., Wang, S., & Liu, S. (2018). Polydopamine-assisted decoration of TiO2 nanotube arrays with enzyme to construct a novel photoelectrochemical sensing platform. *Sensors and Actuators B: Chemical*, 255, 133-139.

[153] Zhuang, W., Zhang, Y., Zhu, J., An, R., Li, B., Mu, L., Ying, H., Wu, J., Zhou, J., Chen, Y., & Lu, X. (2016). Influences of geometrical topography and surface chemistry on the stable immobilization of adenosine deaminase on mesoporous TiO2. *Chemical Engineering Science*, 139, 142-151.

[154] Daaboul, G. G., Vedula, R. S., Ahn, S., Lopez, C. A., Reddington, A., Ozkumur, E., & Ünlü, M. S. (2011). LED-based interferometric reflectance imaging sensor for quantitative dynamic monitoring of biomolecular interactions. *Biosensors and Bioelectronics*, 26(5), 2221-2227.

[155] Xu, J., Shang, F., Luong, J. H., Razeeb, K. M., & Glennon, J. D. (2010). Direct electrochemistry of horseradish peroxidase immobilized on a monolayer modified nanowire array electrode. *Biosensors and Bioelectronics*, 25(6), 1313-1318.

[156] Hola, K., Markova, Z., Zoppellaro, G., Tucek, J., & Zboril, R. (2015). Tailored functionalization of iron oxide nanoparticles for MRI, drug delivery, magnetic separation and immobilization of biosubstances. *Biotechnology advances*, 33(6), 1162-1176.

[157] Bosio, V. E., Islan, G. A., Martínez, Y. N., Durán, N., & Castro, G. R. (2016). Nanodevices for the immobilization of therapeutic enzymes. *Critical reviews in biotechnology*, 36(3), 447-464.

[158] Gupta, U., Agashe, H. B., Asthana, A., & Jain, N. K. (2006). Dendrimers: novel polymeric nanoarchitectures for solubility enhancement. *Biomacromolecules*, 7(3), 649-658.

[159] Zdarta, J., Meyer, A. S., Jesionowski, T., & Pinelo, M. (2018). A general overview of support materials for enzyme immobilization: characteristics, properties, practical utility. *Catalysts*, 8(2), 92.

[160] Qian, G. Q., Zhou, J. Y., Ma, J. B., Wang, D. B., & He, B. L. (1996). Immobilization of E. coli L-Asparaginase on Chitosan Microsphere. *CHEMICAL JOURNAL OF CHINESE UNIVERSITIES-CHINESE EDITION-*, 17, 1147-1150.

[161] Fernandes, A. I., & Gregoriadis, G. (1997). Polysialylated asparaginase: preparation, activity and pharmacokinetics. *Biochimica et Biophysica Acta (BBA)-Protein Structure and Molecular Enzymology*, 1341(1), 26-34.

[162] Allison, J. P., Davidson, L., Gutierrez-Hartman, A., & Kitto, G. B. (1972). Insolubilization of L-asparaginase by covalent attachment to nylon tubing. *Biochemical and biophysical research communications*, 47(1), 66-73.

[163] IuV, G., Chuplygina, E. G., & Klement'eva, T. A. (1981). Immobilization of Citrobacter L-asparaginase in polyacrylamide gel. *Voprosy meditsinskoi khimii*, 27(4), 534-537.

[164] Erdogan, A., Koytepe, S., Ates, B., Yilmaz, I., & Seckin, T. (2014). Preparation of the L-asparaginase-based biosensor with polyimide membrane electrode for monitoring L-asparagine levels in leukemia. *International Journal of Polymeric Materials and Polymeric Biomaterials*, 63(17), 909-917.

[165] Ghosh, S., Chaganti, S. R., & Prakasham, R. S. (2012). Polyaniline nanofiber as a novel immobilization matrix for the anti-leukemia enzyme l-asparaginase. *Journal of molecular catalysis b: enzymatic*, 74(1-2), 132-137.

[166] Youssef, M. M., & Al-Omair, M. A. (2008). Cloning, purification, characterization and immobilization of L-asparaginase II from E. coli W3110. *Asian J. Biochem*, *3*(6), 337-350.

[167] Ulu, A., Noma, S. A. A., Koytepe, S., & Ates, B. (2018). Magnetic Fe3O4@ MCM-41 core–shell nanoparticles functionalized with thiol silane for efficient l-asparaginase immobilization. *Artificial cells, nanomedicine, and biotechnology*, 46(sup2), 1035-1045.

[168] Ulu, A. (2020). Metal–organic frameworks (MOFs): a novel support platform for ASNase immobilization. *Journal of Materials Science*, 55(14), 6130-6144.

[169] Noma, S. A. A., Yılmaz, B. S., Ulu, A., Özdemir, N., & Ateş, B. (2020). Development of L-asparaginase@ hybrid Nanoflowers (ASNase@ HNFs) Reactor System with Enhanced Enzymatic Reusability and Stability. *Catalysis Letters*, 1-11.

[170] Monajati, M., Borandeh, S., Hesami, A., Mansouri, D., & Tamaddon, A. M. (2018). Immobilization of L-asparaginase on aspartic acid functionalized graphene oxide nanosheet: enzyme kinetics and stability studies. *Chemical Engineering Journal*, 354, 1153-1163.

[171] Bahraman, F., & Alemzadeh, I. (2017). Optimization of l-asparaginase immobilization onto calcium alginate beads. *Chemical Engineering Communications*, 204(2), 216-220.

[172] Agrawal, S., Sharma, I., Prajapati, B. P., Suryawanshi, R. K., & Kango, N. (2018). Catalytic characteristics and application of l-asparaginase immobilized on aluminum oxide pellets. *International journal of biological macromolecules*, 114, 504-511.

[173] Uygun, M., Jurado-Sánchez, B., Uygun, D. A., Singh, V. V., Zhang, L., & Wang, J. (2017). Ultrasound-propelled nanowire motors enhance asparaginase enzymatic activity against cancer cells. *Nanoscale*, 9(46), 18423-18429.

[174] Ates, B., Ulu, A., Köytepe, S., Noma, S. A. A., Kolat, V. S., & Izgi, T. (2018). Magnetic-propelled Fe 3 O 4–chitosan carriers enhance l-asparaginase catalytic activity: a promising strategy for enzyme immobilization. *RSC advances*, 8(63), 36063-36075.

[175] Idris, N. M., Gnanasammandhan, M. K., Zhang, J., Ho, P. C., Mahendran, R., & Zhang, Y. (2012). In vivo photodynamic therapy using upconversion nanoparticles as remote-controlled nanotransducers. *Nature medicine*, 18(10), 1580.

[176] Furuta, T., Wang, S. S. H., Dantzker, J. L., Dore, T. M., Bybee, W. J., Callaway, E. M., Denk, W., & Tsien, R. Y. (1999). Brominated 7-hydroxycoumarin-4-ylmethyls: photolabile protecting groups with biologically useful cross-sections for two photon photolysis. *Proceedings of the National Academy of Sciences*, 96(4), 1193-1200.

[177] Guardado-Alvarez, T. M., Sudha Devi, L., Russell, M. M., Schwartz, B. J., & Zink, J. I. (2013). Activation of snap-top capped mesoporous silica nanocontainers using two near-infrared photons. *Journal of the American Chemical Society*, 135(38), 14000-14003.

[178] Gao, H. D., Thanasekaran, P., Chiang, C. W., Hong, J. L., Liu, Y. C., Chang, Y. H., & Lee, H. M. (2015). Construction of a near-infrared-activatable enzyme platform to remotely trigger intracellular signal transduction using an upconversion nanoparticle. *ACS nano*, 9(7), 7041-7051.

[179] del Barrio, M., de Marcos, S., Cebolla, V., Heiland, J., Wilhelm, S., Hirsch, T., & Galbán, J. (2014). Enzyme-induced modulation of the emission of upconverting nanoparticles: Towards a new sensing scheme for glucose. *Biosensors and Bioelectronics*, 59, 14-20.

[180] Carling, C. J., Boyer, J. C., & Branda, N. R. (2009). Remote-control photoswitching using NIR light. *Journal of the American Chemical Society*, 131(31), 10838-10839.

[181] Haase, M., & Schäfer, H. (2011). Upconverting nanoparticles. *Angewandte Chemie International Edition*, 50(26), 5808-5829.

[182] Wu, S., & Butt, H. J. (2016). Near-infrared-sensitive materials based on upconverting nanoparticles. *Advanced Materials*, *28*(6), 1208-1226.

[183] Wang, C., Cheng, L., & Liu, Z. (2011). Drug delivery with upconversion nanoparticles for multi-functional targeted cancer cell imaging and therapy. *Biomaterials*, *32*(4), 1110-1120.

[184] Kumar, R., Nyk, M., Ohulchanskyy, T. Y., Flask, C. A., & Prasad, P. N. (2009). Combined optical and MR Bioimaging using rare earth ion doped $NaYF_4$ nanocrystals. *Advanced Functional Materials*, *19*(6), 853-859.

[185] Xing, H., Bu, W., Zhang, S., Zheng, X., Li, M., Chen, F., He, O., Zhou, L., Peng, W., Hua, Y., & Shi, J. (2012). Multifunctional nanoprobes for upconversion fluorescence, MR and CT trimodal imaging. *Biomaterials*, 33(4), 1079-1089.

[186] Yang, Y., Sun, Y., Cao, T., Peng, J., Liu, Y., Wu, Y., Feng, W., Zhang, Y., & Li, F. (2013). Hydrothermal synthesis of NaLuF4: 153Sm, Yb, Tm nanoparticles and their application in dual-modality upconversion luminescence and SPECT bioimaging. *Biomaterials*, 34(3), 774-783.

[187] Sun, Y., Yu, M., Liang, S., Zhang, Y., Li, C., Mou, T., Yang, W., Zhang, X., Li, B., Huang, C., & Li, F. (2011). Fluorine-18 labeled rare-earth nanoparticles for positron emission tomography (PET) imaging of sentinel lymph node. *Biomaterials*, 32(11), 2999-3007.

[188] Cheng, L., Yang, K., Li, Y., Chen, J., Wang, C., Shao, M., Lee, S. T., & Liu, Z. (2011). Facile preparation of multifunctional upconversion nanoprobes for multimodal imaging and dual-targeted photothermal therapy. *Angewandte Chemie*, 123(32), 7523-7528.

[189] Wang, C., Cheng, L., & Liu, Z. (2011). Drug delivery with upconversion nanoparticles for multi-functional targeted cancer cell imaging and therapy. *Biomaterials*, *32*(4), 1110-1120.

[190] Chen, G., Ohulchanskyy, T. Y., Kumar, R., Ågren, H., & Prasad, P. N. (2010). Ultrasmall monodisperse NaYF4: $Yb3^{+}/Tm3^{+}$ nanocrystals with enhanced near-infrared to near-infrared upconversion photoluminescence. *ACS nano*, 4(6), 3163-3168.

[191] Chen, Z., Chen, H., Hu, H., Yu, M., Li, F., Zhang, Q., Zhou, Z., Yi, T., & Huang, C. (2008). Versatile synthesis strategy for carboxylic acid−functionalized upconverting nanophosphors as biological labels. *Journal of the American Chemical Society*, 130(10), 3023-3029.

[192] Ofelt, G. S. (1962). Intensities of crystal spectra of rare-earth ions. *The journal of chemical physics*, 37(3), 511-520.

[193] Auzel, F. (2004). Upconversion and anti-stokes processes with f and d ions in solids. *Chemical reviews*, 104(1), 139-174.

[194] Durr, N. J., Larson, T., Smith, D. K., Korgel, B. A., Sokolov, K., & Ben-Yakar, A. (2007). Two-photon luminescence imaging of cancer cells using molecularly targeted gold nanorods. *Nano letters*, 7(4), 941-945.

[195] Wang, G., Peng, Q., & Li, Y. (2009). Upconversion luminescence of monodisperse CaF2: $Yb3^{+}/Er3^{+}$ nanocrystals. *Journal of the American Chemical Society*, 131(40), 14200-14201.

[196] Chen, G., Shen, J., Ohulchanskyy, T. Y., Patel, N. J., Kutikov, A., Li, Z., Jie Song, J., Pandey, R. K., Ågren, H., Prasad, P. N., & Han, G. (2012). (aramα-$NaYbF_4$: Tm^{3+})/CaF_2 core/shell nanoparticles with efficient near-infrared to near-infrared upconversion for high-contrast deep tissue bioimaging. *ACS nano*, 6(9), 8280-8287.

[197] Chen, D., Lei, L., Yang, A., Wang, Z., & Wang, Y. (2012). Ultra-broadband near-infrared excitable upconversion core/shell nanocrystals. Chemical Communications, 48(47), 5898-5900.

[198] Wang, L., Qin, W., Liu, Z., Zhao, D., Qin, G., Di, W., & He, C. (2012). Improved 800 nm emission of $Tm3^{+}$ sensitized by $Yb3^{+}$ and $Ho3^{+}$ in β-NaYF 4 nanocrystals under 980 nm excitation. *Optics express*, 20(7), 7602-7607.

[199] Uvarova, T. V., & Kiiko, V. V. (2011). Up-conversion multiwave (White) luminescence in the visible spectral range under excitation by IR laser diodes in the active BaY 2 F 8: Yb 3+, Pr 3+ medium. *Optics and Spectroscopy*, *111*(2), 273-276.

[200] Xin, N., Wei, D., Zhu, Y., Yang, M., Ramakrishna, S., Lee, O., ... & Fan, H. (2020). Upconversion nanomaterials: A platform for biosensing, theranostic and photoregulation. Materials Today Chemistry, 17, 100329.

[201] Wang, F., Chatterjee, D. K., Li, Z., Zhang, Y., Fan, X., & Wang, M. (2006). Synthesis of polyethylenimine/NaYF4 nanoparticles with upconversion fluorescence. *Nanotechnology*, 17(23), 5786.

[202] Mashburn, L. T. (1964). Tumor inhibitory effect of L-asparaginase from Escherichia coli. *Arch. Biochem. Biophys.*, *105*, 450-452.

[203] Hu, D., Li, T., Xu, Z., Liu, D., Yang, M., & Zhu, L. (2018). Self-stabilized silk sericin-based nanoparticles: In vivo biocompatibility and reduced doxorubicin-induced toxicity. *Acta biomaterialia*, 74, 385-396.

[204] Bai, L., Du, Y., Peng, J., Liu, Y., Wang, Y., Yang, Y., & Wang, C. (2014). Peptide-based isolation of circulating tumor cells by magnetic nanoparticles. *Journal of Materials Chemistry B*, 2(26), 4080-4088.

[205] Zhang, K., Zhao, Q., Qin, S., Fu, Y., Liu, R., Zhi, J., & Shan, C. (2019). Nanodiamonds conjugated upconversion nanoparticles for bio-imaging and drug delivery. *Journal of colloid and interface science*, 537, 316-324.

[206] Liu, B., Li, C., Yang, P., Hou, Z., & Lin, J. (2017). 808-nm-Light-excited lanthanide-doped nanoparticles: rational design, luminescence control and theranostic applications. *Advanced Materials*, 29(18), 1605434.

[207] N.E.A. El-Naggar, S.F. Deraz, S.M. El-Ewasy, G.M. Suddek, Purification, characterization and immunogenicity assessment of glutaminase free L-asparaginase from Streptomyces brollosae NEAE-115, BMC Pharmacol. *Toxicol*. (2018) 19-51.

[208] R. V. Mahajan, V. Kumar, V. Rajendran, S. Saran, P.C. Ghosh, R.K. Saxena, Purification and characterization of a novel and robust L-asparaginase having low-glutaminase activity from bacillus licheniformis: *In vitro* evaluation of anti-cancerous properties, *PLoS One*. 9 (2014).

[209] H.A. El-Refai, M.S. Shafei, H. Mostafa, A.M.H. El-Refai, E.M. Araby, F.M. El-Beih, S.M. Easa, S.K. Gomaa, Comparison of free and immobilized L-asparaginase synthesized by gamma-irradiated penicillium cyclopium, *Polish J. Microbiol.* 65 (2016) 43–50.

[210] A.K. Vala, B. Sachaniya, D. Dudhagara, H.Z. Panseriya, H. Gosai, R. Rawal, B.P. Dave, Characterization of L-asparaginase from marine-derived Aspergillus niger AKV-MKBU, its antiproliferative activity and bench scale production using industrial waste, *Int. J. Biol. Macromol*. 108 (2018) 41-46.

[211] Q. Chen, Y. Liu, T. Wang, J. Wu, X. Zhai, Y. Li, W.W. Lu, H. Pan, X. Zhao, Chitosan-PVA monodisperse millimeter-sized spheres prepared by electrospraying reduce the thromboembolic risk in hemorrhage control, *J. Mater. Chem*. B. 5 (2017) 3686-3696.

[212] Zhang, S., Wang, C., Chang, H., Zhang, Q., & Cheng, Y. (2019). Off-on switching of enzyme activity by near-infrared light-induced photothermal phase transition of nanohybrids. *Science advances*, 5(8), eaaw4252.

[212] Yin, W., Yu, J., Lv, F., Yan, L., Zheng, L. R., Gu, Z., & Zhao, Y. (2016). Functionalized nano-MoS2 with peroxidase catalytic and near-infrared photothermal activities for safe and synergetic wound antibacterial applications. *ACS nano*, 10(12), 11000-11011.

[214] Wang, C., Zhang, Q., Wang, X., Chang, H., Zhang, S., Tang, Y., Xu, J., Qi, R., & Cheng, Y. (2017). Dynamic Modulation of Enzyme Activity by Near-Infrared Light. *Angewandte Chemie*, 129(24), 6871-6876.

CURRICULUM VITAE

Name and Surname: Samir Abbas Ali NOMA

Education Status:

- B.Sc., University of Duhok, Faculty of Science, Department of Chemistry. Duhok/IRAQ (2009-2013).

- M.Sc., Aksaray University, Faculty of Science and Arts, Department of Chemistry, Biochemistry division. 68100 Aksaray, Turkey (2014-2016).

- Ph.D., Inonu University, Faculty of Science and Arts, Department of Chemistry, Biochemistry division. 44280 Malatya, Turkey (2016-2021).

Projects

1. **"**Development of Near Infrared Light (NIR) Excited Functional Carrier Systems by Using Upconverting Nanoparticles to Trigger the Activity of Biotechnological Enzyme Drugs**" Scholarship Holder, COST-TÜBİTAK (Scientific and Technological Research Council of Turkey)-KBAG (Project NO: 119Z962), 2020-**

2. **"**Synthesis Characterization and Biological Activities of Benzimidazole Functional N-heterocyclic Carben (NHC) Precursors Containing Thiol Group and Silver and Ruthenium Metal Complexes**"** Researcher, **BAP (Coordinatorship of Scientific Research Projects),** Inonu University Scientific Research Council **(Project ID: 2240).**

3. **"**Preparing Upconverting Nanoparticles for Uricase Immobilization Characterized and Controlling Enzyme Activity Using Near-Infrared NIR**"** Researcher, **BAP (Coordinatorship of Scientific Research Projects),** Inonu University Scientific Research Council **(Project NO: FBG-2020-2173),** 09.06.2020-

4. **"**Synthesis of N-Heterocyclic Carbene (NHC-M, M: Ag, Ru, Pd) Complexes as Drug Agents: Anticancer, Enzyme Inhibition, DNA Binding Properties and Molecular Modification**"** Researcher, **BAP (Coordinatorship of Scientific Research Projects),** Inonu University Scientific Research Council **(Project NO: FOA-2018-1342),** 10.8.2018-

5. **"**Preparation of UV-Curable and Antibacterial Polyurethane-Acrylate Bioadhesives with Zein Protein" Researcher, **BAP (Coordinatorship of Scientific Research Projects),** Inonu University Scientific Research Council **(Project NO: FDP-2018-1284),** 2018-2020.

6. **"**Electrospinning with cyclodextrin-Based Host-guest (Host-Guest) and Implementation Preparation of Polyurethane Dressings Containing Materials Interaction**"** Researcher**, BAP (Coordinatorship of Scientific Research Projects),** Inonu University Scientific Research Council **(Project NO: FCD-2017-956),** 26.12.2017-26.08.2020.

7. "The Preparation and Application of UV-curable, Injectable, Multifunctional Polyurethane Adhesives for Using at Sternal Closure**" Scholarship Holder, 1001 TÜBİTAK (Scientific and Technological Research Council of Turkey)-KBAG (Project NO: 116Z501),** 2017-2019.

8. "Synthesis of some hydrazone Schiff bases, studying antioxidants activities by spectroscopic and x-ray crowning methods of the structures", Researcher, **BAP (Coordinatorship of Scientific Research Projects),** Aksaray University scientific research Council **(Project NO: 2015-085)**.

Scholarships

1. **"**Development of Near Infrared Light (NIR) Excited Functional Carrier Systems by Using Upconverting Nanoparticles to Trigger the Activity of Biotechnological Enzyme Drugs**" Scholarship Holder, COST-TÜBİTAK (Scientific and Technological Research Council of Turkey)-KBAG (Project NO: 119Z962), 2020-**

2. "The Preparation and Application of UV-curable, Injectable, Multifunctional Polyurethane Adhesives for Using at Sternal Closure**" Scholarship Holder, 1001 TÜBİTAK (Scientific and Technological Research Council of Turkey)-KBAG (Project NO: 116Z501),** 2017-2019.

Publications

1. Sevgi BALCIOĞLU, **Samir Abbas Ali Noma**, Ahmet Ulu, Merve Göksin Karaaslan, Onural Ozhan, Suleyman Koytepe, Hakan Parlakpinar,Nigar Vardi, Mehmet Cengiz Colak. **Engineering and Fabrication of Multifunctional Bioadhesives with Broad-Range Tunable Properties for Sternal Closure.** Biomaterials, Submitted.

2. Ülkü Yılmaz, **Samir Abbas Ali Noma**, Tuğba Taşkın Tok[c], Betül Şen, Yetkin Gök, Aydın Aktaş, Burhan Ateş, Muhittin Aygün. **New Pyridine Salts: Synthesis, Characterization, Crystal Structure, Molecular Docking Study, and Investigation of Xanthine Oxidase Inhibitory Effects.** Submitted.

3. Serap Kizilkaya, Ayse Tan, **Samir Abbas Ali Noma**, Burhan Ates, Yunus Kara. **Synthesis, evaluation, and molecular docking studies of novel hybrid isoindole-1,3(2H)-dione derivatives containing 1,2,3-triazole moiety as xanthine oxidase inhibitors.** Bioorganic Chemistry, Submitted.

4. Ayse Tan, Serap Kizilkaya, **Samir Abbas Ali Noma**, Burhan Ates, Yunus Karad. **Novel hybrid isoindole-1,3(2*H*)-dione compounds containing a 1*H*tetrazole moiety: Synthesis, biological evaluation, and molecular docking studies.** *Journal of Biochemical and Molecular Toxicology.* Submitted.

5. Güler Yagiz, **Samir Abbas Ali Noma**, Aliye Altundas, Khattab Al-khafaji, Tugba Taskin-Tok, and Burhan Ates. **Synthesis, Inhibition Studies Against Xanthine Oxidase and Molecular Docking Studies of Dimethyl N-benzyl-1H-1,2,3-triazole-4,5-dicarboxylate and (N-Benzyl-1H-1,2,3-triazole-4,5-diyl)dimethanol Derivatives.** Bioorganic Chemistry. doi.org/10.1016/j.bioorg.2021.104654.

6. **Samir Abbas Ali Noma**, Ömür Acet, Ahmet Ulu, Burcu Önal, Mehmet Odabaşı, Burhan Ateş**. L-asparaginase immobilized p(HEMA-GMA) cryogels: A recent study for biochemical, thermodynamic and kinetic parameters.** Polymer Testing. 93 (2021) 106980.

7. Ferhat Türker, **Samir Abbas Ali Noma**, Aydın Aktaş, Khattab Al Khafaji, Tugba Taşkın Tok, Burhan Ateş, Yetkin Gök. **The (NHC) $PdBr_2$ (2-aminopyridine) Complexes: Synthesis, Characterization, Molecular Docking Study and Inhibitor Effects on the Human Serum Carbonic Anhydrase and Serum Bovine Xanthine Oxidase**. Chemical Monthly, (2020) 151:1557–1567.

8. **Samir Abbas Ali Noma**, Burcu Somtürk Yılmaz, Ahmet Ulu, Nalan Özdemir, Burhan Ateş. **Development of L-asparaginase@hybrid Nanoflowers (ASNase@HNFs) Reactor System with Enhanced Enzymatic Reusability and Stability.** Catalysis Letters, https://doi.org/10.1007/s10562-020-03362-1.

9. Mert Olgun Karataş, **Samir Abbas Ali Noma**, Canbolat Gürses, Sevgi Balcıoğlu, Burhan Ateş, Bülent Alıcı, Ümit Çakır. **Water Soluble Coumarin Quaternary Ammonium Chlorides: Synthesis and Biological Evaluation.** Chem. Biodiversity 2020, 17, 2000258.

10. **Samir Abbas Ali Noma**, Ahmet Ulu, Suleyman Koytepe, Burhan Ateş. Preparation **and characterization of amino and carboxyl functionalized core-shell Fe3O4/SiO2 for L-asparaginase immobilization: A comparison study**. Biocatalysis and Biotransformation, DOI: 10.1080/10242422.2020.1767605. 2020, 38, 392–404.

11. Mustafa Erkan Özgür, Ahmet Ulu, **Samir Abbas Ali Noma**, İmren Özcan, Sevgi Balcıoğlu, Burhan Ateş, Süleyman Köytepe. **Melatonin protects sperm cells of Capoeta trutta from toxicity of titanium dioxide nanoparticles.** Environmental Science and Pollution Research (2020) 27:17843–17853.

12. **Samir Abbas Ali Noma**, Ahmet Ulu, Ömür Acet, Raúl Sanz, Eloy S. Sanz-Pérez, Mehmet Odabaşı, Burhan Ateş. **Comparative study of ASNase Immobilization on Tannic Acid-Modified Magnetic Fe3O4/SBA-15 Nanoparticles to Enhance Stability and Reusability.** *New J. Chem.,* 2020, 44, 4440-4451.

13. **Samir Abbas Ali Noma**, Mahmut Erzengin, Tuncay Tunç, Sevgi Balcıoğlu. **Synthesis, Characterization and Biological Assessment of Novel Hydrazone as a Potential Anticancer Agent and Enzyme Inhibitor.** Journal of Molecular Structure, 1205 (2020) 127550.

14. Özlem GUNDOĞDU, **Samir Abbas Ali NOMA**, Tugba TASKIN-TOK, Burhan ATEŞ, Nurhan KISHALI. **Evaluation of Xanthine Oxidase Inhibitor Properties on isoindoline-1,3-dion derivatives and Calculation of Interaction Mechanism**. Journal of Molecular Structure, 1204 (2020) 127523.

15. Serdar Burmaoglu, Seyda Ozcan, Sevgi Balcioglu, Melis Gencel, **Samir Abbas Ali Noma**, Sebnem Essiz, Burhan Ates, Oztekin Algule. **Synthesis, biological evaluation and molecular docking studies of bischalcone derivatives as xanthine oxidase inhibitors and anticancer agents.** Bioorganic Chemistry, 91 (2019) 103149.

16. Aydın Aktaş, **Samir Abbas Ali Noma**, Duygu Barut Celepci, Fatoş Erdemir, Yetkin Gök, Burhan Ateş. **New 2-Hydroxyethyl Substituted N-Heterocyclic Carbene Precursors: Synthesis, Characterization, Crystal Structure and Inhibitory Properties Against Carbonic Anhydrase and Xanthine Oxidase.** Journal of Molecular Structure (2019), 1184: 487-494.

17. Burhan Ates, Ahmet Ulu, Suleyman Köytepe, **Samir Abbas Ali Noma**, Veli Serkan Kolat, Tekin Izgi. **Magnetic-propelled Fe_3O_4-chitosan carriers enhance L-asparaginase catalytic activity: a promising strategy for enzyme immobilization.** RSC Advances 2018, DOI: 10.1039/c8ra06346j.

18. İbrahim Evren Kıbrız, Mustafa Saçmacı, İsmail Yıldırım, **Samir Abbas Ali Noma**, Tuğba Taşkın Tok, Burhan Ateş. **Xanthine oxidase inhibitory activity of new pyrrole carboxamide derivatives: *In vitro* and in silico studies.** Archiv der Pharmazie 2018, DOI: 10.1002/ardp.201800165.

19. Ahmet Ulu, **Samir Abbas Ali Noma**, Suleyman Koytepe, Burhan Ates. **Chloro-modified magnetic Fe_3O_4@MCM-41 core-shell nanoparticles for L-asparaginase immobilization with improved catalytic activity, reusability and storage stability.** Applied Biochemistry and Biotechnology,187,3, 938-956.

20. Ahmet Ulu, **Samir Abbas Ali Noma**, Suleyman Koytepe & Burhan Ates. **Magnetic Fe_3O_4@MCM-41 core-shell nanoparticles functionalized with thiol silane for efficient L-asparaginase immobilization**. Artificial Cells, Nanomedicine, and Biotechnology 2018, DOI:10.1080/21691401.2018. 1478422.

21. Ahmet Ulu, **Samir Abbas Ali Noma**, Canbolat Gurses, Suleyman Koytepe, Burhan Ates. **Chitosan/Polyvinylpyrrolidone/MCM-41 Composite Hydrogel Films: Structural, Thermal, Surface, and Antibacterial Properties.** Starch - Stärke 2018, 1700303. DOI: 10.1002/star.201700303.

Academic presentation

Oral

1. **Samir Abbas Ali Noma**, Ahmet Ulu, Suleyman Koytepe, Burhan ATEŞ. Preparation and characterization of carboxyl functionalized core-shell Fe3O4/SiO_2 for L-asparaginase immobilization. **2nd INTERNATIONAL CONGRESS on ANALYTICAL and BIOANALYTICAL CHEMISTRY**, 11-14 March 2020 Antalya, Turkey.

2. Burhan Ates, Süleyman Köytepe, Sevgi Balcioglu, Ahmet Ulu, **Samir Abbas Ali Noma**, Imren Özcan. Sternal Kapamada Kullanilmak Üzere Jelatin Içeren UV- Kürlenebilir Poliüretan-Akrilat Sert Doku Yapistiricilarinin Gelistirilmesi. **23 Biyomedikal Bilim ve Teknoloji Sempozyumu** 15-16 Aralık 2018, Acıbadam Mehmet Ali Aydınlar Üniversitesi İstanbul, Turkey.

3. Burhan Ates, Ahmet Ulu, Suleyman Köytepe, **Samir Abbas Ali Noma**, Veli Serkan Kolat, Tekin Izgi. Magnetic Field Enhances Catalytic Activity of L-Asparaginase Conjugated on Fe_3O_4-Chitosan Nanoparticles. **SANKO University Innovation in Medicine Summit-4**, 11-13 Oct 2018, Gaziantep, Turkey.

4. **Samir Abbas Ali Noma**, Ahmet Ulu, Süleyman Köytepe, Burhan Ateş. L-Asparaginase Immobilization on Amino Functionalized Fe_3O_4@SiO_2 Magnetic Nanoparticles. **International Conference on Physical Chemistry and Functional Materials (PCFM'18)**. 19-21 June 2018, Firat University, Elazig-Turkey.

5. Ahmet Ulu, **Samir Abbas Ali Noma**, Süleyman Köytepe, Burhan Ateş. Chloro-Functionalized Magnetic Fe_3O_4@MCM-41 Core-Shell Nanoparticles for Enzyme Immobilization. **International Conference on Physical Chemistry and Functional Materials (PCFM'18).** 19-21 June 2018, Firat University, Elazig-Turkey.

6. **Samir Abbas Ali Noma**, Ahmet Ulu, Suleyman Koytepe, Burhan Ates. Surface Modification of MCM-41-Coated Magnetite Nanoparticles for Covalent Immobilization of L-Asnase. **6th International Attended Drug Chemistry: Design, Synthesis, Production, and Standardization of Drug activity Substances Congress**. 22 – 25 March 2018, Belek, ANTALYA. Maritim Pine Beach Hotel, Turkey.

7. Ahmet Ulu, **Samir Abbas Ali Noma**, Suleyman Koytepe, Burhan Ates. Preparation of Epoxy-Functional Fe_3O_4@MCM-41 Magnetic Nanoparticles and Application of L-Asparaginase Immobilization**. 6th International Attended Drug Chemistry: Design, Synthesis, Production, and Standardization of Drug activity Substances Congress**. 22 – 25 March 2018, Belek, ANTALYA. Maritim Pine Beach Hotel, Turkey.

8. Özlem GÜNDOĞDU, **Samir Abbas Ali NOMA**, Nurhan KİSHALIc, Yunus KARA, Burhan Ates. Xanthine Oxidase Enzyme Inhibition of Some Isoindole-1,3-Dion Derivatives. **6th International Attended Drug Chemistry: Design, Synthesis, Production, and Standardization of Drug activity Substances Congress.** 22–25 March 2018, Belek, ANTALYA. Maritim Pine Beach Hotel, Turkey.

9. **Samir Abbas Ali NOMA**, Merve Goksin KARAASLAN, Sevgi BALCIOGLU, Tuncay TUNC, Burhan ATES, Mahmut ERZENGĠN, Synthesis of Novel Hydrazone Derivatives and Investigation of Their Biological Activities. **Innovation in Medicine Summit-III**, 11-13 May 2017, Gaziantep, Turkey.

Posters

1. Ülkü Yılmaz, Yetkin Gök, Burhan Ateş, **Samir Abbas Ali Noma.** Synthesis of New Pyridine Salts and Investigation their Xanthine Oxidase Inhibitory Effects. **International Conference on Physical Chemistry and Functional Materials** "**PCFM-20"**, **22-24** September 2020 Malatya, Turkey.

2. Ayşe Başak ÇAKMEN, **Samir Abbas Ali NOMA**, Canbolat GÜRSES, Süleyman KÖYTEPE, Burhan ATEŞ, İsmet YILMAZ. The Preparation of Antibacterial Wound Dressing Materials Containing Allantoin via Electrospinning Method. **EURASIA BIOCHEMICAL APPROACHES& ANTALYA CONGRES (2 EBAT),** 26-29 OCTOBER 2019, Antalya, Turkey.

3. Mustafa Nabel Mirdan, **Samir Abbas Ali NOMA**, Burhan ATEŞ and Aliye ALAYLI ALTUNDAŞ. Synthesis Of 1-benzyl-4-phenyl-1*h*-1,2,3-trizole derivatives and investigatoion of biological activity. **7th Drug Chemistry Conference: Design, Synthesis, Production and Standardization of Drug Active Substances,** 14 – 17 March 2019, Kemer, ANTALYA/Turkey.

4. Güler YAĞIZ, **Samir Abbas Ali NOMA**, Burhan ATEŞ and Aliye ALAYLI ALTUNDAŞ. Synthesis of 1-Aryl-1H-1,2,3-Triazole-4,5-Dicarboxylate Derivatives and The Inhibition Effect on The Xanthine Oxidase (XO) Enzyme. **7th Drug Chemistry Conference: Design, Synthesis, Production and Standardization of Drug Active Substances,** 14 – 17 March, 2019, Kemer, ANTALYA/Turkey.

5. Aliye ALAYLI ALTUNDAŞ, **Samir Abbas Ali NOMA**, Güler YAĞIZ and Burhan ATEŞ. The Inhibition Effect of 1H-1,2,3-Triazole Compounds On The Xanthine Oxidase (XO) Enzyme. **7th Drug Chemistry Conference: Design, Synthesis, Production and Standardization of Drug Active Substances,** 14 – 17 March, 2019, Kemer, ANTALYA/Turkey.

6. Ayşe Başak ÇAKMEN, **Samir Abbas Ali NOMA**, Süleyman KÖYTEPE, Burhan ATEŞ, İsmet YILMAZ. Çapraz bağlayıcı olarak trimetilolpropan etoksilatın kullanıldığı alifatik yapıda poliüretanların hazırlanması ve elektrospiNning uygulaması. **EURASIA BIOCHEMICAL APPROACHES& ANTALYA CONGRES (1 EBAT)**, 27-30 OCTOBER 2018, Side Star Elegance Hotel Side/Antalya, Turkey.

7. Sevgi Balcıoğlu, Ahmet Ulu, **Samir Abbas Ali Noma**, Canbolat Gürses, Merve Gökşin Karaaslan, Süleyman Köytepe, Burhan Ateş. Preparation of Sericin Based UV-Curing Multifunctional Polyurethane Tissue Adhesives. **SANKO University Innovation in Medicine Summit-4**, 11-13 Oct 2018, Gaziantep, Turkey.

8. Sevgi Balcioğlu, **Samir Abbas Ali Noma**, Murat ŞİMŞEK Süleyman Köytepe, Burhan Ateş. Nano-Electrospun Wound Dressing Materials Functionalized With Host-Guest Interactions. **14th Nanoscience and Nanotechnology Conference,** 22 - 25 September 2018 / Çeşme, İzmir, Turkey.

9. **Samir Abbas Ali Noma**, Ahmet Ulu, Süleyman Köytepe, Burhan Ateş. Effects of Silica on the Morphology, Structure and Properties of Starch/Poly(vinyl Pyrrolidone) Blends. **VII. Polymer Science and Technology Congress with International Participation**, 09-12 September 2018, Eskişehir, Turkey.

10. Ahmet Ulu, **Samir Abbas Ali Noma**, Süleyman Köytepe, Burhan Ateş. Chloro-Functionalized Magnetic Fe_3O_4@MCM-41 Core-Shell Nanoparticles for Enzyme Immobilization. **International Conference on Physical Chemistry and Functional Materials (PCFM'18).** 19-21 June 2018, Firat University, Elazig-Turkey.

11. Sevgi Balcioğlu, **Samir Abbas Ali Noma**, Süleyman Köytepe, Burhan Ateş. Synthesis and Characterization of Polyurethane Wound Dressing Material. **International Conference on Physical Chemistry and Functional Materials (PCFM'18)**. 19-21 June 2018, Firat University, Elazig-Turkey.

12. Layla Ahmed Othman, Ibrahim A. N. Shaswary, **Samir Abbas Ali NOMA.** Chemical Constituents and Antibacterial Activity of Prosopis-Farcta Fabaceae Family. **6th International Attended Drug Chemistry: Design, Synthesis, Production, and Standardization of Drug activity Substances Congress.** 22 – 25 March 2018, Belek, ANTALYA. Maritim Pine Beach Hotel, Turkey.

13. Tunç T., **Noma, S. A. A.**, Erzengin, M., **"**Synthesis, Crystal Structure, Spectroscopic Studies and Biological activity of 1-(5-bromo-2,3-dimethoxybenzylidene)-2- (pyridine-2-yl) hydrazine Schiff Base Molecule" (Poster Presentation). **ANNUAL MEETING of the German Crystallographic Society (DGK)**, 14–17 March 2016 STUTTGART, Germany.

14. Erzengin M., **Noma, S. A. A.**, Tunç, T., **"**Synthesis of 1-(5-bromo-2,4-dimethoxybenzylidene) -2-(pyridine-2-yl) hydrazine Schiff Base Molecule, Evaluating of its Free Radical Scavenging Activity and Determination of its, *in vitro*, Inhibitory Effect on Purified Human Serum Paraoxonase-1**"**. **ANNUAL MEETING of the German Crystallographic Society (DGK)**, 14–17 March 2016 STUTTGART, Germany.

Participation in seminars, training and workshops

1. "Organization Member for the Biochemistry-5, Summer School Certificate of Attendance,Erciyes University, June 24-27, 2019, Kayseri, Turkey.

2. 23 Biyomedikal Bilim ve Teknoloji Sempozyumu 15-16 Aralık 2018, İstanbul, Turkey.

3. VII. Polymer Science and Technology Congress with International Participation. 09-12 September 2018, Eskişehir, Turkey.

4. International Conference on Physical Chemistry and Functional Materials (PCFM'18). 19-21 June 2018, Firat University, Elazig-Turkey.

5. 6th International Attended Drug Chemistry: Design, Synthesis, Production, and Standardization of Drug activity Substances Congress. 22–25 March 2018, Belek, ANTALYA. Maritim Pine Beach Hotel, Turkey.

6. "Laboratory Animals" Certificate of animal use in experimental research (B), Inönü University Medical School, Ethics Committee for Animal Experiments, 17-26 November 2017**,** Malatya, Turkey.

7. "Organization Member for the Biochemistry-3, Summer School Certificate of Attendance, Aksaray University, July 12-14, 2017, Aksaray, Turkey.

8. "Innovation in Medicine Summit-III", Certificate of Attendance, 11-13 May 2017, Gaziantep, Turkey.

9. "Current Issues in Applied Biochemistry-2", Summer School Certificate of Attendance, Aksaray University 20-23 August 2015, Aksaray, Turkey.

Professional experiences

1. Export Manager in Candy Company Apr 2017- Oct 2017 Malatya/Turkey.
2. Work at DNO Oil Company 26.9.2013-15.11.2013.
3. Training Course in Clinical Central Health Laboratory 28.6.2012-20.9.2012.